DATA-DRIVEN PRIORITIZATION AND EMPIRICAL PREDICTIONS FOR BRIDGE SCOUR IN NEBRASKA

FINAL REPORT

Richard L. Wood (PI), Awgku Ahmad Hashim B. Awg Bolhasan, Basil Abualshar, Christine E. Wittich (co-PI), Chung R. Song (co-PI), Junke Guo (co-PI), Mohammad Ebrahim Mohammadi, Mitra Nasimi, Yijun Liao

University of Nebraska-Lincoln

Department of Civil and Environmental Engineering

900 N 16th St, Lincoln, NE 68588

Sponsored By

Nebraska Department of Transportation and U.S. Department of Transportation Federal Highway Administration

June 2022

NEBRASKA
Good Life. Great Journey.
DEPARTMENT OF TRANSPORTATION

UNIVERSITY OF Nebraska Lincoln

TECHNICAL REPORT DOCUMENTATION PAGE

1. Report No. M104	2. Government Accession No.	3. Recipient's Catalog No.
4. Title and Subtitle Data-Driven Prioritization and Empirical Predictions for Bridge Scour in Nebraska		**5. Report Date** June 2022 **6. Performing Organization Code**
7. Author(s) Awgku Ahmad Hashim B. Awg Bolhasan, Richard L. Wood, Basil Abualshar, Christine E. Wittich (co-PI), Chung R. Song (co-PI), Junke Guo (co-PI), Mohammad Ebrahim Mohammadi, Mitra Nasimi, Yijun Liao		**8. Performing Organization Report No.** SPR-P1(20) M104
9. Performing Organization Name and Address University of Nebraska-Lincoln 1400 R St, Lincoln, NE 68588		**10. Work Unit No.** **11. Contract** 26-1121-4051
12. Sponsoring Agency Name and Address Nebraska Department of Transportation Research Section 1400 Hwy 2 Lincoln, NE 68502		**13. Type of Report and Period Covered** July 2019 – June 2022 **14. Sponsoring Agency Code**
15. Supplementary Notes		

16. Abstract

The effect of scour at the bridge substructure results in an increase in the vulnerability of the overall bridge stability. Previous studies have found that current guidelines are often overly-conservative with respect to scour. This project aims to provide guidance on hydraulic modeling parameters and reasonable scour estimates specific to Nebraska conditions. This will enable engineers to assess bridge sites for scour more precisely for efficient and effective design and countermeasures. Four sites were surveyed for scour changes between the period of December 9, 2020, to April 20, 2021. At these four sites, overland and bathymetry survey data were collected. The data collected were fused to create a high spatial resolution point cloud data of each bridge site. The point cloud datasets were used to analyze and quantify scour changes in the field using a change detection method. Erosion tests were also conducted at each site to classify the soil properties and determine the equivalent grain size parameters. The fused point cloud data and soil parameters were subsequently inputted in hydraulic modeling software, HEC-RAS, to predict bridge scour and to compare changes over time at each of the field sites. The scour analysis data was directly compared with the quantified changes from the point cloud analysis. The project shows that high-resolution geometry and equivalent grain size parameters yield more reasonable scour estimates compared to current guidelines.

17. Key Words	18. Distribution Statement
Bridge scour, flooding, hydraulic modeling, point clouds	No restrictions.

19. Security Classification (of this report)	20. Security Classification (of this page)	21. No. of Pages	22. Price
Unclassified	Unclassified	150	

Form DOT F 1700.7 (8-72) Reproduction of completed page authorized

DISCLAIMER

The contents of this report reflect the views of the authors, who are responsible for the facts and the accuracy of the information presented herein. The contents do not necessarily reflect the official views or policies neither of the Nebraska Department of Transportations nor the University of Nebraska-Lincoln. This report does not constitute a standard, specification, or regulation. Trade or manufacturers' names, which may appear in this report, are cited only because they are considered essential to the objectives of the report.

The United States (U.S.) government and the State of Nebraska do not endorse products or manufacturers. This material is based upon work supported by the Federal Highway Administration under SPR-P1(20) M104. Any opinions, findings and conclusions, or recommendations expressed in this publication are those of the author(s) and do not necessarily reflect the views of the Federal Highway Administration."

This report also serves as the thesis for Awgku Ahmad Hashim B. Awg Bolhasan under the advisement of Prof. Richard L. Wood.

Table of Contents

List of Tables

List of Figures

ABSTRACT

The effect of scour at the bridge substructure results in an increase in the vulnerability of the overall bridge stability. Previous studies have found that current guidelines are often overly-conservative with respect to scour. This project aims to provide guidance on hydraulic modeling parameters and reasonable scour estimates specific to Nebraska conditions. This will enable engineers to assess bridge sites for scour more precisely for efficient and effective design and countermeasures.

Four sites were surveyed for scour changes between the period of December 9, 2020, to April 20, 2021. At these four sites, overland and bathymetry survey data were collected. The data collected were fused to create a high spatial resolution point cloud data of each bridge site. The point cloud datasets were used to analyze and quantify scour changes in the field using a change detection method. Erosion tests were also conducted at each site to classify the soil properties and determine the equivalent grain size parameters. The fused point cloud data and soil parameters were subsequently inputted in hydraulic modeling software, HEC-RAS, to predict bridge scour and to compare changes over time at each of the field sites. The scour analysis data was directly compared with the quantified changes from the point cloud analysis. The project shows that high-resolution geometry and equivalent grain size parameters yield more reasonable scour estimates compared to current guidelines.

ACKNOWLEDGEMENTS

This project was funded by the Nebraska Department of Transportation (NDOT) under project number M104 – Data-Driven Prioritization and Empirical Predictions for Bridge Scour in Nebraska. The research team would also like to appreciate the support and assistance of the Technical Advisory Committee (TAC) throughout this project. This includes the following member (in alphabetical order): Jason Dayton, Mark Fischer, Lieska Halsey, David Hansen, Kirk Harvey, Fouad Jaber, and Mark Traynowicz.

CHAPTER 1 – INTRODUCTION

1.1. PROJECT OVERVIEW

Bridge scour is a leading cause of bridge closures and failures in the country and Nebraska based on (Nebraska Legislature, 2014). Over the last few years, high-profile bridge closures in Nebraska have been widely publicized in the media-citing scour as the primary issue. Within the FHWA specified process, two critical steps rely on site-specific details (FHWA, 2012). Within the FHWA process, step 2 is to develop hydraulic parameters and step 5 is to evaluate the results for reasonableness. Different materials will scour at various rates. Loose granular soils can rapidly erode by flowing water, whereas cohesive soils, which are common to specific areas of Nebraska, are more scour-resistant. However, Section 3.1 of HEC-18 (FHWA, 2012), conservatively assumes that the ultimate scour in cohesive soils can be as deep as the scour in loose granular soils (or sands). While this assumption is expected to be conservative because of the increased critical shear stress in cohesive soils, this can lead to highly inaccurate scour estimates and the potential for over-designed and costly bridge foundations. However, significant challenges arise to verify the magnitude of scour for these varying soils. This is primarily due to the cyclic nature of the scour process where scour is deepest during the peak of a flood but may be hardly visible as floodwaters recede and scour holes fill with sediment. Therefore, there is a critical need to develop improved hydraulic parameters and to provide guidance on reasonableness for scour estimates that reflect Nebraska soils.

1.1.1. Bridge Scour

Bridge scour is the gradual removal or the erosion of sediment and soil from the areas of a bridge foundation such as piers and abutments, resulting in significantly reduced capacity and

safety of the bridge. As shown in Figure 1.1, the bridge scour that occurs at the foundation of the bridge (pier) is caused by the water discharged from upstream of the river, removing the sediment and soils around the bridge pier, causing the scour holes at the foundation of the bridge. The sediments removed and carved upstream are then carried downstream of the river, where the sediments will be deposited. The region of separation caused by the bridge pier is known as the wake flow region. This is the region of disturbed flow downstream of a solid body of water. As seen in the figure, the scour hole caused a significant change in the bridge foundation, compromising the bridge's structural integrity.

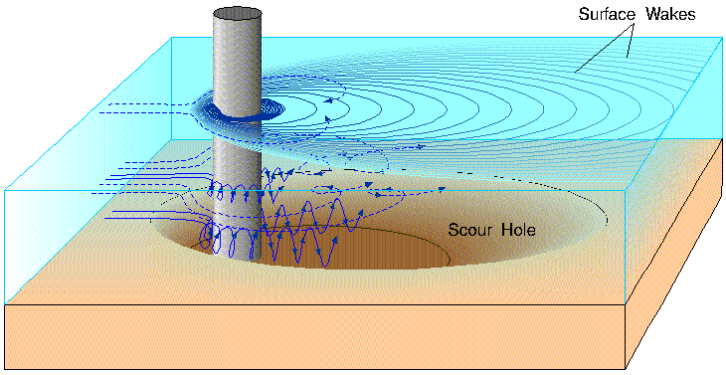

Figure 1.1: Overview of scour mechanisms (courtesy of USGS, 2016).

1.1.2. Bridge Scour Classifications

There are two general classifications of bridge scour. The first is known as general scour. This is the lowering (degradation) of the streambed across the stream, which develops with or without the presence of a structure along the river such as a bridge (Khassaf, 2021). General scour can be further classified as long-term or short-term general scour. Long-term is a streambed profile change over a long period of time. Short-term is the (general) scour and fill-in over long-term streamflow runoff cycle. Short-term general scour depends on the process of sediment transport in the river and will result in filling in areas of long-term scour.

The second type is localized scour which is due to the presence of a human-made structure along the river, such as a bridge. Localized scour can further be classified as the combination of contraction scour and local scour. Contraction scour occurs due to the flow contraction that occurs between the bridge foundations, such as the abutment and the piers of the bridge (as shown in Figure 1.2). The upstream flow converges when the flow under the opening of the bridge. The accelerated flow caused by the flow convergence, caused contraction scour. The increase in speed of water as it moves through a bridge opening that is narrower than the natural river channel, to maintain the same flow rate (often known as Q). Moreover, there are also the clear-water scour and the live-bed scour. The difference is that during clear water scour, the bed material is not in motion, meaning the sediment removed by the scour, is not replenished by the upstream flow. In contrast to the live-bed scour, the scour sediment is constantly transported into the local scour hole.

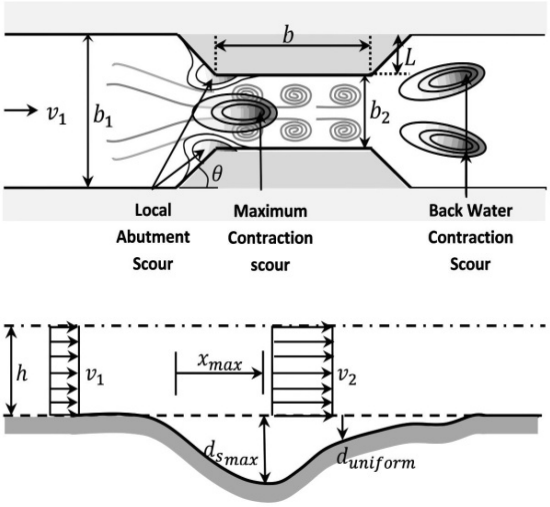

Figure 1.2: Overview of contraction scour (courtesy of Ghazvinei, Mohammad, Ghazali, and Huat, 2012).

1.2. RESEARCH MOTIVATIONS AND OBJECTIVES

This project aims to provide guidance on hydraulic parameters and reasonable scour estimates specific to Nebraska conditions. This will enable engineers to assess bridge sites for scour more confidently. Most bridge foundations designed before 1987 did not consider scour as part of the design and post-1987 bridges are very conservatively designed against scour (Briaud et al., 2018), or minimally perceived to be conservative.

1.2.1 Objectives

The first objective of this project is to reduce the uncertainty in the scour prediction equations specific to Nebraska soils and hydraulic conditions using empirical field data collected. Particular attention will be paid to the scour predictions of clayey and cohesive soils, which are currently presumed to be overly conservative in the existing FHWA HEC-18 approach. The second objective of this project is to evaluate and provide guidance on reasonable scour estimates for Nebraska soil and hydraulic conditions. This objective is done to address engineering judgment on whether the numerical scour predictions are "unconservative" or "over-conservative". Guidance will be provided using real field measurements to benchmark and clarify the ranges of acceptable scour in this area from the highly detailed, high-fidelity site assessments.

1.2.2. Expected Benefits

In addition to these direct outcomes, this project is expected to result in the following benefits: reduced bridge closures, structural savings for new bridge design, validation and/or limitations of existing scour predictions, enhanced knowledge of scour and model for other states/agencies.

1.3. RESEARCH TASKS

Research tasks were done for this project divided into five tasks. These are described below as individual subsections. Task 5 relates to the reporting, which includes this document.

1.3.1. Literature Review (Task 1)

The initial literature review motivated the study of this research. The initial literature reading is based on previous work and studies on the observational method on bridge scour. The previous works discuss and address the conservatism in the current procedures. This research task is discussed in Chapter 2.

1.3.2. Geometric Data Collection and Temporal Scour Rate (Task 2)

High accuracy and high-fidelity geospatial data were collected between December 9th, 2020, to April 20th, 2021. The data collection is split between *overland* and *bathymetry* data. Lidar surveys produce geometrically accurate overland point cloud data, which supplement areas of occlusion and for efficient data collection. Uncrewed aerial system (UAS or commonly known as drones) surveys the surrounding soils and upstream and downstream channels. The RTK echo and sonar soundings collect bathymetry data to provide the (underwater) river streambed profile. The overland and bathymetry data are then fused to create a three-dimensional model for all the four bridge sites selected for the study.

The temporal scour rate is analyzed by importing the combined geospatial data collected into HEC-RAS. HEC-RAS is an open-source software capable of creating models of hydraulic water flow in rivers that can also perform hydraulic calculations of the rivers. The HEC-RAS is used to perform the scour calculations for this project. This software is considered given its extensive and exclusive use by NDOT.

1.3.3. Site Characterization (Task 3)

The initial site selection was recommended by NDOT and was surveyed in January 2020. The initial four sites selected were located in Hooper, Waterloo, Lincoln, and Falls City. The initial site locations are shown in Figure 1.3 below.

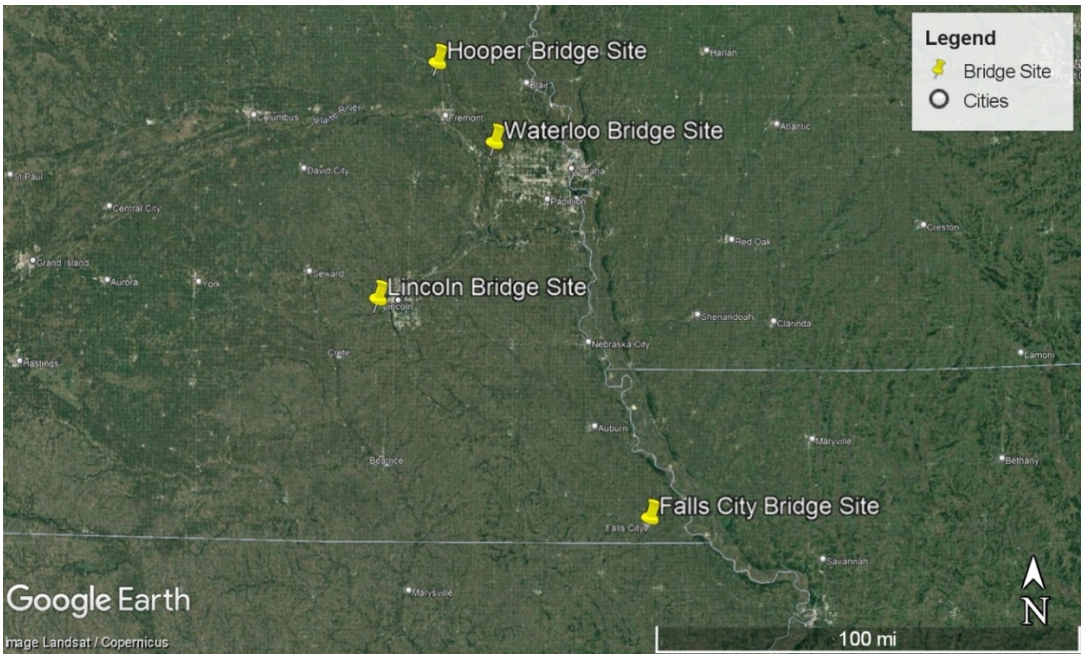

Figure 1.3: Initial site selection.

From north to south, the Hooper bridge site crosses Maple Creek, and spans over 30.8 meters (101 feet) and is located south of the city of Hooper. South of the Hooper bridge site is the Waterloo bridge site. The Waterloo bridge site is located north-east of the village and spans over 123.1 meters (404 feet) and crosses the Elkhorn River. The next bridge site is located southwest of Lincoln. The bridge in Lincoln crosses Haines Branch with a bridge length of 31.1 meters (102 feet). The final initial bridge site location selected is south of Falls City, with a bridge length of 115.8 meters (380 feet) crossing the Big Nemaha River. The details of the initial bridges selected are tabulated in Table 1.1.

From the initial site selection, only two of the sites made it to the final site selection, which is the Hooper and Lincoln bridge site. The two sites that did not make it to the final selection are the Waterloo and Falls City bridge sites.

Table 1.1: Initial site summary.

Bridge Site	Hooper	Waterloo	Lincoln	Falls City
Structure Number	C002713910	S064 06033	C005521315	S073 00248
Year Built	1967	1984	1991	1981
Length (m)	30.8	123.1	31.1	115.8
Length (ft)	101	404	102	380
Number of Spans	1	3	3	3
Number of Piers	0	2	2	2
Peak Flow Rate (ft^3/sec)	35000	100000	5060	71600
Average Flow Rate (ft^3/sec)	4627	17647	1180	25978

The figure below shows the pictures of the Waterloo and Falls City bridge sites during the initial site survey visit in January 2020. The Waterloo bridge site was not chosen due to inaccessibility on two out of the four corners of the bridge (posted private property limiting access as this survey is also conducted outside of the right-of-way). On the other hand, the Falls City bridge site does have accessibility issues that cause safety issues. The Falls City bridge site was not selected due to safety. The limited accessibility at these sites causes would result in insufficient data to conduct this study, as ground and aerial surveys are conducted both inside and outside of the streams (on the banks and surrounding areas).

(a) (b)

Figure 1.4: Elkhorn River Bridge site near Waterloo.

(a) (b)

Figure 1.5: Big Nemaha Bridge site near Falls City.

Consequently, the two bridge sites that were not selected were replaced by two new bridge sites. The two new bridge sites for the final site selections are located in Wilber and Beatrice. The Wilber bridge site crosses Turkey Creek and spans over 73.8 meters (242feet) and is located west of the city of Hooper. The bridge in Beatrice crosses the Big Blue River with a bridge length of 132.6 meters (435 feet). The details of the final four bridge site locations (shown in Figure 1.6) have greater variability with accessibility on most of the banks (up and downstream of the bridge). These sites are discussed in more detail in Chapter 3.

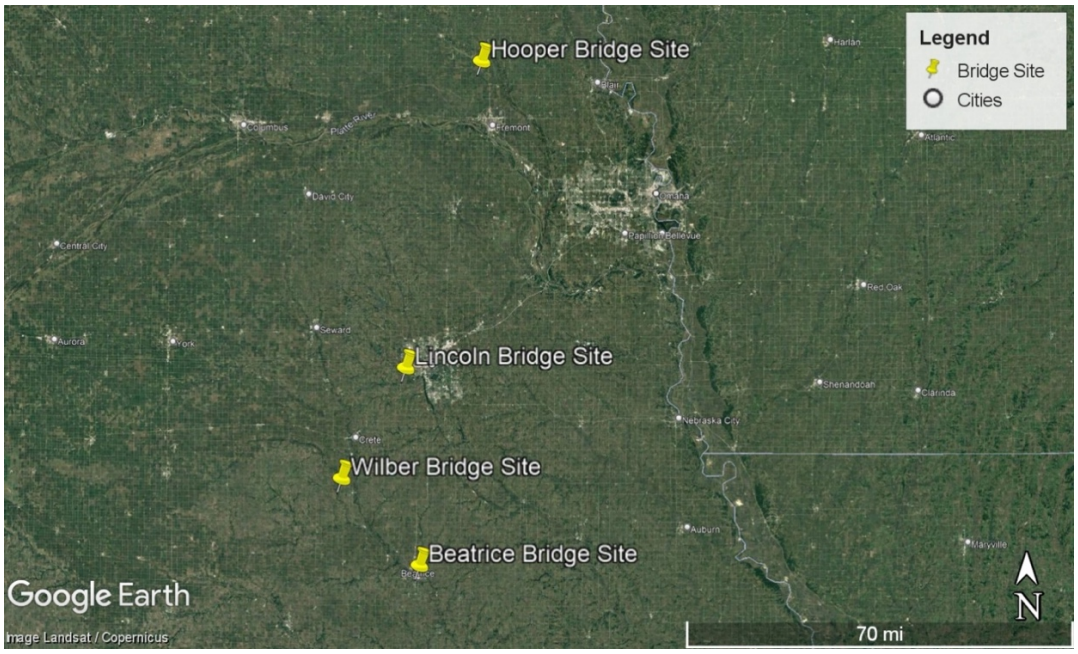

Figure 1.6: Final site selection (courtesy of Google Earth).

Soil samples were taken from the riverbed at the four different bridge sites for geotechnical analysis. As control specimens and to validate the behavior of the different soils collected, four samples were taken from two different locations at the University of Nebraska-Lincoln City Campus. The collected soil samples were then tested and analyzed to obtain an equivalent D_{50} value for each of the sites. The process of soil characterization is further discussed in Chapter 4.

1.3.4. Data-Driven Scour Validation (Task 4)

Data observations are made to achieve the objectives of the project and outline recommendations. The hydraulic model is created on HEC-RAS by using the rasterized combined point cloud data consisting of overland and bathymetry data. HEC-RAS is used for the bridge scour analysis, similar to the existing methods at NDOT. The combined point cloud data are also used to analyze and observe scour changes on CloudCompare. Using the M3C2 computations on CloudCompare, the scour analysis data from HEC-RAS is then directly compared with the

quantified changes detected with the M3C2 computations. This provides a confirmation of the field-measured changes at each of the four sites.

1.4. REPORT ORGANIZATION

The report consists of six chapters discussing the process for data-driven prioritization and empirical predictions for bridge scour at the four different site selected locations. Chapter 1 provides the project overview, scope, tasks, and motivation of the overall study. Chapter 2 discusses the literature review that motivates this project. The chapter describes the general literature review done on current site characterization and scour process. In chapter 3, the process of field surveying is discussed. The chapter outlines how the 3D survey is performed using different equipment to collect 3D point cloud data for topography and bathymetry datasets. Chapter 4 outlines the site characterization done to determine the soil characteristics of the four different sites in Nebraska. This includes the procedure to classify the type of soil and quantify a D_{50} value for each site based on the equivalent value. Chapter 5 then would discuss the implementation of the point cloud data within a 1D hydraulic HEC-RAS model to run scour analysis and confirm the site characterizations. Chapter 6 concludes the study by discussing the results and recommendations for a revised scour analysis procedure. Chapter 7 concludes the study and outline potential future research studies. Appendices include the detailed results of the site characterization and the HEC-RAS report of the scour analysis.

CHAPTER 2 – LITERATURE REVIEW

This chapter discusses a brief literature review that outlines and guides the project as well as represents Task 1 in the research project. The current guidelines used may be considered as an over-conservative evaluation of scour; however, this is not definite for all cases. Briaud and others have done research on an observational scour study approach to estimate scour that is less conservative and found that the hydraulic guideline is often overly-conservative. These specific studies are detailed in this chapter. This research focuses on the possibility of merging the simplicity and the future of the point cloud data surveying and detecting changes in scour using point cloud data to calculate scour using a one-dimensional hydraulic model within HEC-RAS.

2.1. FRAGILITY OF BRIDGES TO SCOUR IN NEBRASKA

The effect of scour (by displacing and carving out sediments) at the bridge foundation, results in an increase in the vulnerability of the overall bridge structure. Therefore, it is crucial to consider the impact of scour to the structural integrity of the bridge. Figure 2.1 shows the potential damage that could occur due to ineffective scour capacity. Figure 2.1(a) shows the bridge collapse on Route SC 418 crossing Enoree River in South Carolina and Figure 2.1(b) shows an approach slab failure at a bridge crossing the Elkhorn River, Nebraska State Route 57 just south of Stanton, Nebraska.

(a) (b)

Figure 2.1: Bridge failure due to scour (a) Enoree river bridge (photograph by Michael Hall, 1995), (b) Stanton County bridge (photograph by Richard Wood, 2019).

The state of Nebraska has 3,522 bridges with a length greater than 20 feet that it is responsible for maintaining on the state highway system, (Nebraska Legislature, 2014). Nebraska's cities and 93 counties have a total of 11,763 bridges that span longer than 20 feet. According to this report, bridges under 20 feet are not generally inspected and thus no count generally exists, but the number may be in the tens of thousands when considering both state and local crossings. The increased size and weight of agricultural equipment combined with the simple passage of time have put increased stress on Nebraska's county bridges. Moreover, an exacerbated effect exists in some areas of Nebraska with the degradation of the water channel the county bridge spans, or in other words the process of water eroding the channel's banks and threatening the integrity of the bridge. Or in other words, scour degrades the structural integrity of the foundation and its supported superstructure.

This report also identifies that environmental factors and modern vehicles are stressing rural bridges, many of which were built in the first half of the twentieth century, highlighting the age of Nebraska's bridges, which is similar to other states. With environmental factors like channel

deepening and erosion (also known as scour in this project) and it is easy to see why bridges require some form of rehabilitation, repair, or replacement. Moreover, agricultural equipment (such as grain carts and combines; which is inclusive of husbandry vehicles (NCHRP Research Report 951, 2020), semi-trailers, school busses, and ambulances are all heavier today and put great stress and concentrated weight on bridges, given if the bridges have adequate width for safe operation and usage.

Risk is defined as the product of the probability of occurrence times the value of the consequences. The probability that an event will be exceeded is commonly denoted as POE (probability of exceedance). The annual POE is the probability that an event will be exceeded in any one year. Figure 2.2 shows the various risk of civil engineering amongst other common factors that contribute to fatalities or monetary loss. There are four different failure modes observed in bridge scour as shown in Figure 2.3. About 26% of the observed occurrence of bridge scour are large scour holes. The other 74% of the observed scour caused by a compromised bridge foundation may contribute to or cause a structural collapse.

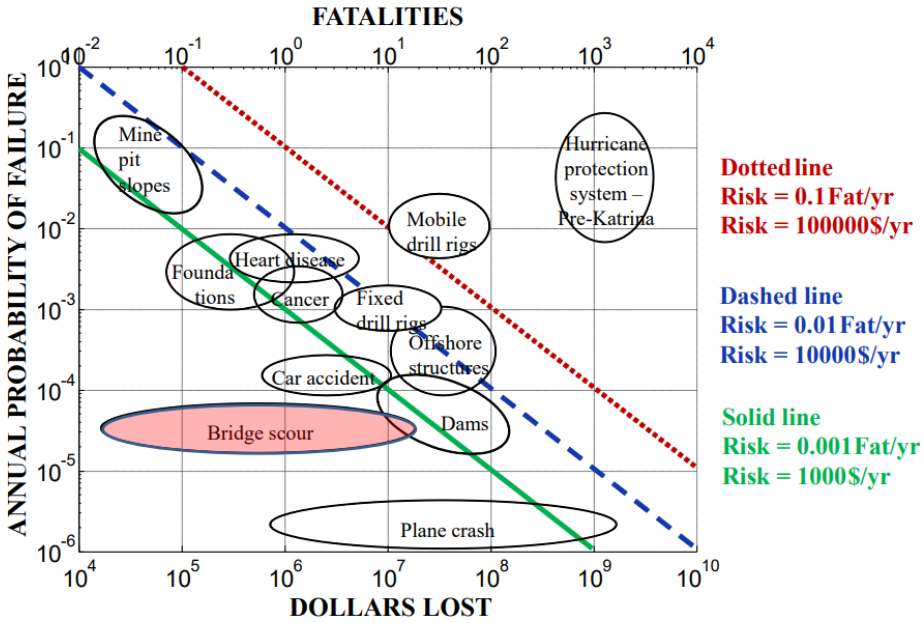

Figure 2.2: Annual probability of failure of bridge scour (courtesy of Briaud et al., 2014).

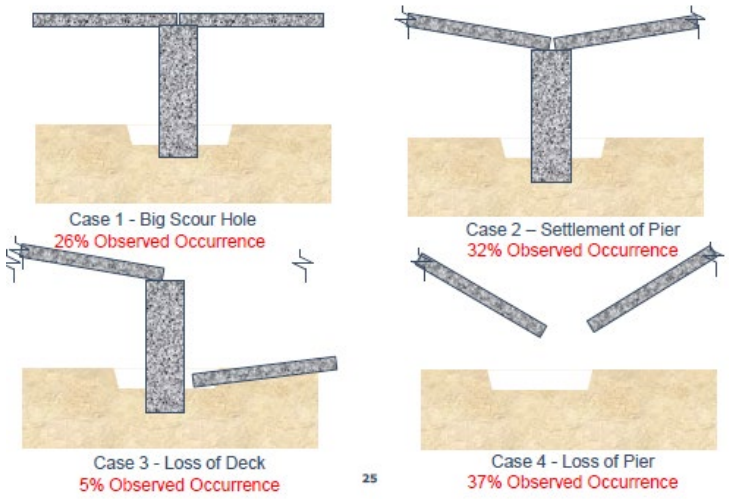

Figure 2.3: Observed failure modes of bridge due to scour (courtesy Briaud et al., 2014).

It is also important to note that there are three types of scour depth to consider. This includes abutment, pier, and contraction scour. Figure 2.4 visualizes the different types of scour depth. Abutment scour occurs near the abutment and the pier scour occurs around the pier, where the discharge of the upstream flow accelerates around the structural bridge's abutment and the

piers. At the contracted cross-section of the bridge opening, the contraction scour occurs across where the water upstream accelerates between the bridge opening.

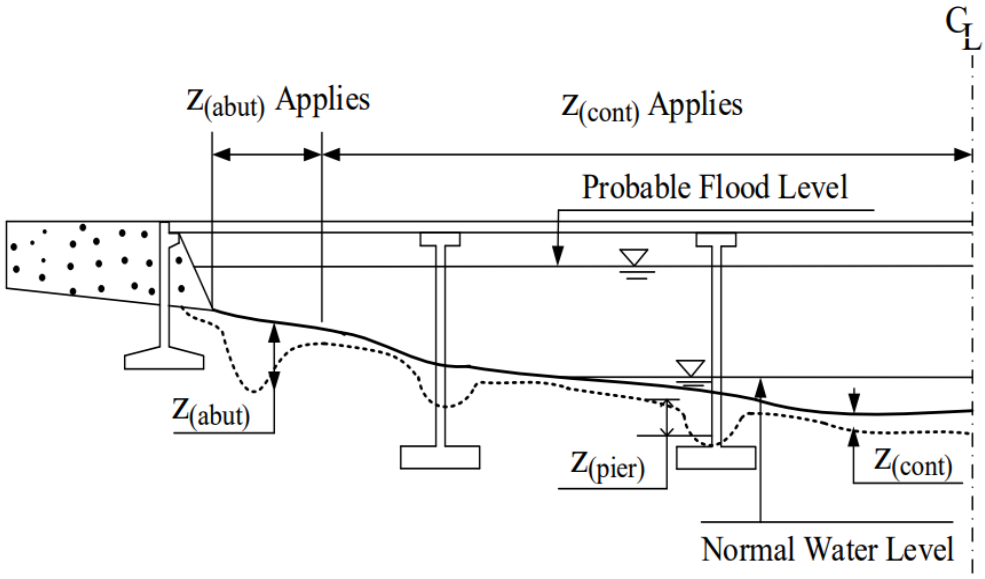

Figure 2.4: Different types of scour depth (courtesy Briaud et al., 2014).

2.2. PREDICTION OF BRIDGE SCOUR

Scour predictions are usually made based on conventional regression methods. These methods while are useful but are presumed to conservative and may overpredict scour results which is uneconomical. The most current method used does not consider the soil resistance to erosion, thereby giving the same scour depth whether the bridge was founded in fine sand or in weathered rock. While a typical non-cohesive bed erodes particle by particle, a cohesive or sand-clay mixture bed erodes chunk by chunk, particle by particle, or aggregate by aggregate (Chaudhuri and Debnath 2013).

The Observation Method for Scour (OMS) was developed to address the conservatism inherent in the current procedures by relying significantly on past observations at the bridge

(Briaud et al., 2018). OMS is based primarily on observed measurements by obtaining the maximum observed scour depth and the highest flood of the bridge which help predict the future scour depth for a chosen future flood by extrapolating the observations. These results aim to reduce the over-conservatism of current practice but do have limitations. The limitation of this method is that OMS requires that the user estimate the possibility and magnitude of infilling. The OMS method has evolved to create the TAMU-OMS software (Govindasamy et al.,2014).

2.2.1. CURRENT HYDRAULIC ANALYSIS GUIDELINES

The method and formulations from Hydraulic Engineering Circular No. 18 (HEC-18, 2012) have been found to be consistently over-conservative (Briaud et al., 2018). The method is recommended for sandy soils but is very conservative for clay streambeds. Moreover, contraction and pier scour depths for sandy soils may be calculated using equations from Chapters 6 and 7 of HEC-18.

Figure 2.5 shows the flow chart for scour and stream stability analysis and evaluation by the Federal Highway Administration (FHWA). HEC-20 is the initial process and data collection in understanding and evaluating the river system. The four major variables to consider for scour are channel configuration, stream velocity, soil grain size, and underlying bed material. Once these are determined analysis or evaluation will progress to the HEC-18 process which consists of a seven-step process as described in the manual.

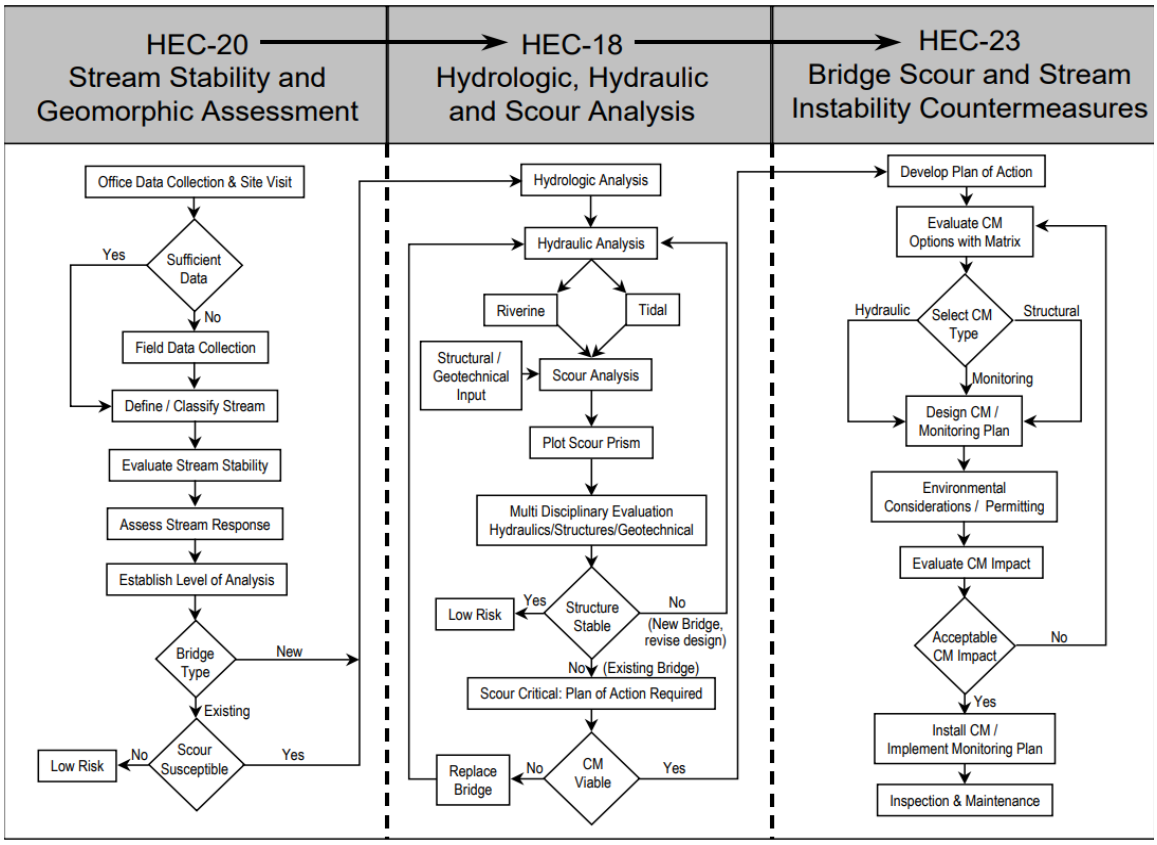

Figure 2.5: Flow chart for scour and stream stability analysis and evaluation by FHWA (courtesy of FHWA, 2012).

The equations that are used in HEC-18 were primarily developed based on laboratory small-scale flume studies on uniform non-cohesive soil. Thus, it can be said that the HEC-18 method tends to overestimate the scour depth as there is the presence of stratified soil with varying cohesion in real bridge site (Gjunsburgs et al. 2014). That is cohesive soils should be increased resistance to scour.

2.2.2. BRIDGE SCOUR ANALYSIS

Evaluation of scour on a bridge pier can be computed using the hydraulic model HEC-RAS. HEC-RAS was designed originally in 1995 by the United States Army Corps of Engineers Hydrologic Engineering Center's River Analysis System allows an analyst to perform one-

dimensional steady and unsteady flow river hydraulics calculations, sediment transport-mobile bed modeling, and water temperature analyses. This software employs Preissmann's finite difference second-order scheme with an implicit linearized system to settle the mass and momentum conservation equations. The left-right overbank and channel are expected to have a similar level of water surface in a cross-section. This software has the capacity to calculate profiles of water surface for constant discharge as well as the daily discharge with subcritical, super critical, and mixed type flow (Brunner, 2002).

2.3. SOIL CHARACTERIZATION

The site characterization performed with this study involves determining the site's D_{50} value. D_{50} is the sediment particles with diameters that are cumulatively smaller or larger than 50%. D_{50} is also defined as the median particle diameter or size (grain size). This value is a critical input within any hydraulic HEC-RAS model. To help determine the D_{50} of the soil properties at the four different bridge sites, this study utilizes the mini-JET erosion test (further discussed in Chapter 4). The results obtained were then compared to previous research conducted as well as control locations.

Research conducted by Hanson and Simon et al. (2001) on the cohesive streambeds in midwestern areas in the US, indicated that there is a wide variation of erosion resistance results at the streambed of Western Iowa, Eastern Nebraska, and Yalobusha River Basin, Mississippi. Based on the work by Hanson & Simon et al., (2001), 83 submerged jet tests in cohesive streambeds were conducted with results confirming a wide variation in the erosion resistance of the cohesive streambed, as shown in Figure 2.6. The results obtained from this study were then compared to the

research conducted by Hanson & Simon et al. (2001), by assessing the material resistance of the locations to help classify the values for the HEC-RAS models developed within this project.

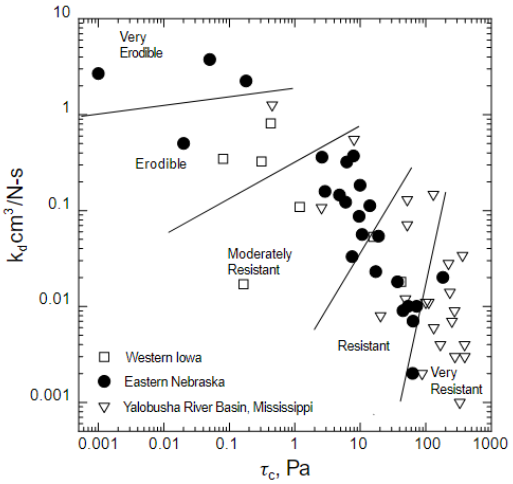

Figure 2.6: Critical shear stress vs. erodibility coefficient from cohesive streambed tests (courtesy Hanson and Simon, 2001).

The results from this research were also compared with the study done by Simon et al. (2010). Figure 2.7 shows the data scatter of the combining of all available data, which results in a steeper regression with a higher coefficient than the original relation published by Hanson and Simon et al. (2001).

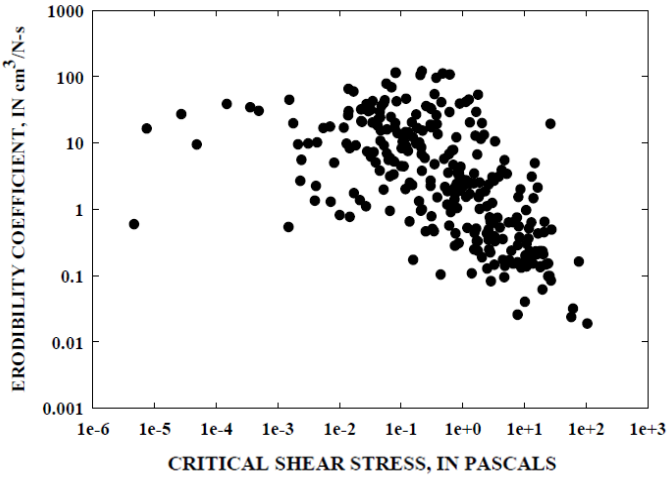

Figure 2.7: Critical shear stress vs. erodibility coefficient (courtesy Simon et al., 2010).

The mean grain size, D_{50}, vs. the critical shear stress were plotted in a previous study conducted by Briaud et al. (2017). Figure 2.8 shows that the critical shear stress is governed by the mean grain size for any diameter larger than 0.2 mm, but the case is different for the soils with a diameter smaller than 0.2 mm. This difference is due to the other factors that may come into play such as cohesion, plasticity index (PI), void ratio, percent of fines, dispersion ratio, soil temperature, water temperature, etc.

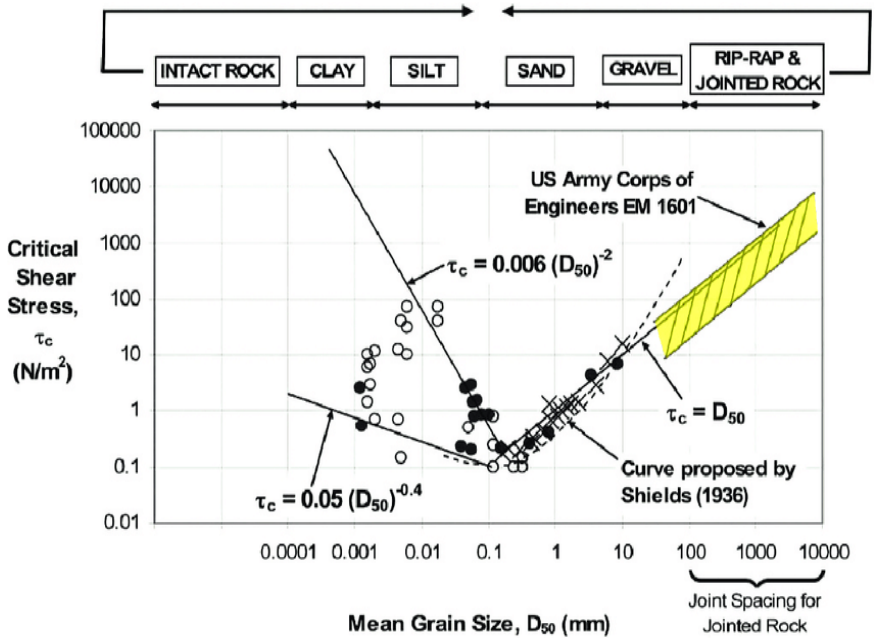

Figure 2.8: Mean grain size D_{50} vs. critical shear stress (Briaud et al., 2017).

2.4. APPLICATION TO THE PROJECT

As this project is informed by the literature review that is cited here, a few key points can be made. The project goals and achievement strategy were developed in light of this literature review. The background of bridge scour help establishes the importance of scour design. Previous work has shown improved ways exist for scour design. Previous work has shown improved ways

exist for scour design. Previous studies done by Briaud et al. (2018) and Govindasamy et al. (2014) show the over-conservative assumptions of the current hydraulic guidelines. This is the key motivation for this project. The current guideline of HEC-18 shows the over-conservative assumptions of cohesive soils. An update on soil characterization is done for this project based on previous studies. The survey method used for this project to collect field data is presented to provide a holistic geometric view of the site to closely simulated the field condition. This is done in a time-effective manner and with safety in mind (particularly when collecting bathymetry data).

CHAPTER 3 – SITE OVERVIEW AND GEOMETRIC DATA COLLECTION

This chapter discusses the site selection and data collection techniques used throughout the project. Moreover, this chapter summarizes Task 2 of the research project. Four sites were surveyed for scour changes between the period of December 9, 2020, to April 20, 2021, over a period of nearly five months with the largest flow events of the 2021 calendar year. At these four sites, the team collected survey data consisting of overland and bathymetry data. The two data collected were then combined to create a high spatial resolution point cloud data of each bridge site. These data are then inputted in HEC-RAS (discussed in Chapter 5) to create a hydraulic model to run bridge scour analysis as well as compared for temporal changes at each of the field site (discussed in Chapter 6).

3.1 SELECTED SITES

The four sites selected for the projects are located in the eastern part of Nebraska as shown in Figure 3.1. In the discussion of these sites, these are presented from north to south, starting with Hooper. Summary information of each site including the discharge of the recurrence interval of the flood year is summarized in Table 3.1. The first site is located south of Hooper as shown in Figure 3.2. The Hooper bridge site crosses Maple Creek and spans over 30.8 meters (101 feet). This bridge carries County Road 20. As shown in Figure 3.4, the pictures of the bridge show a single-span crossing (without any piers). Therefore, the pier scour is not considered on the Hooper site location. The 100-year flood local scour values have been determined by NDOT to be 11 feet (36 meters).

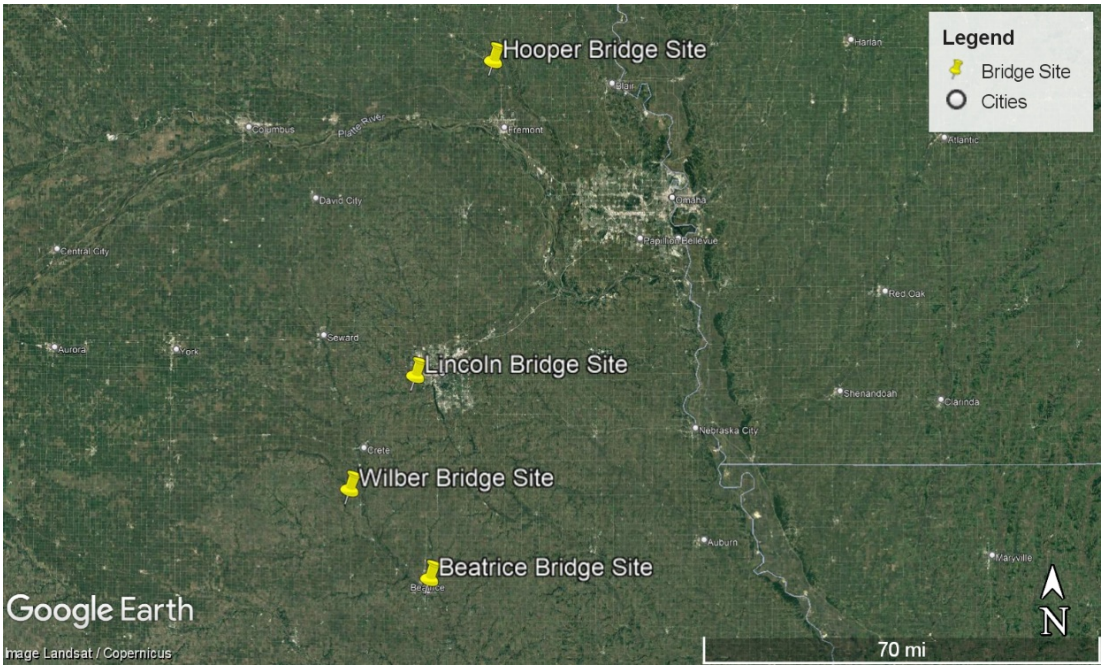

Figure 3.1: Selected bridge sites.

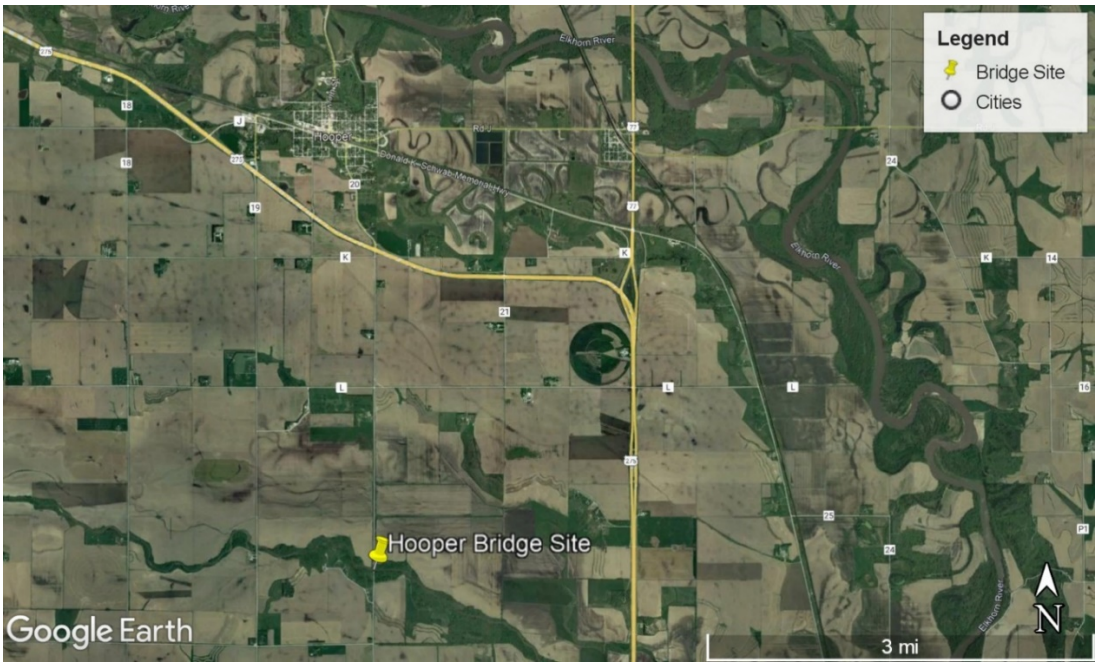

Figure 3.2: Hooper bridge site location.

(a) (b)

Figure 3.3: Field visit photos of the Hooper site.

The second site is located southeast of Lincoln as shown in Figure 3.4. The Lincoln bridge site crosses Haines Branch and spans over 31.1 meters (102 meters). This bridge carries SW 56th Street. As shown in Figure 3.5, the bridge consists of three spans and two piers. The 100-year flood local scour values have been determined by NDOT to be 12 feet (4 meters).

Figure 3.4: Lincoln bridge site location.

(a) (b)

Figure 3.5: Field visit photos of the Lincoln site.

The third site is located west of Wilber as shown in Figure 3.6. The Lincoln bridge site crosses Turkey Creek and spans over 73.8 meters (242 feet). This bridge carries Nebraska Highway 41. As shown in Figure 3.7, the bridge also consists of three spans and two piers. The 100-year flood local scour values have been determined by NDOT to be 2.4 feet (0.7 meters) for the Wilber site.

Figure 3.6: Wilber bridge site location.

(a) (b)

Figure 3.7: Field visit photos of the Wilber site.

The fourth and final site is located south of Beatrice as shown in Figure 3.8. The Beatrice bridge site crosses the Big Blue River and spans over 132.6 meters (435 feet). This bridge carries US-77 just south of the downtown region of Beatrice. As shown in Figure 3.9, the site contains four piers and five spans. The 100-year flood local scour values have been determined by NDOT to be 8.0 feet. Upstream of the river, there is a railroad bridge as shown in Figure 3.10.

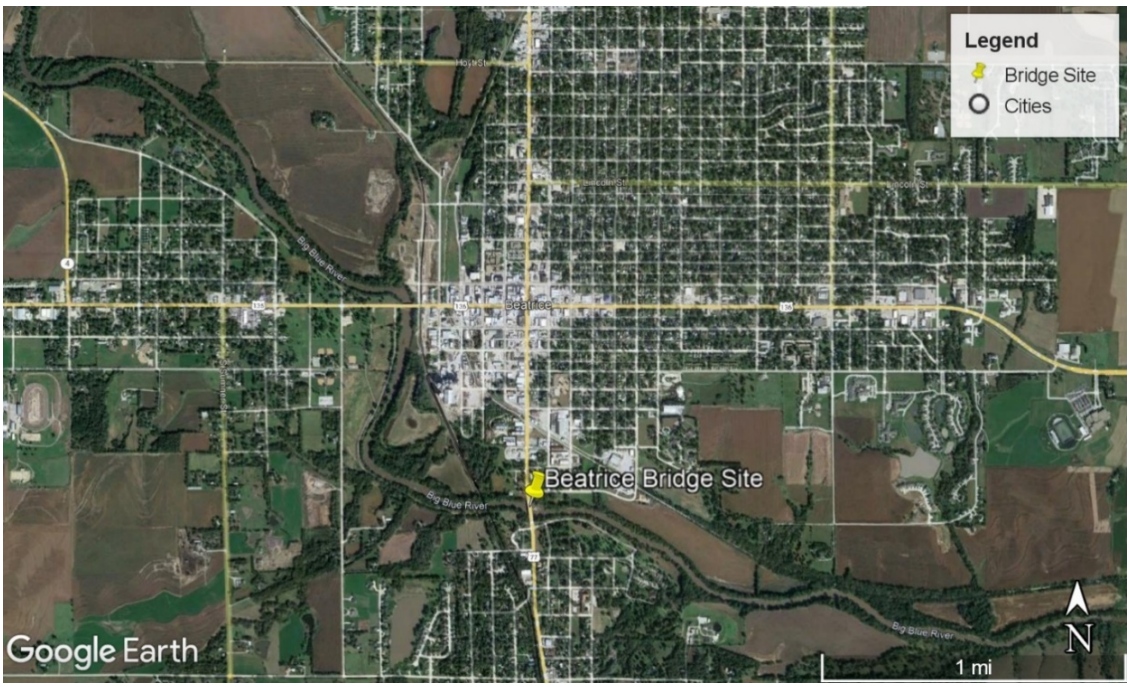

Figure 3.8: Beatrice bridge site location.

(a) (b)

Figure 3.9: Field visit photos of the Beatrice site.

Figure 3.10: Railroad bridge upstream of the Beatrice bridge.

Table 3.1: Final site selection summary.

Site	Hooper	Lincoln	Wilber	Beatrice
Structure Number	C002713910	C005521315	S041 05764	S077 02160
Year Built	1967	1991	1993	1976
Length (m)	30.8	31.1	73.8	132.6
Length (ft)	101	102	242	435
Number of Spans	1	3	3	5
Number of Piers	0	2	2	4
Crossing	Maple Creek	Haines Branch	Turkey Creek	Big Blue River
Stream Gage Owner	USGS	USGS	NE-DNR	NE-DNR
Gage Name	6800000	6803093	6881200	6881500
Q2 (cfs) [1]	3,241	1,200	2,181	9,030
Q10 (cfs) [1]	8,558	2,946	6,246	29,066
Q25 (cfs) [1]	11,955	3,892	9,338	42,910
Q50 (cfs) [1]	15,749	4,596	12,168	54,605
Q100 (cfs) [1]	17,745	5,291	15,491	67,350
Q500 (cfs) [1]	25,515	6,864	25,501	100,94249
Q100 Local Scour (feet) [2]	11	12	2.4	8.2
General Soil Type	Alluvium (well drained, silty soils in alluvium) and Loess (well drained, silty soil)	Loess and till (well-drained. silty soil with clayey subsoils)	Loess (well drained, silty soil with clayey subsoils)	Alluvium (silty soils formed in alluvium)
Degradation-Determined Soil Type	Sandy Silt	Clayey Sand	Sandy Lean Clay, Clayey Sand	Sandy Silty Clay, Silt with Sand

[1] To convert from cfs (cubic feet per second) to m^3/s, multiple by 0.028316847.

[2] Local scour values as determined by NDOT.

3.2 WORKFLOW OF DATA COLLECTION

A summary of the data collection workflow that was performed in this project is shown in Figure 3.11. Two different types of data were collected during the surveying period – which is the overland data and the bathymetry data. The overland data were collected using two different methods. The first survey method used is the post-processing kinematic uncrewed (or unmanned) aerial survey (PPK-UAS). The PPK-UAS equipment used for the site survey is a modified DJI Mavic Pro 2 and Wingtra Fixed Wing UAS. A modified DJI Mavic Pro 2 was used in the initial site visit in January 2020 but was then changed to higher quality UAS equipment, a WingtraOne UAS for improved accuracy, detail, and efficiency. The second piece of equipment for the overland data collection is a ground-based lidar. The specific equipment used was a FARO Focus S350 Laser Scanner.

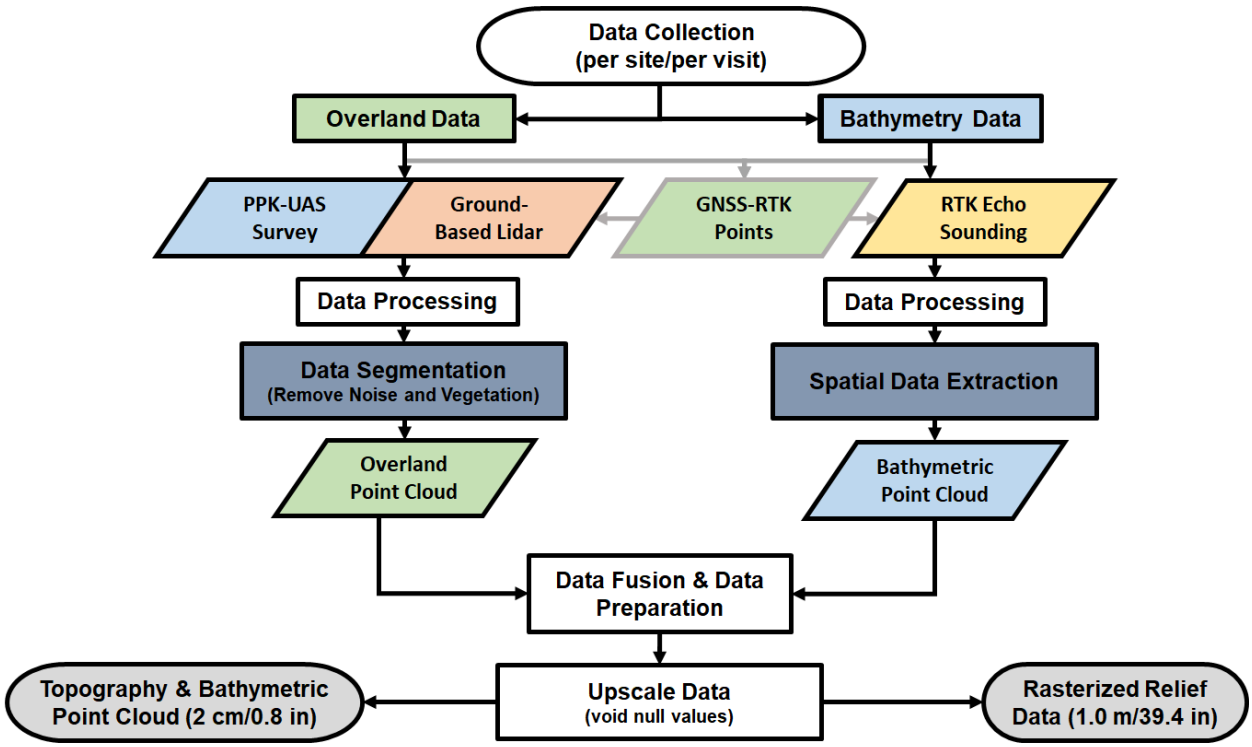

Figure 3.11: Data collection workflow.

The overland data were also collected using two different methods for efficiency in the field. The Global Navigation Satellite System (GNSS) Real-Time Kinematic (RTK) rovers were also used to collect profile points as references for bank segmentations. Specific for the bathymetry data, RTK Echo Sounding was used to collect a more detailed bathymetry data (the ground underneath the water surface). The GNSS also operated in an RTK mode with dual receiver units to achieve centimeter-level accuracy. The GNSS surveys consist of two units – one is the base station acting as the reference point, and the other is the rover collecting and receiving measurements.

Once the data has been collected, the overland and bathymetry data undergo various data processing steps. Once the data has been processed and translated into the Nebraska State Plane Coordinates (SPC, in meters), the data is then cleaned by removing any noises and vegetation. The vegetation is segmented out as this data is not of interest to this project. The process of data fusion is then conducted by combining the overland and bathymetry data. The data are then upscaled to remove any voids and null values (or holes) that will affect the analysis. Once the data has been upscaled, the data is ready for various analyses.

3.3. INTRODUCTION TO PLATFORMS USED

3.3.1. PPK-UAS Data Collection

The use of UAS equipment saves time and costs in comparison to other surveying tools. The equipment used for the PPK-UAS data collection is the Wingtra Fixed Wing UAS (shown in Figure 3.12(a)), which is a mapping drone that collects consistent, high spatial survey data. This is also a vertical take and landing (VTOL) fixed-wing platform. At the initial site survey, the DJI

Mavic Pro 2 (modified) was used for data collection (Figure 3.12(b)), as it was the only UAS available in the research group at that time. Both platforms used Post Processed kinematic (PPK) correction technology; however, the VTOL fixed-wing platform is much more efficient.

(a) (b)

Figure 3.12: PPK-UAS survey: (a) Wingtra and (b) DJI Mavic Pro 2 (DJI, 2022).

The benefit of using the PPK technology is a faster on-site survey because error corrections are calculated post-survey. The PPK system also does not require a connection throughout its survey to a GNSS base station. This is advantageous for areas with high tree cover or interference, which was prevalent at all the sites. The WingtraOne UAS does capture more ground larger area per flight and a more detailed picture with its 42 MP RGB camera, compared to the 20.8 MP DJI Mavic Pro 2. The PPK UAS has a local horizontal accuracy on the order of 1 cm (0.4 in), as specified and confirmed by the manufacturer on rigid surfaces. The UAS flew approximately over 2000 meters (6562 feet) of the Hooper site. Figure 3.13 shows the flight path taken by the UAS along the river of the Hooper site. Figure 3.14 shows the three-dimensional point cloud data overview of the Hooper site.

Figure 3.13: UAS flight path along the river for the Hooper site.

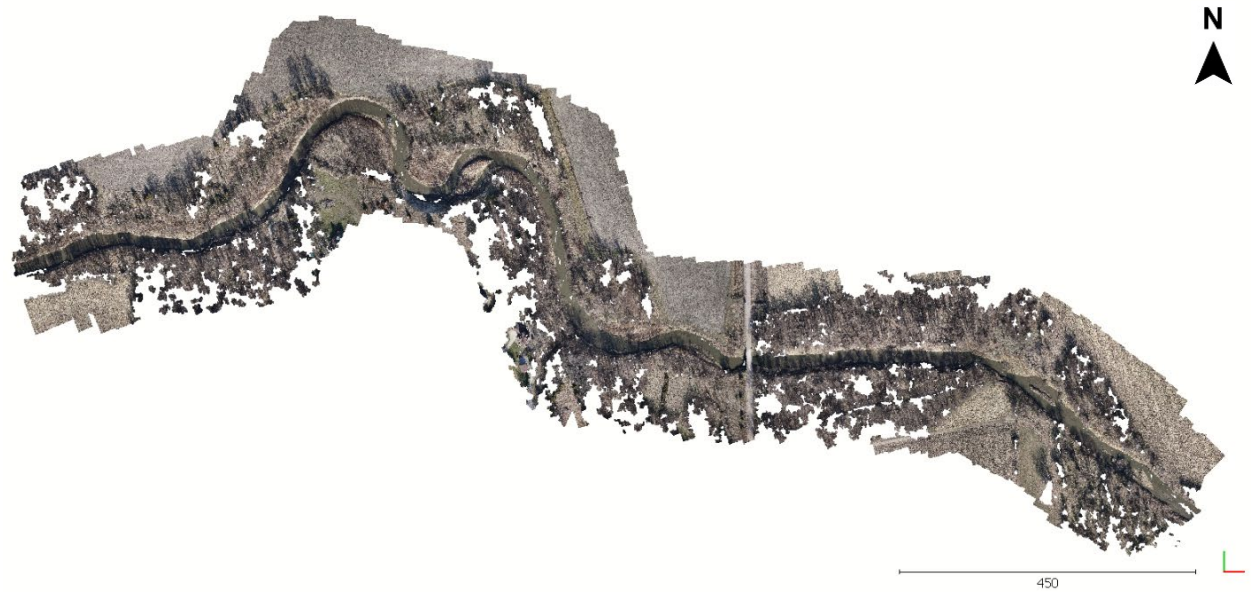

Figure 3.14: Hooper UAS point-cloud overview (approximately 2000 meters, 6562 feet).

The flight paths taken by the UAS along the river for each of the bridge sites are shown in Figure 3.13, Figure 3.15, Figure 3.17, and Figure 3.19. The three-dimensional point cloud data overviews for each of the bridge sites are shown in Figure 3.14, Figure 3.16, Figure 3.18, and

Figure 3.20. The UAS covered approximately 1800 meters (5906 feet) at the Lincoln site, 2000 meters (6562 feet) at the Wilber site, and 2100 meters (6890 feet) at the Beatrice site. The flight paths did vary at each site given the constraints at each site to always keep the UAS in line-of-sight (LOS). The UAS flights were conducted by Richard Wood, a Federal Aviation Administration (FAA) Part 107 licensed small UAS airman.

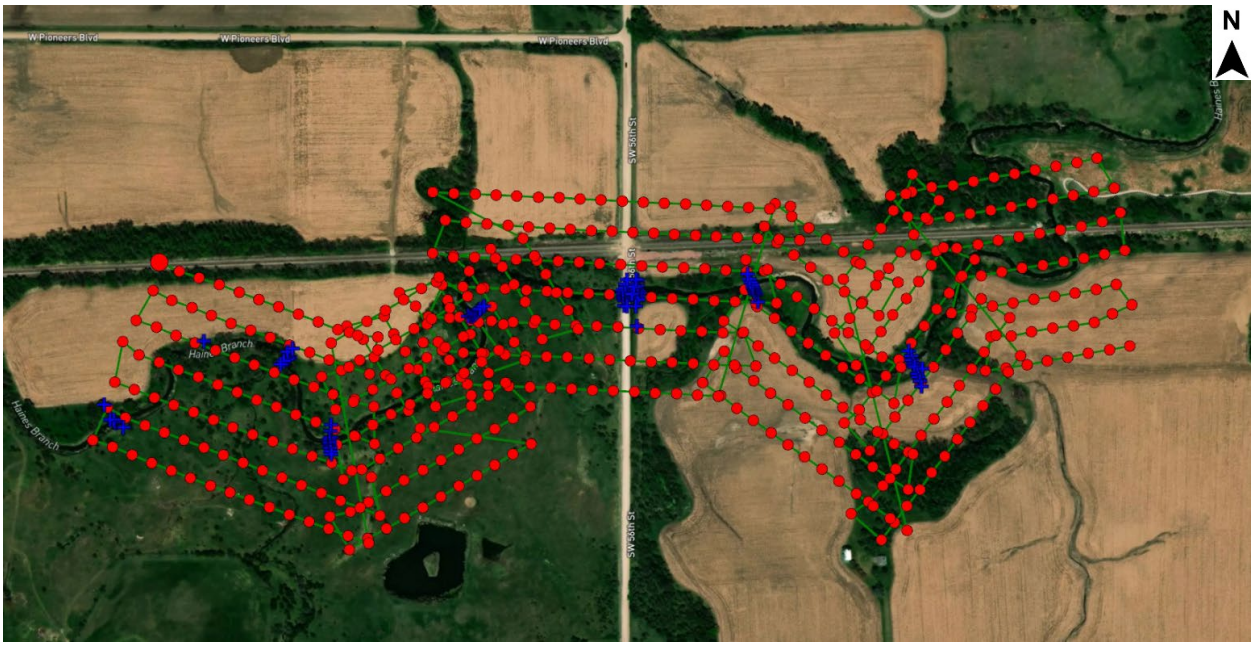

Figure 3.15: UAS flight path along the river for the Lincoln site.

Figure 3.16: Lincoln UAS point-cloud overview (approximately 1800 meters, 5906 feet).

Figure 3.17: UAS flight path along the river for the Wilber site.

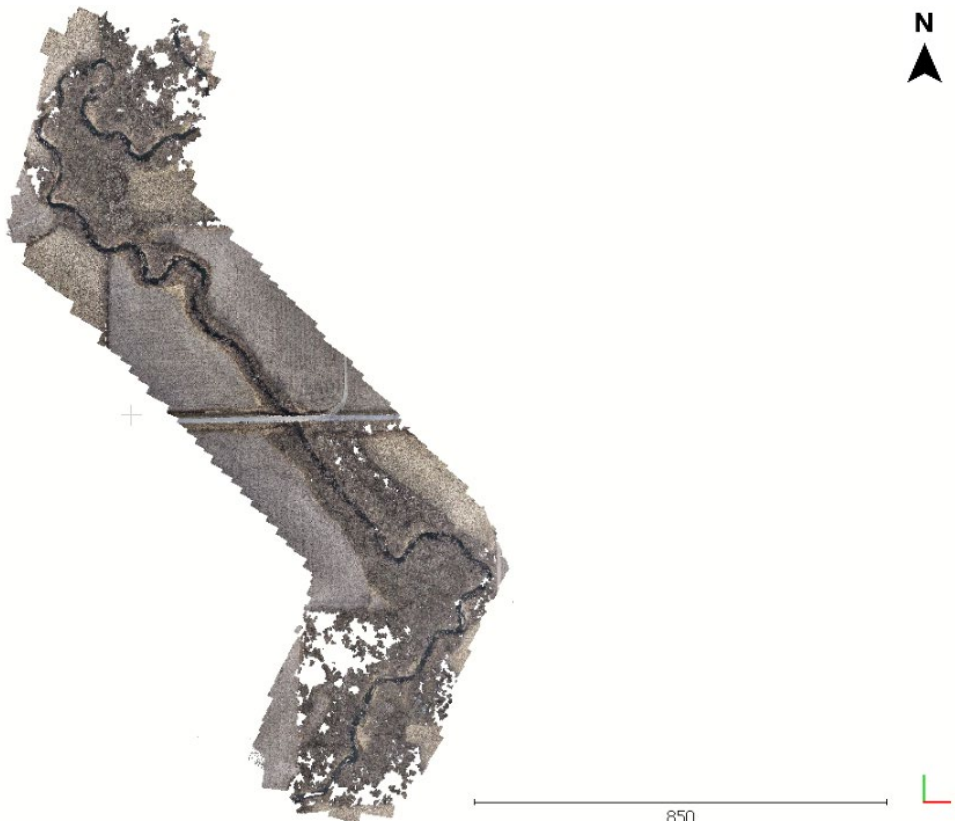

Figure 3.18: Wilber UAS point-cloud overview (approximately 2000 meters, 6562 feet).

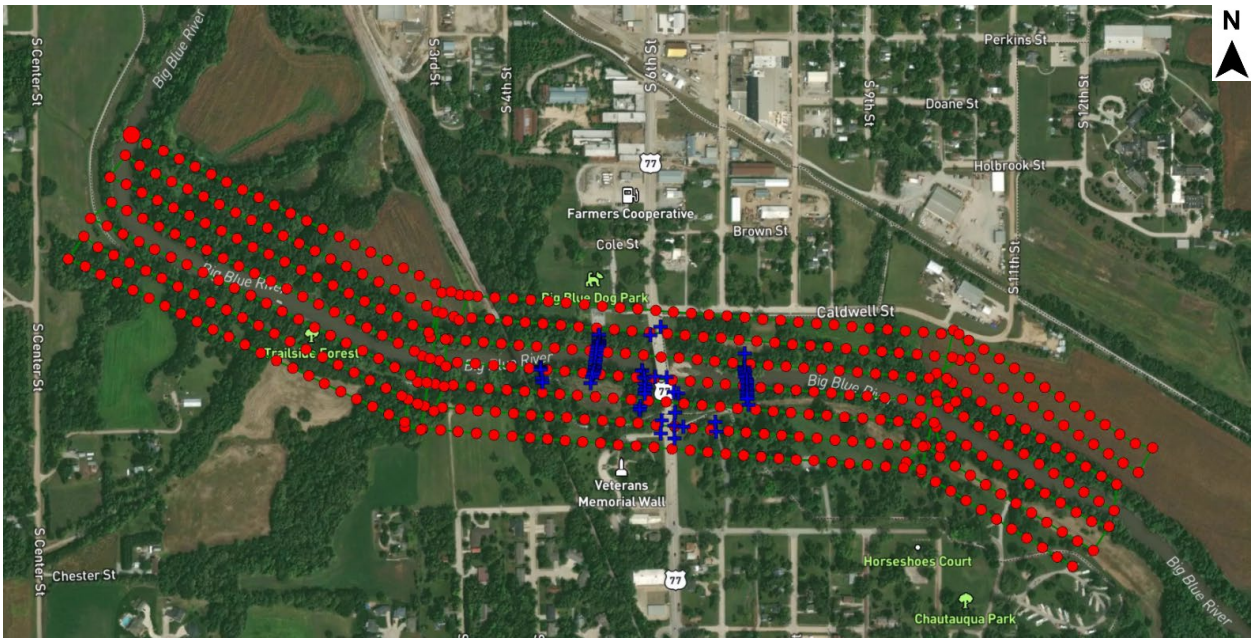

Figure 3.19: UAS flight path along the river for the Beatrice site.

Figure 3.20: Beatrice UAS point-cloud overview (approximately 2100 meters, 6890 feet).

3.3.2. Ground-Based Lidar Data Collection

The FARO Focus S350 Laser Scanner is the selected ground-based lidar equipment used for this project (Figure 3.21). The ground-based lidar data collection captures fast and accurate measurements of detailed topographic terrain. The FARO Focus S350 offers a long range of 350 meters with a 2 mm accuracy. Since a UAS is not able to collect point cloud data under the bridges, the FARO Focus S350 aids in capturing the detailed point cloud data on and under the bridge deck. The lidar scanner also offers more details of the terrain near the bridges given its close range to the ground level.

Figure 3.21: Lidar scanner used at the Hooper site.

The location of each site is represented by the blue dots. The location of the lidar scanner is dependent on the accessibility of the bridge site and where it would create a clear point cloud model of the bridge deck and under the bridge. In Hooper, there are four different locations the lidar scanner is set up (Figure 3.22). The lidar scanners are set up at each corner of the bridge.

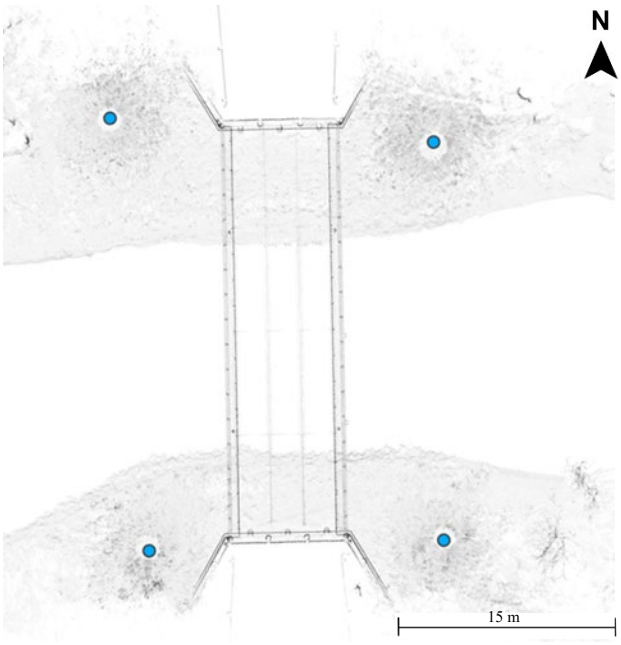

Figure 3.22: Location of the lidar scanners (shown as blue circles) at Hooper.

The lidar scanner is set up at five different locations at the Lincoln site (Figure 3.23). Each corner of the bridge in Lincoln (except for the northwest corner), as this location is heavily vegetated. The lidar scanner is instead set up at two different locations on the north side of the bridge and the south side of the bridge, with each position focusing on the west and east side. This is detailed in Figure 3.23. There are six lidar scanners set up at the Wilber site (Figure 3.24). One on the deck, four underneath the bridge, and one on the southeast corner of the bridge. Since Beatrice is the largest bridge site on this project spans over 132.6 meters (435 feet), and there are eight lidar locations selected (Figure 3.25). Two lidar scan positions are placed on the island on the south side of the bridge. The bank of the north side of the bridge is not accessible due to large trees and heavy vegetation. Consequently, the lidar scanning positions are optimized for the greatest coverage.

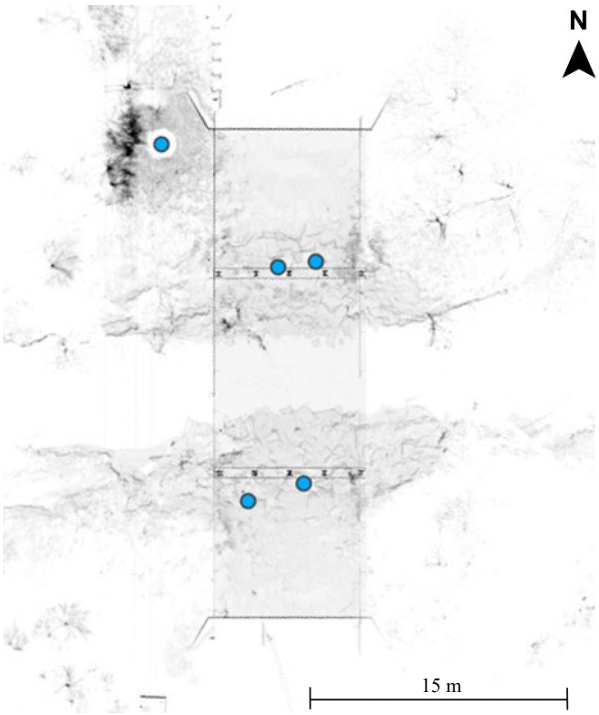

Figure 3.23: Location of the lidar scanners at Lincoln.

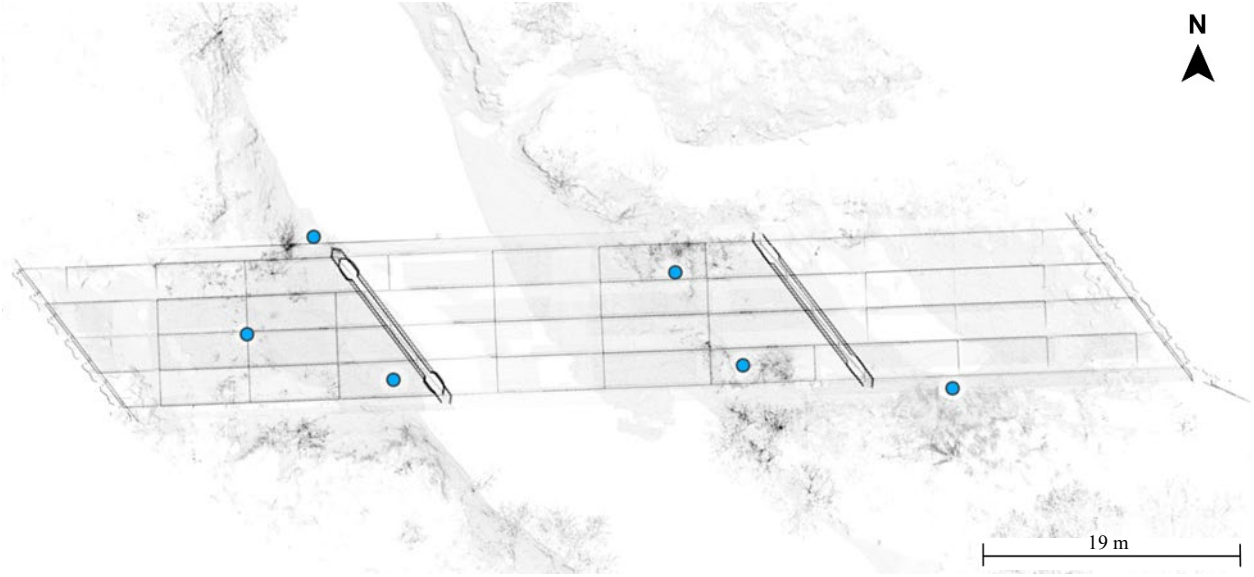

Figure 3.24: Location of the lidar scanners at Wilber.

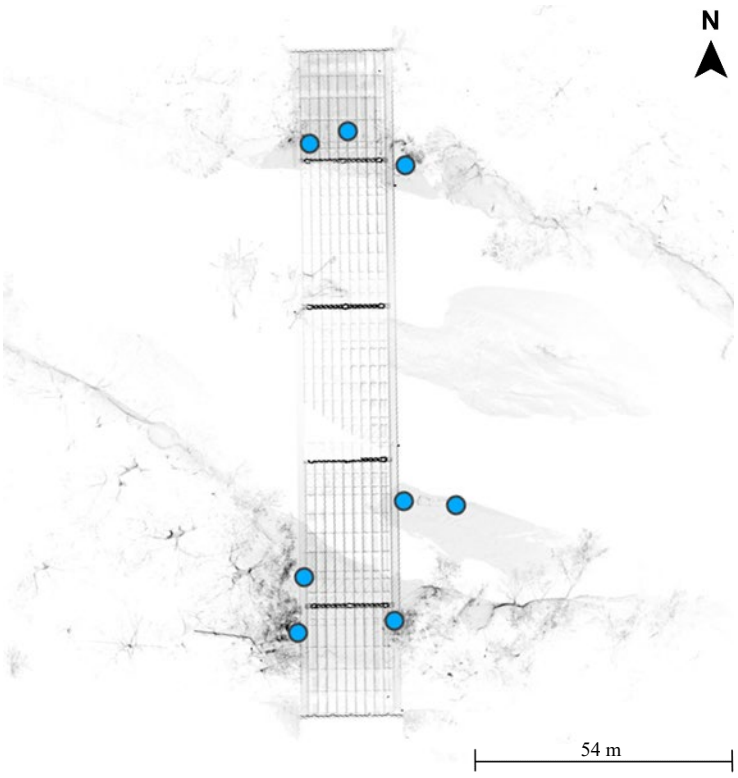

Figure 3.25: Location of the lidar scanners at Beatrice.

Each 3D point cloud data created by the lidar scanner are collected in independent coordinate systems. It is necessary to register the point clouds into a uniform coordinate system for each site. This is done using the proprietary software, Faro Scene. The registered point clouds are then segmented manually for noise (moving vehicles, vegetation, etc.) The point cloud view for each site is shown in Figure 3.26 to Figure 3.29.

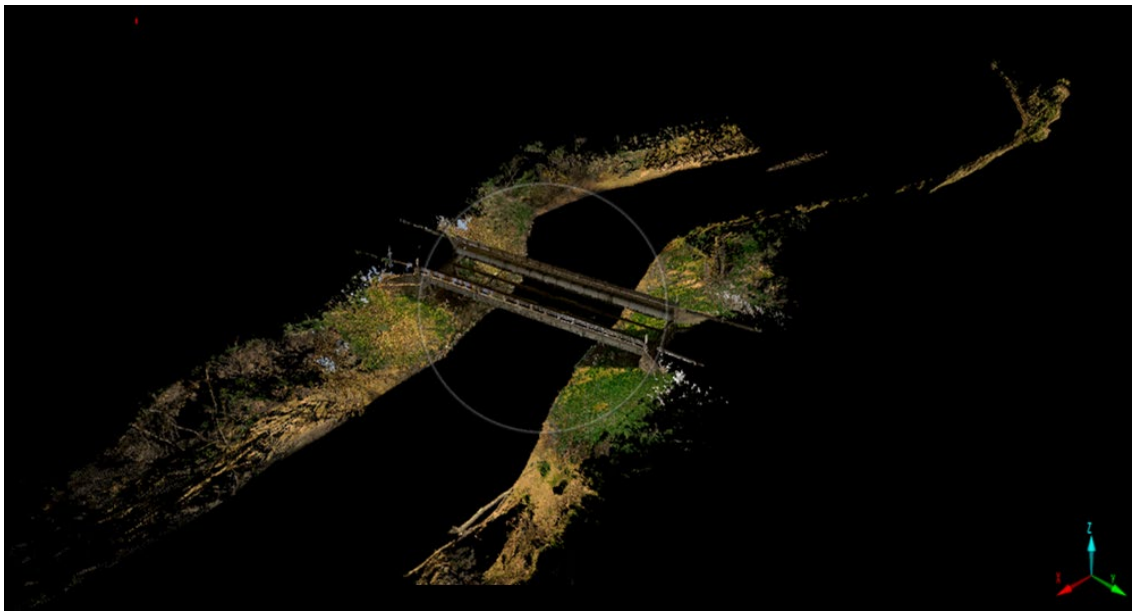

Figure 3.26: Lidar point cloud data for the Hooper site (arbitrary isometric view).

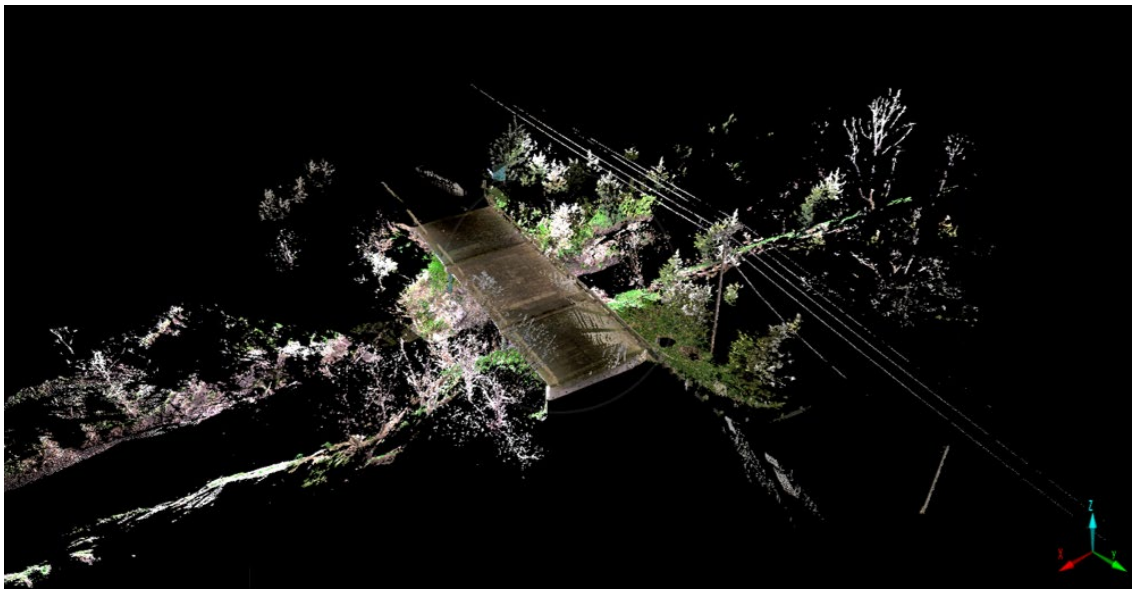

Figure 3.27: Lidar point cloud data for the Lincoln site (arbitrary isometric view).

Figure 3.28: Lidar point cloud data for the Wilber site (arbitrary isometric view).

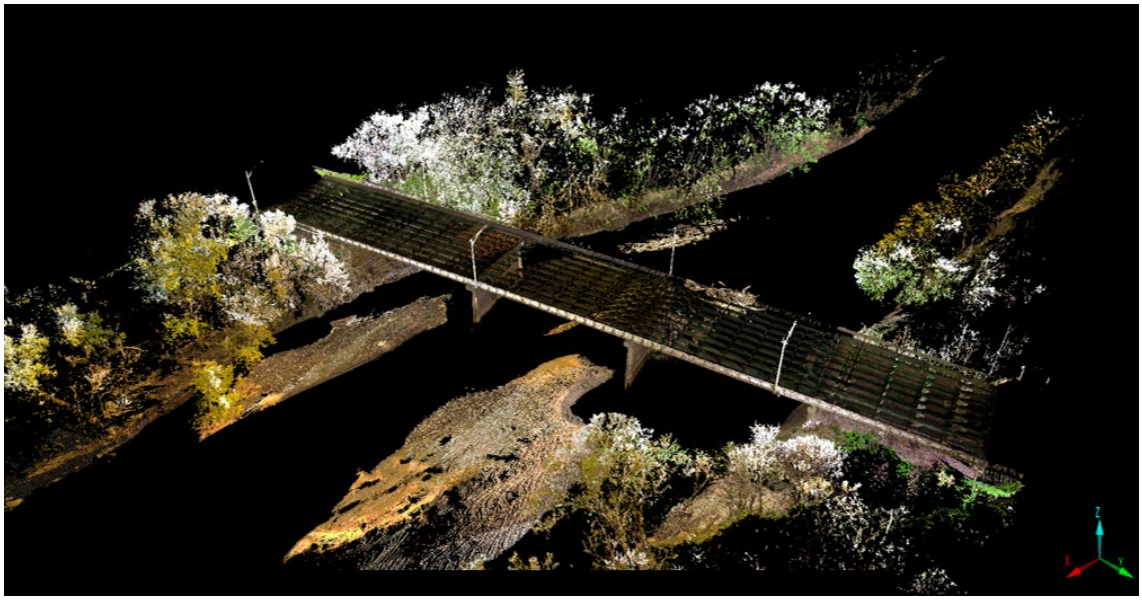

Figure 3.29: Lidar point cloud data for the Beatrice site (arbitrary isometric view).

3.3.3. GNSS-RTK Points

The GNSS-RTK equipment is used as a base receiver for the UAS and a RTK-Echo sounder as well as to collect cross-sectional profile points (Figure 3.30). Note that cross-sectional profiles were only done at sites and locations that permitted safe wading by the team members. The GNSS receivers consist of two units – one is the base station acting as the reference point, and the other is the rover collecting and receiving measurements. The collected profile points are used as a reference point to compare the accuracy of the point cloud data (for the UAS overland points) as well as provide bathymetric depths for Hooper, Lincoln, and Wilber.

Figure 3.30: On-site GNSS-RTK data collection.

The cross-section profiles for each site are shown in Figure 3.31, Figure 3.32, Figure 3.33, and Figure 3.34. At each site, there are five cross-sections upstream and three cross-sections downstream. The exception to this was the Beatrice site. At Beatrice, the river was too deep in numerous locations for the team to wade safely; however, this data was captured via sonar device (fish finder).

Figure 3.31: Overview map targets and profile location at the Hooper site.

Figure 3.32: Overview map targets and profile location at the Lincoln site.

Figure 3.33: Overview map targets and profile location at the Wilber site.

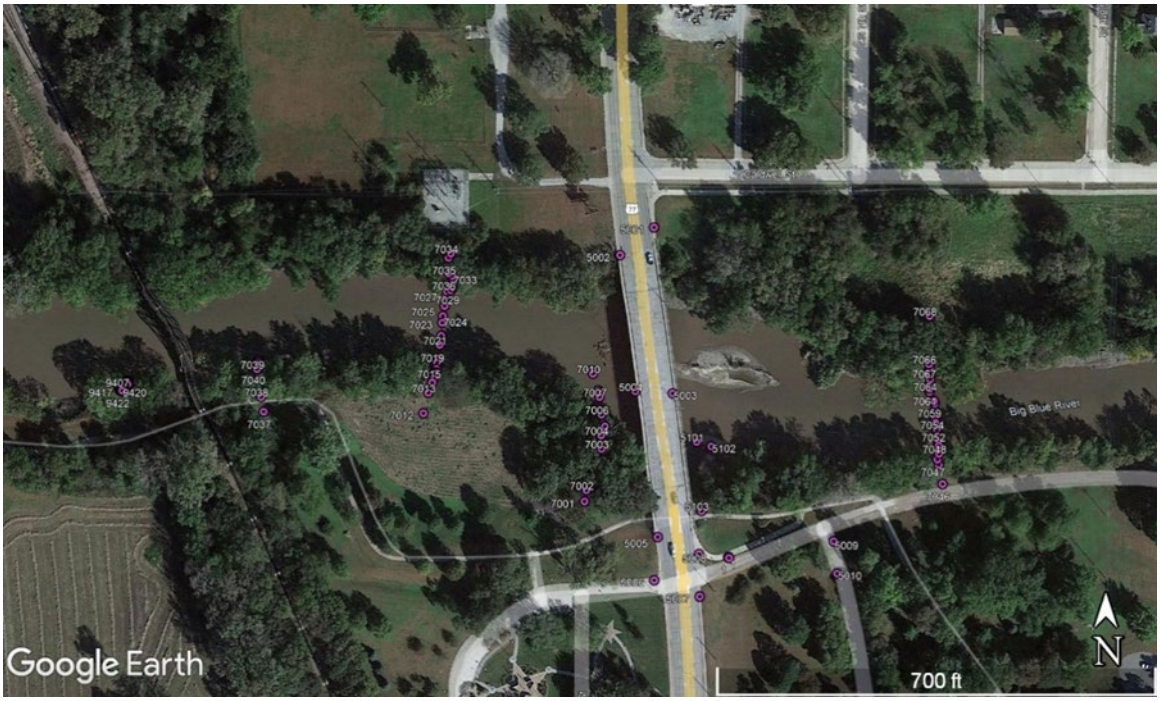

Figure 3.34: Overview map targets and profile location at the Beatrice site.

3.3.4. RTK Echo Sounding

The platform used to collect the bathymetry data is an RTK Echo Sounding system. The RTK unit is mounted on a CEE-Line single beam for the bathymetry survey on shallow waters where it is accessible by the surveyors with waders. For the deeper parts of the water, mainly at the Hooper, Wilber, and Beatrice site, an echo-sounder-based fish finder is used with an external GPS antenna. The echo sounder equipment is attached to the bottom of the vessel (Figure 3.35 (b)) to collect bathymetry data within the deeper parts of the river. Attached to the vessel is a Humminbird sonar device (with external GPS for Beatrice) to help visualize and capture the bathymetry data with ease on the vessel (Figure 3.35(a)).

The sonar survey efficiently creates a precise acoustic image of the streambed. This helped the team capture a much more detailed overview of the streambed topography which otherwise is not captured by the UAS and ground-based lidar equipment. The on-site survey in the deeper parts of the water is as shown in Figure 3.36.

(a) (b)

Figure 3.35: Echo sounder and sonar survey: (a) Humminbird Sonar and (b) Vessel-based survey equipment.

Figure 3.36: On-site vessel-based survey.

The bathymetric contours and the side-scan sonar in the result of the on-site survey are shown in Figure 3.37 and Figure 3.38, respectively for the Beatrice site. At Beatrice, the bathymetric depths were determined exclusively from the fish finder device, given the size and depth of the river. Bathymetric depths were also compared at Hooper and Wilber for equipment validation. This data is able to be translated into discrete depths using the ReefMaster software suite and incorporated into the rest of the point cloud data. The combined point cloud for all sites is then uploaded into CloudCompare for the next step of data fusion. The three-dimensional point cloud data for each site are shown in Figure 3.39 to Figure Figure 3.42. As shown in this figure, there is a decrease in the elevation of the streambed going from upstream to downstream of the river, as expected.

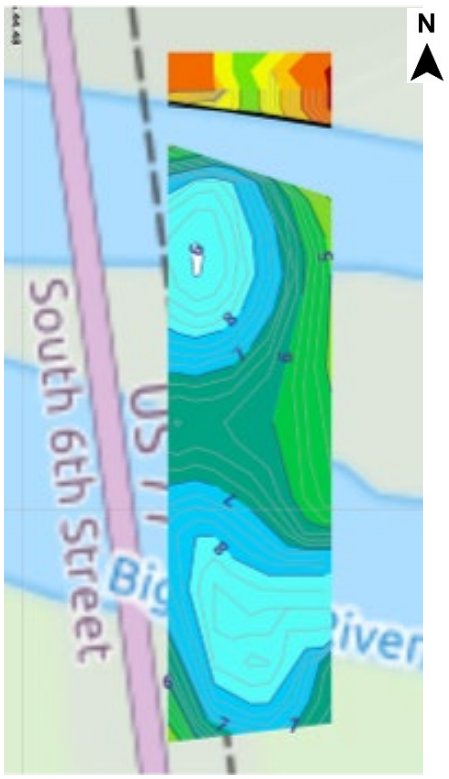

Figure 3.37: Bathymetric contours at Beatrice.

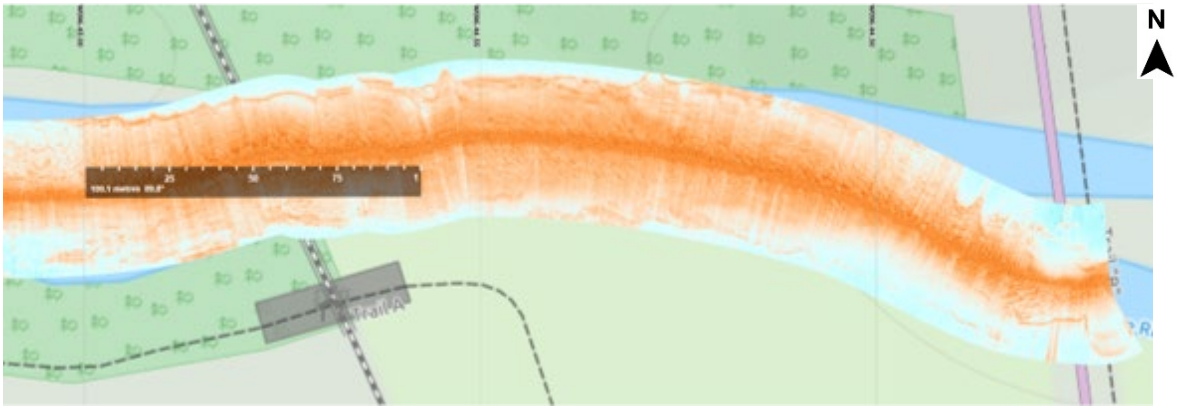

Figure 3.38: Side-scan sonar at Beatrice.

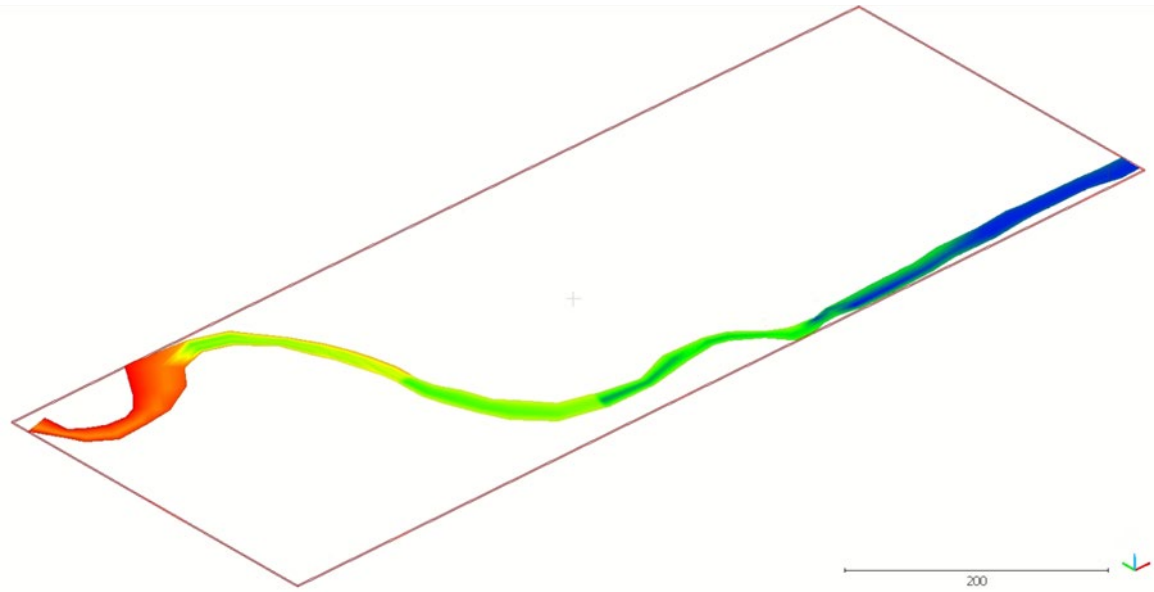

Figure 3.39: Bathymetry depth interpolation at the Hooper.

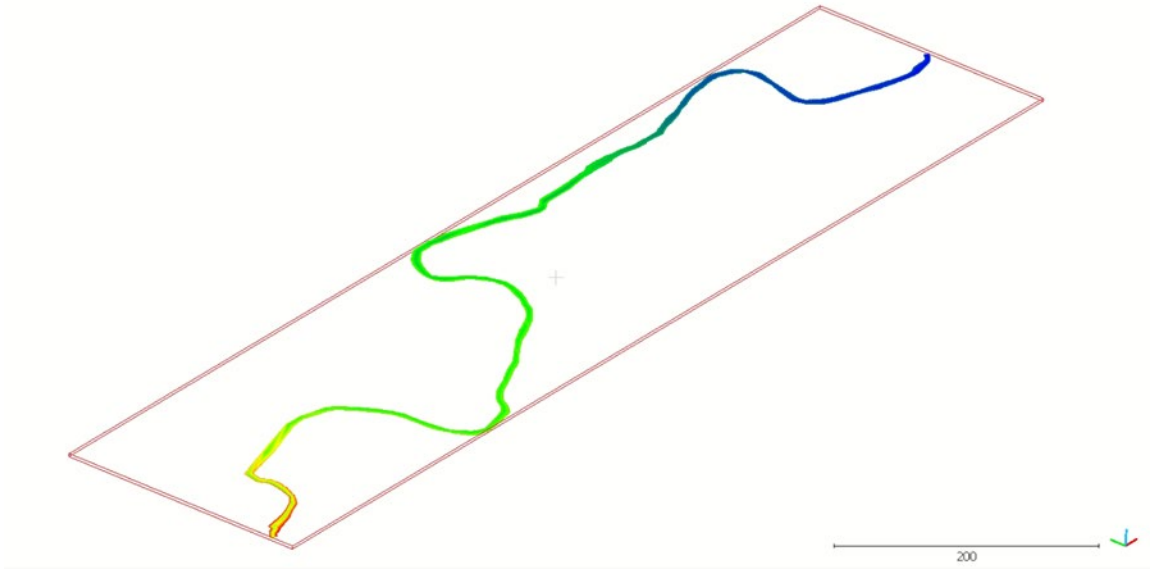

Figure 3.40: Bathymetry depth interpolation at the Lincoln.

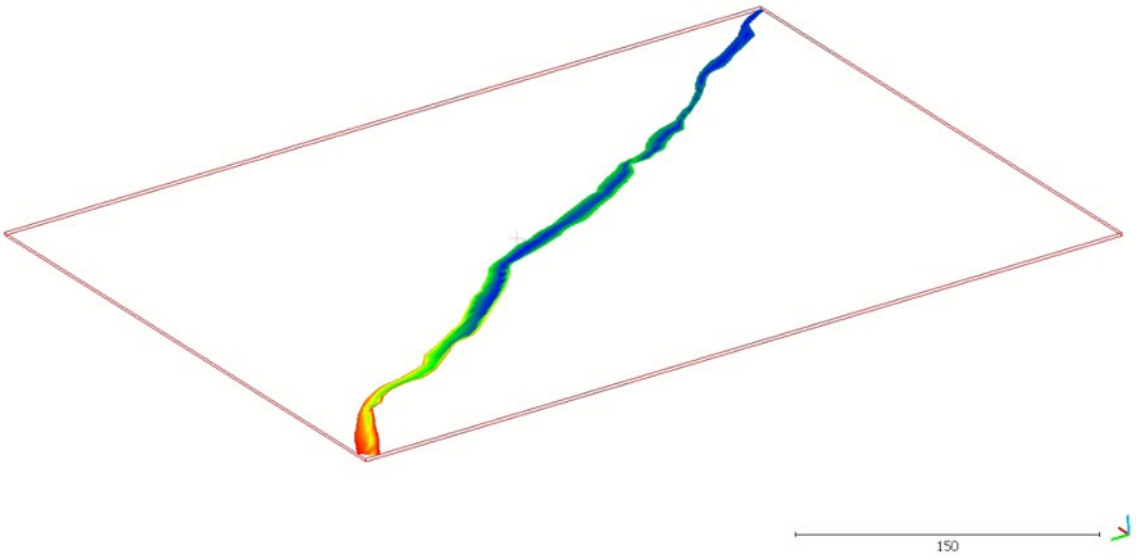

Figure 3.41: Bathymetry depth interpolation at the Wilber.

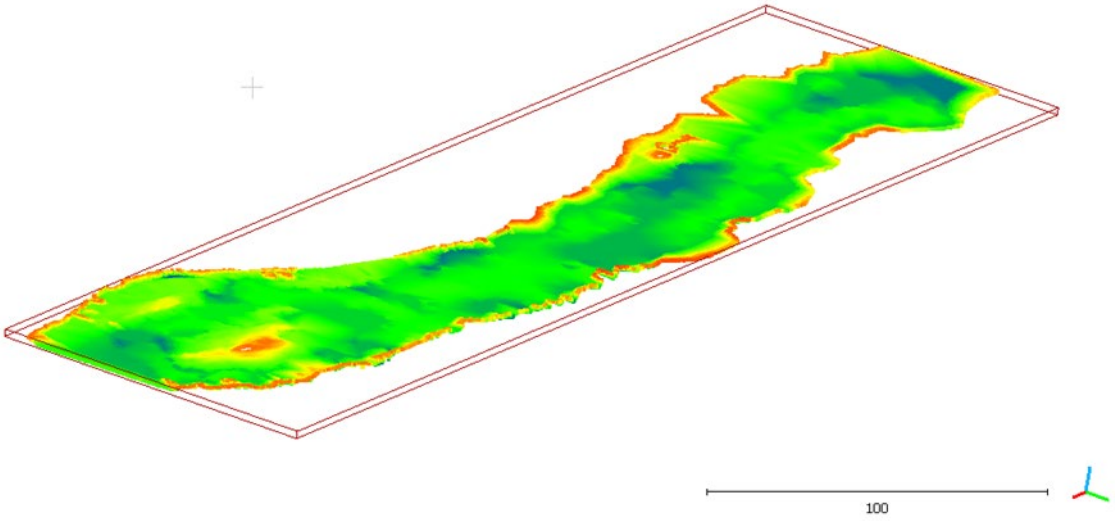

Figure 3.42: Bathymetry depth interpolation at the Beatrice.

3.4. DATA FUSION AND DATA PREPARATION

The process of data fusion is the combination of the overland and bathymetry data creating a detailed overview of the entire site. The combined data for each site is the finalized version used

to analyze the scour changes. The first step of the data fusion process is the registration of lidar to UAS point cloud data. This alignment was performed using a spectral value decomposition (SVD) technique (Liao and Wood, 2020). The alignment was done based on the static points on the sites as a point of reference, such as the bridge deck, the bridge railing and the light posts. The registration of the lidar to the UAS point cloud data have an alignment accuracy of 2 cm. The alignment of these two data provide a detailed and holistic view of the overland data.

Once the data have been registered, the next step in the process is the manual bank segmentation. Using the overland data for each site, the bank points are manually selected between the cross-sectional profiles (data collected using GNSS-RTK). This process is to create an interpolated bathymetry dataset of each site (Figure 3.43 & Figure 3.44). The interpolation of the bathymetric depths is invoked using the bank pairs and the GNSS profiles for Hooper, Lincoln, and Wilber. This interpolation was done using MATLAB.

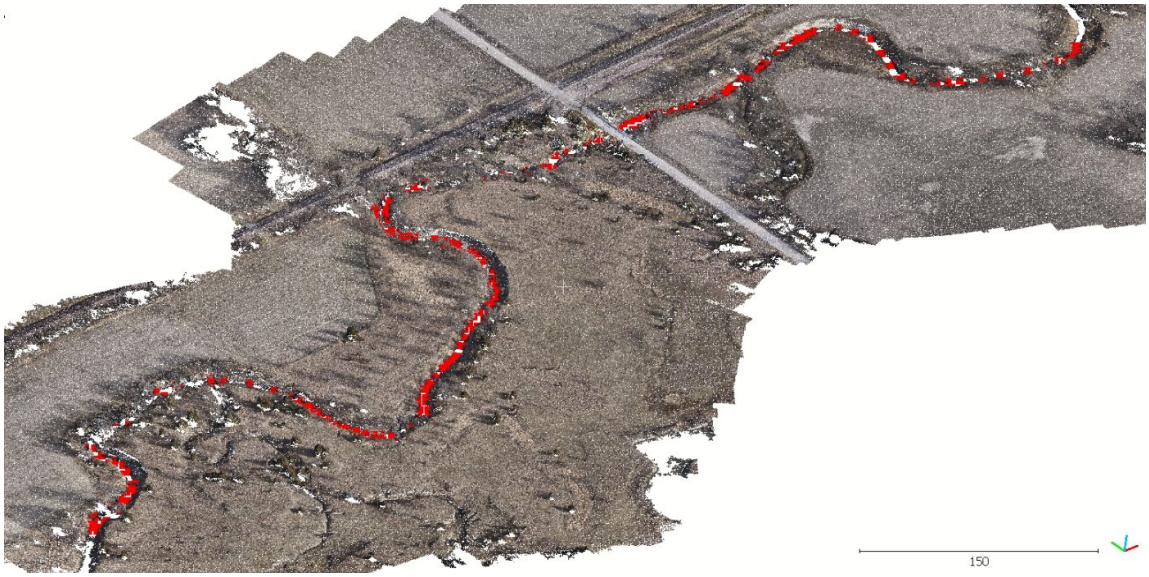

Figure 3.43: Manual bank segmentation at the Lincoln site.

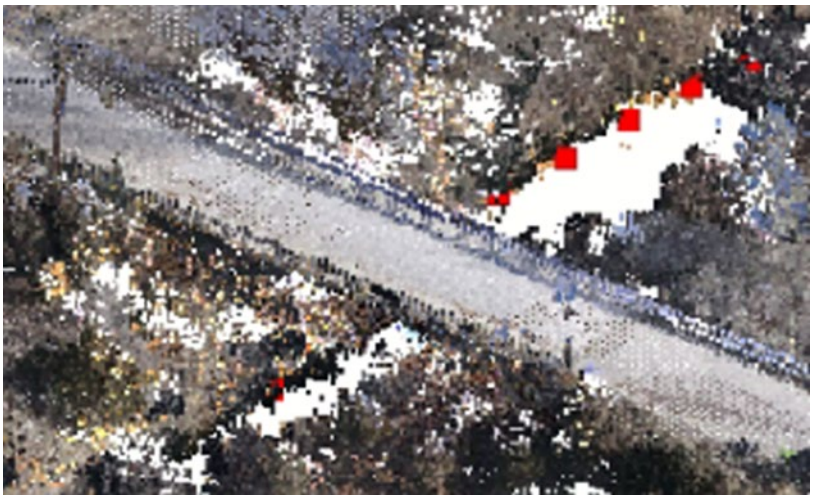

Figure 3.44: Close-up of bank segmentation at the Lincoln site.

Once the bank segmentation is complete, the cross-sectional profile points are then interpolated to create the bathymetry data. The bathymetry data is then combined with the software CloudCompare as shown in Figure 3.45.

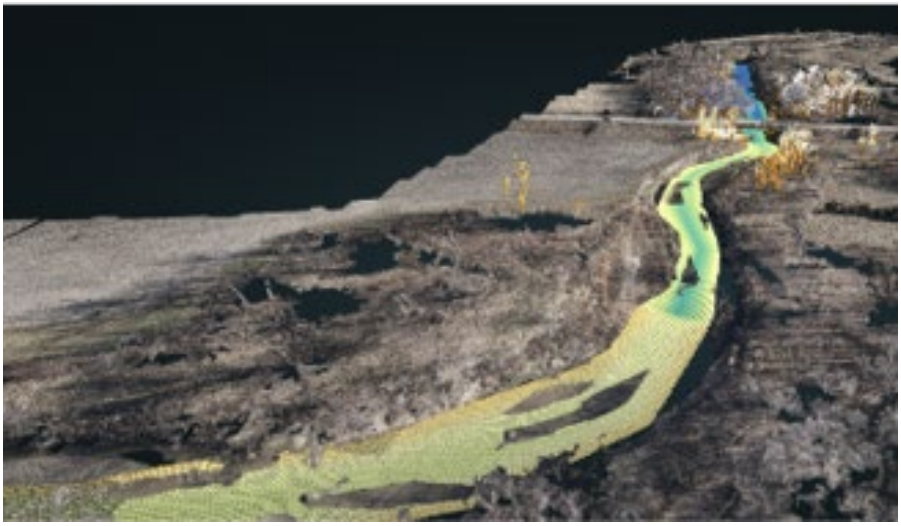

Figure 3.45: Bathymetry depth combined with lidar and UAS point cloud data (Hooper).

Once the overland and bathymetry data are combined, the topography and bathymetry point cloud with an estimated horizontal accuracy of 2 cm (0.8 cm) goes through the change detection process (discussed in Chapter 5). Due to the high vegetation and noise area around the riverbanks,

these point cloud data is removed to reduce any significant error. Due to some missing data points that were not captured, the null values are voided by upscaling the data. Figure 3.46 to Figure 3.49 shows each site point cloud data before the upscaling process.

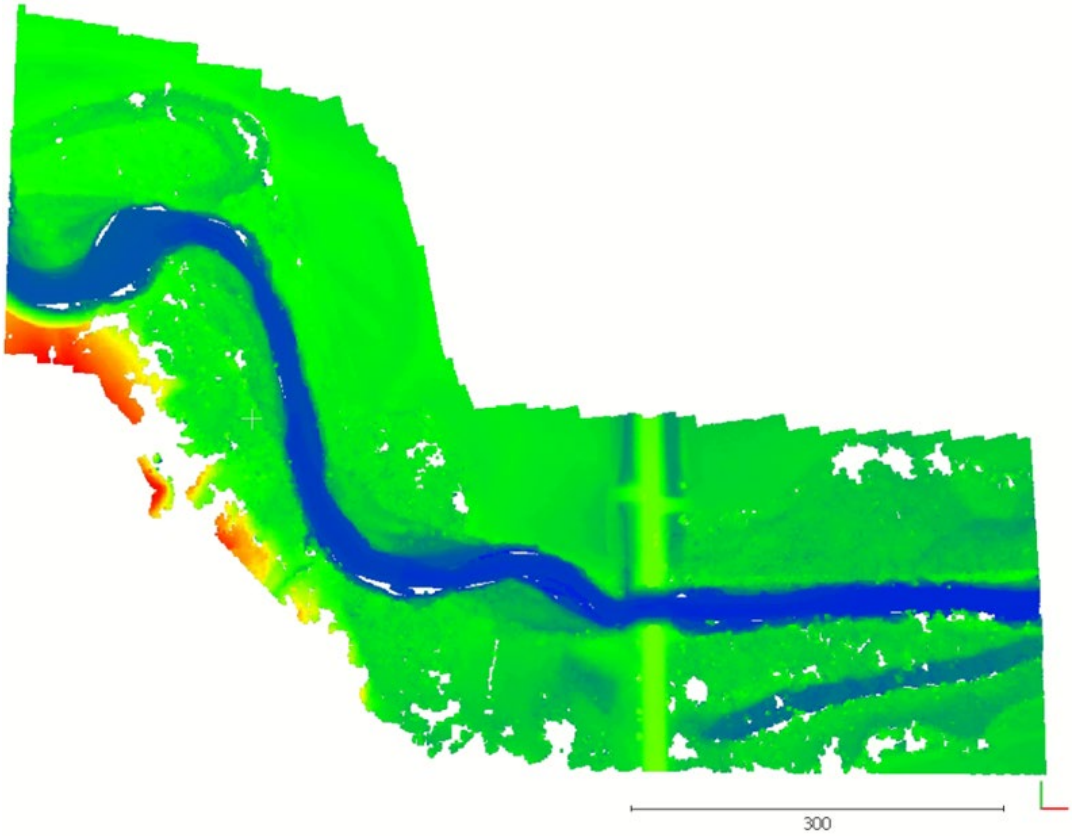

Figure 3.46: Point cloud data before upscaling at the Hooper site.

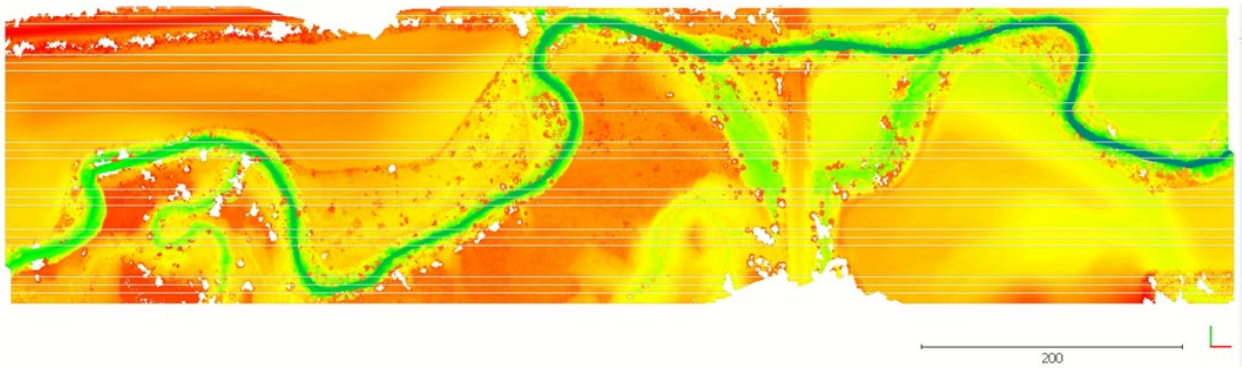

Figure 3.47: Point cloud data before upscaling at the Lincoln site.

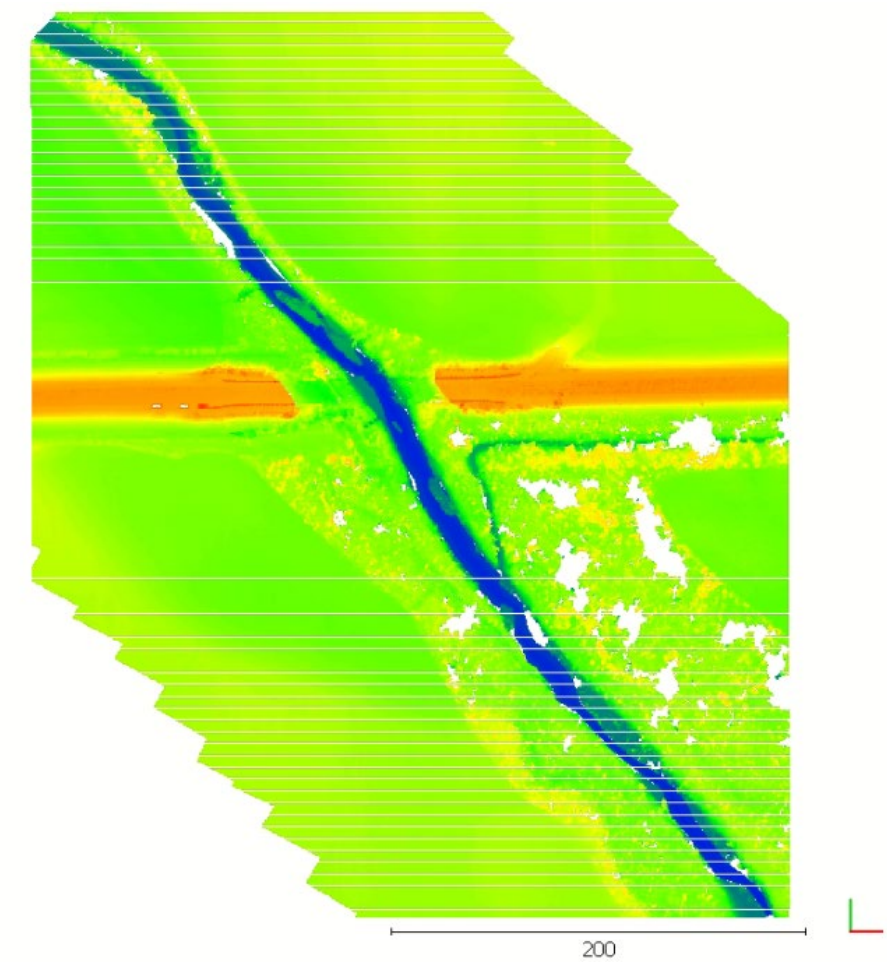

Figure 3.48: Point cloud data before upscaling at the Wilber site.

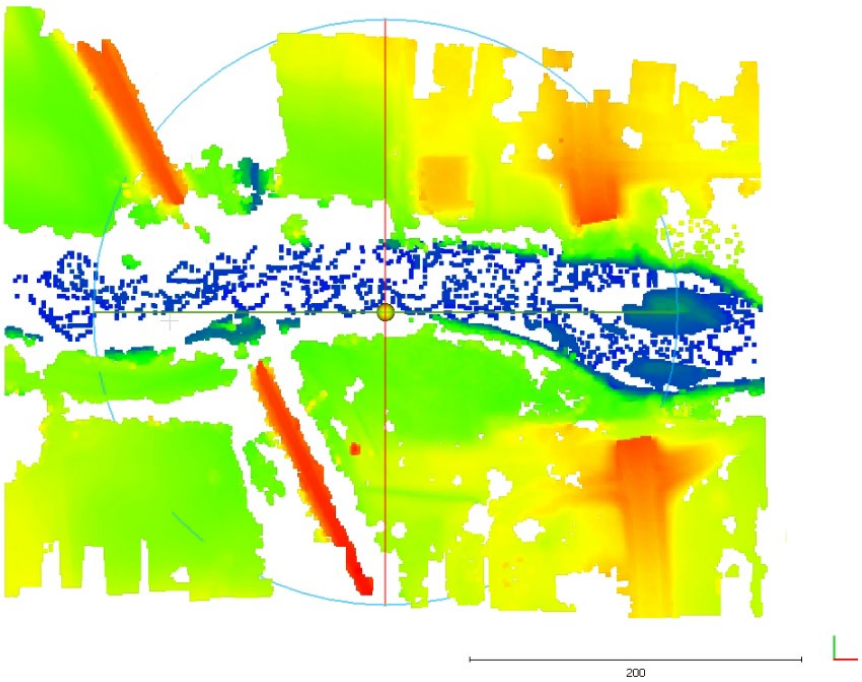

Figure 3.49: Point cloud data before upscaling at the Beatrice site.

This point cloud is also rasterized into a 1-meter grid (39 inches) before being imported into the hydraulic modeling software, HEC-RAS. This 1-meter grid rasterization was needed to prevent any sharp geometric locations from creating unusual river flows. These rasterized figures are shown in Figure 3.50 to Figure 3.53. These rasterized data are used as the terrain for the hydraulic computations done on HEC-RAS to determine bridge scour depths. The rasterized data are exported as a *.tif file format prior being loaded on HEC-RAS, which will be discussed in Chapter 5.

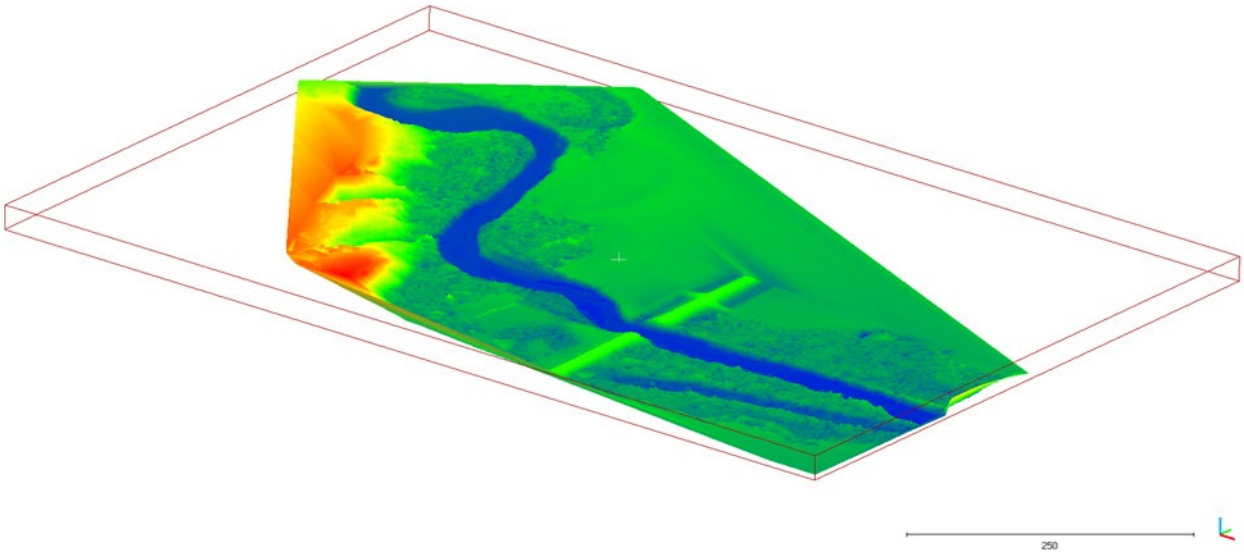

Figure 3.50: Rasterized bathymetry and topography point cloud data at Hooper site.

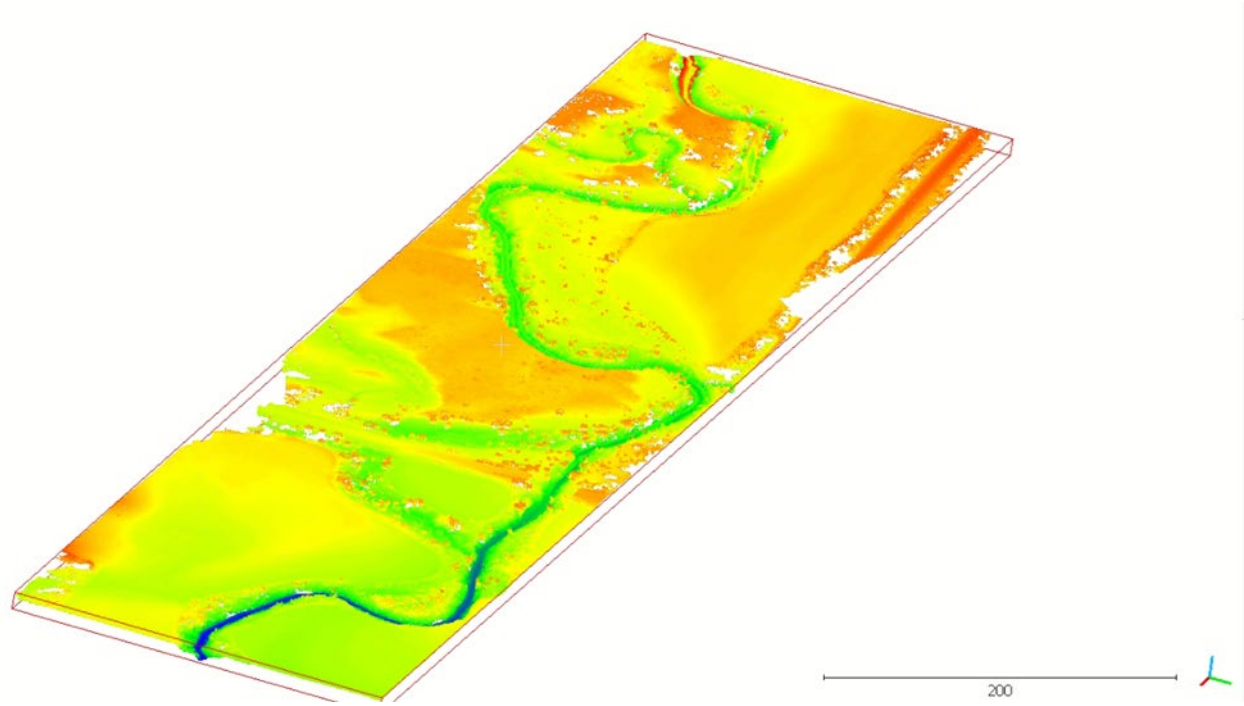

Figure 3.51: Rasterized bathymetry and topography point cloud data at Lincoln site.

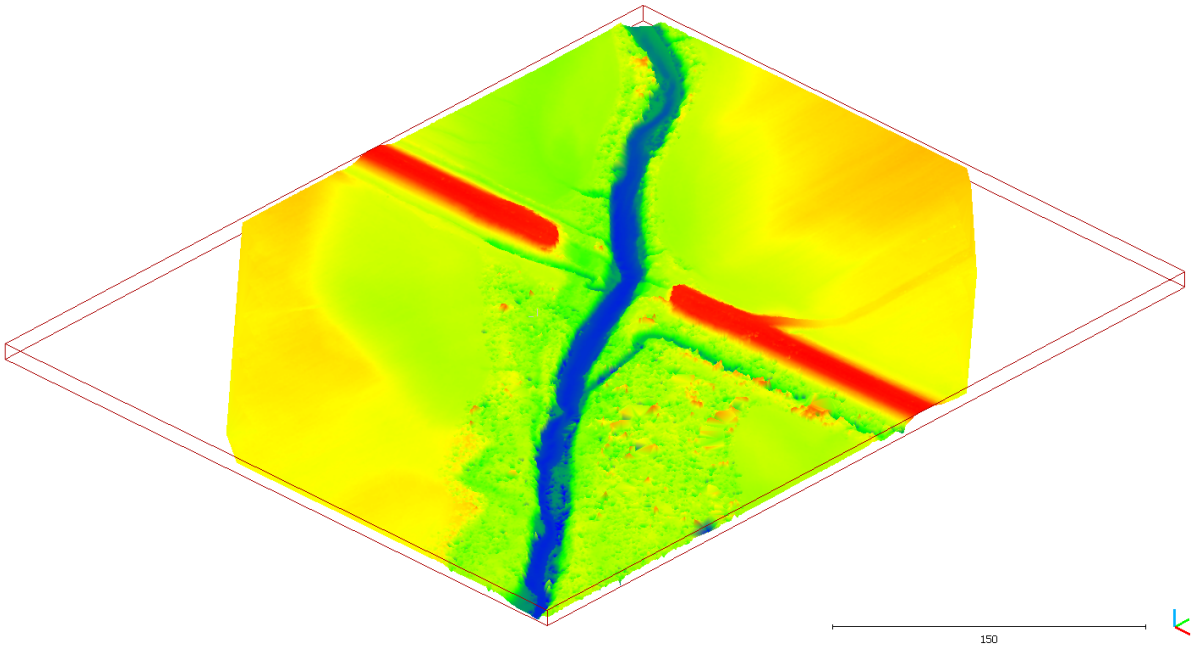

Figure 3.52: Rasterized bathymetry and topography point cloud data at Wilber site.

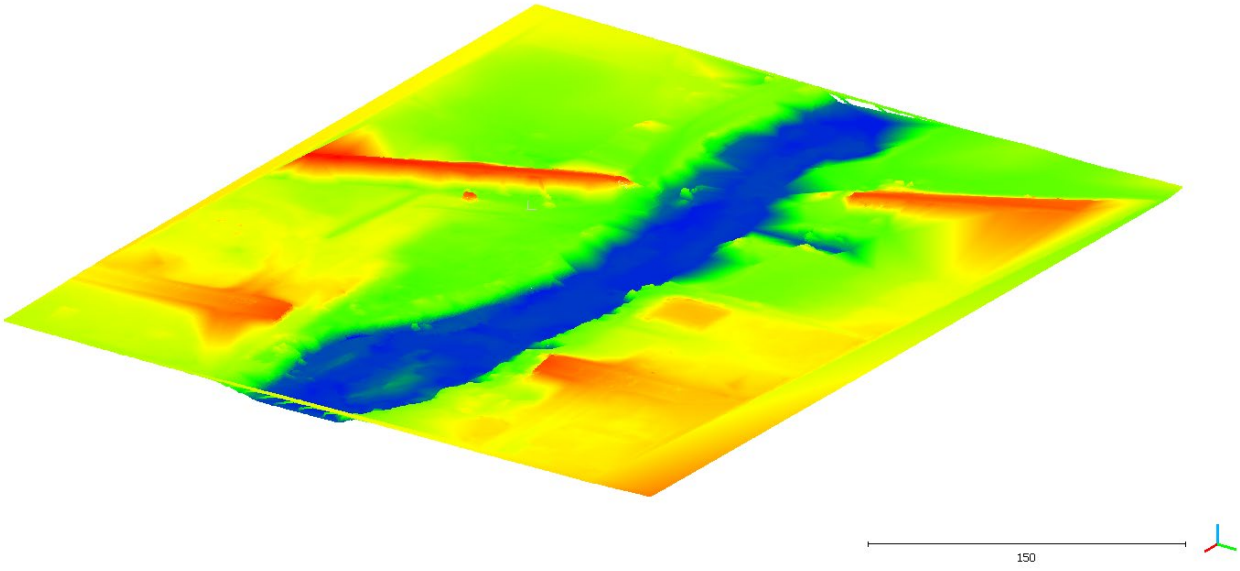

Figure 3.53: Rasterized bathymetry and topography point cloud data at Beatrice site.

CHAPTER 4 – SITE CHARACTERIZATION

This chapter discusses the site characterization to determine the soil characteristics at the four different sites in Nebraska as well as represents Task 3 in the research project. Nearly all of the soils at the selected sites are characterized as cohesive soils. Cohesive soils have many factors that affect the erodibility compared to cohesionless soils. Therefore, compared to cohesive soils, cohesionless soils can be correlated to D_{50}. Twenty-one erosion tests were conducted to classify the soil properties (Abualshar, 2022). The properties will help identify the equivalent D_{50} value needed for the hydraulic model input for each site.

4.1. SOIL SAMPLING AND TESTING

4.1.1. Soil Sample Locations

A total of twenty-one soil samples were collected. Seventeen soil samples were taken from four different sites in Nebraska (soil sampling location coordinates specified in Table 4.1). The streams where the soil samples were collected are Maple Creek (Hooper site), Haines Branch (Lincoln site), Turkey Creek (Wilber site), and the Big Blue River (Beatrice site). In addition, four samples were taken from the University of Nebraska-Lincoln at the City Campus (40.829722, -96.656349), and at the East Campus (40.821569, -96.688980) as control specimens to confirm the behavior of different soils.

Table 4.1: Soil sampling locations at each of the four sites.

Site	Latitude	Longitude	Sample #	Local Location	Comments
Hooper	41.5612	-96.5411	S1	NW	
			S2	SE	
			S3	NE	
			S4	SW	
Lincoln	40.7675	-96.7966	S1	SW	
			S2	NW	
			S3	SW	Same location of S1
Wilber	40.4802	-97.0131	S1	NW	
			S2	SW	
			S3	SE	
			S4	NE	
Beatrice	40.2562	-96.7466	S1	SE	
			S2	SW	
			S3	SW	Further distance toward the upper stream
			S4	SC	C means for centrally located
			S5	NE	

4.1.2. Testing Equipment

Numerous methods and devices are used to predict the erodibility coefficient of soils such as Flume Tests, Erosion Function Apparatus, submerged jets, and large-scale testing. This study utilizes a Mini-JET device for the erosion test shown in Figure 4.1 (Hanson and Cook, 2004) and (Al-Madhhachi et al., 2013). Figure 4.2 (b) shows the general details of the excess shear stress-based erosion testing method. The mini-JET is the miniature version of the JET device which has

the advantage of being able to be used in the field. The mini-JET is used to measure values for the critical shear stress and erodibility coefficient.

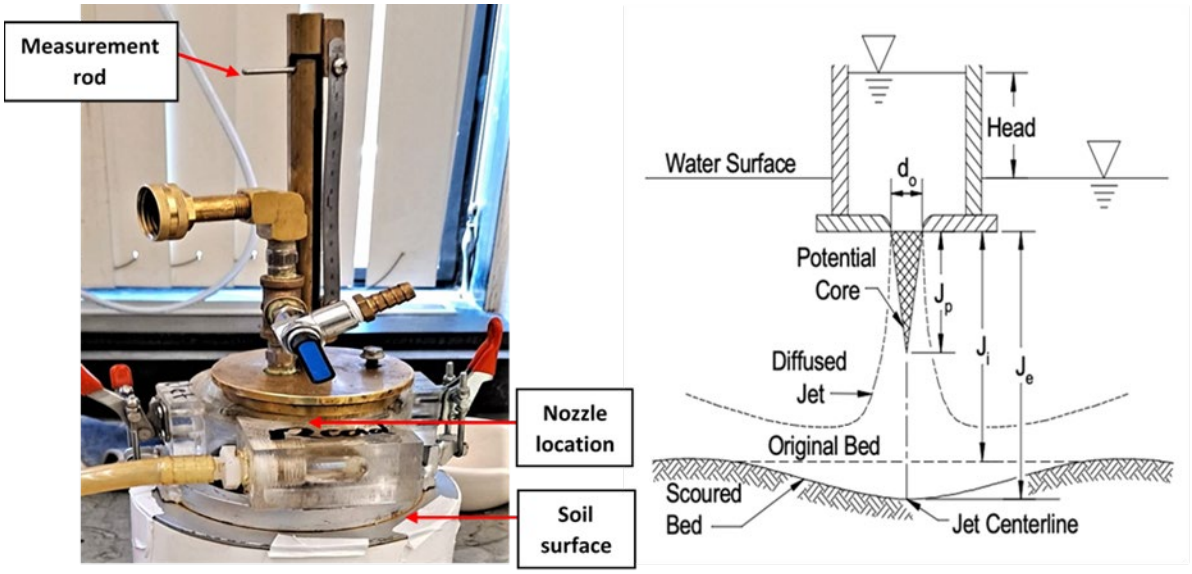

(a) (b)

Figure 4.1: JET erodibility test.

4.2. SOIL PROPERTIES

To classify the soil samples, the following tests were conducted:

- ASTM: Standard D-2216: Determination of Water Content.
- ASTM Standard D-422: Sieve Analysis.
- ASTM Standard D-422: Hydrometer Analysis.
- ASTM Standard D-4318: Liquid Limit (Test-Percussion Cup Method).
- ASTM Standard D-4318: Plastic Limit.
- ASTM Standard D-2974: Determination of Organic Content.

The soil samples were then classified based on the Unified Soil Classification System (USCS). All soil properties and classification are shown in Table 4.2. In Addition, the gradation curves are presented in Appendix B.

Table 4.2: Soil properties and classifications.

Site	Sample #	Water Content %	Organic Content %	LL	PL	PI	C_c	C_u	Passing #200	% Silt	% Clay	D_{50}	Symbol	Name
Lincoln	S1	NA [1]	NA [1]	NA[1]	NA[1]	NA[1]	NA[1]	NA[1]	46	28	18	0.087	SC	Clayey Sand
	S2	35.6	5.3	30.6	19.4	11.2	NA	NA	46	28	18	0.087	SC	Clayey Sand
	S3	40.2	5.1	35.1	20.3	14.8	NA	NA	35	25	10	0.183	SC	Clayey Sand
	S4	NA	NA	NA	NA	NA	NA	NA	46	28	18	0.087	SC	Clayey Sand
Wilber	S1	46.8	2.1	36.8	22	14.8	NA	NA	65	49	16	0.037	CL	Sandy Lean Clay
	S2	52.6	3.5	43.4	24.7	18.7	NA	NA	36	20	16	0.425	SC	Clayey Sand
	S3	13.9	NA	NP	NP	NP	0.694	4	0.6	NA	NA	0.842	SP	Poorly Graded Sand
	S4	13.5	NA	NP	NP	NP	0.756	6.07	1.75	NA	NA	1.350	SP	Poorly Graded Sand
Hooper	S1	52.5	2.8	27.3	25.5	1.5	NA	NA	64	59	5	0.057	ML	Sandy Silt
	S2	36	2.7	23.8	21.7	2.1	NA	NA	52	48	4	0.073	ML	Sandy Silt
	S3	18	NA	NP	NP	NP	0.858	2.5	0.7	NA	NA	0.570	SP	Poorly Graded Sand
	S4	33.4	2.6	26.7	22.2	4.5	NA	NA	54	48	6	0.069	ML	Sandy Silt
Beatrice	S1	20.4	NA	NA	NA	NA	0.762	2.679	0.6	NA	NA	0.610	SP	Poorly Graded Sand
	S2	42.2	5.1	34.9	26.9	8	NA	NA	76	63	13	0.041	ML	Silt with Sand
	S3	10.9	NA	NP	NP	NP	2.813	1.25	0.1	NA	NA	1.280	SP	Poorly Graded Sand
	S4	49.3	4.7	24.3	17.5	6.8	NA	NA	59	50	9	0.073	CL-ML	Sandy Silty Clay
	S5	48.9	1.2	35.3	26.6	8.7	NA	NA	52	36	16	0.037	ML	Silt with Sand
UNL City Campus	S1	21.7	NA	48.8	31.9	16.9	NA	NA	29	22	7	0.390	SM	Silty Sand
	S2	15.1	NA	47.7	33	14.7	NA	NA	19	14	5	0.688	SM	Silty Sand
UNL East Campus	S1	20.1	NA	42	24.7	17.3	NA	NA	50	32	18	0.075	CL	Sandy Lean Clay
	S2	21.1	NA	42.3	25.01	17.29	NA	NA	48	26	22	0.048	CL	Sandy Lean Clay

[1]: The properties of sample 1 are not available directly by testing. However, sample 3 was taken from the same location of sample 1.

4.3. EROSION TEST AND CALCULATIONS

Erosion occurs when the shear stress caused by the flowing water is higher than the critical shear stress. The erosion rate can be predicted using the excess shear stress equation (Hanson & Cook, 1997), which is defined as:

$$\epsilon_r = k_d(\tau_o - \tau_c)^a \qquad \text{[Equation 1]}$$

Where,

ϵ_r = Erosion rate (m/sec)

k_d = Erodibility coefficient (m^3/ N•sec)

τ_o = Average hydraulic boundary shear stress/ Maximum stress caused by jet (Pa)

τ_c = Critical shear stress (Pa)

a = Empirical exponent commonly used as unity

4.3.1. Scour Plots

The mini-JET was used to plot the scour versus time plot for all samples which can be used to predict the excess shear stress parameters. Figure 4.2 to Figure 4.5 show the plots for all four sites and the four (control) samples from the University of Nebraska-Lincoln.

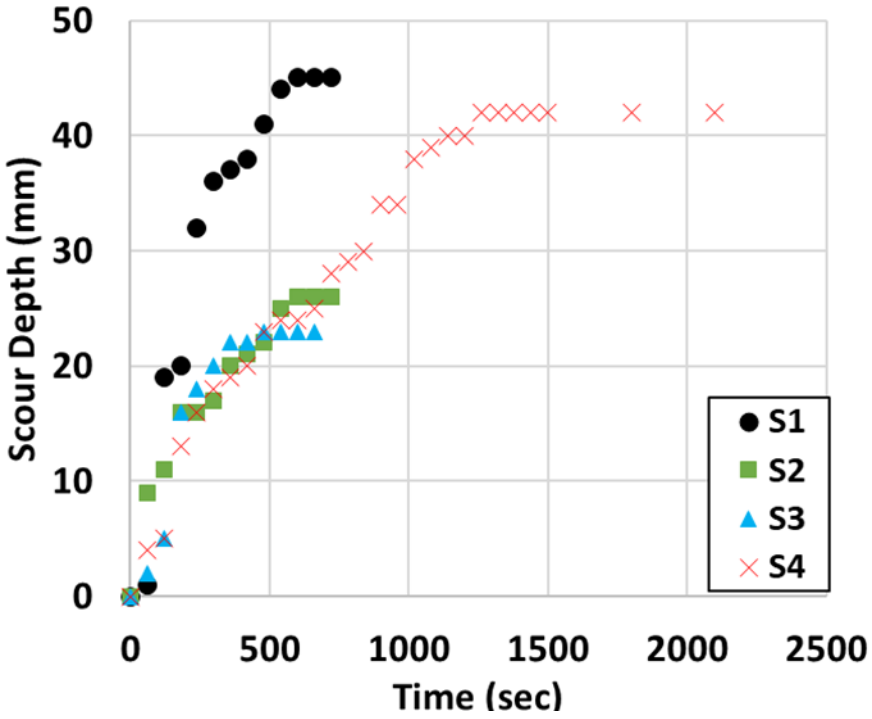

Figure 4.2: Scour vs. time for Lincoln site.

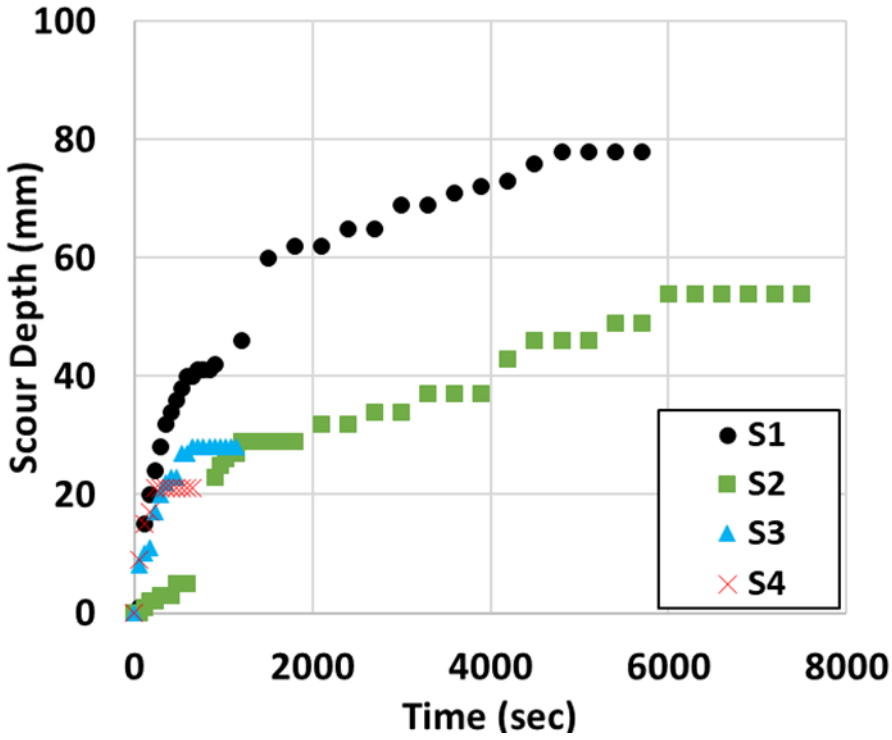

Figure 4.3: Scour vs. time for Wilber site.

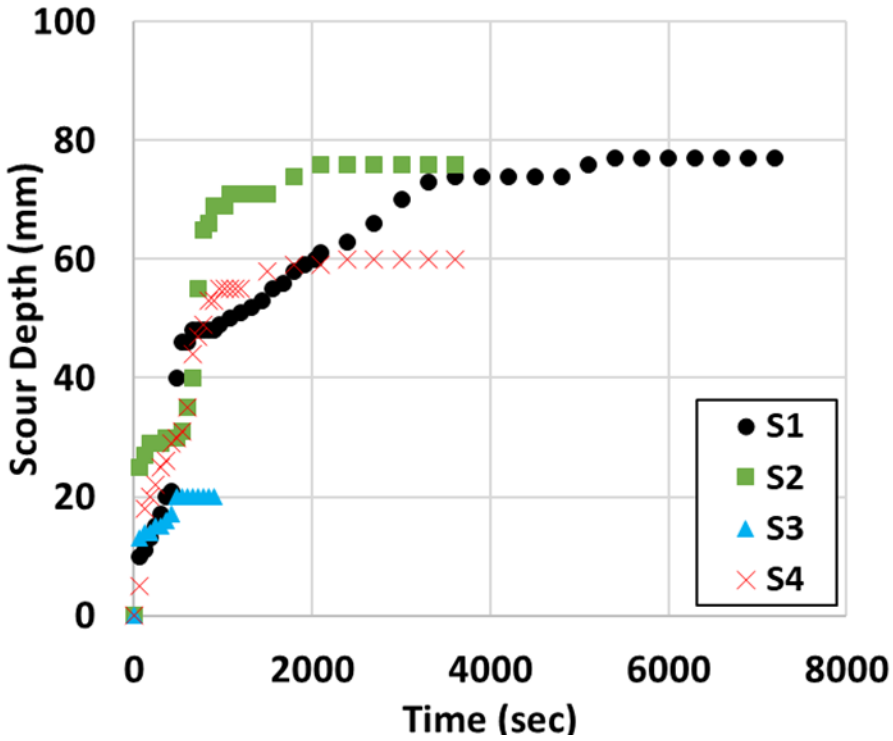

Figure 4.4: Scour vs. time for Hooper site.

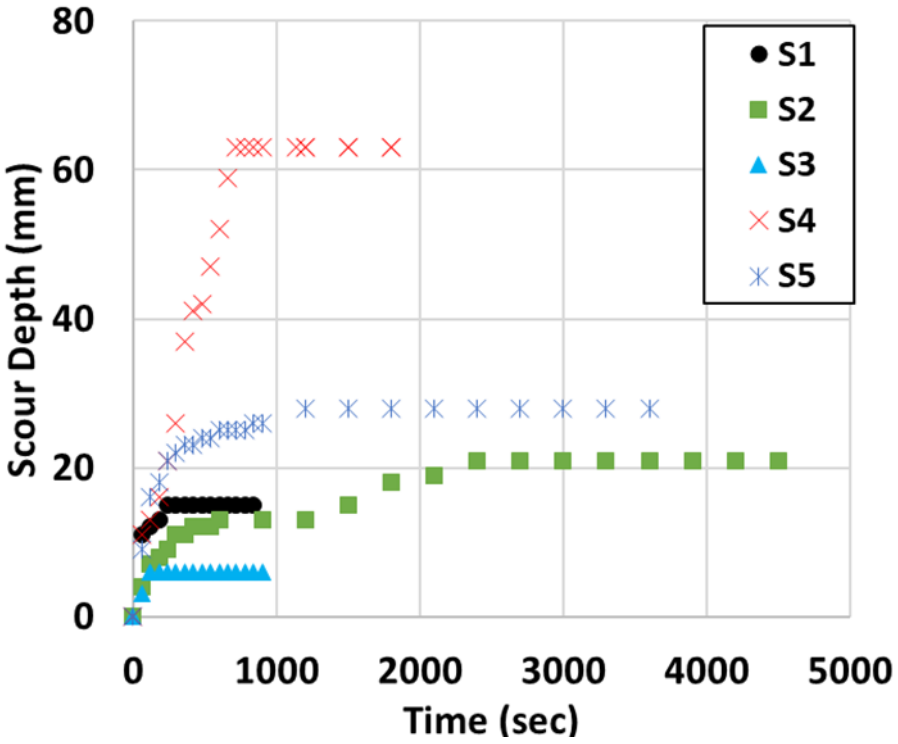

Figure 4.5: Scour vs. time for Beatrice site.

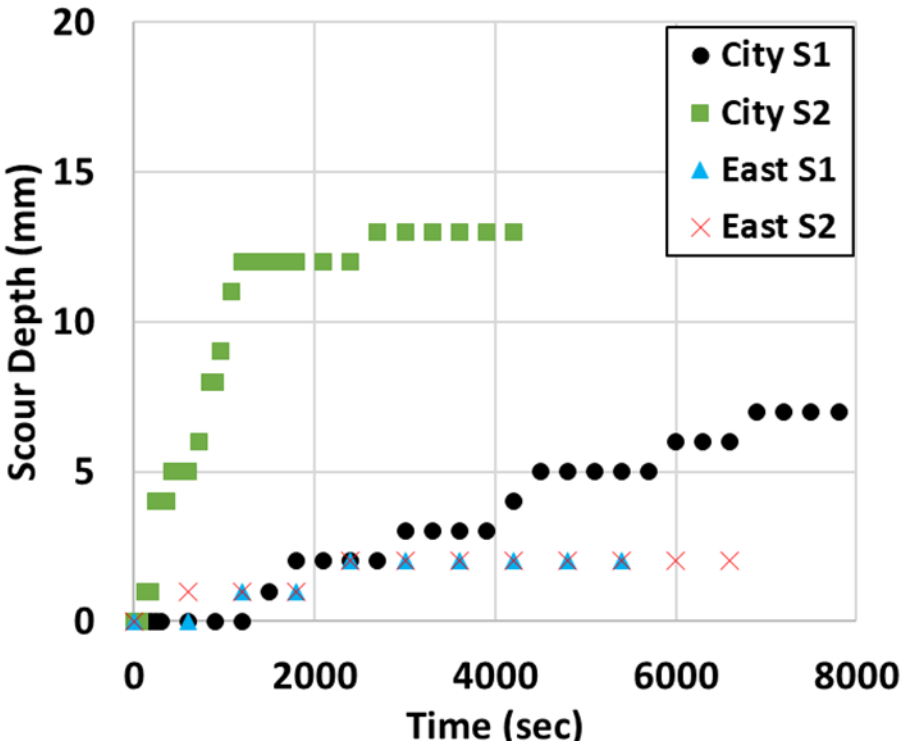

Figure 4.6: Scour vs. time for UNL campuses.

The scour curves show a wide variety in the erosion behavior of soils from different locations and at the same site location. The equilibrium erosion varies from 2 mm to around 80 mm, indicating a wide range of critical shear stress. In addition, the shape of the curves indicates the erodibility coefficient. The curves show the highest critical shear stress in the samples from the UNL campuses, which is expected as these samples do not correspond to soils obtained from the riverbed. However, lower critical shear stress is observed for some samples in Hooper and Wilber locations. Furthermore, some curves show different portions such as S2 in Wilber which indicates the behavior of layered soils.

4.3.2. Critical Shear Stress and Erodibility Coefficient

The critical shear stress represents how deep the erosion can develop, while the erodibility coefficient shows how fast the erosion can be. To find the magnitude of the critical shear stress and the erodibility coefficient, the method provided by Hanson & Cook (1997) is used for this study. The testing results are summarized in Table 4.3.

Table 4.3: Erosion testing results.

Site	Sample #	J_e (m)	τ_c (Pa)	K_d (cm^3/N•sec)
Lincoln	S1	0.1116	1.36	101.63
	S2	0.0881	2.18	63.17
	S3	0.0699	3.45	32.46
	S4	0.1097	1.41	39.44
Wilber	S1	0.1222	1.13	20.31
	S2	0.0911	2.04	5.36
	S3	0.0729	3.18	24.14
	S4	0.0651	3.99	47.23
Hooper	S1	0.1184	1.21	15.4
	S2	0.1187	1.2	44.17
	S3	0.0613	4.5	23.5
	S4	0.1002	1.69	21.17
Beatrice	S1	0.0553	5.52	32.35
	S2	0.0592	4.83	4.42
	S3	0.0461	7.95	25
	S4	0.1147	1.29	49.89
	S5	0.0658	3.91	12.01
UNL City Campus	S1	0.0421	9.55	0.42
	S2	0.049	7.02	2.66
UNL East Campus	S1	0.0383	11.54	0.96
	S2	0.0392	11	1.06

It was noticed that the erodibility coefficient is high for riverbed soils, this being at each of the four sites in this project. To make sure that the testing device is giving reliable parameters, four control samples were taken from UNL campus and tested in different conditions; without submerging them for a day. The test results show the expected results indicating that the device is giving reliable results.

To further detail this validation, the Beatrice soil sample S2 is used as a sample calculation is done to help verify the results. The raw data for the Beatrice S2 soil sample is presented in Table 4.4. The input parameters used to calculate the velocity of the water, the potential core length, and the fluid-induced shear stress are summarized in Table 4.5.

Table 4.4: Beatrice soil sample S2 raw data.

Time (sec)	Reading (m)
0	0.037
60	0.041
120	0.044
180	0.045
240	0.046
300	0.048
360	0.048
420	0.049
480	0.049
540	0.049
600	0.05
900	0.05
1200	0.05
1500	0.052
1800	0.055
2100	0.056
2400	0.058
2700	0.058
3000	0.058
3300	0.058
3600	0.058
3900	0.058
4200	0.058
4500	0.058

Table 4.5: Input parameters used in the calculation procedure.

Parameter	Magnitude	Unit	Reference
Density of water	1000	Kg/m^3	
Diameter of nozzle	0.00318	m	(Al-Madhhachi et al., 2013)
Diffusion coefficient	6.3	-	(Al-Madhhachi et al., 2013)
Head	0.914	m	(Al-Madhhachi et al., 2013)
Friction coefficient	0.00416	-	(Al-Madhhachi et al., 2013)
Discharge coefficient	0.75	-	(Al-Madhhachi et al., 2013)

The maximum velocity which is the velocity at the jet nozzle is computed as follows (Hanson and Cook, 2004) and (Al-Madhhachi et al., 2013):

$$U_o = C\sqrt{2gh} \qquad \text{[Equation 2]}$$

Where,

C = Discharge coefficient (0.7-0.75) for the Mini-JET and 1 for the original JET.

g = Gravitational acceleration 9.81 m/sec^2

h = head in cm (0.91 m)

The core length represents the distance from the jet orifice whereas the jet velocity at the jet center is still the same as the velocity at the orifice. The potential core length is defined as follows.

$$J_p = C_d^2 d_o \qquad \text{[Equation 3]}$$

Where,

C_d^2 = Diffusion coefficient squared ≈ (6.3)

d_o= Nozzle Diameter (m) = (0.00318) (Al-Madhhachi et al., 2013)

The maximum fluid-induced shear stress with the designated et velocity at the nozzle (Pa) is computed as follows:

$$\tau_o = C_f \rho U_o^2 \qquad \text{[Equation 4]}$$

Where,

C_f = Friction Coefficient (0.00416) (Hanson and Cook, 2004)

ρ= Fluid density = 1000 Kg/m^3

Therefore, the calculated maximum velocity of the jet nozzle (Equation 2), potential core length (Equation 3), maximum fluid-induced shear stress (Equation 4), and can be found as:

$$U_o = 0.75\sqrt{2 * 9.81 * 0.9} = 3.18\, m/sec$$

$$J_p = C_d d_o = 6.3 * 0.00318 = 0.020034\, m$$

$$\tau_o = 0.00414 * 1000 * 3.18^2 = 41.97\, Pa$$

The equilibrium depth prediction is done based on the hyperbolic technique (Duncan and Chang, 1970). The calculations to obtain the t/J vs t curve is presented in Table 4.6 and the t/J vs t curve is plotted in Figure 4.7.

Table 4.6: Calculations to predict equilibrium depth.

Time (sec)	**Test reading (m)**	**Scour reading (m)**	**t/*J***
0	0.037	0	-
60	0.041	0.004	15000
120	0.044	0.007	17142.8571
180	0.045	0.008	22500
240	0.046	0.009	26666.6667
300	0.048	0.011	27272.7273
360	0.048	0.011	32727.2727
420	0.049	0.012	35000
480	0.049	0.012	40000
540	0.049	0.012	45000
600	0.05	0.013	46153.8462
900	0.05	0.013	69230.7692
1200	0.05	0.013	92307.6923
1500	0.052	0.015	100000
1800	0.055	0.018	100000
2100	0.056	0.019	110526.316
2400	0.058	0.021	114285.714
2700	0.058	0.021	128571.429
3000	0.058	0.021	142857.143
3300	0.058	0.021	157142.857
3600	0.058	0.021	171428.571
3900	0.058	0.021	185714.286
4200	0.058	0.021	200000
4500	0.058	0.021	214285.714

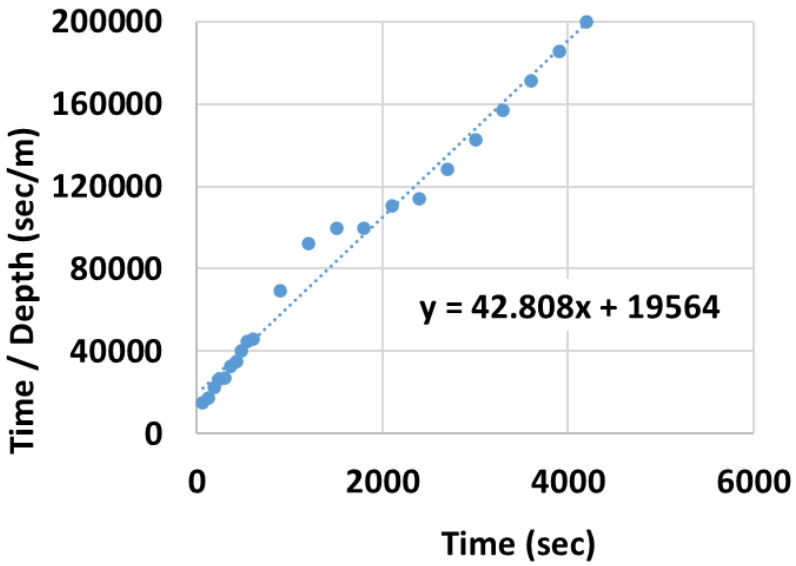

Figure 4.7: Hyperbolic curve (Duncan and Chang, 1970).

4.3.3. Data Validation

To check how this technique fits the data, the erosion curve is plotted using the obtained equation as follows and presented in Figure 4.8.

$$J = \frac{t}{42.808t + 19564} \qquad \text{[Equation 5]}$$

Where,

t = time (sec)

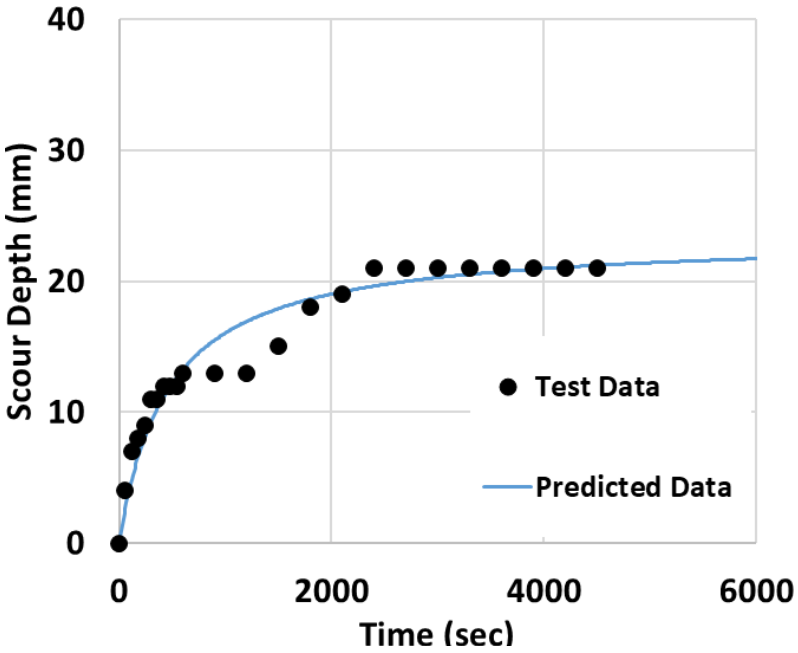

Figure 4.8: Erosion coefficient comparing actual and predicted over referenced time.

From Figure 4.8, the maximum depth is 1/slope of the line = 1/ 42.808 = 0.0234 m. In this calculation, the initial depth is not considered. So, the initial depth should be added to get the equilibrium depth.

$$J_e = 0.0234 + 0.037 = 0.0604 \text{ m}$$

Based on Hanson and Cook (1997), the critical stress is defined as the stress at which the soil detachment starts to occur. The critical stress is determined using Equation 6 as following:

$$\tau_c = \tau_o(\frac{J_p}{J_e})^2 \qquad \text{[Equation 6]}$$

Where,

τ_o= Average hydraulic boundary shear stress/ Maximum stress caused by jet (Pa)

J_p= Potential core depth (m)

J_e= Erosion depth (m)

The calculated critical stress (Equation 6) is as follows,

$$\tau_c = \tau_o \left(\frac{J_p}{J_e}\right)^2 = 41.97 * \left(\frac{0.020034}{0.0604}\right)^2 = 4.62\ Pa$$

For the calculation purpose, additional terms need to be defined including the reference time and the dimensionless scour terms. The reference time is calculated using the following equation:

$$T_r = \frac{J_e}{\tau_c\, k_d} \qquad \text{[Equation 7]}$$

The dimensionless scour terms are defined using the following equations:

$$J_p^* = \frac{J_p}{J_e} \qquad \text{[Equation 8]}$$

$$J^* = \frac{J}{J_e} \qquad \text{[Equation 9]}$$

Equation 10 can be used to determine the reference time.

$$T_m = T_r \left[0.5 \ln\left(\frac{1+J^*}{1-J^*}\right) - J^* - 0.5 \ln\left(\frac{1+J_i^*}{1-J_i^*}\right) + J_i^*\right] \qquad \text{[Equation 10]}$$

Based on the definition of the reference time, Equation 10 is rewritten as:

$$T_m = \frac{J_e}{\tau_c\, K_d} \left[0.5 \ln\left(\frac{1+J^*}{1-J^*}\right) - J^* - 0.5 \ln\left(\frac{1+J_i^*}{1-J_i^*}\right) + J_i^*\right] \qquad \text{[Equation 11]}$$

In Equation 7, everything is known except k_d. Starting with an initial value of $k_d = 0.1$, $T_{m(Predicted)}$ was determined for each measured depth in the dimensionless term, J*. Then, the difference between $T_{m(Predicted)}$, and $T_{m(Actual)}$ was computed as R. After this step, the difference (R) was squared (R^2), and the summation of R^2 was obtained. Finally, the summation of R^2 was

minimized using a solver and revising the k_d value. With the assistance of a solver with the testing data and predetermined critical shear stress, k_d is determined by reducing the error squared.

$$k_d = 3.48\ cm^3/N \cdot sec$$

To double-check that the obtained excess shear stress parameters are representative of the erosion behavior of the soil. Equation 10 can be rewritten as:

$$2\frac{T_m}{T_r} + \ln\left(\frac{1+J_i^*}{1-J_i^*}\right) - 2J_p^* = \ln\left(\frac{1+J^*}{1-J^*}\right) - 2J^* \qquad \text{[Equation 12]}$$

At any time, the left side of the equation is known. So, the equation is solved for one unknown which is J* based on the calculated parameters and the erosion profile is plotted as shown in Figure 4.9.

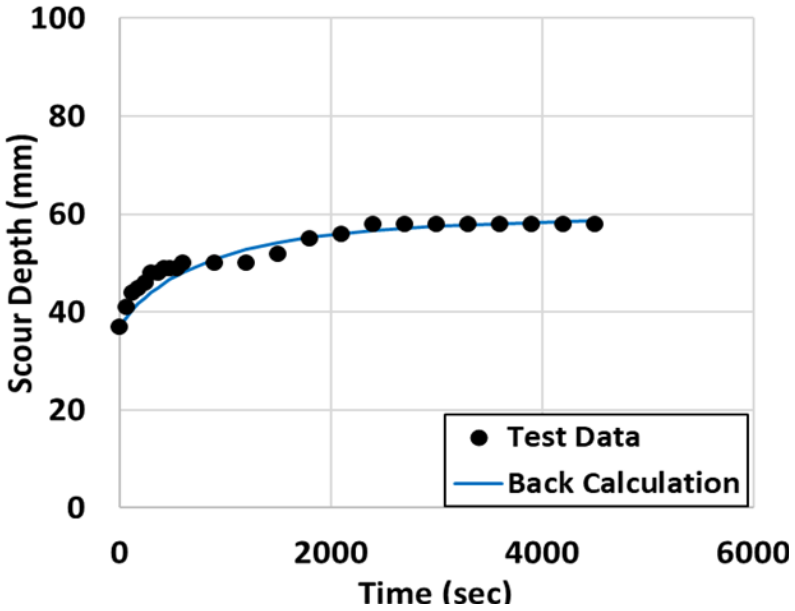

Figure 4.9: Test data vs. ack calculated data.

The plot shows a good agreement between the back-calculated data and the original data. This indicates that the mini-Jet characterization is reasonable and usable for the needs of this project.

4.4. COMPARISON WITH PREVIOUS RESEARCH

A study was conducted by Hanson & Simon (2001) on the cohesive streambeds in the midwestern area of the US. Their focus was particularly on western Iowa, eastern Nebraska, and Yalobusha River Basin, Mississippi. Figure 4.10 shows the data from Hanson & Simon (2001) in addition to the data from the current study. Figure 4.10 show that there is a good match between the current and previous study in terms of the critical shear stress. However, the erodibility coefficient is higher. The overall erosion behavior of the tested soils at the four sites is that they may erode fast but not deep.

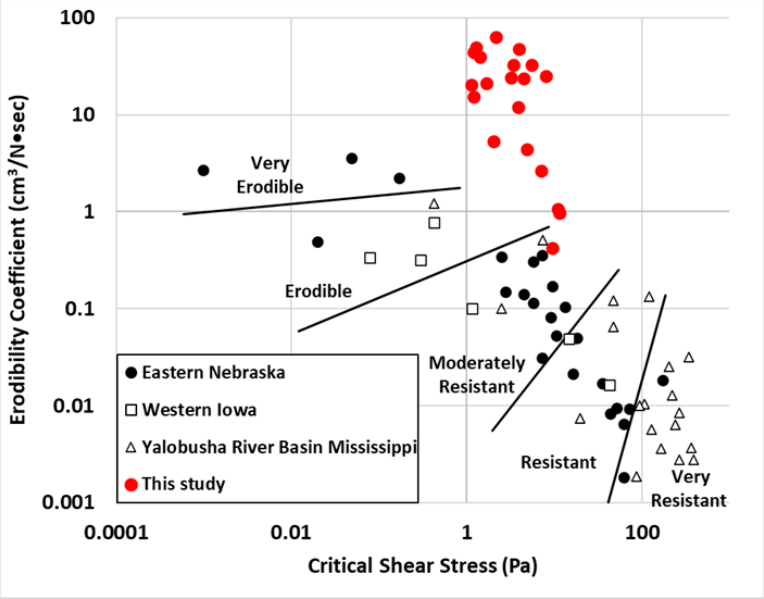

Figure 4.10: Critical shear stress vs. erodibility coefficient replotted from (after Hanson and Simon, 2001).

A second study is selected for further comparison and analyze the results of this study. The test results were compared with another research conducted by Simon et al. (2010). As shown in Figure 4.11, the riverbed data is located in the right upper portion. This indicates that the obtained data are within the normal anticipated range.

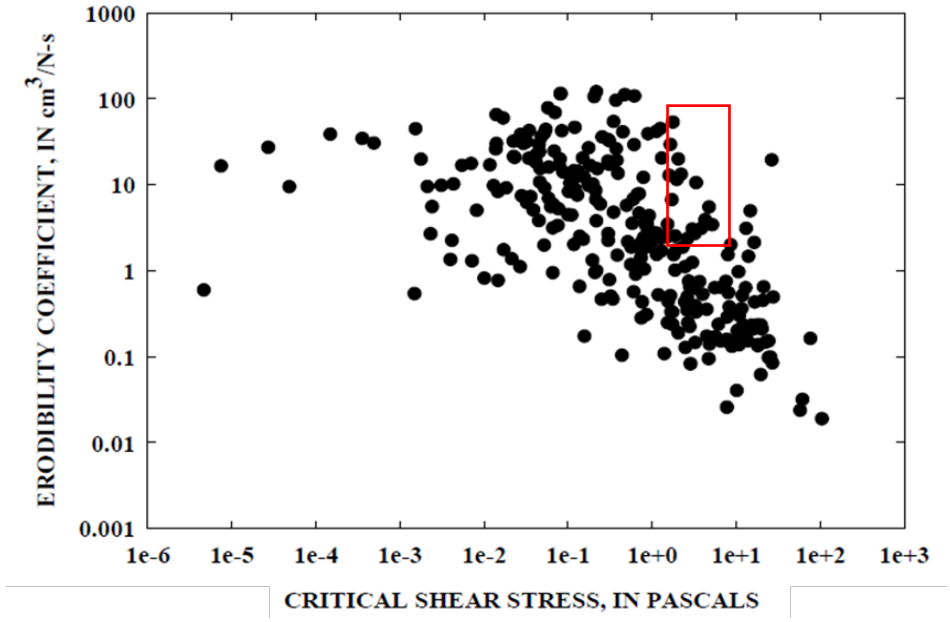

Figure 4.11: Critical shear stress vs. erodibility coefficient (after Simon et al., 2010).

4.5. EQUIVALENT D_{50} VALUES

Another study conducted translated the erosion testing results into the mean grain size D_{50} value (Briaud et al., 2017). This is an important parameter and one that is a direct input into the HEC-RAS models. In the reference, an equivalent sand plot can be constructed for each site. These figures demonstrate that the critical shear stress is governed by the mean grain size for any diameter larger than 0.2 mm. However, the case is different for the soils with a diameter smaller than 0.2 mm. This difference is due to the other factors that may come into play such as cohesion, plasticity index, void ratio, fine's percent, dispersion ratio, soil temperature, water temperature, etc.

In analyzing, the results of this project with Briaud et al. (2017), the samples with D_{50} more than 0.2 mm show a higher erosion resistance (τ_c). On the other hand, the samples with D_{50} less

than 0.2 mm show about the same erosion resistance (τ_c) as the upper limit of the previous study. This similarity can validate the upper limit equation given by Briaud et al. (2017) for the silty soils around the Lincoln area. Based on this, one can predict an equivalent sand particle for the cohesive soils that will give the same erosion resistance (τ_c) which is used as an input to some software as follows.

$$D_{50(Sand\ Equivalent)} = 0.006\left(D_{50(Gradation)}\right)^{-2} \qquad \text{[Equation 13]}$$

Where the calculation for the equivalent sand D_{50} (Hooper),

$$D_{50(Sand\ Equivalent)} = 0.006(0.057\ mm)^{-2} = 1.847\ mm$$

The equivalent sand plot and representative D_{50} values for each site are shown in the following Table 4.7 and in Figures 4.12 to 4.15. In this table, an equivalent D_{50} value is computed as also compared to the NDOT provided values. The NDOT D_{50} values are obtained from the NDOT provided HEC-RAS models, where the D_{50} values are used to calculate the general scour depth. These project-specific D_{50} values are inputted into the HEC-RAS models that are discussed in Chapter 5. Moreover, the results of this project are also overlaid into the previous work to demonstrate a similar range of results as a quick comparison (Figure 4.16).

Table 4.7: The actual, equivalent sand, and representative D_{50} values for each site.

Site	Actual D_{50}	Equivalent Sand D_{50}	Representative D_{50}	NDOT D_{50}
Hooper	0.057	1.847	1.201	0.01
	0.073	1.126		
	0.57	-		
	0.069	1.261		
Lincoln	0.0867	0.799	0.645	0.1
	0.0867	0.799		
	0.183	0.18		
	0.0867	0.799		
Wilber	0.0371	4.36	1.745	0.1
	0.425	-		
	0.842	-		
	1.35	-		
Beatrice	0.61	-	2.211	0.1
	0.0408	3.605		
	1.28	-		
	0.073	1.126		
	0.0368	4.431		

All units are in mm.

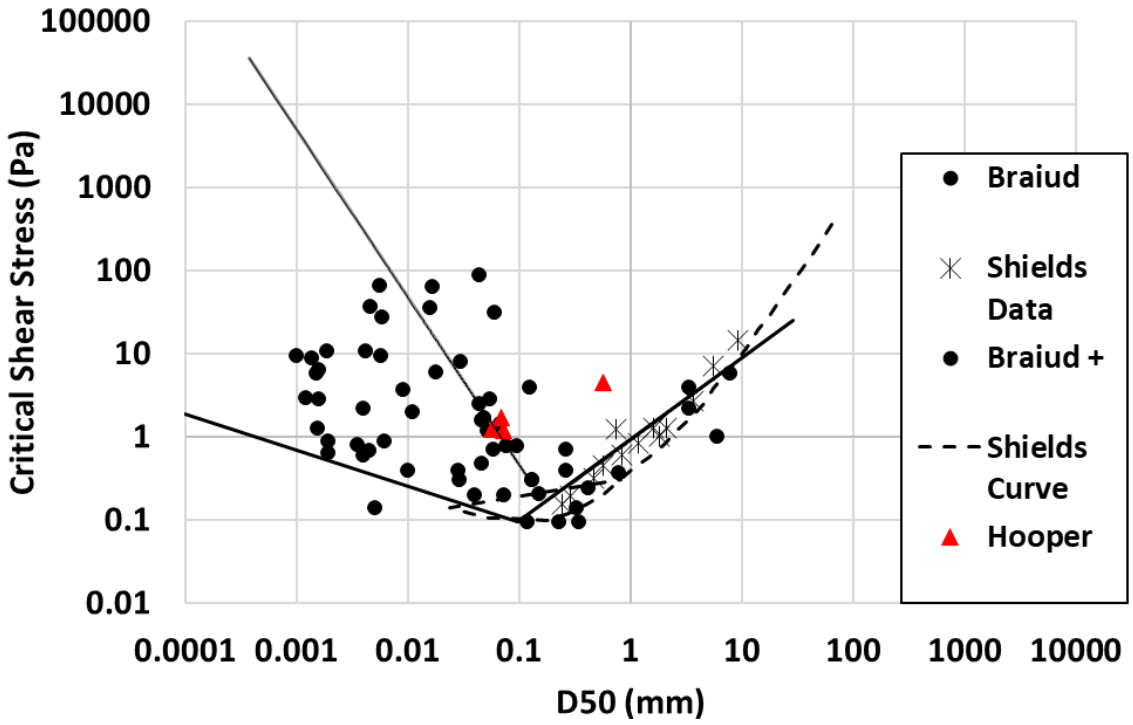

Figure 4.12: Equivalent sand D_{50} plot for the Hooper site.

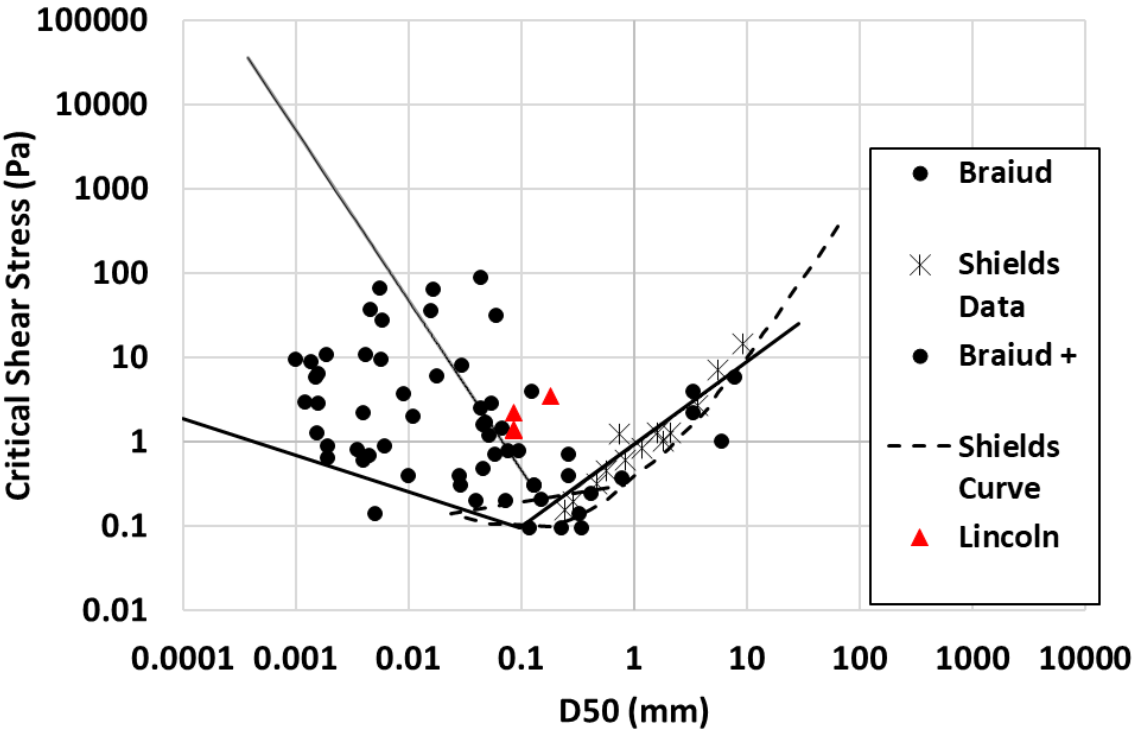

Figure 4.13: Equivalent sand D_{50} plot for the Lincoln site.

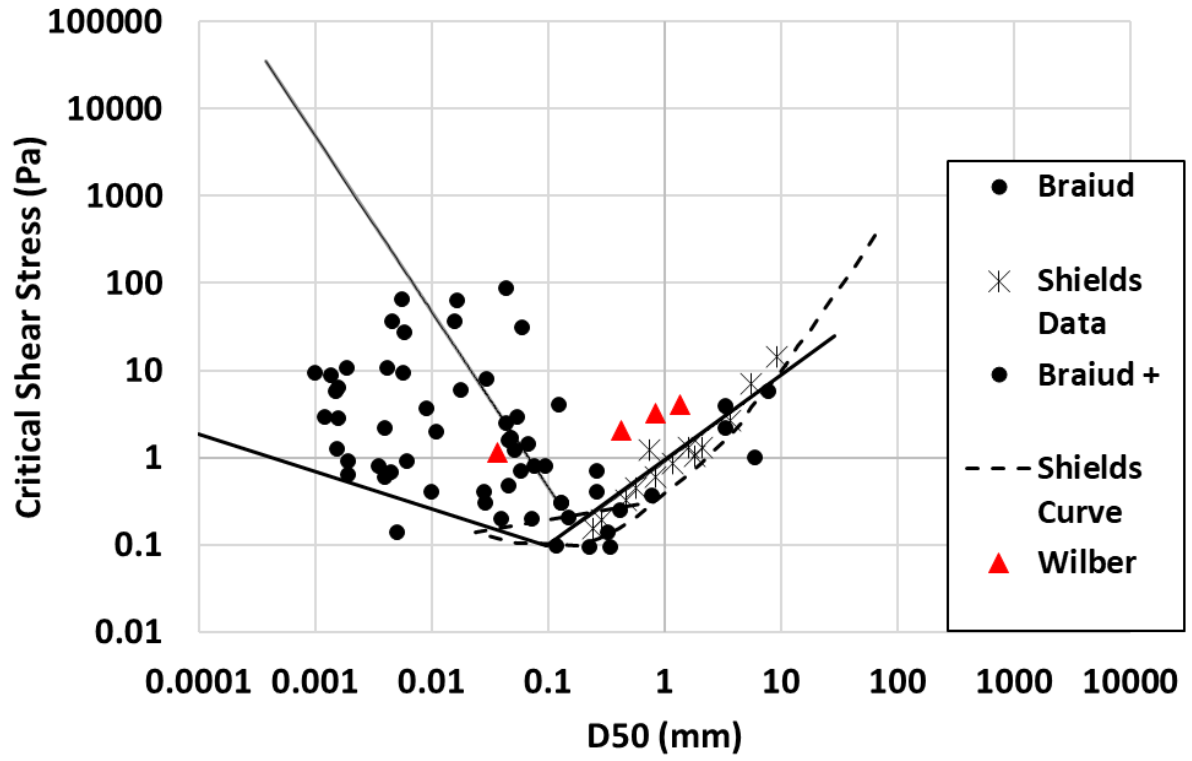

Figure 4.14: Equivalent sand D_{50} plot for the Wilber site.

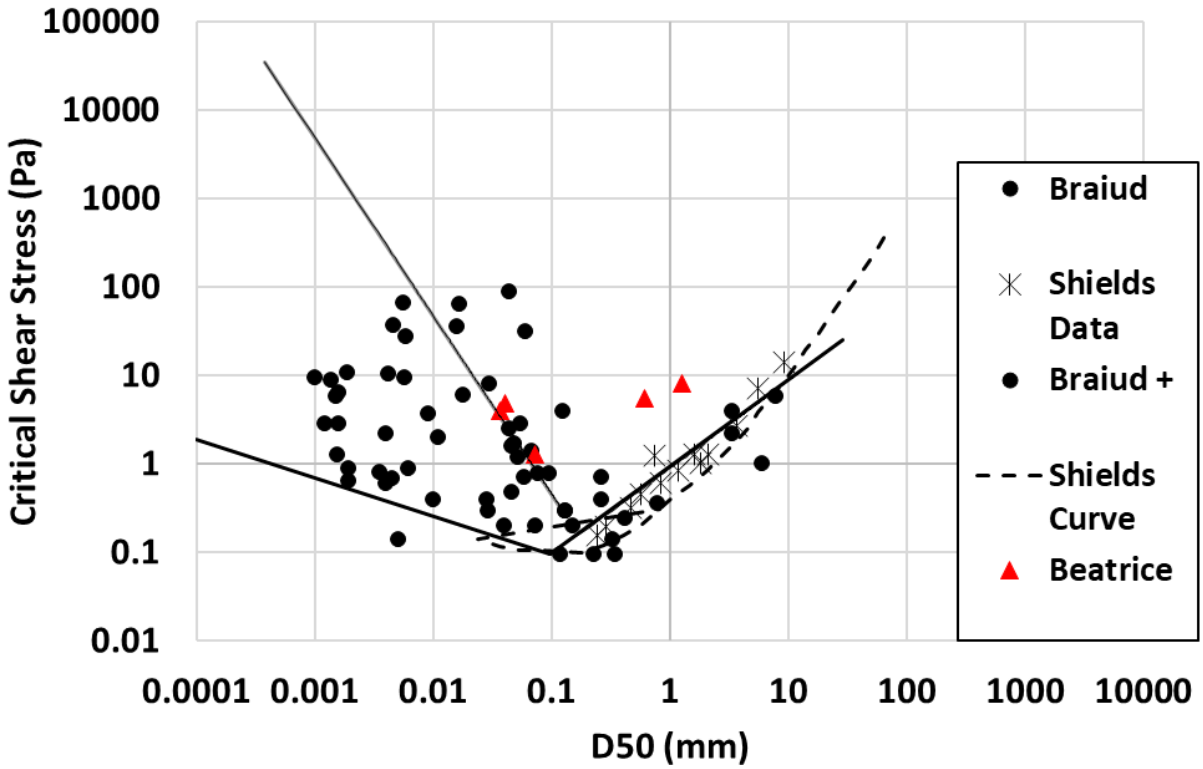

Figure 4.15: Equivalent sand D_{50} plot for the Beatrice site.

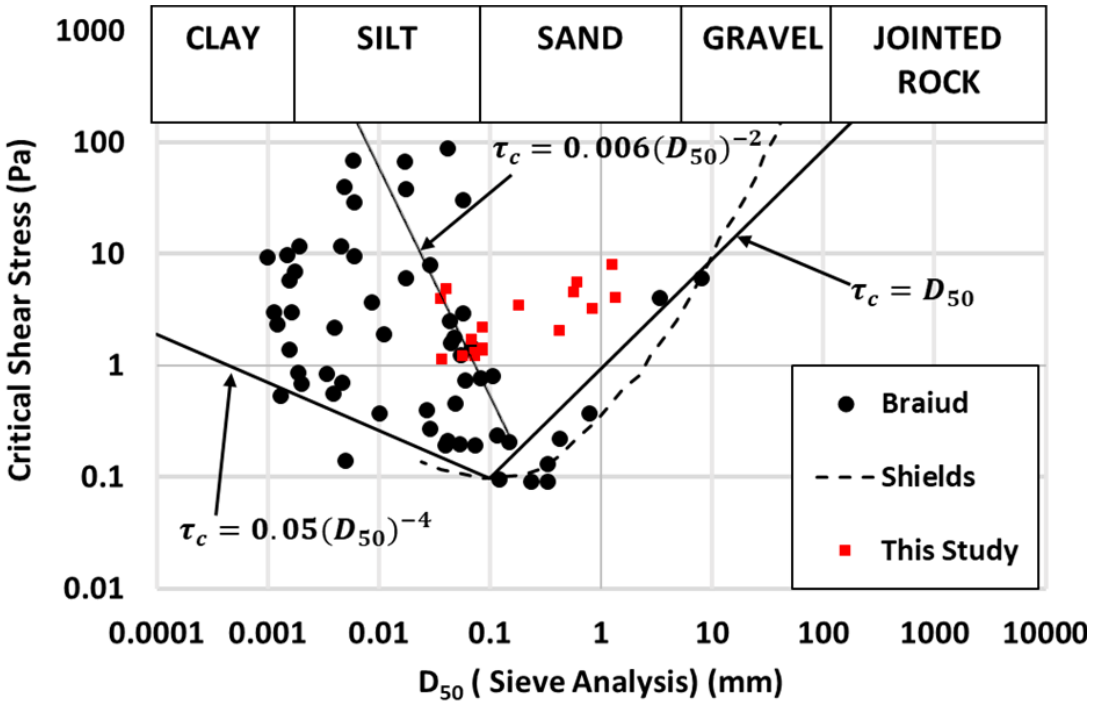

Figure 4.16: Mean grain size D_{50} vs. critical shear stress (Briaud et al., 2017).

4.6. CONCLUSION

The erosion test (e.g., erodibility coefficient) results show a high erosion coefficient with a relatively high critical shear stress, which indicates that the riverbed soils at each of the sites can generally erode fast but not deep. Note this is noted to be in good agreement with similar studies in the region (Hanson and Simon, 2001) as well as validation of the upper limit equation given by Briaud et al., (2017). Moreover, this methodology outputted a project-specific D_{50} value that as field-validated is used within the HEC-RAS models as discussed in Chapter 5. The validity of this D_{50} value within hydraulic modeling will be explored in more detail in Chapter 6.

CHAPTER 5 – HYDRAULIC MODELING

This chapter discusses the implementation of the point cloud data within a 1D hydraulic HEC-RAS model to run scour analysis and confirm the site characterizations. This chapter and the next encompass Task 4 of the research project. The workflow of the implementation of the rasterized terrain model created using the point cloud data will be discussed in detail. This workflow is presented in a detailed manner and includes step-by-step overviews. The hydraulic computations for the 100-year flood event are performed to examine the values and compare with the 100-year local scour rate obtained from NDOT.

5.1. HYDRAULIC MODELING (HEC-RAS)

The Hydrologic Engineering Center's River Analysis System (HEC-RAS) is a computer software platform that allows users to create a hydraulic model for rivers and channels to perform one-dimensional steady flow, one and two-dimensional unsteady flow calculations, sediment transport, and water temperature quality modeling (Brunner, 2002). HEC-RAS makes it easier for a user to visualize these data graphically. HEC-RAS is widely used for hydraulic computations and is easily accessible. Using point cloud data as a terrain file does have the benefit of providing a more detailed overview of the site terrain.

5.1.1. Hydraulic Modeling Workflow

Before performing bridge scour analysis using HEC-RAS, the user needs to create a hydraulic model initially. The hydraulic model consists of the river and bridge geometry bridge

data. Figure 5.1 shows the workflow for the procedure performed within this study to create a hydraulic model and to analyze the scour changes of the four sites using HEC-RAS.

Figure 5.1: HEC-RAS Workflow.

As discussed in Chapter 3, the point cloud data obtained from the data collection period are cleaned to remove noises that would impact results and upscaled to void null values in the point cloud data. These input point clouds contain both overland and bathymetry data points. Using the point cloud data that has been prepared, the data are rasterized to 1.0 meter/39.4 inches on CloudCompare as shown in Figure 5.2 and Figure 5.3.

The raster files are then exported in the *.tif file format before being loaded into RAS Mapper. RAS Mapper is a tool on HEC-RAS where the terrain models can be developed for 1D and 2D hydraulic modeling. These terrain models can be created by importing raster files. These terrain models are more detailed and an easier way to create more detailed geometric data.

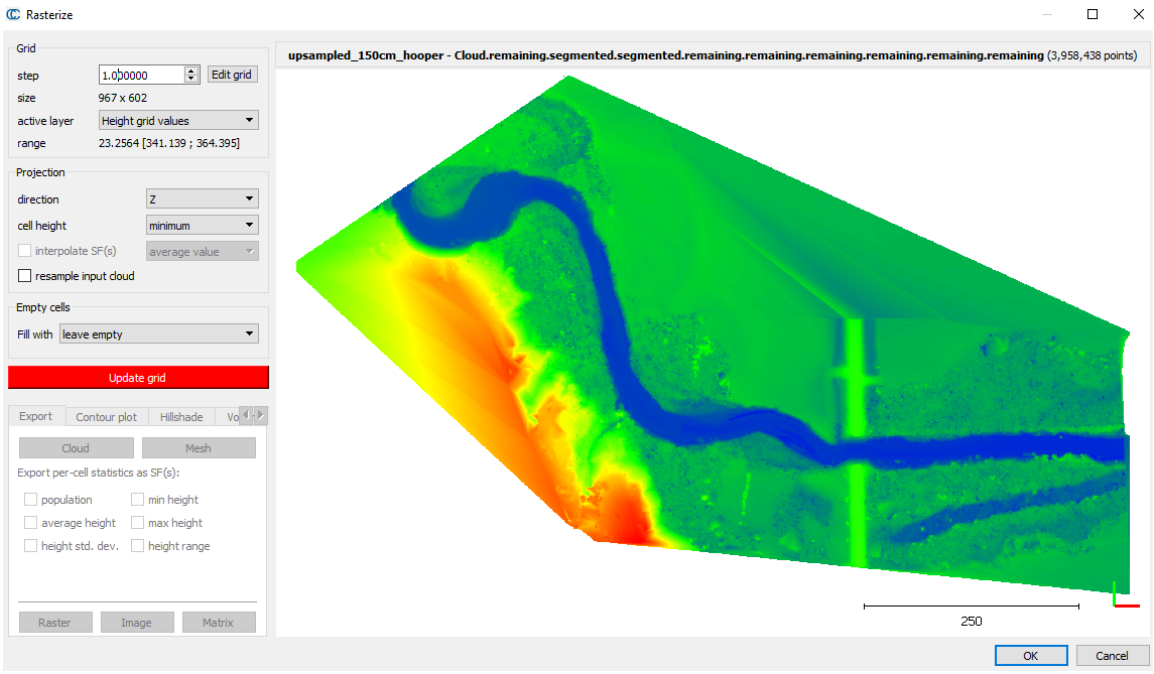

Figure 5.2: Rasterize point cloud data on CloudCompare for the Hooper site.

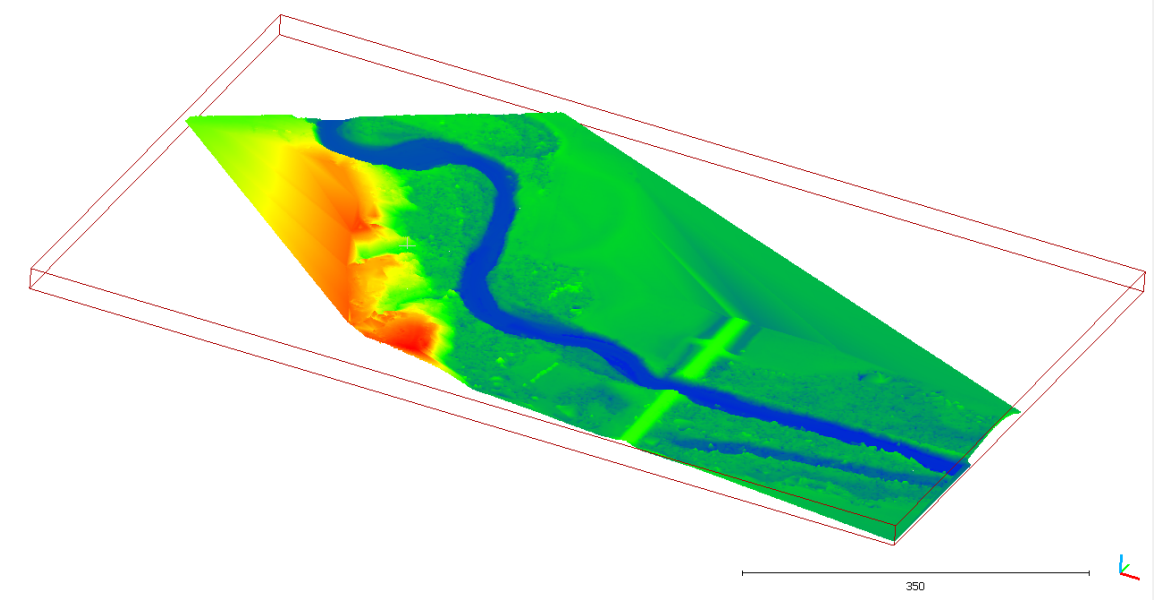

Figure 5.3: Point cloud data rasterized up to 1 meter for the Hooper site.

The first step before importing the raster file into RAS Mapper is to create a new project for a hydraulic model. Once a new project has been created, RAS Mapper can be accessed on the main menu. Before importing the raster file, the user needs to identify and select the correct project

file to set the terrain file on the correct coordinates. For this project, the projection file is based on the defined GNSS coordinate projection file. Then the user can right-click 'Terrain' and select 'Create a New RAS Terrain' and load the rasterized data (Figure 5.4 (a) and Figure 5.4 (b)). To verify if the input data is projected in the right coordinates, right-click 'Map Layers', select 'Add Web Imagery Layer', and select Google Satellite. The uploaded rasterized point cloud data is then shown with an overlay of the Google Satellite imagery as a base map. This is shown in Figure 5.4 (c).

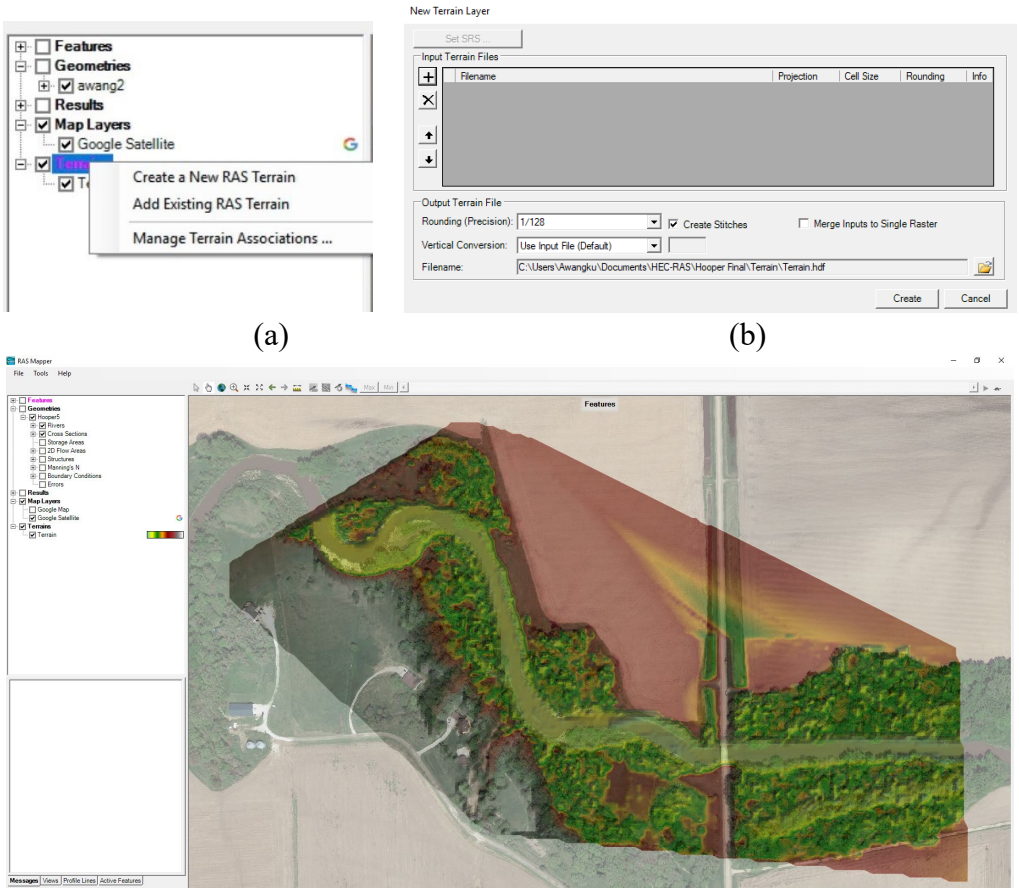

Figure 5.4: (a) Accessing terrain options, (b) Importing point cloud data to HEC-RAS for the Hooper site, (c) Loaded terrain file.

Once the terrain has been uploaded, the geometric data of the stream is created. On RAS Mapper, right-click ‘River’, select ‘Edit Geometry’ (Figure 5.5 (a)), and draw the river reach from upstream to downstream. Once the river reach has been defined, stop editing the geometry by right-clicking ‘Rivers’ and selecting ‘Stop Editing’. Once the river's reach has been defined, the bank lines and flow path of the river can be defined. To define bank lines and flow paths, expand ‘Rivers’, select ‘Bank Lines’, and select ‘Edit Geometry’ (Figure 5.5 (b)), and draw the right bank line from upstream to downstream. Then a similar process can be performed for the left bank. Using the similar procedure as ‘Bank Lines’, the flow paths are then defined next. This is done using the ‘Edit Geometry’ item and drawing the flow paths on both sides of the riverbanks from upstream to downstream. Figure 5.5 (c) shows the defined river reach, bank lines, and flow paths for Maple Creek at the Hooper site.

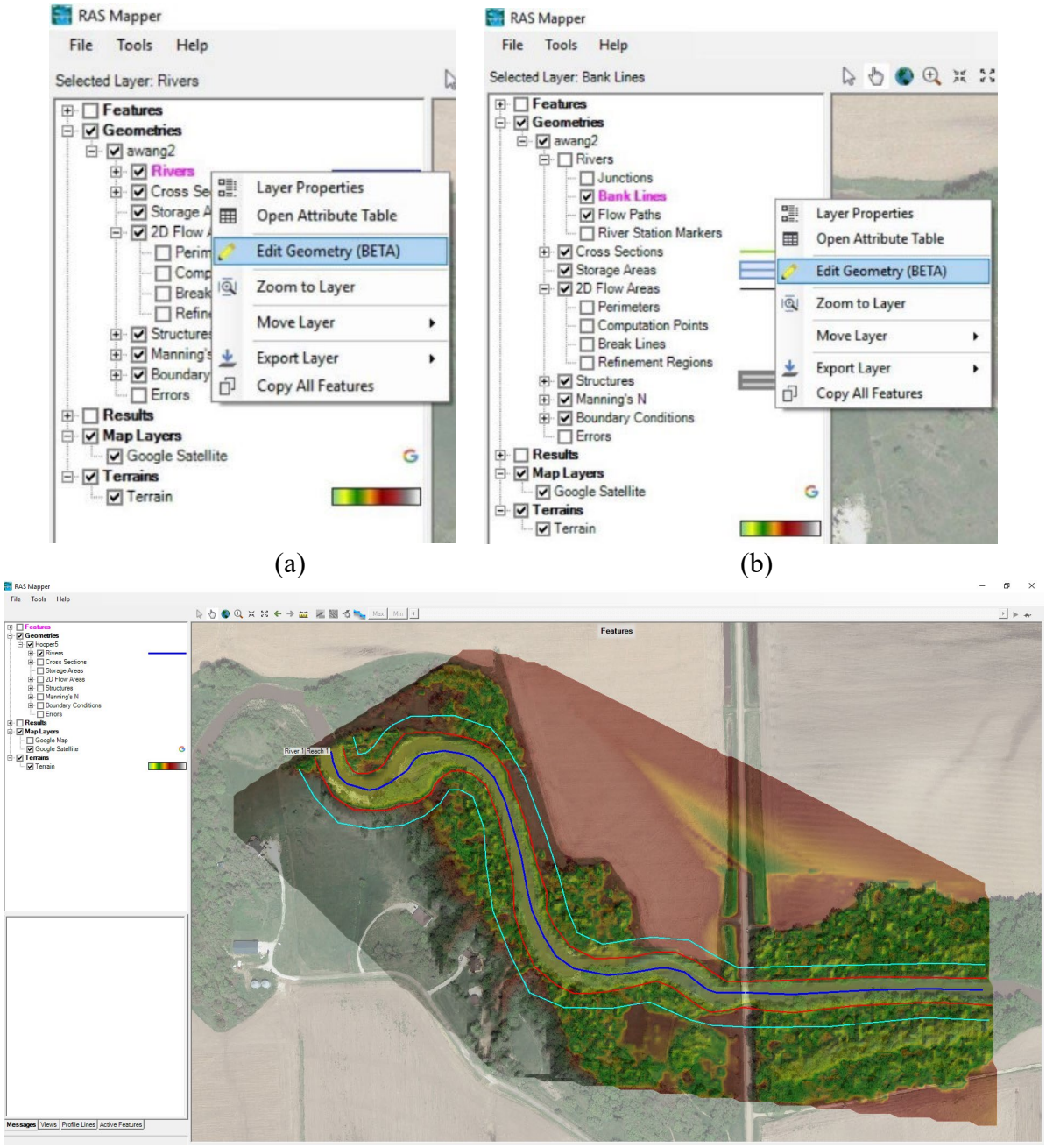

(a) (b)

(c)

Figure 5.5: (a) Editing river reach geometry, (b) Editing bank lines and flow paths geometry, (c) Geometry of the river reach, bank lines, flow paths defined at the Hooper site.

The next step within RAS Mapper is to create cross-sections. The user can right-click 'Cross Sections', and select 'Edit Geometry' (Figure 5.6 (a)) to draw the cross-sections across the river. Cross-sections are created perpendicular to the river flow and at every bank turn (Figure 5.6 (b)). Once the cross-sections are defined within RAS Mapper, close the window and open up the 'View/Edit geometry data' in the main menu. At this point, the user will interpolate the cross-sections within the river reach. The cross-section interpolation tool can be accessed under the 'Tools' tab. To create a detailed geometry of the stream, the cross-section is interpolated with a maximum distance between the cross-sections of 5 meters (16 feet, Figure 5.6 (c)). The interpolated cross-section is shown in Figure 5.6 (d) for the Hooper site.

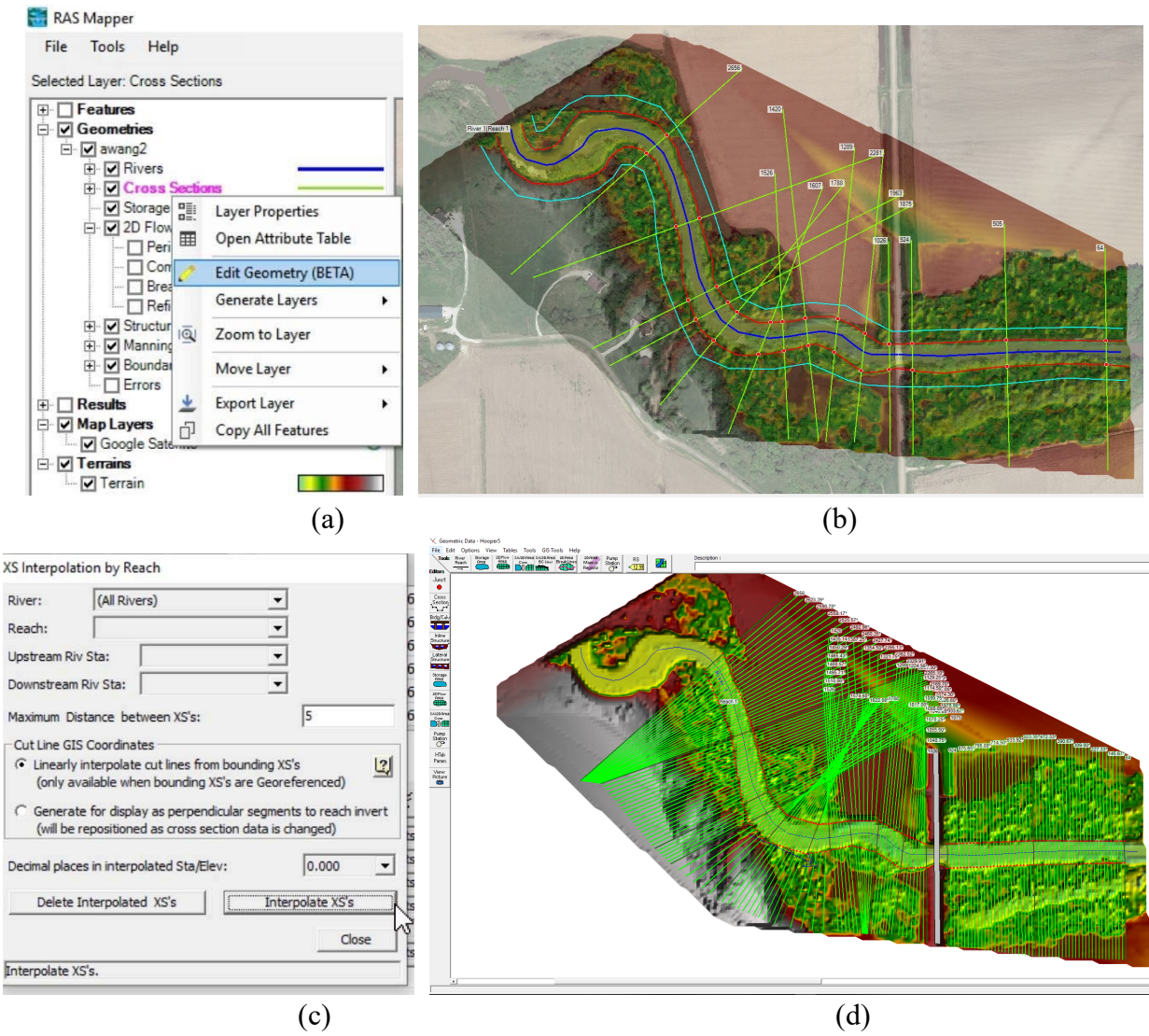

Figure 5.6: (a) Editing cross-section geometry, (b) Geometry of the cross-sections defined at the Hooper site, (c) Cross-section interpolation within reach, (d) Geometry of the interpolated cross-sections defined at the Hooper site.

Once the cross-sections have been created, they can be updated in the cross-section under the ‘Geometric Data’ window. The cross-sections may also be filtered if there are excessive or repetitive points using the ‘Cross Section Points Filter’ under the ‘Tools’ tab. Figure 5.7 shows what a typical cross-section would look like. The next step of the analysis is to add the bridge structure geometry data. The bridge geometry data is based on the information given by NDOT and the bridge plan layout (Appendix A). To create a bridge geometry, the user can first add the ‘Deck/Roadway’ data (Figure 5.8 (a)) of the bridge and then the ‘Stopping Abutment’ and ‘Pier’ data for each site (Figure 5.8 (b)). Figure 5.8 (c) shows the bridge geometry created crossing for Turkey Creek at the Wilber site. Note this site is shown here as there are no piers at the Hooper site.

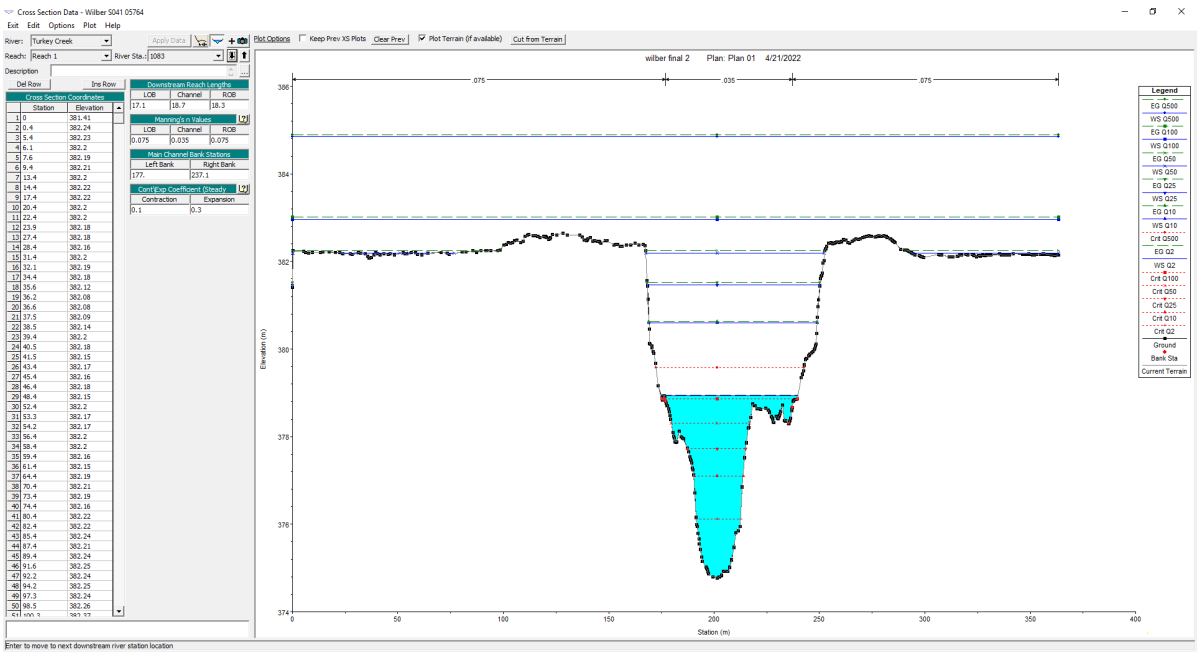

Figure 5.7: Cross section data.

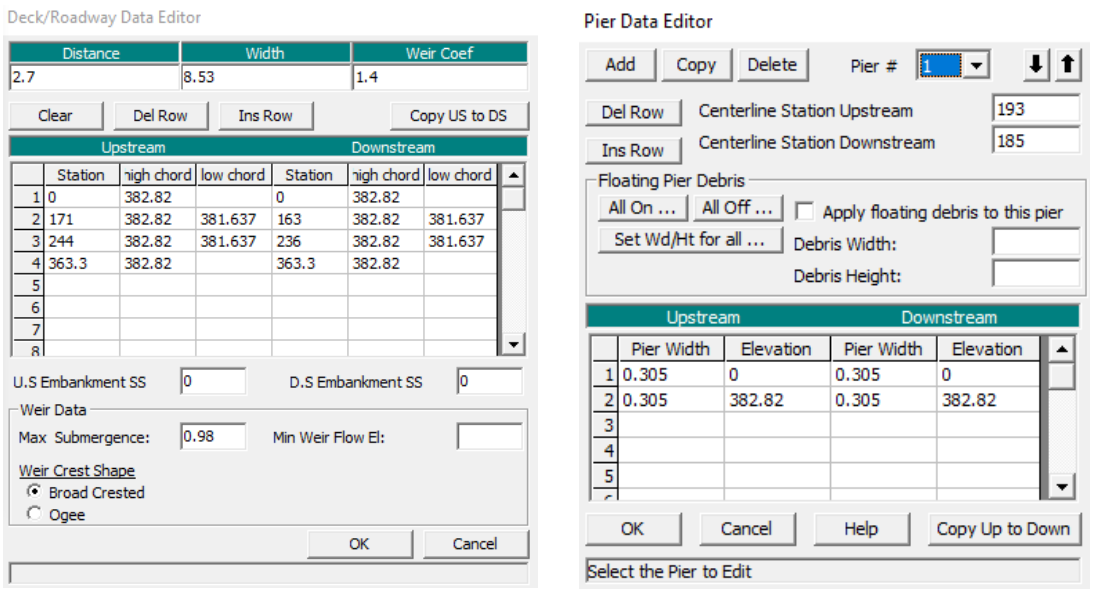

(a) (b)

(c)

Figure 5.8: (a) Deck/roadway data editor, (b) Pier data editor, (c) Bridge geometry data for the Wilber site.

Once the geometry data has been created and finalized, the next step is to input the flow data. The values input for this study includes the flood year event discharge flow rates and the peak flow discharge events that occurred within the period of this study (Figure 5.9 (a)). The steady flow boundary conditions are also defined by the river stream's normal depth (Figure 5.9 (b)). Once the flow data have been updated and saved, the next step is to run the steady flow analysis. To perform this task and in the main menu, click the 'Perform a steady flow simulation' and select 'Compute' (Figure 5.10(a)) to run the steady flow analysis. Once the steady flow analysis is run, the finished computations window will be displayed (Figure 5.10 (b)).

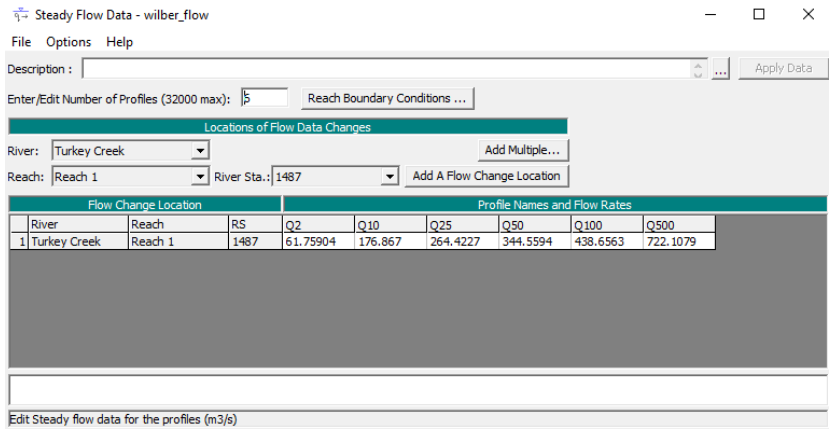

(a)

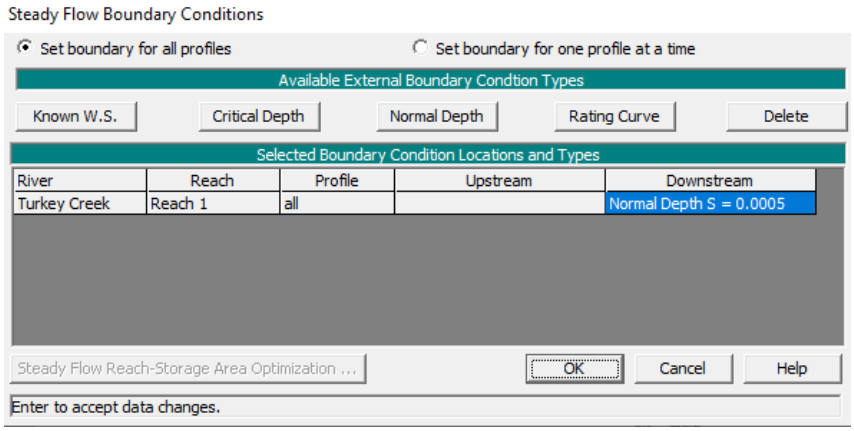

(b)

Figure 5.9: (a) Flow discharge input, (b) Normal depth boundary condition.

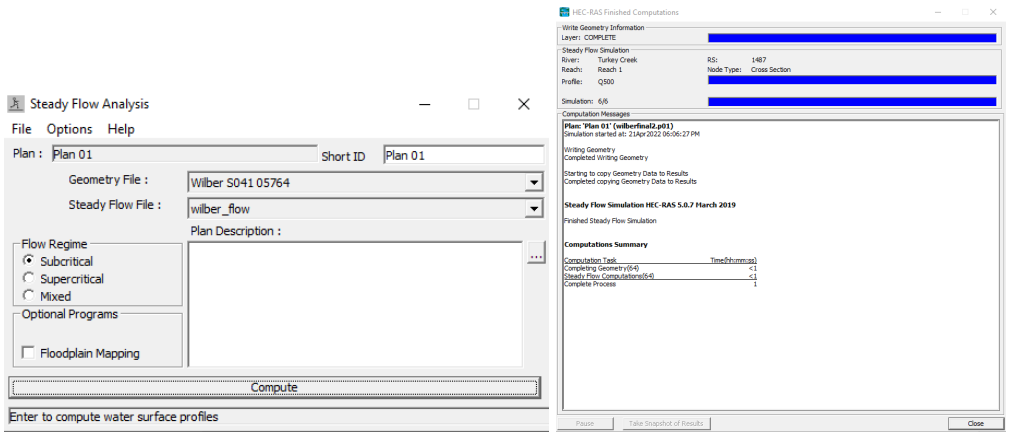

(a) (b)

Figure 5.10: (a) Compute steady flow analysis, (b) Computed steady flow analysis.

After the steady flow analysis is complete, the next step is to compute the bridge scour depths. Under the main menu, click 'Perform hydraulic design computations.' The input data for the bridge scour analysis is based on the representative D_{50} value from Chapter 4. Note other input parameters (e.g., Manning's coefficient) into the hydraulic model were set to the same values as obtained from NDOT and/or its consultants. This was done for consistency in comparison, but it is expected that some variation of these parameters may occur with different engineering judgments. The other input parameters were held constant for this study. This study focusses on how to account for cohesive soils. Moreover, the D_{50} value accounts for the median particle, and is taken as independent of other parameters. The total bridge scour depths consist of three types of bridge scour analyses – contraction scour, abutment scour, and pier scour. Once the hydraulic design computations have been finalized, the window will display the scour depths (Figure 5.11) and a report will be generated.

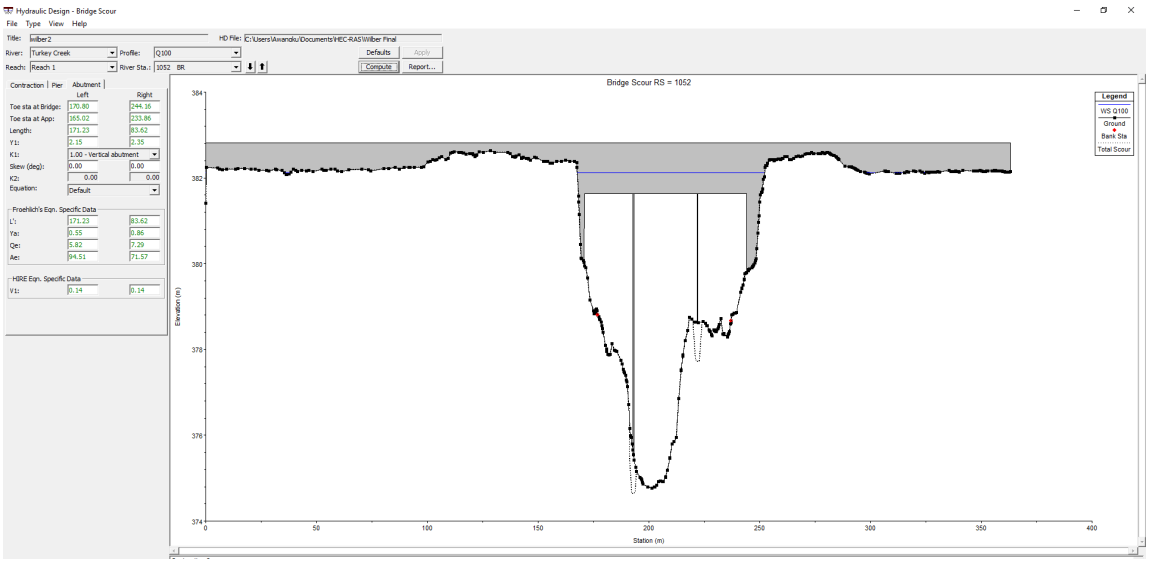

Figure 5.11: Perform hydraulic design computations.

5.1.2. Hydraulic Models

The following figures (Figure 5.12 to Figure 5.15) show the hydraulic models created for each site. These models were constructed in the same process as described below. Note for each of the sites, the scour input data (including D_{50}) changes.

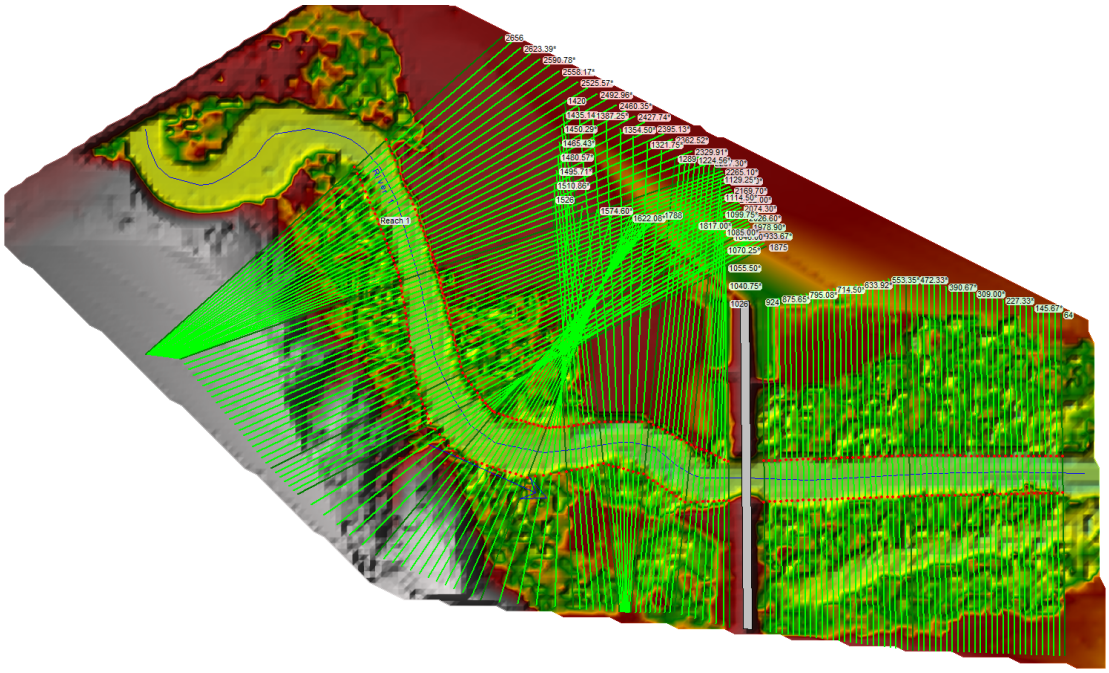

Figure 5.12: Hydraulic model for the Hooper site.

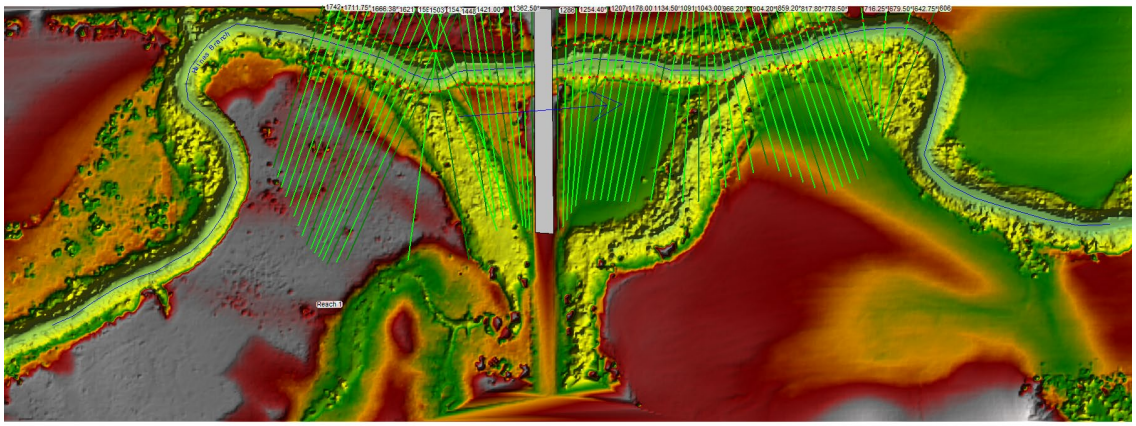

Figure 5.13: Hydraulic model for the Lincoln site.

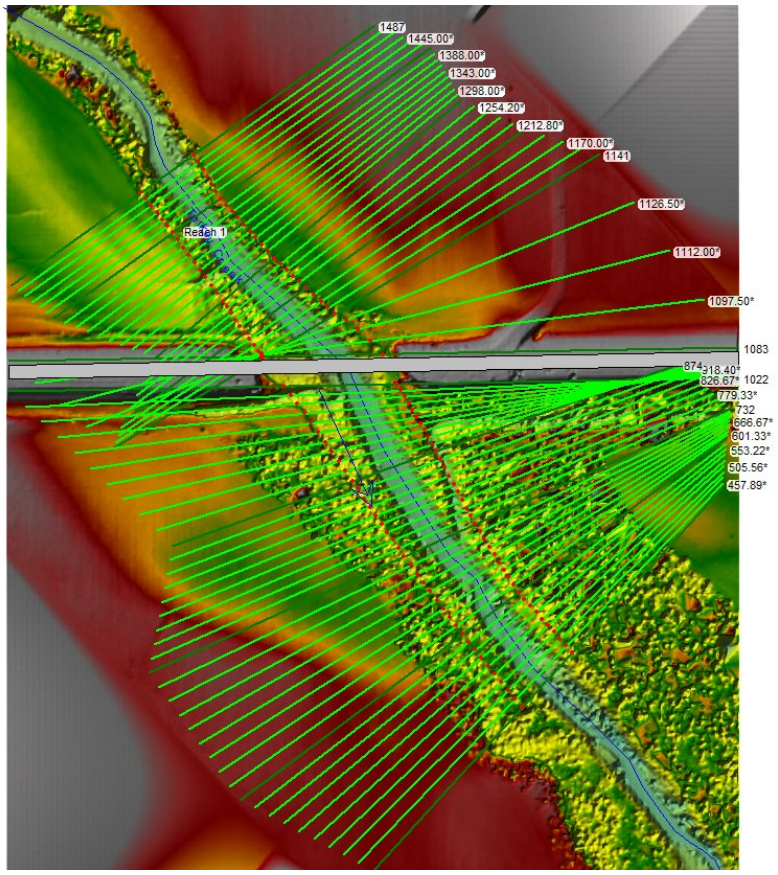

Figure 5.14: Hydraulic model for the Wilber site.

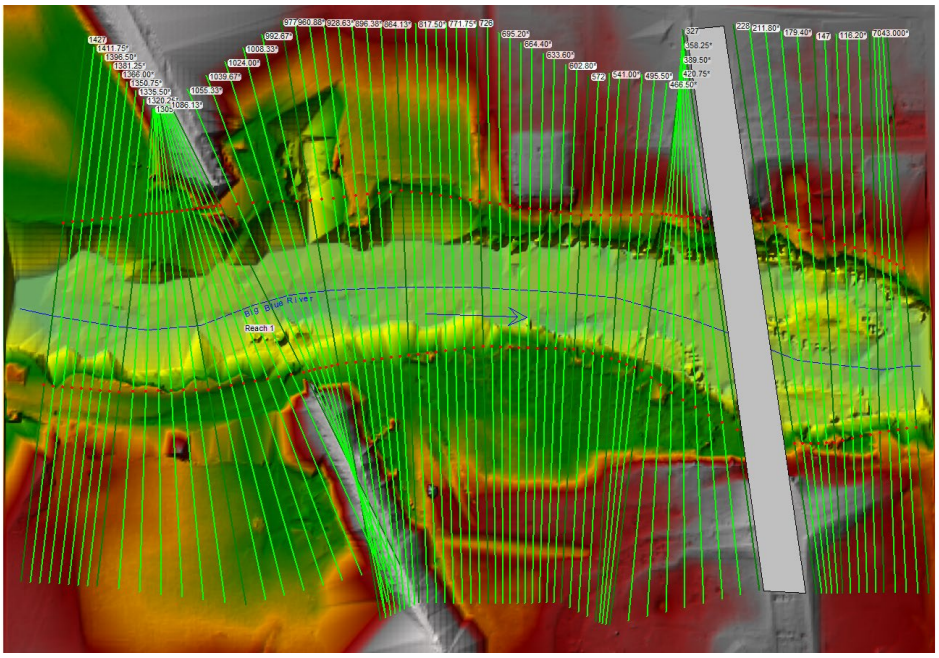

Figure 5.15: Hydraulic model for the Beatrice site.

5.2. BRIDGE SCOUR ANALYSES

The local scour for each site based on the 100-flood year event has been determined by NDOT (as shown in Table 3.1) to be 11ft (3.4 m) for the Hooper site, 2.4 ft (0.73 m) for the Wilber site, and 8.2 ft (2.5 m) for the Beatrice site. The information for the local scour depth for the Lincoln site is not available. The NDOT has also provided its HEC-RAS models which are attached to Appendix F of this report. Note some of these models were developed by NDOT consultants. These models are used for guidance and comparison in this project, with the salient differences being the input geometry and the grain size (D_{50} value).

Contraction scour can be computed in HEC-RAS by either Laursen's clear-water (Laursen, 1963) or live-bed (Laursen, 1960) contraction scour equations. This project utilizes the Laursen's clear-water to compute for contraction scour (Laursen, 1963). This equation can be found in the

HEC-18 documentation under Chapter 6 – Contraction Scour, which is Equation (6.4). The contraction scour equation utilizes the site specific D_{50} values obtained (from Chapter 4), and the K_1 value is calculated based on the equivalent D_{50}. Note, all other variables are obtained automatically from the HEC-RAS output file.

The pier scour can be computed by either the Colorado State University (CSU) equation (Richardson, et al, 1990) or the Froehlich (1988) equation. This study uses the CSU equation to compute the pier scour for each site. This equation can be found in the HEC-18 documentation under Chapter 7 – Pier Scour (7.1).

The 100-year flood event for each site has been computed based on the hydraulic models created using the point cloud data collected for this study. The hydraulic computations for each site are shown in Figure 5.16 to Figure 5.19. These hydraulic computations are based on the representative D_{50} value obtained by this study as described in Chapter 4.

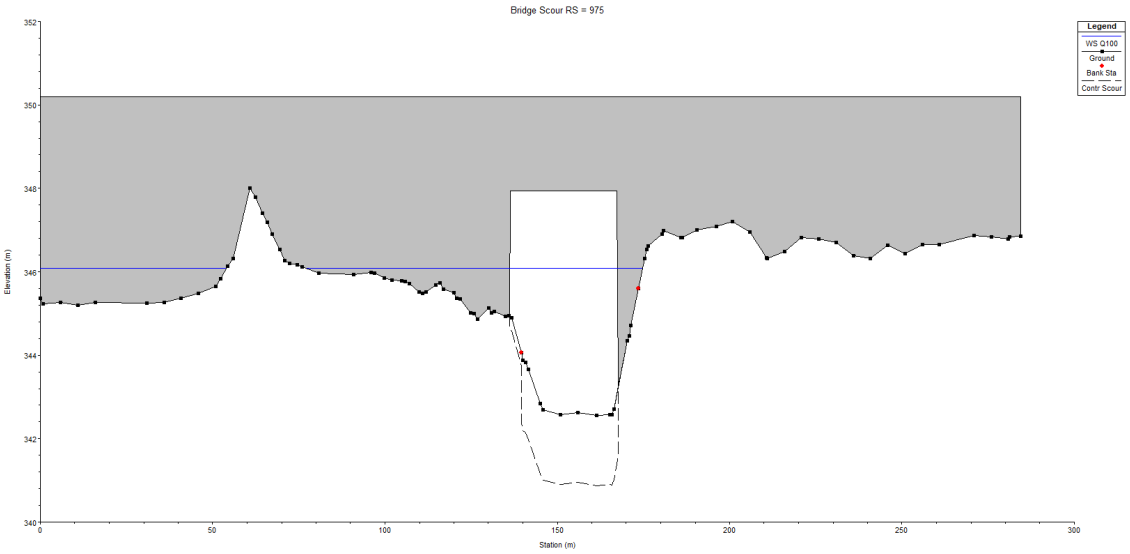

Figure 5.16: Hydraulic design computation for Q100 at the Hooper site.

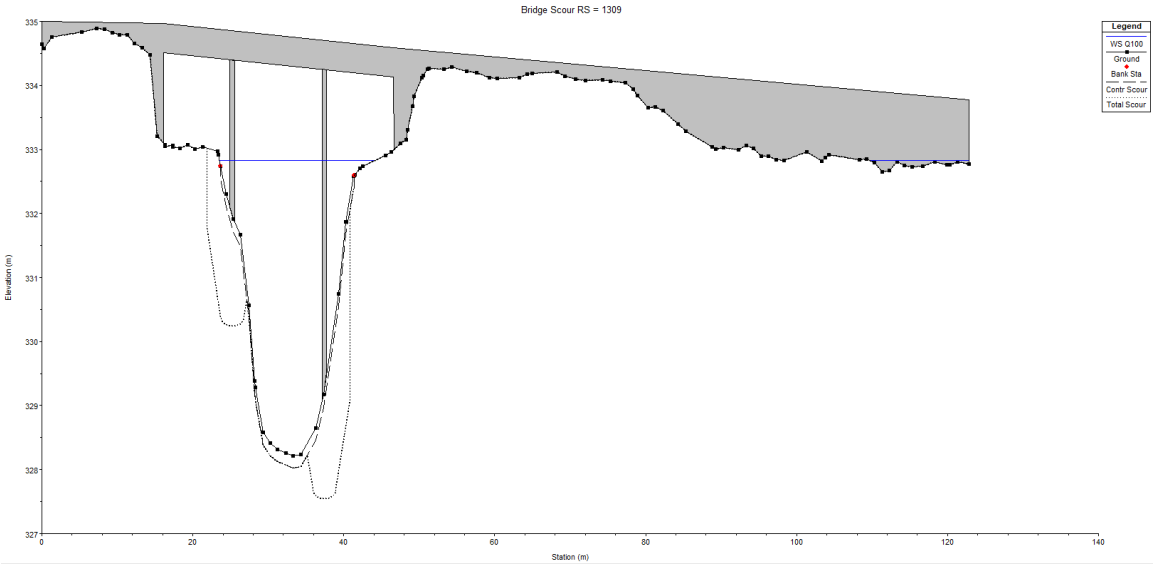

Figure 5.17: Hydraulic design computation for Q100 at the Lincoln site.

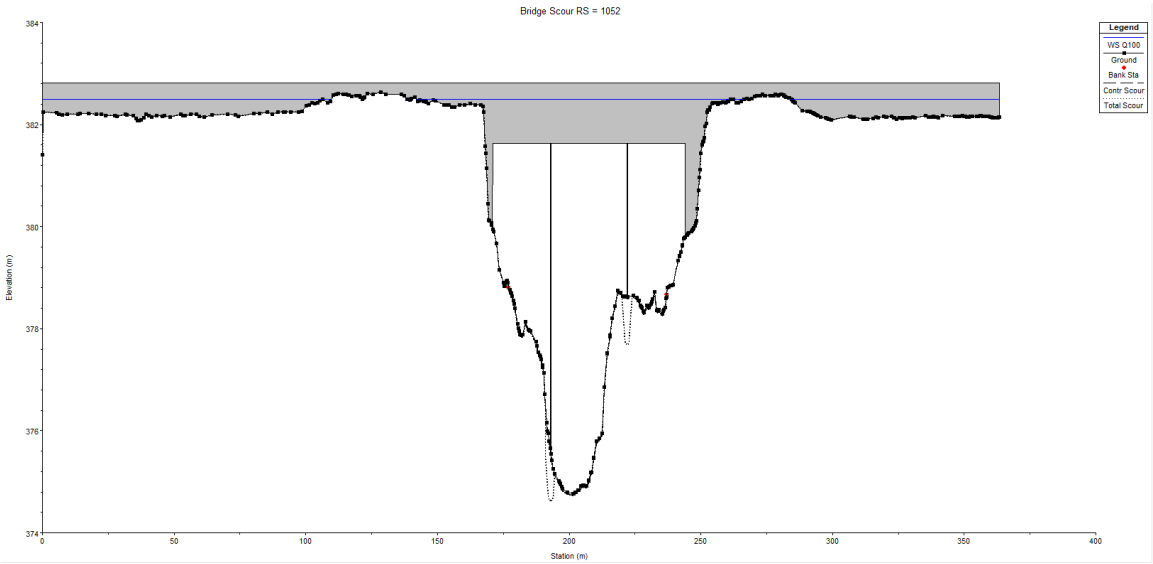

Figure 5.18: Hydraulic design computation for Q100 at the Wilber site.

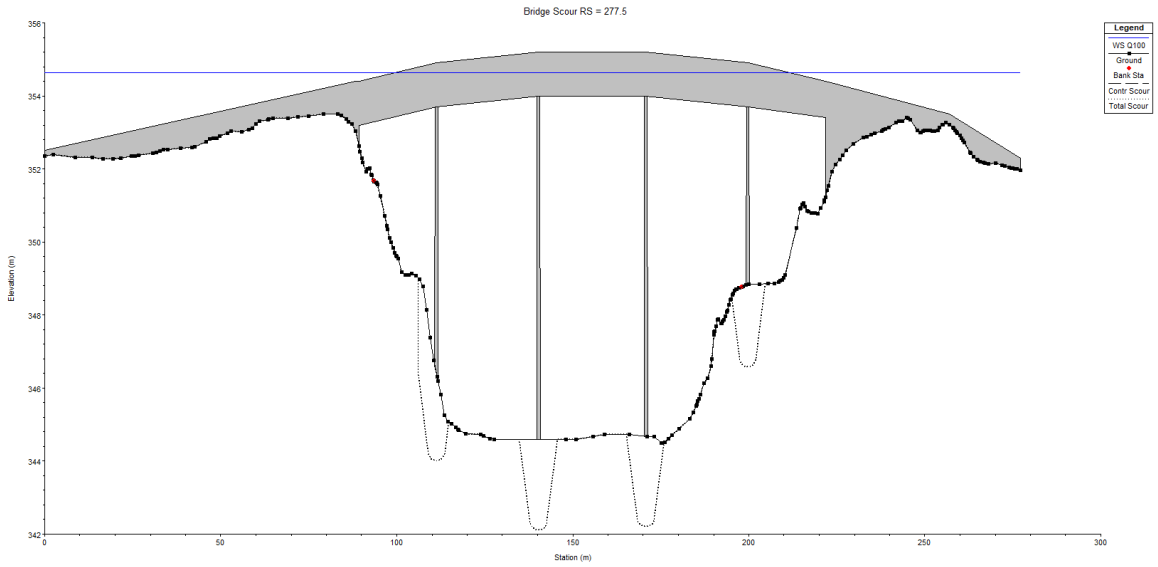

Figure 5.19: Hydraulic design computation for Q100 at the Beatrice site.

Table 5.1 shows the tabulated data comparing the scour depth between the 100-year flood event based on NDOT findings using NDOT's HEC-RAS models and the 100-year flood event calculated based on the hydraulic model created using the point cloud data. The data shows that the combined scour depths are approximately the same between the two models. However, there is a lower combined scour depth for the Hooper and Lincoln site. The Wilber site shows the combined scour depth to be a little higher than the scour depth as provided by NDOT. The combined scour findings using the point cloud data are also a little lower for the Beatrice site. This data comparison is shown in Table 5.1.

Table 5.1: Scour findings vs. NDOT's scour finding for Q100.

Site Location	Contraction Scour (m)	Pier Scour (m)	Combined Scour (m)	NDOT Combined Scour (m)	Difference in Combined Scour (m)
Hooper	1.68	0	1.68	3.35	**+1.67**
Lincoln	0.2	1.54	1.74	3.76	**+2.02**
Wilber	0	0.89	0.89	0.73	**-0.16**
Beatrice	0	2.47	2.47	2.49	**+0.02**

5.3. CONCLUSION

The results show that the hydraulic computations done based on the findings of the representative D_{50} values with point cloud data on HEC-RAS are either similar or significantly smaller than the current HEC-RAS models. This method shows that the current method employed by NDOT, or its consultants is conservative for simulated Q100 flow events. However, this will be revisited in the next chapter (Chapter 6), where the HEC-RAS model results will be compared against the field-measured scour and stream degradation values during the monitoring period.

CHAPTER 6 – DATA-DRIVEN SCOUR VALIDATION

This chapter discusses the field-measured scour depths and stream changes, as compared to the hydraulic models. Moreover, this chapter also discusses the results and recommendations for a revised scour analysis procedure. The change detection process, as applied to the various field datasets, using CloudCompare software is outlined in this chapter, and the results of the findings are examined. These results are compared and analyzed with the bridge scour analysis method using HEC-RAS based on the highly detailed terrain model. This chapter summarizes the concluding part of Task 4 of the data-driven scour validation.

6.1. CHANGE DETECTION

Change detection is an approach to compare two or more temporal datasets of point clouds. The data used for this study are the terrain data comprising the overland and bathymetry data. Using the point cloud data from the two different dates of the data collection, we could use the change detection process to quantify changes over time. This method will help us analyze the difference in the topographic changes between the two periods of time. The process of change detection can be processed using CloudCompare software's plugin - the M3C2 algorithm (Lague, et al., 2013).

6.1.1. M3C2 Algorithm

The multiscale model to model cloud comparison (M3C2) is an algorithm on CloudCompare that computes distances between two different point clouds (Figure 6.1, Lague, et al., 2013). The algorithm detects signed changes at the voxel step by counting the number of added

and removed points. For this study, the added points are accretion, and the removed points are scour changes (or stream degradation). The change detection process helps us determine the scour and accretion changes at the site. However, the changes measured can also be influenced by vegetation at the site and other environmental factors.

Figure 6.1: Application of M3C2 on example data (courtesy of Lague et al., 2013).

6.1.2. M3C2 Analysis and Results

For this study, the focus of the M3C2 results is the statistical changes in the negative direction, which is the lowering of the data between the temporal point cloud datasets. That is for a specific voxel, the vertical reduction in elevation. The removal of these points represents scour and stream degradation changes that occur at the four different sites. The addition (accretion) of the points is not the focus of this study, but it is included for completeness. The increase in elevation may be associated with vegetation growth, leaves, debris, etc.

The first site discussed in the analysis is the Hooper site. The study at the Hooper site compares point cloud data first collected on December 10, 2020, to that of April 23, 2021. There are two regions of interest for the Hooper site. 'Region 1' is located upstream of Maple Creek, where the stream meanders, and 'Region 2' is in the proximity of the bridge (Figure 6.2). These two regions

were then run under the M3C2 algorithm to examine the change detection that occurs between the two point cloud datasets. The M3C2 output of a new point cloud data showing the statistical changes between the temporal cloud data is shown in Figure 6.3. The statistical data of the M3C2 point cloud are then plotted in a histogram to quantify the scour and accretion values, as shown in Figure 6.4.

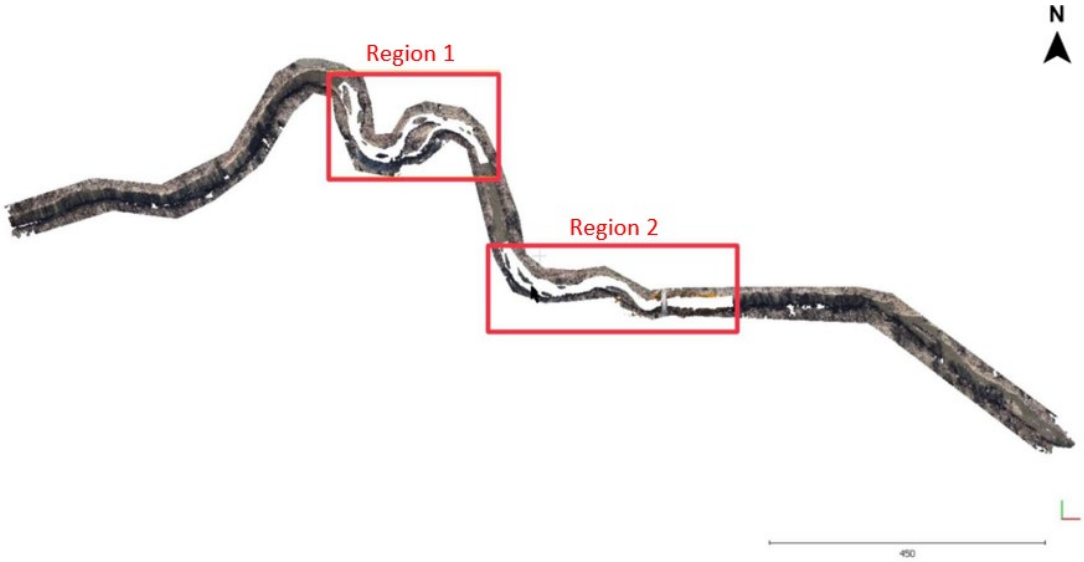

Figure 6.2: Region of interest for the Hooper site (approximately 2100 meters).

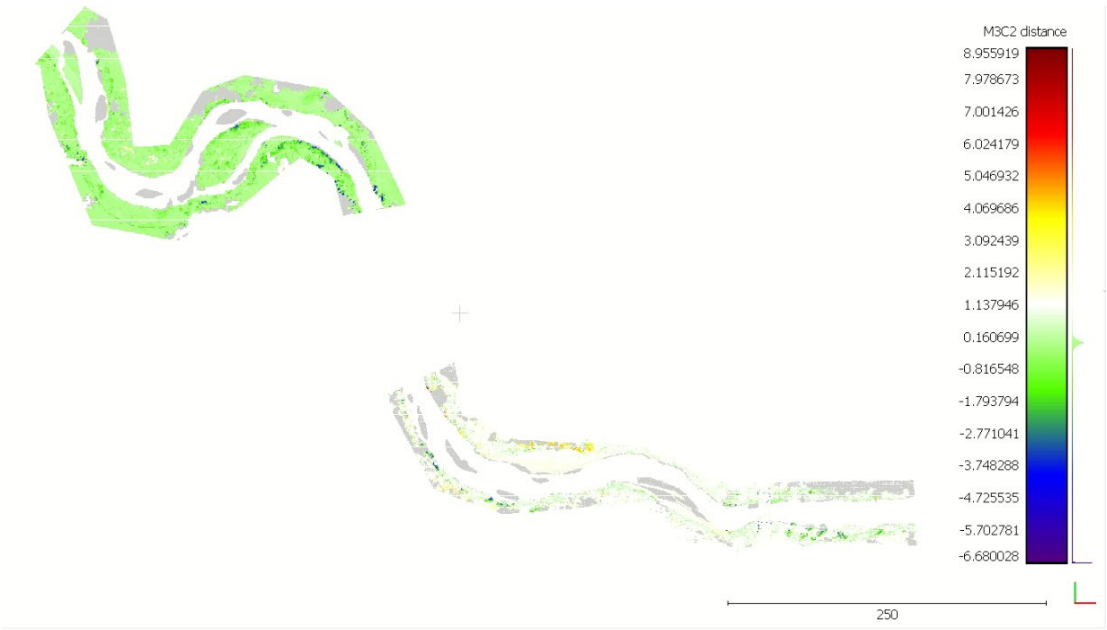

Figure 6.3: Change detection via M3C2 algorithm for the Hooper site.

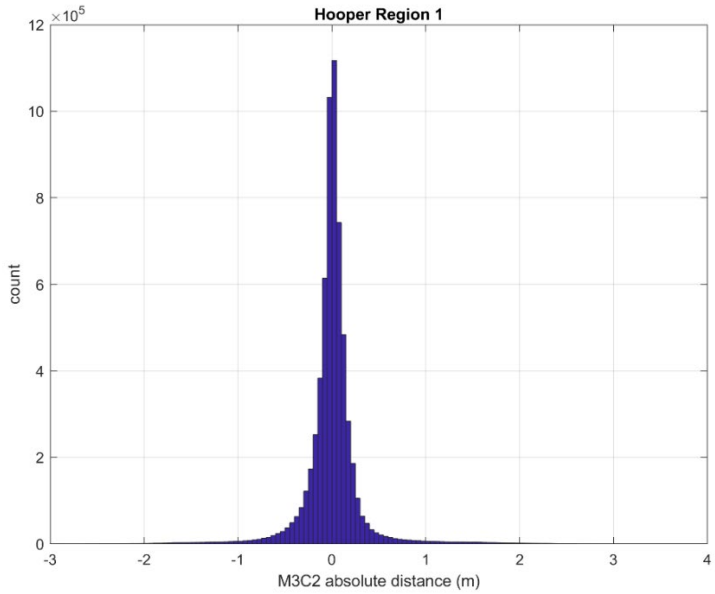

(a)

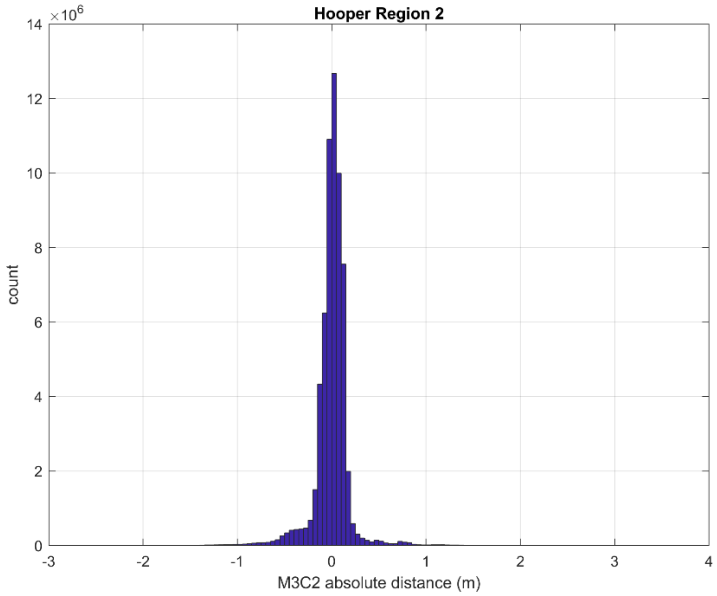

(b)

Figure 6.4: Change detection results for the Hooper site (a) Region 1 (b) Region 2.

The median and mean value from the histogram is calculated and tabulated in Table 6.1. The tabulated data shows the point removal (negative values) and point addition (positive value) between the temporal point cloud data. The negative value represents the scour data, and the positive value is the accretion data. The scour values are the values of interest for this analysis. The mean value considers the overall average of the negative point changes, including the noise, erroneous points, and outliers. While there is inherent noise in the data as well as an anticipated Gaussian distribution to the measured and realistic values, the value of interest is taken conservatively at the 95% confidence interval, this relates to approximately the mean plus two standard deviations, as the Gaussian distribution is assumed to be dual tailed. The equation used to determine the 95% confidence value more precisely is the mean plus 1.96 of the standard deviations.

The data shows a median scour change of 0.09 meters in 'Region 1' and scour change of 0.07 meters in 'Region 2', where the 95% confidence value is 0.39 meters (the region closest to the bridge). These values are also summarized for all sites later in this chapter in Table 6.14.

Table 6.1: M3C2 results for the Hooper site.

Direction	Negative (Scour)		Positive (Accretion)	
Site Location	Region 1	Region 2	Region 1	Region 2
Median	-0.09	-0.07	0.08	0.07
Mean	-0.18	-0.14	0.17	0.13

The study at the Lincoln site compares point cloud data first collected on December 9, 2020, to that of April 23, 2021. Figure 6.5 shows the four regions of interest for the change detection at the Lincoln site. 'Regions 1 and 2" are located upstream at Haines Branch, 'Region 3' is in the proximity of the bridge, and 'Region 4' is located downstream of the stream. Figure 6.6 shows the M3C2 point cloud data output. The result of the statistical changes between the temporal point cloud data for each region is plotted in Figure 6.7. The median and mean value from the histogram is calculated and tabulated in Table 6.2. For this site, the data shows a median scour change of 0.17 meters in 'Region 1', 0.16 meters in 'Region 2' and 'Region 3', and scour change of 0.33 meters in 'Region 4', where the 95% confidence value is 0.56 meters (the region closest to the bridge).

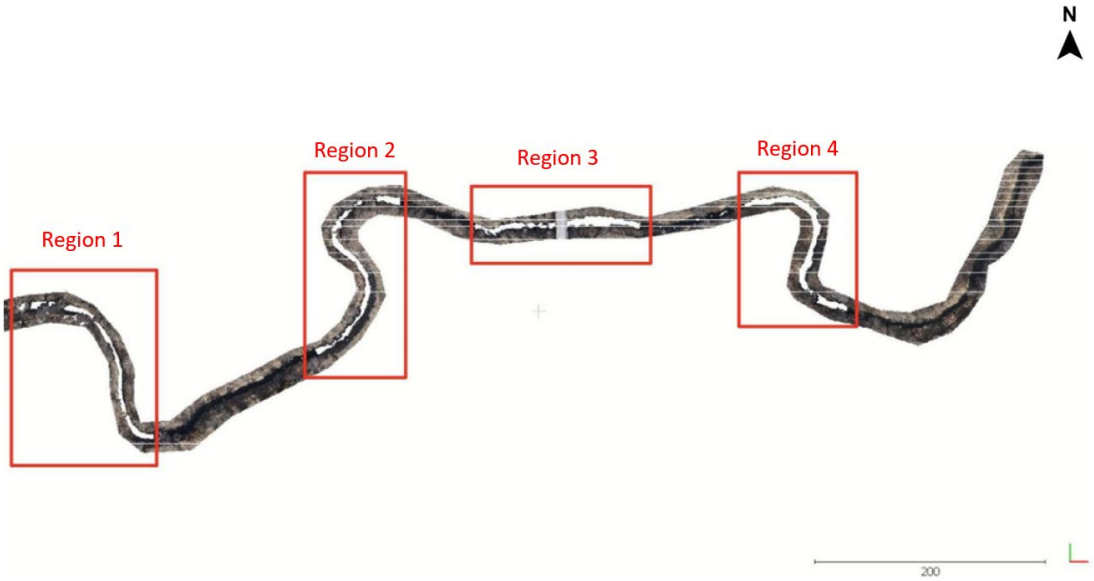

Figure 6.5: Region of interest for the Lincoln site.

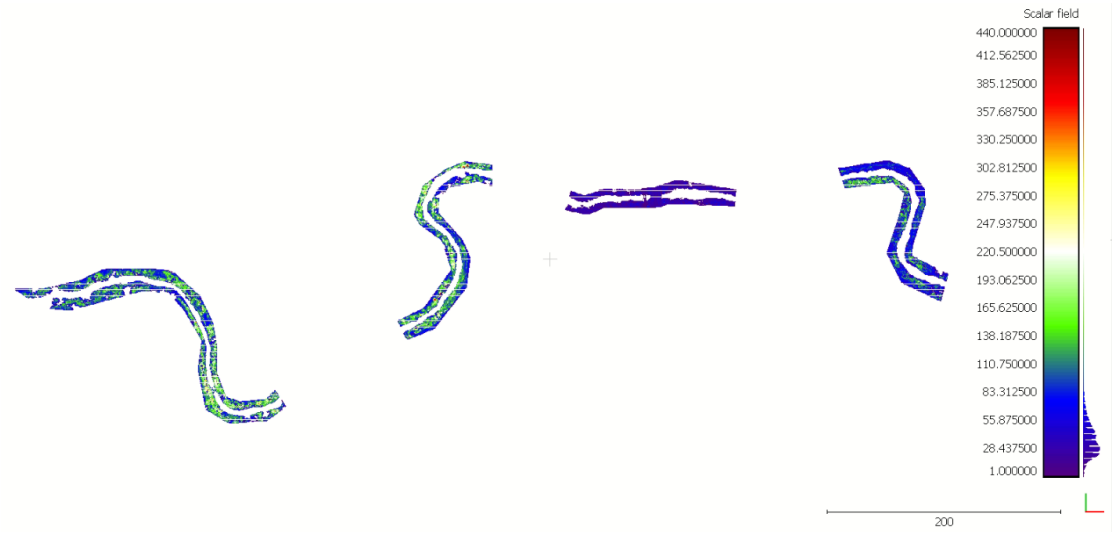

Figure 6.6: Change detection via M3C2 algorithm for the Lincoln site.

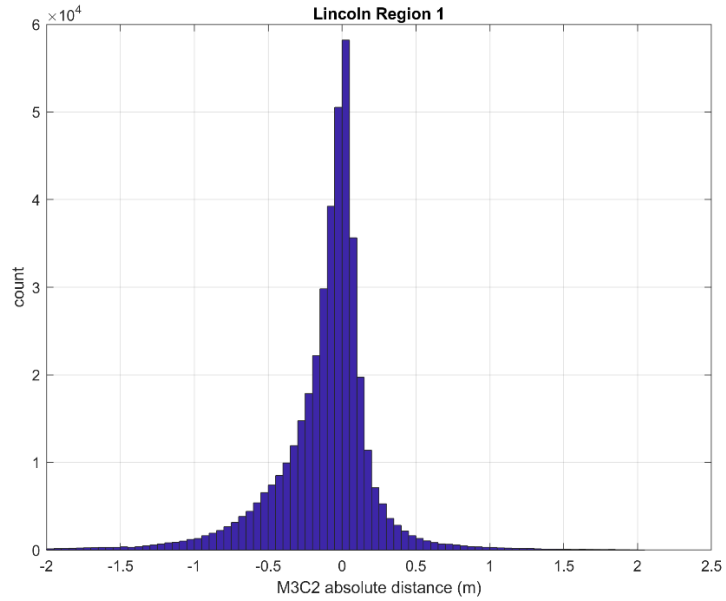
Lincoln Region 1
×10^4
6
5
4
3
2
1
0
count
-2
-1.5
-1
-0.5
0
0.5
1
1.5
2
2.5
M3C2 absolute distance (m)

(a)

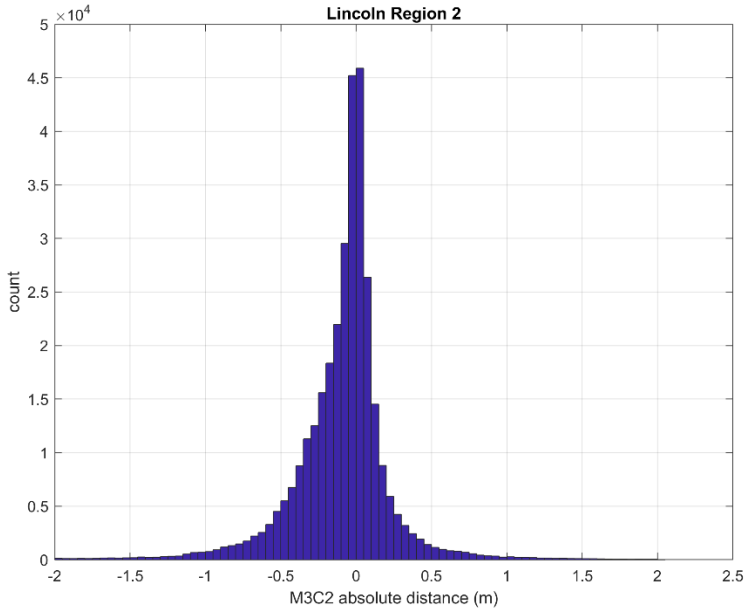
Lincoln Region 2
×10^4
5
4.5
4
3.5
3
2.5
2
1.5
1
0.5
0
count
-2
-1.5
-1
-0.5
0
0.5
1
1.5
2
2.5
M3C2 absolute distance (m)

(b)

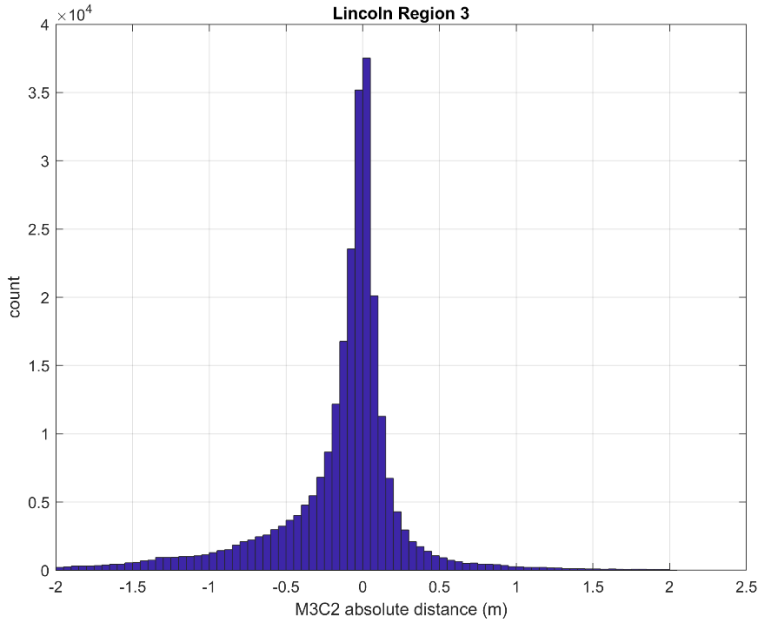

(c)

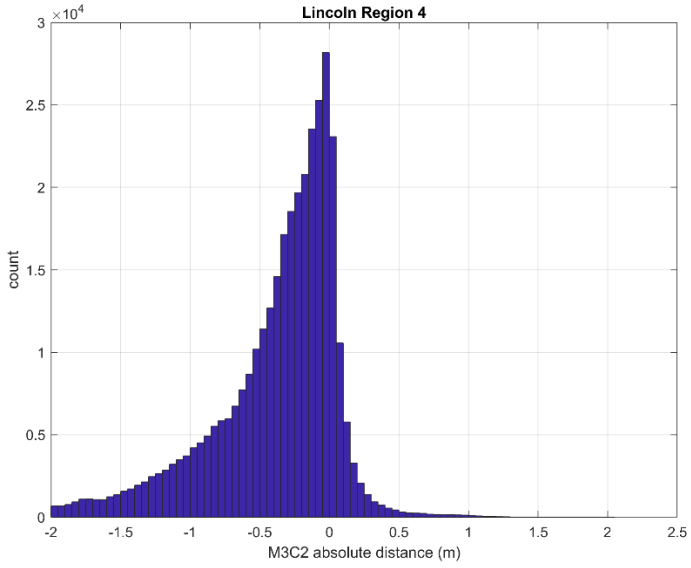

(d)

Figure 6.7: Change detection results for the Lincoln site (a) Region 1 (b) Region 2 (c) Region 3 (d) Region 4.

Table 6.2: M3C2 results for Lincoln site.

Direction	Negative (Scour)				Positive (Accretion)			
Site Location	Region 1	Region 2	Region 3	Region 4	Region 1	Region 2	Region 3	Region 4
Median	-0.1680	-0.1629	-0.1609	-0.3340	0.0741	0.0761	0.0749	0.0591
Mean	-0.2868	-0.2793	-0.3460	-0.4924	0.1527	0.1632	0.2124	0.1244

The study at the Wilber site compares point cloud data first collected on December 10, 2020, to that of April 24, 2021. Figure 6.8 shows the two regions of interest for the change detection at the Wilber site. ‘Region 1’ is located upstream of Turkey Creek, and ‘Region 2’ is located around the location of the bridge. Figure 6.9 shows the M3C2 point cloud data output. The result of the statistical changes between the temporal point cloud data for each region is plotted in Figure 6.10. The median and mean value from the histogram is calculated and tabulated in Table 6.3. For this site, the data shows a median scour change of 0.15 meters in ‘Region 1’, and 0.14 meters for ‘Region 2’, where the 95% confidence value is 0.66 meters (the region closest to the bridge).

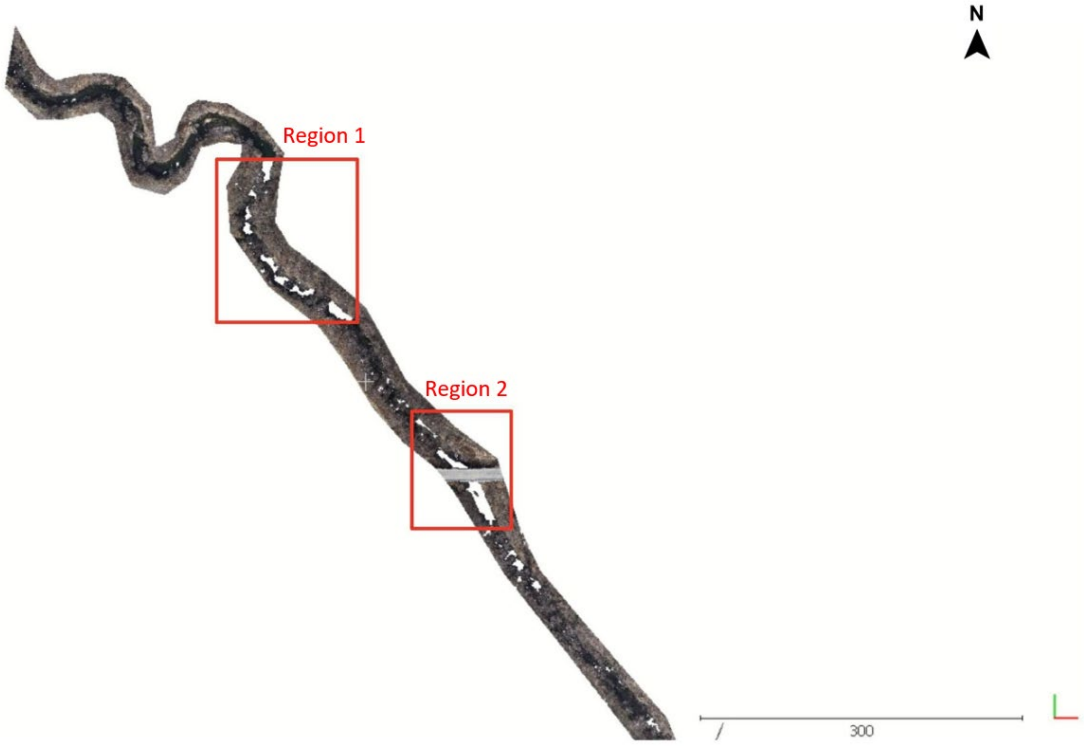

Figure 6.8: Region of interest for the Wilber site.

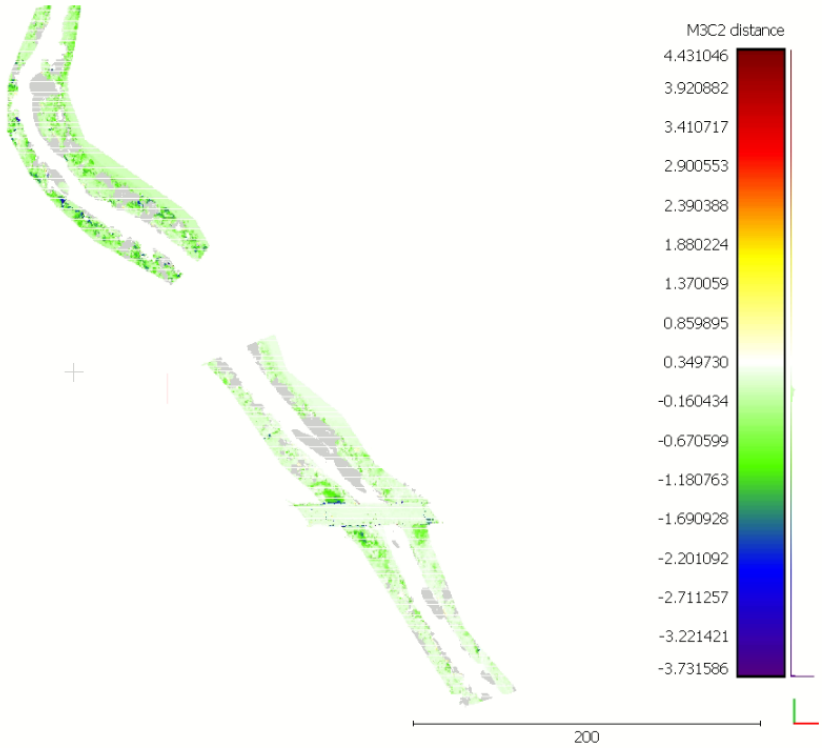

Figure 6.9: Change detection via M3C2 algorithm for the Wilber site.

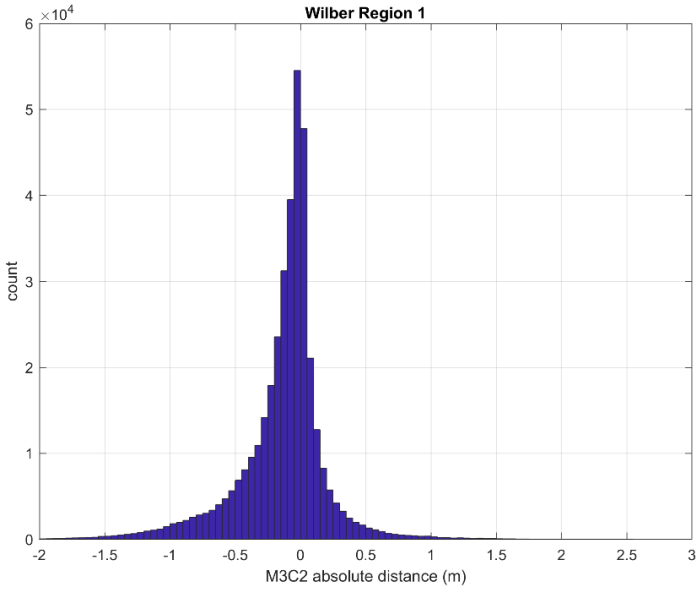

(a)

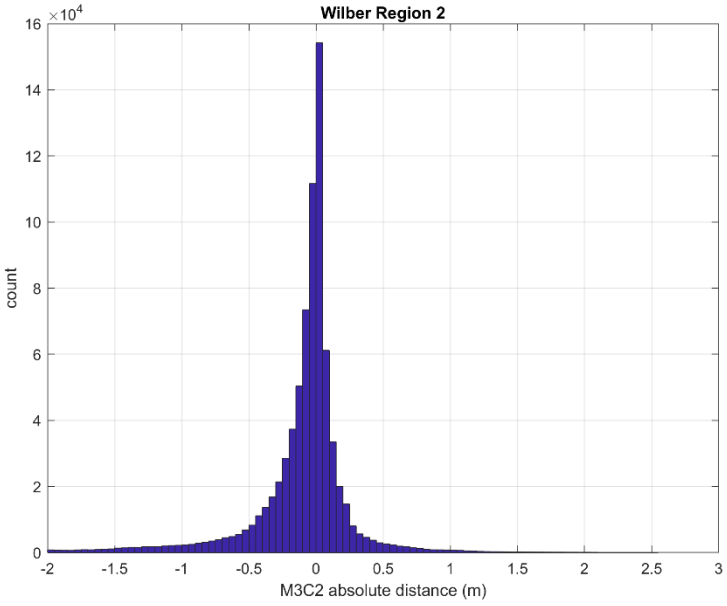

(b)

Figure 6.10: Change detection results for the Wilber site (a) Region 1 (b) Region 2.

Table 6.3: M3C2 results for Wilber site.

Direction	Negative (Scour)		Positive (Accretion)	
Site Location	Region 1	Region 2	Region 1	Region 2
Median	-0.1579	-0.1371	0.0735	0.0573
Mean	-0.2713	-0.3130	0.1632	0.1911

The study at the Beatrice site compares point cloud data first collected on December 10, 2020, to that of April 23, 2021. Figure 6.11 shows the two regions of interest for the change detection at the Wilber site. 'Region 1' is located upstream of the Big Blue River, and 'Region 2' is located around the location of the bridge. Figure 6.12 shows the M3C2 point cloud data output. The result of the statistical changes between the temporal point cloud data for each region is plotted in Figure 6.13. The median and mean value from the histogram is calculated and tabulated in Table 6.4. For this site, the data shows a median scour change of 0.08 meters in 'Region 1' and in 'Region 2', where the 95% confidence value is 0.93 meters (the region closest to the bridge).

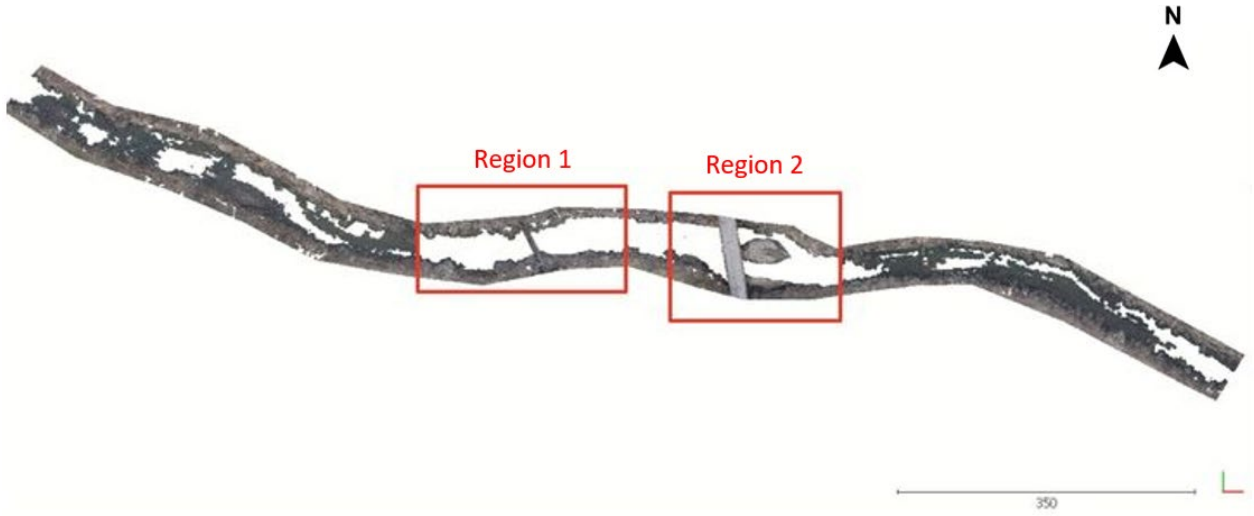

Figure 6.11: Region of interest for Beatrice site.

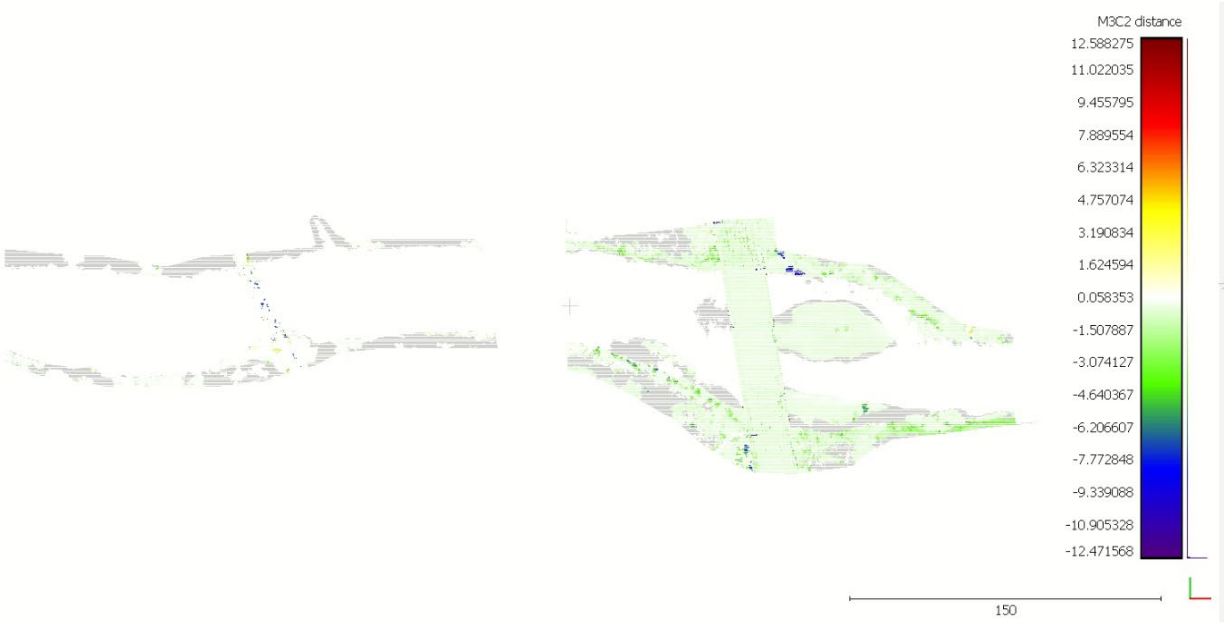

Figure 6.12: Change detection via M3C2 algorithm for Beatrice site.

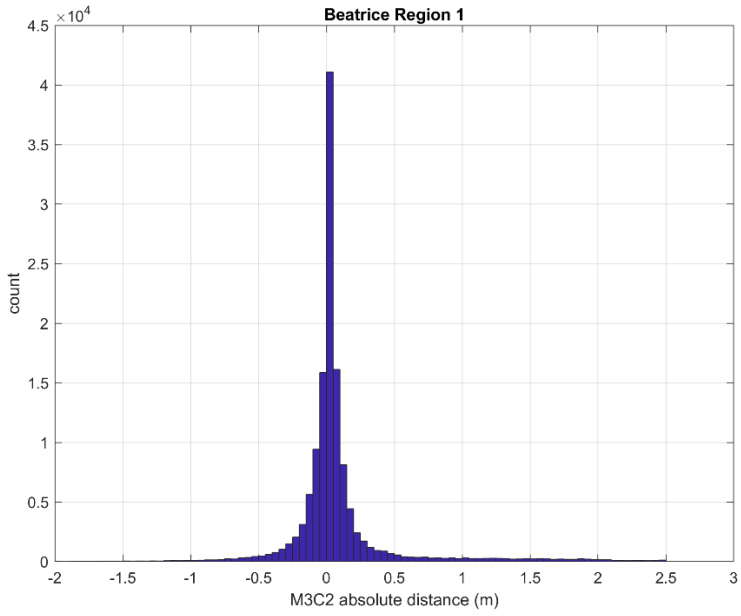

(a)

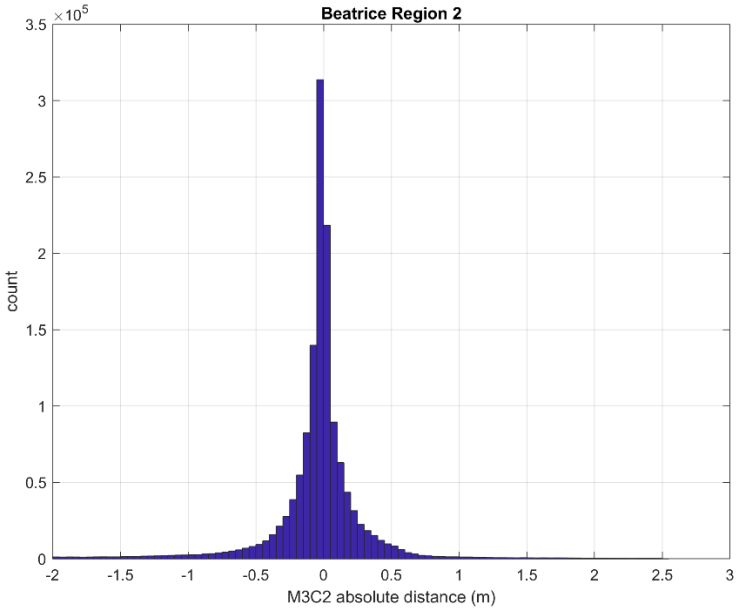

(b)

Figure 6.13: Change detection results for the Beatrice site (a) Region 1 (b) Region 2.

Table 6.4: M3C2 results for Beatrice site.

Direction	Negative (Scour)		Positive (Accretion)	
Site Location	Site 1	Site 2	Site 1	Site 2
Median	-0.0799	-0.0799	0.0654	0.0948
Mean	-0.3193	-0.2659	0.7595	0.5159

The representative change detection data are tabulated in Table 6.5. The representative value is the value which is closest to the real value of the statistical change measurements. The representative value, exclude those values that would be considered as point cloud data noises.

The representative median is the value of interest. The median shows there is an approximate scour change of 0.08 meters at the Hooper site, 0.07 meters at the Lincoln site, 0.15 meters at the Wilber site, and 0.08 meters at the Beatrice site.

Table 6.5: Summary of change detection values for all sites.

Site	Number of Locations	Representative Mean (m)	Representative Median (m)
Hooper	2	0.16	0.08
Lincoln	4	0.16	0.07
Wilber	2	0.29	0.15
Beatrice	2	0.29	0.08

The registration of lidar to UAS point cloud data have an alignment accuracy of 2 cm. The alignment was done based on the static points on the sites as a point of reference, such as the bridge deck, the bridge railing and the light posts.

6.2. DISCHARGE FLOW HISTORY

The project surveying period varies slightly for each site. For Hooper, this is between December 10, 2020, to April 23, 2021. For Lincoln, this monitoring period was from December 9, 2020, to April 23, 2021. At Wilber, this period is from December 10, 2020, to April 24, 2021, and finally, at Beatrice, this was from December 10, 2020, to April 23, 2021. Note these surveying periods are slightly different given the time and weather constraints in the field. Figure 6.14 to Figure 6.17 shows the discharge history of these sites during the surveying period. Note there were no substantial flows during these monitoring periods for any of the sites.

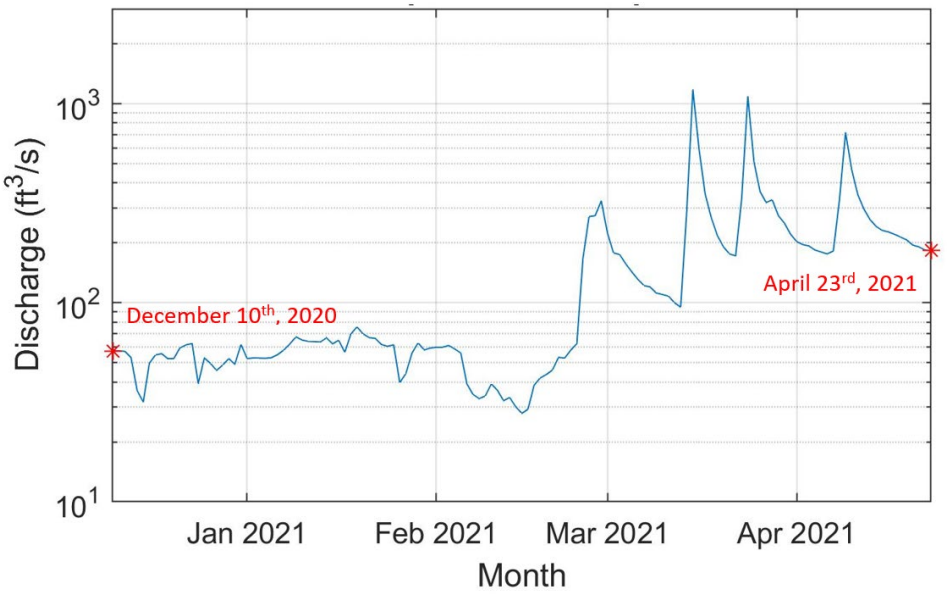

Figure 6.14: Discharge history for Hooper site.

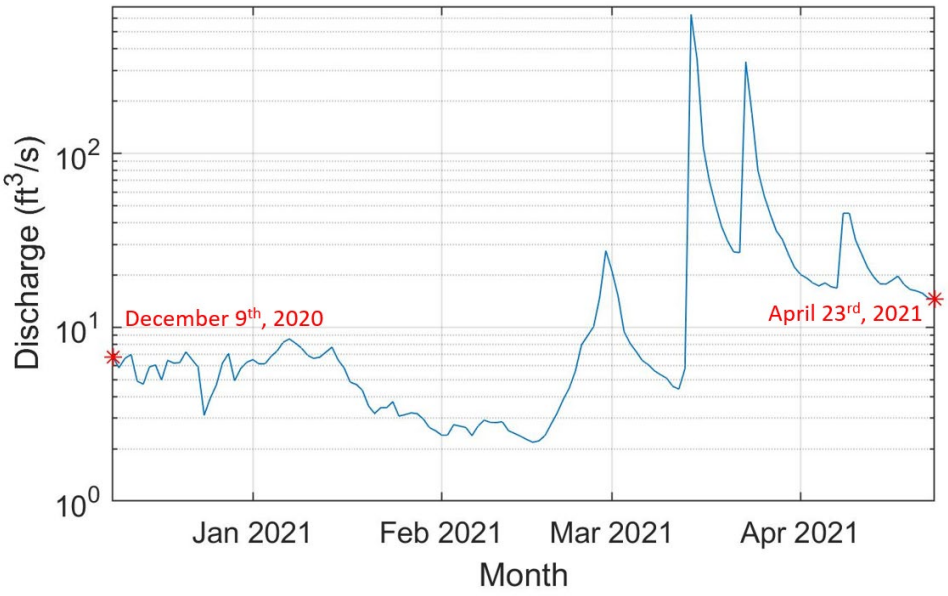

Figure 6.15: Discharge history for Lincoln site.

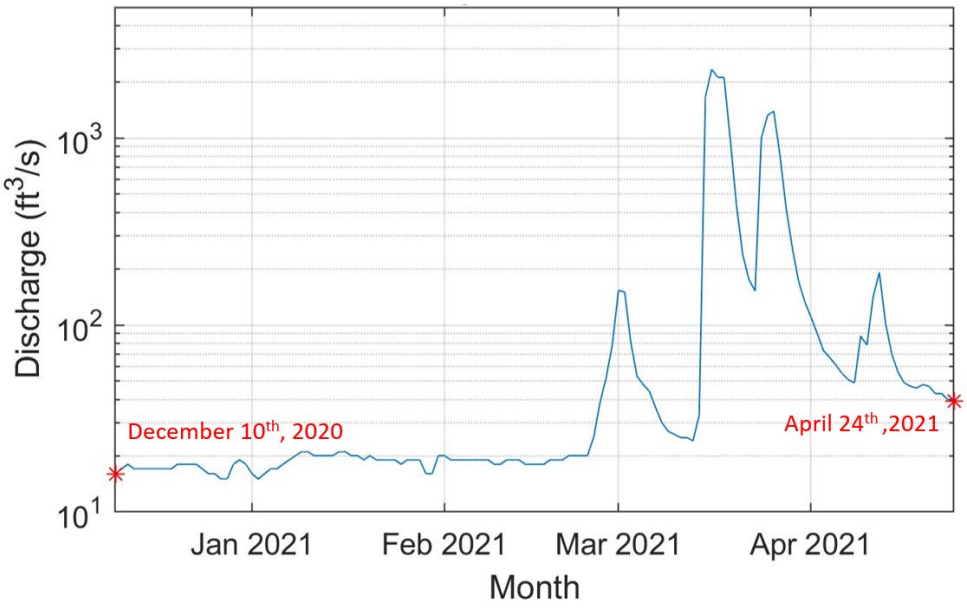

Figure 6.16: Discharge history for Wilber site.

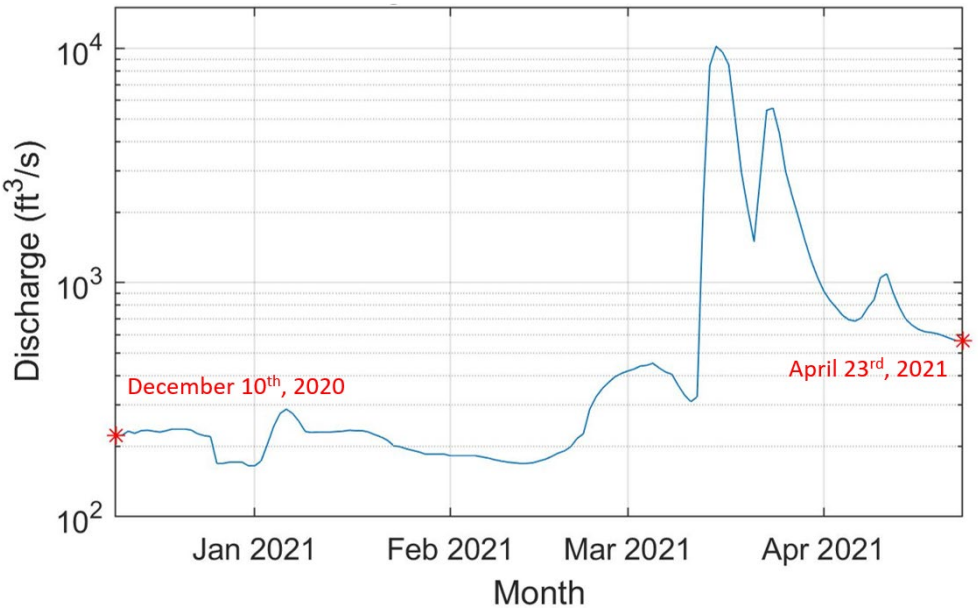

Figure 6.17: Discharge history for Beatrice site.

From the graphical plot of the discharge history, it shows that there are four prominent peak discharge events that occur during the surveying period at the Hooper, Lincoln, and Wilber sites. The Beatrice site however has prominent three peak discharge events. The highest flow discharges occurred around March 14 – 16, 2021. The peak flow discharge events and values are

tabulated in Table 6.6 and the peak flow discharge values associated with the stream's Q2 flood year event discharge is tabulated in Table 6.7. The maximum peak discharge event will be inputted into the hydraulic models and then compared with the previous M3C2 change detection values.

Table 6.6: Flow discharge events at each site.

Site	Event Date	Discharge, Q [ft^3/s]
Hooper	2/28/2021	325
	3/15/2021	1180
	3/24/2021	1090
	4/9/2021	716
Lincoln	2/28/2021	27.6
	3/14/2021	630
	3/23/2021	336
	4/8/2021	45.3
Wilber	2/28/2021	153
	3/15/2021	2330
	3/25/2021	1390
	4/11/2021	191
Beatrice	3/16/2021	10200
	3/25/2021	5560
	4/12/2021	1090

Table 6.7: Summary of peak flow for each site.

Site	Initial Visit	Final Visit	Peak Flow (cfs)	Associated Flow (years)
Hooper	December 10, 2020	April 23, 2021	1180	< Q2 (moderate)
Lincoln	December 09, 2020	April 23, 2021	630	< Q2 (moderate)
Wilber	December 10, 2020	April 24, 2021	2330	> Q2 (slightly)
Beatrice	December 10, 2020	April 23, 2021	10200	> Q2 (moderate)

6.3. BRIDGE SCOUR ANALYSIS

The bridge scour analysis is computed with HEC-RAS using the highly detailed terrain model created from the data collection as well as the HEC-RAS model provided by NDOT. The NDOT HEC-RAS model is used as a guideline and comparison of the two different geometric models. This analysis shows the difference in the scour depths findings between the two models.

There are ten hydraulic computations done for Hooper, Lincoln, and the Wilber site, one for each of the peak discharge events during the surveying period on both hydraulic models. Moreover, nine hydraulic computations were done for Beatrice due to only three flow discharge events being considered for this site. Each of these flow discharge events is run on our hydraulic model and NDOT's hydraulic model. These data are used to give an overview of the scour depths occurrence at the different flood year events and the scour changes during the study period.

6.3.1. Discharge Events

Using the peak discharge events tabulated in Tables 6.6 and 6.7, the scour results for each of these events are tabulated in Table 6.8 for the hydraulic model created with the highly detailed geospatial data. Moreover, and for comparison, Table 6.9 summarizes these scour computations for the model provided by NDOT. The hydraulic computations based on our hydraulic model and NDOT's model show that there are no scour depth changes occurring at Hooper. The difference between the combined scour depth is 0.36 meters for Lincoln, and 0.03 meters for Wilber for the first peak flow discharge on February 28, 2021.

The second discharge event between March 14-16, 2021, is considered for all four of the sites. The difference between the combined scour computed on our hydraulic model and NDOT's model is 0.02 meters for Hooper, 0.32 meters for Lincoln, 0.03 meters for Wilber, and 0.12 meters

at Beatrice. The third discharge event occurs between March 23-24, 2021. The difference between the combined scour depths is 0.02 meters for Hooper, 0.35 meters for Lincoln, 0.02 meters for Wilber, and 0.11 meters at the Beatrice site. The final discharge event occurs between April 8-12, 2021. The difference in the combined scour is 0.01 meters for Hooper, 0.34 meters for Lincoln, 0.01 meters for Wilber, and 0.40 meters at the Beatrice site.

From the results, NDOT computed zero scour depths for the sites during the surveying period at Hooper, but our hydraulic models did find there is contraction scour at the Hooper site, but it was minimal. Due to the limitations of this project, mainly being discharge events only at or below the Q2 flowrates, there was little to no contraction scour changes recorded during the monitoring period. Since Hooper only considers contraction scour, the scour changes recorded at this site is not as significantly larger than the other sites (which include pier scour). The Lincoln, Wilber, and Beatrice sites all demonstrate lower scour depths than that of the NDOT models. As long as these scour computations are accurate, this illustrates that the provided hydraulic models are more conservative. That is, in other words, the hydraulic models that were developed in this project with detailed terrain as equivalent D_{50} values often produced smaller scour depths.

Table 6.8: Discharge events during the surveying period based on the highly detailed terrain and equivalent D_{50} models.

Site	Event Date	Discharge, Q [ft^3/s]	**Combined Scour (m)**
Hooper	2/28/2021	325	**0.00**
	3/15/2021	1180	**0.02**
	3/24/2021	1090	**0.02**
	4/9/2021	716	**0.01**
Lincoln	2/28/2021	27.6	**0.58**
	3/14/2021	630	**1.10**
	3/23/2021	336	**0.98**
	4/8/2021	45.3	**0.65**
Wilber	2/28/2021	153	**0.31**
	3/15/2021	2330	**0.54**
	3/25/2021	1390	**0.54**
	4/11/2021	191	**0.34**
Beatrice	3/16/2021	10200	**1.60**
	3/25/2021	5560	**1.40**
	4/12/2021	1090	**0.95**

Table 6.9: Discharge events during the surveying period based on the NDOT provided hydraulic models.

Site	Event Date	Discharge, Q [ft^3/s]	**Combined Scour (m)**
Hooper	2/28/2021	325	**0.00**
	3/15/2021	1180	**0.00**
	3/24/2021	1090	**0.00**
	4/9/2021	716	**0.00**
Lincoln	2/28/2021	27.6	**0.94**
	3/14/2021	630	**1.42**
	3/23/2021	336	**1.33**
	4/8/2021	45.3	**0.99**
Wilber	2/28/2021	153	**0.34**
	3/15/2021	2330	**0.57**
	3/25/2021	1390	**0.52**
	4/11/2021	191	**0.35**
Beatrice	3/16/2021	10200	**1.72**
	3/25/2021	5560	**1.51**
	4/12/2021	1090	**1.35**

6.3.2. Flood-Year Events

Using the HEC-RAS hydraulic model, the scour depths of the typical flood year events are calculated. These flood year events are the 2-year, 10-year, 25-year, 50-year, 100-year, and 500-year flood events. The scour depth findings for the hydraulic models are tabulated in Table 6.10 to Table 6.15. These events are provided for future validation and investigation, but all of these events are either similar or slightly smaller than that of the NDOT-provided hydraulic models.

Table 6.10: Scour findings for Q2 with the highly detailed terrain and equivalent D_{50} model.

Site Location	Contraction Scour (m)	Pier Scour (m)	**Combined Scour (m)**
Hooper	0.04	0.00	**0.04**
Lincoln	0.00	1.24	**1.24**
Wilber	0.00	0.53	**0.53**
Beatrice	0.00	1.42	**1.42**

Table 6.11: Scour findings for Q10 with the highly detailed terrain and equivalent D_{50} model.

Site Location	Contraction Scour (m)	Pier Scour (m)	**Combined Scour (m)**
Hooper	0.06	0.00	**0.06**
Lincoln	0.10	1.52	**1.62**
Wilber	0.00	0.69	**0.69**
Beatrice	0.00	1.65	**1.65**

Table 6.12: Scour findings for Q25 with the highly detailed terrain and equivalent D_{50} model.

Site Location	Contraction Scour (m)	Pier Scour (m)	**Combined Scour (m)**
Hooper	0.45	0.00	**0.45**
Lincoln	0.11	1.62	**1.74**
Wilber	0.00	0.77	**0.77**
Beatrice	0.00	2.03	**2.03**

Table 6.13: Scour findings for Q50 with the highly detailed terrain and equivalent D_{50} model.

Site Location	Contraction Scour (m)	Pier Scour (m)	**Combined Scour (m)**
Hooper	1.16	0.00	**1.16**
Lincoln	0.14	1.69	**1.82**
Wilber	0.00	0.83	**0.83**
Beatrice	0.00	2.16	**2.16**

Table 6.14: Scour findings for Q100 with the highly detailed terrain and equivalent D_{50} model.

Site Location	Contraction Scour (m)	Pier Scour (m)	**Combined Scour (m)**
Hooper	1.68	0.00	**1.68**
Lincoln	0.20	1.54	**1.74**
Wilber	0.00	0.89	**0.89**
Beatrice	0.00	2.47	**2.47**

Table 6.15: Scour findings for Q500 with the highly detailed terrain and equivalent D_{50} model.

Site Location	Contraction Scour (m)	Pier Scour (m)	**Combined Scour (m)**
Hooper	3.19	0.00	**3.19**
Lincoln	0.52	1.83	**2.34**
Wilber	0.00	0.96	**0.96**
Beatrice	0.59	2.70	**3.29**

6.4. DATA-DRIVEN SCOUR VALIDATION

This section discusses the data-driven observations made to achieve the objectives of the project and outlines recommendations for potential implementation. The change detection results of the combined point cloud data (overland and bathymetry data) are used to analyze and observe scour changes on CloudCompare, using the M3C2 computations on CloudCompare. The hydraulic computations of the hydraulic models on HEC-RAS are used for the bridge scour analysis, similar to the existing methods at NDOT.

The scour analysis data from HEC-RAS is directly compared with the quantified changes detected with the M3C2 computations which are tabulated in Table 6.16. The table also includes the comparison of the scour depths using the NDOT models. Both models were subjected to identical flow rates.

The comparison of these values shows that the M3C2 data obtained from the change detection process is lower than the combined scour calculated through HEC-RAS, but on the same order of magnitude. During the project period, the hydraulic computations show that the contraction scour at the Wilber and Beatrice is zero, while the pier scour is 0.54 meters for the Wilber site and 1.60 meter for the Beatrice site. This is mainly because the M3C2 results cannot

accurately measure the pier scour. Therefore, the obtained M3C2 data would not be able to be compared to the combined scour data. This limitation of the M3C2 data results from accretion and deposit of sediment following peak discharge events.

During this project, two high-flood events were assessed during this project using an additional surveying tool of a sonar device (or fish finder). These surveys were conducted at Wilber and Beatrice. At the Lincoln site, pier scour calculations from HEC-RAS do not account for the riprap (or large stones) providing some scour protection. At Wilber, pier scour depths were measured to be similar to that of the predicted depths in the field, but in this early deployment of the equipment (without an external GPS antenna) this data was not able to be saved and plotted reliably in map form. However, at Beatrice, the pier scour measured during the peak discharge event is very similar to that as predicted within HEC-RAS, indicating the HEC-RAS models are in close agreement with that as measured in the field. The contour created based on the data captured by Humminbird sonar device shows 5 feet (1.5 meters) pier scour depth as shown in Figure 6.18.

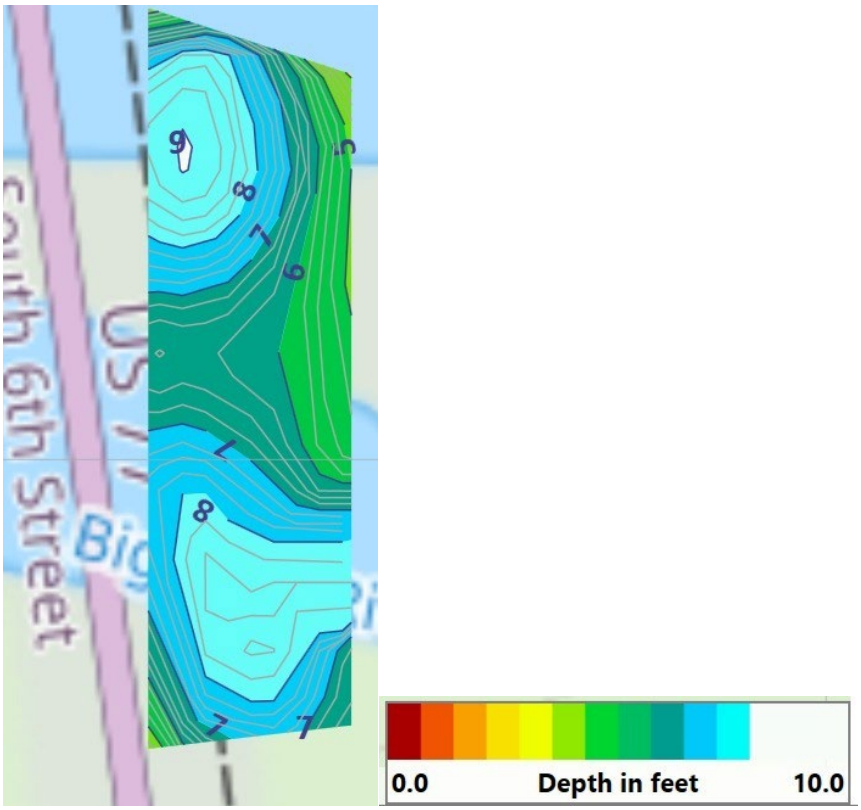

Figure 6.18: Beatrice contour based on the Humminbird sonar device for the pier scour.

Moreover, the hydraulic computations performed using the developed HEC-RAS model yield a lower peak combined scour in comparison to the NDOT-provided models. The HEC-RAS model created incorporates both high-resolution geometry (from the UAS, lidar, and bathymetry) and equivalent D_{50} values. The developed Hooper site hydraulic model shows that there is indeed a contraction scour of 0.02 meters at the site for the peak discharge event during the project period. This value is non-zero while the NDOT model does not compute contraction scour for Hooper. Based on the Q100 flow rate (Table 6.14) of the Hooper site, the contraction scour is overall lower by 1.67 meters than the NDOT Q100 contraction scour (1.68 meters versus 3.35 in the NDOT model).

The data also shows that the peak discharge scour is 1.14 meters for the Lincoln site, 0.54 meters for the Wilber site, and 1.60 meters for the Beatrice site for our hydraulic model. The scour

depths are lower by 0.28 meters for the Lincoln site, 0.03 meters for the Wilber site, and 0.12 meters for the Beatrice site. The lower scour depth findings identify that high-resolution geometry and the equivalent D_{50} values findings are less conservative than the current procedures and appear to be reasonable based on the field observations.

Table 6.16: Scour depth comparison of the peak flow discharge of our model, NDOT model and the change detection values (M3C2).

	Our Model			**NDOT model**			**M3C2 Data**		
Site	**Peak Total Discharge Scour (m)**	**Peak Pier Scour (m)**	**Peak Contraction Scour (m)**	**Peak Total Discharge Scour (m)**	**Peak Pier Scour (m)**	**Peak Contraction Scour (m)**	**Median (m)**	**Mean (m)**	**95% Confidence Interval (m)**
Hooper	0.02	0.00	0.02	0.00	0.00	0.00	0.08	0.16	0.39
Lincoln	1.14	1.10	0.04	1.42	1.08	0.35	0.07	0.16	0.56
Wilber	0.54	0.54	0.00	0.57	0.57	0.00	0.15	0.29	0.66
Beatrice	1.60	1.60	0.00	1.72	1.72	0.00	0.08	0.29	0.93

6.5. CONCLUSIONS

The findings based on the data-driven scour validation demonstrate the following conclusions:

- The hydraulic computations done with the developed HEC-RAS model yield a lower peak combined scour in comparison to the NDOT-provided model. This incorporates both high-resolution geometry (from the UAS, lidar, and bathymetry) and equivalent D_{50} values.
- The developed Hooper site model shows that there is indeed contraction scour of 0.02 meter at the site for the peak discharge event during the project period.
- The M3C2 data obtained from the change detection process is lower than the combined scour calculated through HEC-RAS, but on the same order of magnitude. This is mainly because the M3C2 results cannot accurately measure the pier scour. Therefore, the obtained M3C2 data would not be able to be compared to the combined scour data. This limitation of the M3C2 data results from accretion and deposit of sediment following peak discharge events. Note that many of the deeper pier scour holes typically fill up with transported sediment.
- During this project, two high-flood events were assessed during this project. This was at Wilber and Beatrice. At Wilber, pier scour depths were measured to be similar to that of the predicted depths in the field, and at Beatrice, the pier scour measured during the peak discharge event is very similar to that as predicted within HEC-RAS, indicating the HEC-RAS models are in close agreement with that as measured in the field.
- Based on the computations made and with the limitations of this project, mainly being discharge events only at or below the Q2 flowrates, the combination of the highly detailed

terrain model and the soil characterization findings of the D_{50} value produce values closer to the field-verified conditions.

CHAPTER 7 – CONCLUSIONS

7.1. REPORT SUMMARY

Bridge scour is a leading cause of bridge closures and failures in the country and Nebraska (Nebraska Legislature, 2014), and it is crucial to consider the impact of scour to the structural integrity of the bridge for continued operation and life safety. The current guidelines used by the state of Nebraska, which match that of HEC 18, may be considered as an over-conservative evaluation of scour, however, this is not definite for all cases. This study concentrates on how the uncertainty of the scour predictions can be reduced by evaluating and providing guidance on reasonable scour estimates for Nebraska soil and hydraulic conditions. This study addresses whether the current numerical scour predictions are "unconservative" or "over-conservative".

Four sites were surveyed for scour changes between December 9, 2020, to April 20, 2021, which are located in Hooper, Lincoln, Wilber, and Beatrice. High accuracy and high-fidelity geospatial data of the overland and bathymetry data were collected between these periods. The overland and bathymetry data are then fused to create a three-dimensional model for all the four bridge sites selected for the study. The temporal scour rate is analyzed by importing the combined geospatial data collected into HEC-RAS.

HEC 18 (FHWA, 2012) conservatively assumes that the ultimate scour in cohesive soils can be as deep as the scour in loose granular soils (or sands), which leads to potentially highly inaccurate scour estimates and the potential for over-designed and costly bridge foundations. Cohesive soils have many factors that affect erodibility compared to cohesionless soils. Therefore, compared to cohesive soils, cohesionless soils can be correlated to D_{50} easily. The equivalent D_{50}

value needed for the hydraulic model input for each site is based on the soil properties results made from the twenty-one soil erosion tests using the mini-JET erosion test.

The temporal scour rate is determined by implementing the rasterized combined geospatial data and the equivalent D_{50} values to the 1D hydraulic HEC-RAS models. Data observations are made to achieve the objectives of the project and outline recommendations. The combined point cloud data are also used to analyze and observe scour changes using the change detection method based on the M3C2 computations within CloudCompare. The scour analysis data from HEC-RAS is then directly compared with the quantified changes detected with the M3C2 computations. The study is concluded by discussing the findings and results and providing recommendations for a revised scour analysis procedure.

7.2. CONCLUSIONS

Based on the findings and results of the study, the following conclusions are made:

1. The mini-JET erosion test results show a high erosion coefficient with a relatively high critical shear stress, indicating that the riverbed soils at each site can generally erode fast but not deep. The results of this study are in good agreement with similar studies in the region (Briaud et al., 2017). Moreover, this methodology outputs a project-specific D_{50} value that is field-validated and used within the HEC-RAS models.
2. The results show that the hydraulic computations based on the representative D_{50} values with point cloud data on HEC-RAS are either similar or significantly smaller than the current HEC-RAS models. This method shows that the current method employed by

NDOT, or its consultants are potentially more conservative for simulated Q100 flow events.

3. The bridge scour analysis is computed with HEC-RAS using the highly detailed terrain model created from the data collection as well as other input parameters held consistent from the HEC-RAS model provided by NDOT. This analysis shows the difference in the scour depths findings between the two models. The lower scour depth findings show that high-resolution geometry and the equivalent D_{50} values are less conservative than the current procedures. This validates the limitations of the existing scour procedure and the promise of the proposed implementation.
4. The method of using high-fidelity geospatial data for bridge scour analysis yields scour values that are more reasonable therefore would lead to reduced bridge closures, structural savings for new bridge design, and enhanced knowledge of scour models.
5. The obtained M3C2 data would not be able to be compared to the combined scour data. This limitation of the M3C2 data alone results from accretion and deposit of sediment following peak discharge events at piers. However, the project team was able to verify consistent pier scour holes before they were filled through the use of a sonar device.

7.3. FUTURE WORK AND RECOMMENDATIONS FOR EXISTING WORKFLOWS

The conclusions identified the limitations of the change detection process presented in this study that could potentially be done for future research work to be implemented and improved upon. This includes the following:

1. Additional periods of monitoring should be considered, particularly during intervals that experience large peak discharge events. This current student was only able to examine events below the Q2 threshold.
2. The topography data may be improved using ground-based lidar for more scans. This is particularly true for riverbanks with a significant amount of vegetation. However, while this may produce more data points, the registration errors associated with an open traverse would compound. The benefits and limitations of this would have to be explored for feasibility.
3. The use of FLOW-3D can be explored. FLOW-3D is a detailed computational fluid dynamics (CFD) software. This software can incorporate the three-dimensional point cloud data for a more detailed scour computation. FLOW-3D would be the ideal local scour simulator for short episodic time scales; however, this level of analysis may not be considered for potential implementation into routine practice.
4. Implementing the study of stratified soil profiles for detailed site characterization and classification would yield a more accurate D_{50} value. With the presence of stratified soil with different erosion rates at varying layers, the mean of the particle size for each layer is of value to determine a more accurate scour depth. Since the varying flood events affect the different scour depths, the findings of the stratified soil properties along with the varying flood events would yield a much less conservative scour depth value. This is particularly true for large flow events; however, these flow events were not experienced during the monitoring period.

REFERENCES

Arneson, L. A., Zevenbergen, L. W., Lagasse, P. F., & Clopper, P. E. (2012). Evaluating scour at bridges (No. FHWA-HIF-12-003). National Highway Institute (US).

Al-Madhhachi, A. S. T., Hanson, G. J., Fox, G. A., Tyagi, A. K., & Bulut, R. (2013). Measuring soil erodibility using a laboratory "mini" JET. Transactions of the ASABE, 56(3), 901-910.Chicago

Briaud, J. L., Jung, I., Govindasamy, A., Kim, D., & Lee, J. (2018). The Observation Method for Bridge Scour: Case Histories. ISSMGE International Journal of Geoengineering Case Histories, 4(3), 185-202.

Briaud, J. L., Govindasamy, A. V., & Shafii, I. (2017). Erosion charts for selected geomaterials. Journal of geotechnical and geoenvironmental engineering, 143(10), 04017072.

Briaud, J. L., Gardoni, P., & Yao, C. (2014). Statistical, risk, and reliability analyses of bridge scour. Journal of Geotechnical and Geoenvironmental Engineering, 140(2), 04013011.

Brunner, G. W. (2002). Hec-ras (river analysis system). In North American water and environment congress & destructive water (pp. 3782-3787). ASCE.

Chaudhuri, S., & Debnath, K. (2013). Observations on initiation of pier scour and equilibrium scour hole profiles in cohesive sediments. ISH Journal of Hydraulic Engineering, 19(1), 27-37.

DJI Mavic Pro 2. (2022). DJI. photograph. Retrieved from https://www.dji.com/mavic-2.

Duncan, J. M., & Chang, C. Y. (1970). Nonlinear analysis of stress and strain in soils. Journal of the soil mechanics and foundations division, 96(5), 1629-1653.

Fu, G., Wang, Q., Chi, J., Lwin, M., & Corotis, R. (2020). Proposed AASHTO Load Rating Provisions for Implements of Husbandry (No. Project 12-110).

Ghazvinei, P. T., Mohamed, T. A., Ghazali, A. H., & Huat, B. K. (2012). Scour hazard assessment and bridge abutment instability analysis. Electron. J. Geotech. Eng, 17, 2213-2224.

Gjunsburgs, B., Govsha, J., & Lauva, O. (2014). Scour at layered riverbed: reason of the structures failure. In Environmental Engineering. Proceedings of the International Conference on Environmental Engineering. ICEE (Vol. 9, p. 1). Vilnius Gediminas Technical University, Department of Construction Economics & Property.

Govindasamy, A. V., & Briaud, J. L. (2014). Application of the observation method for scour to two Texas bridges. In Geo-Congress 2014: Geo-characterization and Modeling for Sustainability (pp. 2640-2654).

Hall, M. (1995). Calibration of the Maryland Abutment-Scour Equation Using a Modified Critical Velocity. https://www2.usgs.gov/water/southatlantic/sc/projects/bridgescour/index.html

Hanson, G. J., & Cook, K. R. (2004). Apparatus, test procedures, and analytical methods to measure soil erodibility in situ. Applied engineering in agriculture, 20(4), 455.

Hanson, G. J., & Simon, A. (2001). Erodibility of cohesive streambeds in the loess area of the midwestern USA. Hydrological processes, 15(1), 23-38.

Hanson, G. J., & Cook, K. R. (1997). Development of excess shear stress parameters for circular jet testing. ASAE Paper, 972227.

Muhsen, N. A., Khassaf S. (2021). Effect of Local Scour Interference Between Circular Bridge Pier and Different Shapes of Abutment.

Nebraska legislature (2014). The alarming conditions of Nebraska's Rural Bridges study report: L.R. 528 Study Report. Nebraska Legislature Transportation & Telecommunications Committee. https://nebraskalegislature.gov/pdf/reports/committee/transport/2014_lr528.pdf

Simon, A., Bankhead, N., Thomas, R., & Klimetz, L. (2010). Iterative bank-stability and toe-erosion modeling for predicting streambank loading rates and potential load reductions. USDA-ARS, National Sedimentation Laboratory.

Wood, R. L., Kim, Y. R., Liao, Y., & Mohammadi, M. E. (2020). Improvement of Low Traffic Volume Gravel Roads in Nebraska.

Appendix A
Bridge Plans

List of Figures

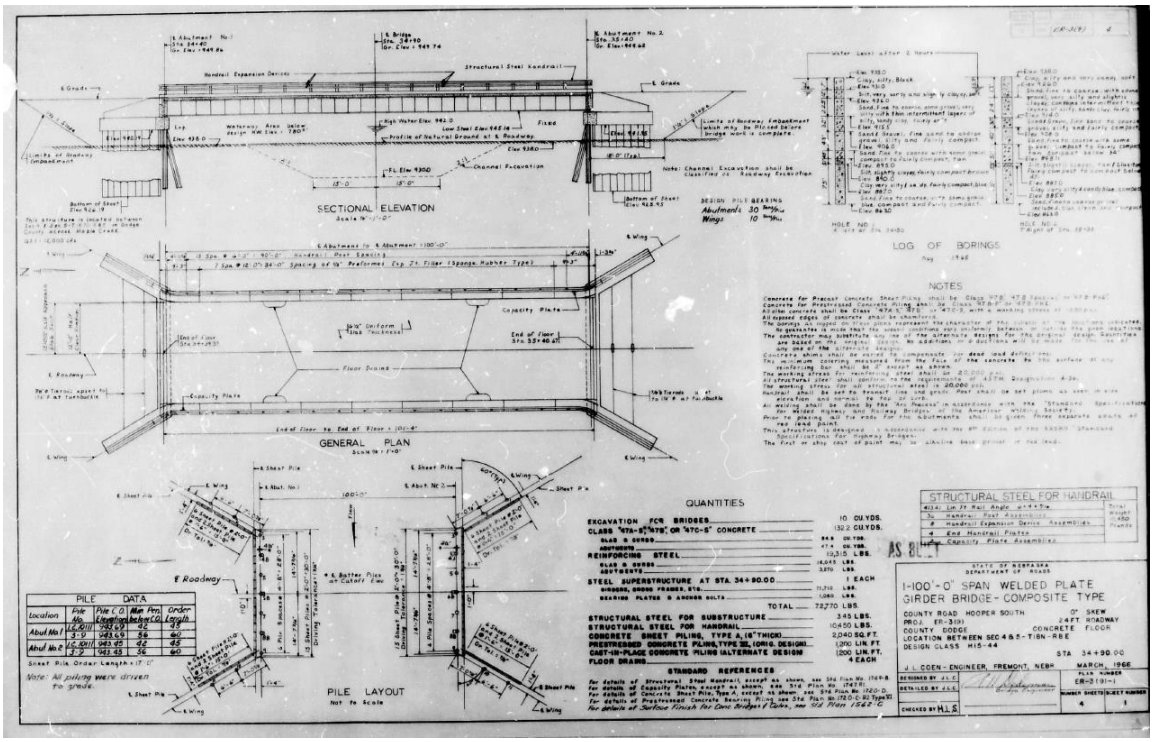

Figure A.1: Hooper Bridge Plan (courtesy of NDOT).

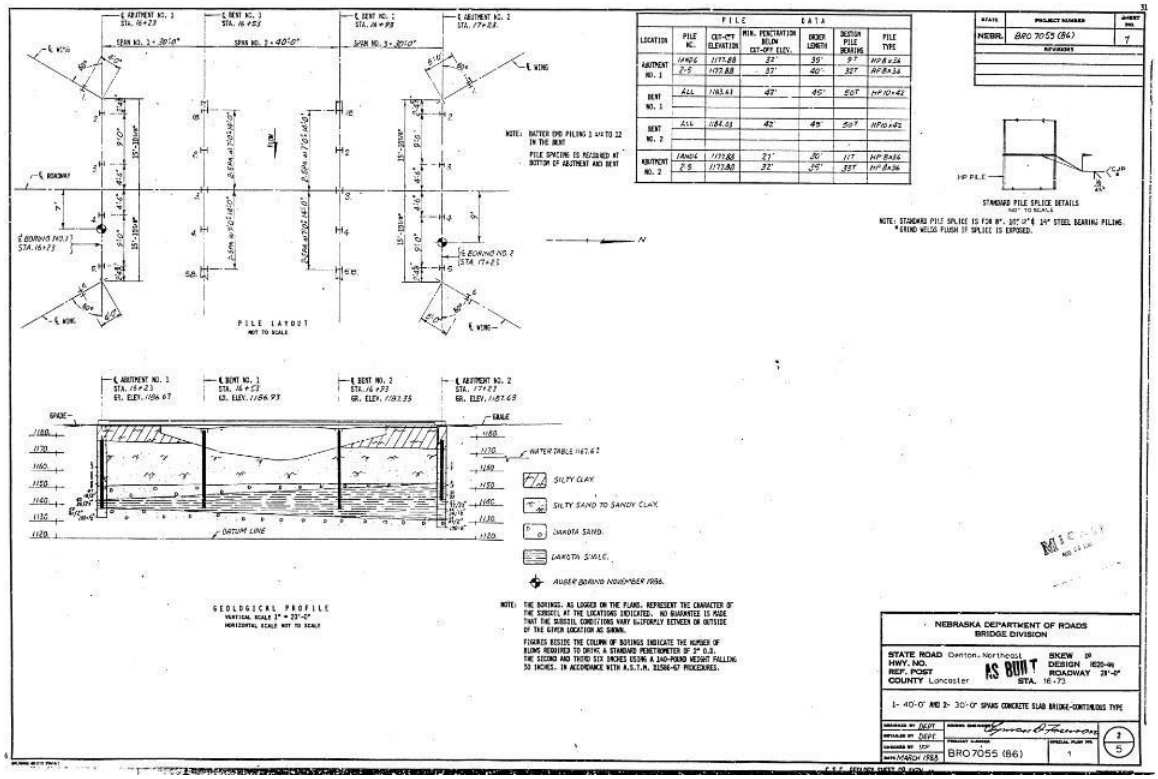

Figure A.2: Lincoln Bridge Plan (courtesy of NDOT).

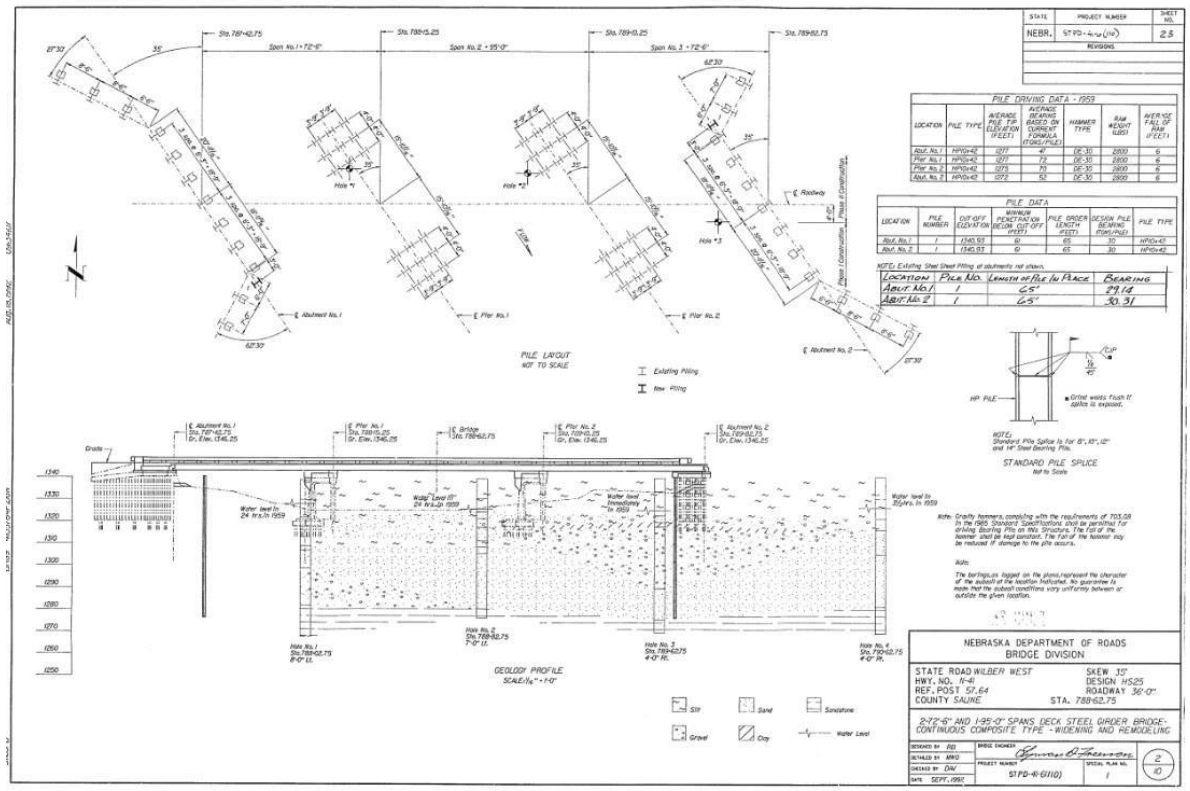

Figure A.3: Wilber Bridge Plan (courtesy of NDOT).

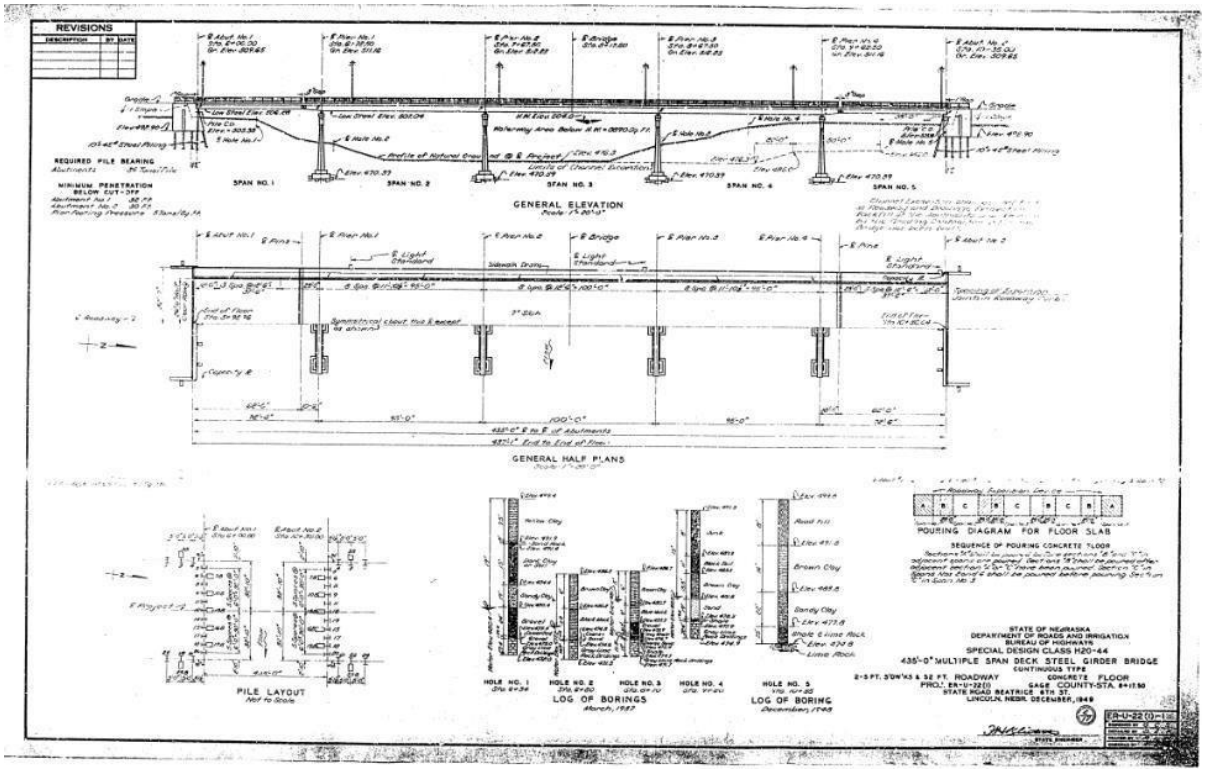

Figure A.4: Beatrice Bridge Plan (courtesy of NDOT).

Appendix B

Gradation Curves

List of Figures

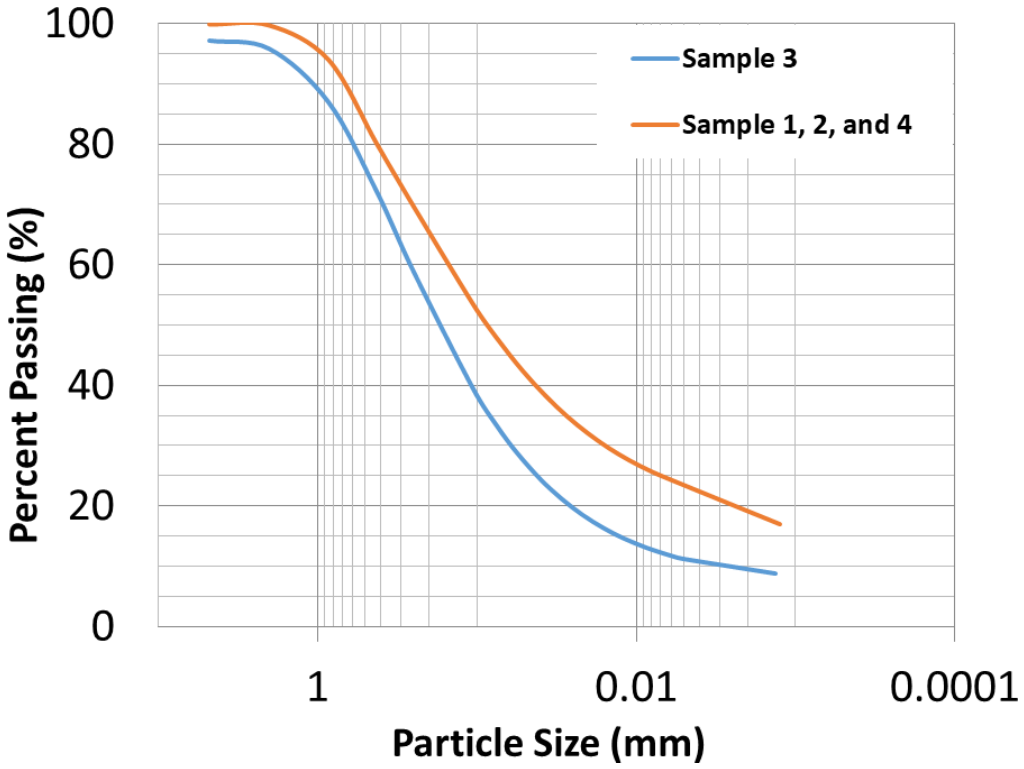

Figure B.1: Gradation curves for samples in Lincoln site.

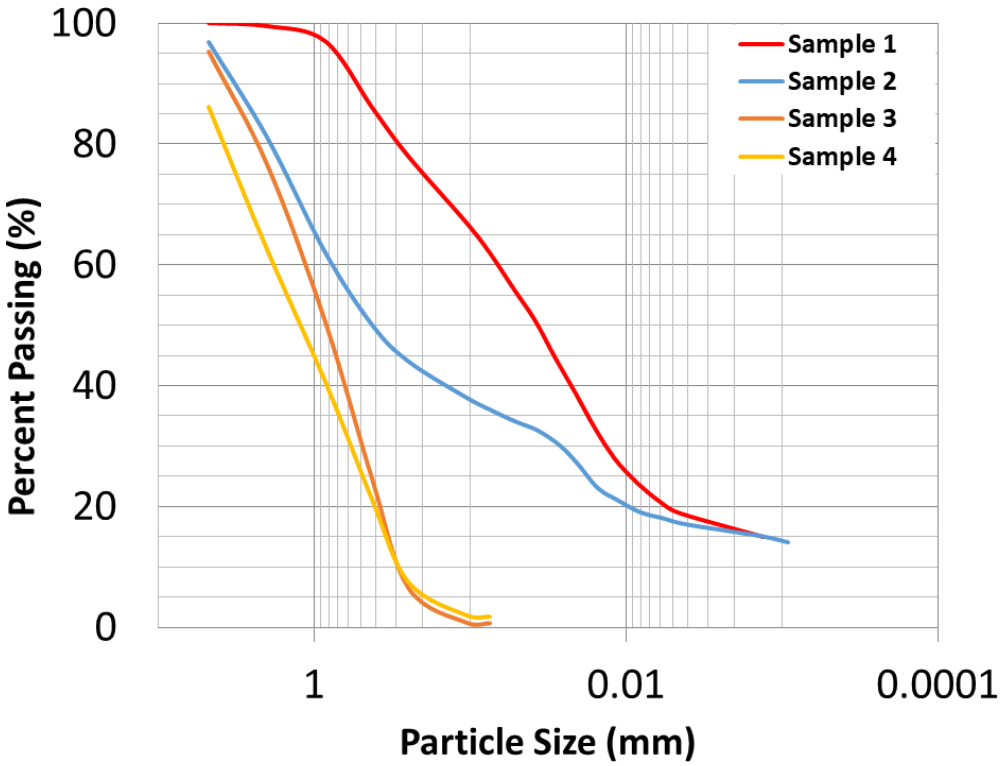

Figure B.2: Gradation curves for samples in Wilber site.

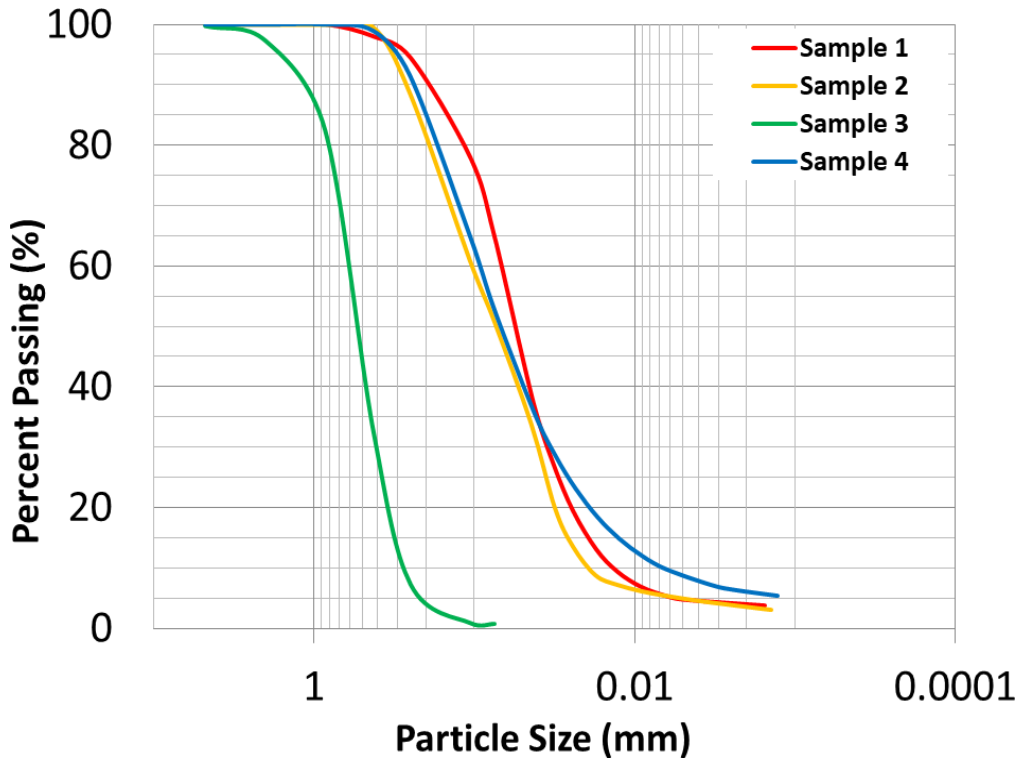

Figure B.3: Gradation curves for samples in Hooper site.

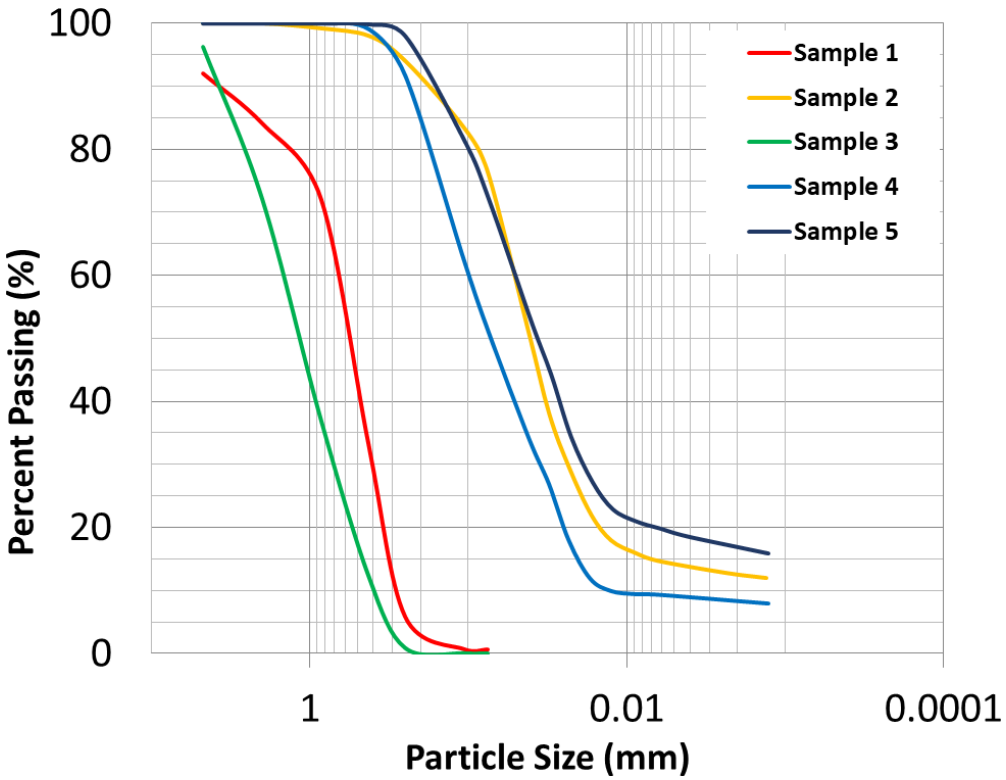

Figure B.4: Gradation curves for samples in Beatrice site.

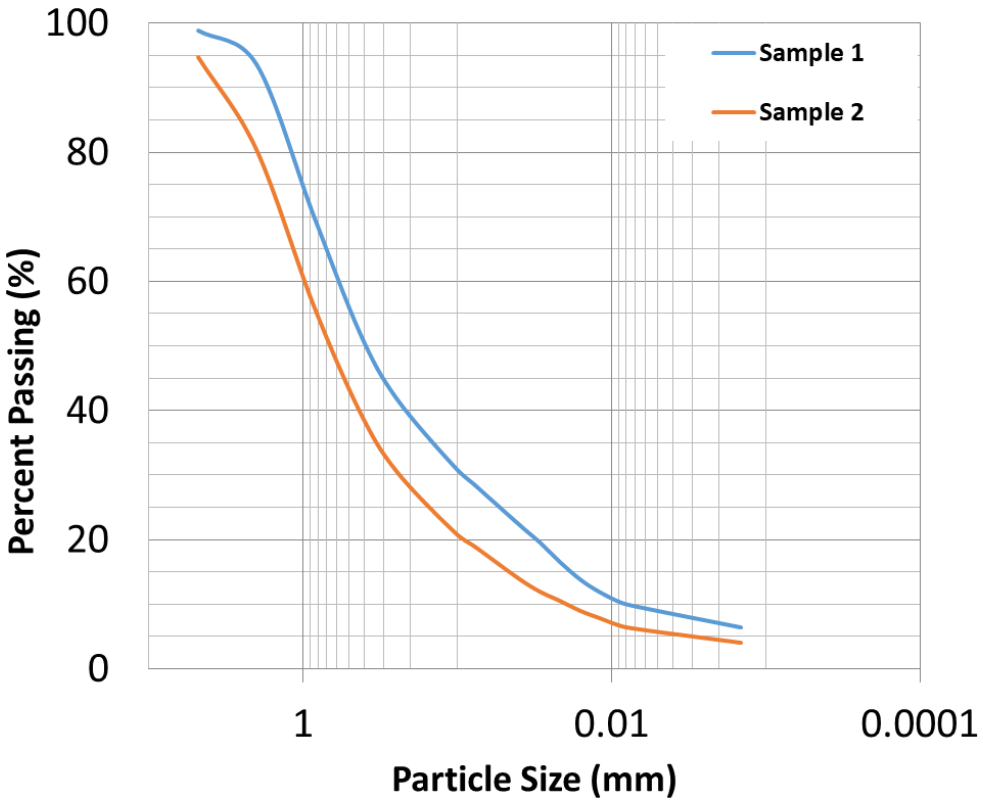

Figure B.5: Gradation curves for samples in Whittier Building site.

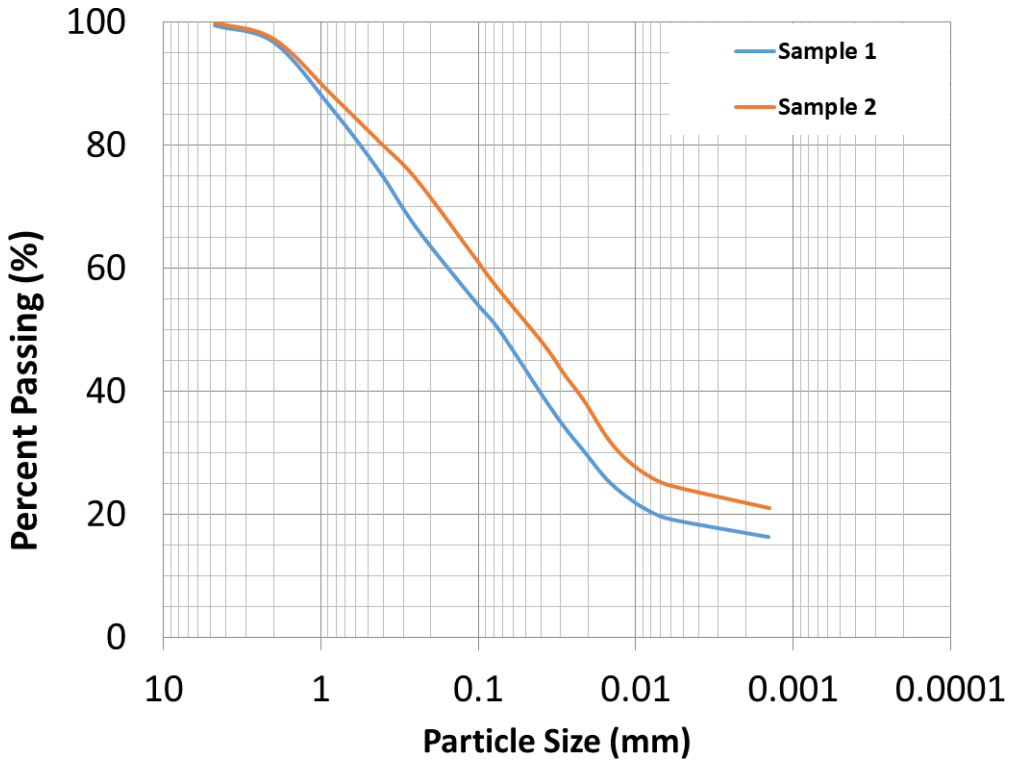

Figure B.6: Gradation curves for samples in East Campus site.

Appendix C

Highly Detailed Terrain HEC-RAS Model Output Reports

HOOPER:

Q2 flood year event:

Contraction Scour

		Left	Channel	Right
Input Data				
	Average Depth (m):	0.16	2.15	
	Approach Velocity (m/s):	0.13	1.69	
	Br Average Depth (m):	0.22	2.34	
	BR Opening Flow (m3/s):	0.06	91.72	
	BR Top WD (m):	1.48	28.45	
	Grain Size D50 (mm):	1.20	1.20	1.20
	Approach Flow (m3/s):	0.02	91.75	
	Approach Top WD (m):	1.05	33.43	
	K1 Coefficient:	0.590	0.640	
Results				
	Scour Depth Ys (m):	0.00	0.04	
	Critical Velocity (m/s):	0.48	0.75	
	Equation:	Clear	Live	

Combined Scour Depths

Q10 flood year event:

Contraction Scour

		Left	Channel	Right
Input Data				
	Average Depth (m):	0.40	3.36	0.17
	Approach Velocity (m/s):	0.24	2.39	0.13
	Br Average Depth (m):	0.98	3.98	
	BR Opening Flow (m3/s):	1.78	240.56	
	BR Top WD (m):	3.60	28.25	
	Grain Size D50 (mm):	1.20	1.20	1.20
	Approach Flow (m3/s):	8.95	233.37	0.02
	Approach Top WD (m):	93.48	36.12	0.91
	K1 Coefficient:		0.640	
Results				
	Scour Depth Ys (m):		0.06	
	Critical Velocity (m/s):		0.80	
	Equation:		Live	

Combined Scour Depths

O25 flood year event:

Contraction Scour

		Left	Channel	Right
Input Data				
	Average Depth (m):	0.80	3.52	0.19
	Approach Velocity (m/s):	0.35	2.50	0.15
	Br Average Depth (m):	1.33	4.10	
	BR Opening Flow (m3/s):	3.15	335.38	
	BR Top WD (m):	3.53	28.19	
	Grain Size D50 (mm):	1.20	1.20	1.20
	Approach Flow (m3/s):	38.70	298.99	0.83
	Approach Top WD (m):	138.74	36.12	28.29
	K1 Coefficient:	0.640	0.640	0.590
Results				
	Scour Depth Ys (m):	0.00	0.45	
	Critical Velocity (m/s):	0.63	0.81	
	Equation:	Clear	Live	

Combined Scour Depths

Q50 flood year event:

Contraction Scour

		Left	Channel	Right
Input Data				
	Average Depth (m):	1.44	3.62	0.57
	Approach Velocity (m/s):	0.42	2.37	0.23
	Br Average Depth (m):	1.53	4.11	
	BR Opening Flow (m3/s):	4.58	441.38	
	BR Top WD (m):	3.49	28.15	
	Grain Size D50 (mm):	1.20	1.20	1.20
	Approach Flow (m3/s):	88.72	343.01	14.24
	Approach Top WD (m):	146.12	36.12	109.11
	K1 Coefficient:	0.640	0.640	0.640
Results				
	Scour Depth Ys (m):	0.15	1.16	
	Critical Velocity (m/s):	0.70	0.81	
	Equation:	Clear	Live	

Abutment Scour

		Left	Right
Input Data			
	Station at Toe (m):	136.10	167.73
	Toe Sta at appr (m):	149.93	183.59
	Abutment Length (m):	146.12	114.99
	Depth at Toe (m):	2.13	3.80
	K1 Shape Coef:	1.00 - Vertical abutment	
	Degree of Skew (degrees):	0.00	0.00
	K2 Skew Coef:	0.00	0.00
	Projected Length L' (m):	146.12	114.99
	Avg Depth Obstructed Ya (m):	1.44	0.75
	Flow Obstructed Qe (m3/s):	88.72	70.01
	Area Obstructed Ae (m2):	210.08	85.84
Results			
	Scour Depth Ys (m):	0.00	0.00
	Froude #:	0.10	0.42
	Equation:	HIRE	HIRE

Combined Scour Depths

Left abutment scour + contraction scour (m):	0.15
Right abutment scour + contraction scour (m):	1.16

Q100 flood year event:

Contraction Scour

		Left	Channel	Right
Input Data				
	Average Depth (m):	1.77	3.78	0.95
	Approach Velocity (m/s):	0.43	2.26	0.29
	Br Average Depth (m):	1.56	4.20	
	BR Opening Flow (m3/s):	5.23	497.26	
	BR Top WD (m):	3.49	28.15	
	Grain Size D50 (mm):	1.20	1.20	1.20
	Approach Flow (m3/s):	115.42	357.41	29.66
	Approach Top WD (m):	150.11	36.12	109.11
	K1 Coefficient:	0.640	0.640	0.640
Results				
	Scour Depth Ys (m):	0.32	1.68	
	Critical Velocity (m/s):	0.72	0.82	
	Equation:	Clear	Live	

Combined Scour Depths

Q500 flood year event:

Contraction Scour

		Left	Channel	Right
Input Data				
	Average Depth (m):	3.13	3.95	2.35
	Approach Velocity (m/s):	0.45	1.96	0.37
	Br Average Depth (m):	2.36	4.30	
	BR Opening Flow (m3/s):	9.31	713.19	
	BR Top WD (m):	3.34	28.02	
	Grain Size D50 (mm):	1.20	1.20	1.20
	Approach Flow (m3/s):	217.64	408.90	95.96
	Approach Top WD (m):	153.34	36.12	109.11
	K1 Coefficient:	0.640	0.640	0.640
Results				
	Scour Depth Ys (m):	0.84	3.19	
	Critical Velocity (m/s):	0.79	0.83	
	Equation:	Clear	Live	

Combined Scour Depths

Peak discharge event 1:

Contraction Scour

		Left	Channel	Right
Input Data				
	Average Depth (m):		0.54	
	Approach Velocity (m/s):		0.68	
	Br Average Depth (m):		0.64	
	BR Opening Flow (m3/s):		9.20	
	BR Top WD (m):		23.81	
	Grain Size D50 (mm):	1.20	1.20	1.20
	Approach Flow (m3/s):		9.20	
	Approach Top WD (m):		24.88	
	K1 Coefficient:		0.640	
Results				
	Scour Depth Ys (m):		0.00	
	Critical Velocity (m/s):		0.59	
	Equation:		Live	

Peak discharge event 2:

Contraction Scour

		Left	Channel	Right
Input Data				
	Average Depth (m):		1.26	
	Approach Velocity (m/s):		1.17	
	Br Average Depth (m):		1.30	
	BR Opening Flow (m3/s):		33.41	
	BR Top WD (m):		26.72	
	Grain Size D50 (mm):	1.20	1.20	1.20
	Approach Flow (m3/s):		33.41	
	Approach Top WD (m):		28.67	
	K1 Coefficient:		0.640	
Results				
	Scour Depth Ys (m):		0.02	
	Critical Velocity (m/s):		0.68	
	Equation:		Live	

Combined Scour Depths

Peak discharge event 3:

Contraction Scour

		Left	Channel	Right
Input Data				
	Average Depth (m):		1.21	
	Approach Velocity (m/s):		1.14	
	Br Average Depth (m):		1.24	
	BR Opening Flow (m3/s):		30.87	
	BR Top WD (m):		26.53	
	Grain Size D50 (mm):	1.20	1.20	1.20
	Approach Flow (m3/s):		30.87	
	Approach Top WD (m):		28.36	
	K1 Coefficient:		0.640	
Results				
	Scour Depth Ys (m):		0.02	
	Critical Velocity (m/s):		0.68	
	Equation:		Live	

Combined Scour Depths

Peak discharge event 4:

Contraction Scour

		Left	Channel	Right
Input Data				
	Average Depth (m):		0.95	
	Approach Velocity (m/s):		0.96	
	Br Average Depth (m):		0.97	
	BR Opening Flow (m3/s):		20.27	
	BR Top WD (m):		25.67	
	Grain Size D50 (mm):	1.20	1.20	1.20
	Approach Flow (m3/s):		20.27	
	Approach Top WD (m):		26.89	
	K1 Coefficient:		0.640	
Results				
	Scour Depth Ys (m):		0.01	
	Critical Velocity (m/s):		0.65	
	Equation:		Live	

Combined Scour Depths

LINCOLN:

Q2 flood year event:

Contraction Scour

		Left	Channel	Right
Input Data				
	Average Depth (m):		2.00	
	Approach Velocity (m/s):		1.39	
	Br Average Depth (m):		1.98	
	BR Opening Flow (m3/s):		33.98	
	BR Top WD (m):		12.80	
	Grain Size D50 (mm):	0.65	0.65	0.65
	Approach Flow (m3/s):		33.98	
	Approach Top WD (m):		12.23	
	K1 Coefficient:		0.640	0.640
Results				
	Scour Depth Ys (m):		0.00	
	Critical Velocity (m/s):		0.60	
	Equation:		Live	

Pier Scour

All piers have the same scour depth

Input Data		
	Pier Shape:	Round nose
	Pier Width (m):	0.61
	Grain Size D50 (mm):	0.65000
	Depth Upstream (m):	1.97
	Velocity Upstream (m/s):	1.40
	K1 Nose Shape:	1.00
	Pier Angle:	0.00
	Pier Length (m):	9.68
	K2 Angle Coef:	1.00
	K3 Bed Cond Coef:	1.10
	Grain Size D90 (mm):	2.00000
	K4 Armouring Coef:	1.00
Results		
	Scour Depth Ys (m):	1.24
	Froude #:	0.32
	Equation:	CSU equation

Q10 flood year event:

Contraction Scour

		Left	Channel	Right
Input Data				
	Average Depth (m):		2.64	
	Approach Velocity (m/s):		2.07	
	Br Average Depth (m):		2.65	
	BR Opening Flow (m3/s):		83.42	
	BR Top WD (m):		14.35	
	Grain Size D50 (mm):	0.65	0.65	0.65
	Approach Flow (m3/s):		83.42	
	Approach Top WD (m):		15.30	
	K1 Coefficient:		0.640	
Results				
	Scour Depth Ys (m):		0.10	
	Critical Velocity (m/s):		0.63	
	Equation:		Live	

Pier Scour

All piers have the same scour depth

Input Data		
	Pier Shape:	Round nose
	Pier Width (m):	0.61
	Grain Size D50 (mm):	0.65000
	Depth Upstream (m):	2.60
	Velocity Upstream (m/s):	2.07
	K1 Nose Shape:	1.00
	Pier Angle:	0.00
	Pier Length (m):	9.68
	K2 Angle Coef:	1.00
	K3 Bed Cond Coef:	1.10
	Grain Size D90 (mm):	2.00000
	K4 Armouring Coef:	1.00
Results		
	Scour Depth Ys (m):	1.52
	Froude #:	0.41
	Equation:	CSU equation

Combined Scour Depths

Pier Scour + Contraction Scour (m):

	Channel:	1.62

Q25 flood year event:

Contraction Scour

		Left	Channel	Right
Input Data				
	Average Depth (m):		2.77	
	Approach Velocity (m/s):		2.37	
	Br Average Depth (m):		2.80	
	BR Opening Flow (m3/s):		110.21	
	BR Top WD (m):		15.56	
	Grain Size D50 (mm):	0.65	0.65	0.65
	Approach Flow (m3/s):		110.21	
	Approach Top WD (m):		16.84	
	K1 Coefficient:	0.640	0.640	0.640
Results				
	Scour Depth Ys (m):		0.11	
	Critical Velocity (m/s):		0.63	
	Equation:		Live	

Pier Scour

All piers have the same scour depth

Input Data		
	Pier Shape:	Round nose
	Pier Width (m):	0.61
	Grain Size D50 (mm):	0.65000
	Depth Upstream (m):	2.75
	Velocity Upstream (m/s):	2.37
	K1 Nose Shape:	1.00
	Pier Angle:	0.00
	Pier Length (m):	9.68
	K2 Angle Coef:	1.00
	K3 Bed Cond Coef:	1.10
	Grain Size D90 (mm):	2.00000
	K4 Armouring Coef:	1.00
Results		
	Scour Depth Ys (m):	1.62
	Froude #:	0.46
	Equation:	CSU equation

Combined Scour Depths

	Pier Scour + Contraction Scour (m):		
		Channel:	1.74

Q50 flood year event:

Contraction Scour

		Left	Channel	Right
Input Data				
	Average Depth (m):		2.92	0.04
	Approach Velocity (m/s):		2.55	0.10
	Br Average Depth (m):		2.91	0.02
	BR Opening Flow (m3/s):		130.14	0.00
	BR Top WD (m):		16.31	0.28
	Grain Size D50 (mm):	0.65	0.65	0.65
	Approach Flow (m3/s):		130.09	0.05
	Approach Top WD (m):		17.42	11.44
	K1 Coefficient:	0.640	0.640	0.640
Results				
	Scour Depth Ys (m):		0.14	
	Critical Velocity (m/s):		0.64	
	Equation:		Live	

Pier Scour

All piers have the same scour depth

Input Data		
	Pier Shape:	Round nose
	Pier Width (m):	0.61
	Grain Size D50 (mm):	0.65000
	Depth Upstream (m):	2.89
	Velocity Upstream (m/s):	2.55
	K1 Nose Shape:	1.00
	Pier Angle:	0.00
	Pier Length (m):	9.68
	K2 Angle Coef:	1.00
	K3 Bed Cond Coef:	1.10
	Grain Size D90 (mm):	2.00000
	K4 Armouring Coef:	1.00
Results		
	Scour Depth Ys (m):	1.69
	Froude #:	0.48
	Equation:	CSU equation

Combined Scour Depths

Pier Scour + Contraction Scour (m):

	Channel:	1.82

Q100 flood year event:

Contraction Scour

		Left	Channel	Right
Input Data				
	Average Depth (m):	0.03	3.10	0.16
	Approach Velocity (m/s):	0.07	2.71	0.21
	Br Average Depth (m):	0.05	3.08	0.09
	BR Opening Flow (m3/s):	0.00	149.77	0.05
	BR Top WD (m):	0.16	16.48	2.79
	Grain Size D50 (mm):	0.65	0.65	0.65
	Approach Flow (m3/s):	0.00	148.76	1.07
	Approach Top WD (m):	0.12	17.70	31.68
	K1 Coefficient:	0.590	0.690	0.640
Results				
	Scour Depth Ys (m):		0.20	0.00
	Critical Velocity (m/s):		0.65	0.39
	Equation:		Live	Clear

Pier Scour

All piers have the same scour depth

Input Data		
	Pier Shape:	Round nose
	Pier Width (m):	0.61
	Grain Size D50 (mm):	0.65000
	Depth Upstream (m):	2.63
	Velocity Upstream (m/s):	2.13
	K1 Nose Shape:	1.00
	Pier Angle:	0.00
	Pier Length (m):	12.20
	K2 Angle Coef:	1.00
	K3 Bed Cond Coef:	1.10
	Grain Size D90 (mm):	2.00000
	K4 Armouring Coef:	1.00
Results		
	Scour Depth Ys (m):	1.54
	Froude #:	0.42
	Equation:	CSU equation

Combined Scour Depths

Pier Scour + Contraction Scour (m):

	Channel:	1.74

O500 flood year event:

Contraction Scour

		Left	Channel	Right
Input Data				
	Average Depth (m):	0.26	3.61	0.57
	Approach Velocity (m/s):	0.27	2.84	0.45
	Br Average Depth (m):	0.19	3.46	0.40
	BR Opening Flow (m3/s):	0.52	192.65	1.20
	BR Top WD (m):	7.63	16.48	5.31
	Grain Size D50 (mm):	0.65	0.65	0.65
	Approach Flow (m3/s):	0.61	181.46	12.29
	Approach Top WD (m):	8.69	17.70	48.13
	K1 Coefficient:	0.640	0.640	0.640
Results				
	Scour Depth Ys (m):	0.00	0.52	0.04
	Critical Velocity (m/s):	0.43	0.66	0.49
	Equation:	Clear	Live	Clear

Pier Scour

All piers have the same scour depth

Input Data		
	Pier Shape:	Round nose
	Pier Width (m):	0.61
	Grain Size D50 (mm):	0.65000
	Depth Upstream (m):	3.60
	Velocity Upstream (m/s):	2.87
	K1 Nose Shape:	1.00
	Pier Angle:	0.00
	Pier Length (m):	9.68
	K2 Angle Coef:	1.00
	K3 Bed Cond Coef:	1.10
	Grain Size D90 (mm):	2.00000
	K4 Armouring Coef:	1.00
Results		
	Scour Depth Ys (m):	1.83
	Froude #:	0.48
	Equation:	CSU equation

Combined Scour Depths

Pier Scour + Contraction Scour (m):

	Channel:	2.34

Peak discharge event 1:

Contraction Scour

		Left	Channel	Right
Input Data				
	Average Depth (m):		0.29	
	Approach Velocity (m/s):		0.42	
	Br Average Depth (m):		0.25	
	BR Opening Flow (m3/s):		0.78	
	BR Top WD (m):		12.80	
	Grain Size D50 (mm):	0.65	0.65	0.65
	Approach Flow (m3/s):		0.78	
	Approach Top WD (m):		6.46	
	K1 Coefficient:		0.640	
Results				
	Scour Depth Ys (m):		0.00	
	Critical Velocity (m/s):		0.44	
	Equation:		Clear	

Pier Scour

All piers have the same scour depth

Input Data		
	Pier Shape:	Round nose
	Pier Width (m):	0.61
	Grain Size D50 (mm):	0.65000
	Depth Upstream (m):	0.25
	Velocity Upstream (m/s):	0.46
	K1 Nose Shape:	1.00
	Pier Angle:	0.00
	Pier Length (m):	12.20
	K2 Angle Coef:	1.00
	K3 Bed Cond Coef:	1.10
	Grain Size D90 (mm):	2.00000
	K4 Armouring Coef:	1.00
Results		
	Scour Depth Ys (m):	0.58
	Froude #:	0.29
	Equation:	CSU equation

Peak discharge event 2:

Contraction Scour

		Left	Channel	Right
Input Data				
	Average Depth (m):		1.42	
	Approach Velocity (m/s):		1.17	
	Br Average Depth (m):		1.44	
	BR Opening Flow (m3/s):		17.84	
	BR Top WD (m):		11.00	
	Grain Size D50 (mm):	0.65	0.65	0.65
	Approach Flow (m3/s):		17.84	
	Approach Top WD (m):		10.76	
	K1 Coefficient:		0.640	
Results				
	Scour Depth Ys (m):		0.00	
	Critical Velocity (m/s):		0.57	
	Equation:		Live	

Pier Scour

All piers have the same scour depth

Input Data		
	Pier Shape:	Round nose
	Pier Width (m):	0.61
	Grain Size D50 (mm):	0.65000
	Depth Upstream (m):	1.41
	Velocity Upstream (m/s):	1.18
	K1 Nose Shape:	1.00
	Pier Angle:	0.00
	Pier Length (m):	12.20
	K2 Angle Coef:	1.00
	K3 Bed Cond Coef:	1.10
	Grain Size D90 (mm):	2.00000
	K4 Armouring Coef:	1.00
Results		
	Scour Depth Ys (m):	1.10
	Froude #:	0.32
	Equation:	CSU equation

Peak discharge event 3:

Contraction Scour

		Left	Channel	Right
Input Data				
	Average Depth (m):		0.98	
	Approach Velocity (m/s):		1.00	
	Br Average Depth (m):		1.02	
	BR Opening Flow (m3/s):		9.51	
	BR Top WD (m):		9.02	
	Grain Size D50 (mm):	0.65	0.65	0.65
	Approach Flow (m3/s):		9.51	
	Approach Top WD (m):		9.72	
	K1 Coefficient:		0.640	
Results				
	Scour Depth Ys (m):		0.01	
	Critical Velocity (m/s):		0.53	
	Equation:		Live	

Pier Scour

All piers have the same scour depth

Input Data		
	Pier Shape:	Round nose
	Pier Width (m):	0.61
	Grain Size D50 (mm):	0.65000
	Depth Upstream (m):	0.97
	Velocity Upstream (m/s):	1.02
	K1 Nose Shape:	1.00
	Pier Angle:	0.00
	Pier Length (m):	12.20
	K2 Angle Coef:	1.00
	K3 Bed Cond Coef:	1.10
	Grain Size D90 (mm):	2.00000
	K4 Armouring Coef:	1.00
Results		
	Scour Depth Ys (m):	0.98
	Froude #:	0.33
	Equation:	CSU equation

Combined Scour Depths

	Pier Scour + Contraction Scour (m):		
		Channel:	0.99

Peak discharge event 4:

Contraction Scour

		Left	Channel	Right
Input Data				
	Average Depth (m):		0.35	
	Approach Velocity (m/s):		0.54	
	Br Average Depth (m):		0.31	
	BR Opening Flow (m3/s):		1.28	
	BR Top WD (m):		7.19	
	Grain Size D50 (mm):	0.65	0.65	0.65
	Approach Flow (m3/s):		1.28	
	Approach Top WD (m):		6.90	
	K1 Coefficient:		0.640	
Results				
	Scour Depth Ys (m):		0.03	
	Critical Velocity (m/s):		0.45	
	Equation:		Live	

Pier Scour

All piers have the same scour depth

Input Data		
	Pier Shape:	Round nose
	Pier Width (m):	0.61
	Grain Size D50 (mm):	0.65000
	Depth Upstream (m):	0.31
	Velocity Upstream (m/s):	0.57
	K1 Nose Shape:	1.00
	Pier Angle:	0.00
	Pier Length (m):	12.20
	K2 Angle Coef:	1.00
	K3 Bed Cond Coef:	1.10
	Grain Size D90 (mm):	2.00000
	K4 Armouring Coef:	1.00
Results		
	Scour Depth Ys (m):	0.65
	Froude #:	0.32
	Equation:	CSU equation

Combined Scour Depths

	Pier Scour + Contraction Scour (m):		
		Channel:	0.68

WILBER:

Q2 flood year event:

Contraction Scour

		Left	Channel	Right
Input Data				
	Average Depth (m):	0.13	1.86	0.20
	Approach Velocity (m/s):	0.02	0.61	0.02
	Br Average Depth (m):	0.05	1.82	0.10
	BR Opening Flow (m3/s):	0.00	61.75	0.00
	BR Top WD (m):	2.04	59.49	2.62
	Grain Size D50 (mm):	1.75	1.75	1.75
	Approach Flow (m3/s):	0.00	61.74	0.01
	Approach Top WD (m):	1.94	54.74	2.91
	K1 Coefficient:		0.590	0.590
Results				
	Scour Depth Ys (m):		0.00	
	Critical Velocity (m/s):		0.83	
	Equation:		Clear	

Pier Scour

All piers have the same scour depth

Input Data		
	Pier Shape:	Round nose
	Pier Width (m):	0.31
	Grain Size D50 (mm):	1.75000
	Depth Upstream (m):	1.82
	Velocity Upstream (m/s):	0.56
	K1 Nose Shape:	1.00
	Pier Angle:	0.00
	Pier Length (m):	8.53
	K2 Angle Coef:	1.00
	K3 Bed Cond Coef:	1.10
	Grain Size D90 (mm):	2.00000
	K4 Armouring Coef:	1.00
Results		
	Scour Depth Ys (m):	0.53
	Froude #:	0.13
	Equation:	CSU equation

Q10 flood year event:

Contraction Scour

		Left	Channel	Right
Input Data				
	Average Depth (m):	1.16	3.44	1.11
	Approach Velocity (m/s):	0.08	0.92	0.08
	Br Average Depth (m):	1.28	3.43	1.34
	BR Opening Flow (m3/s):	0.67	175.38	0.82
	BR Top WD (m):	6.27	59.49	7.09
	Grain Size D50 (mm):	1.75	1.75	1.75
	Approach Flow (m3/s):	0.71	175.26	0.90
	Approach Top WD (m):	8.01	55.57	10.69
	K1 Coefficient:	0.590	0.640	0.590
Results				
	Scour Depth Ys (m):	0.00	0.00	0.00
	Critical Velocity (m/s):	0.76	0.92	0.76
	Equation:	Clear	Live	Clear

Pier Scour

All piers have the same scour depth

Input Data		
	Pier Shape:	Round nose
	Pier Width (m):	0.31
	Grain Size D50 (mm):	1.75000
	Depth Upstream (m):	3.43
	Velocity Upstream (m/s):	0.85
	K1 Nose Shape:	1.00
	Pier Angle:	0.00
	Pier Length (m):	8.53
	K2 Angle Coef:	1.00
	K3 Bed Cond Coef:	1.10
	Grain Size D90 (mm):	2.00000
	K4 Armouring Coef:	1.00
Results		
	Scour Depth Ys (m):	0.69
	Froude #:	0.15
	Equation:	CSU equation

Q25 flood year event:

Contraction Scour

		Left	Channel	Right
Input Data				
	Average Depth (m):	1.74	4.19	1.75
	Approach Velocity (m/s):	0.11	1.12	0.11
	Br Average Depth (m):	2.09	4.18	2.13
	BR Opening Flow (m3/s):	1.48	261.17	1.77
	BR Top WD (m):	6.08	59.49	6.96
	Grain Size D50 (mm):	1.75	1.75	1.75
	Approach Flow (m3/s):	1.67	260.57	2.18
	Approach Top WD (m):	9.03	55.57	11.54
	K1 Coefficient:	0.590	0.640	0.590
Results				
	Scour Depth Ys (m):	0.00	0.00	0.00
	Critical Velocity (m/s):	0.82	0.95	0.82
	Equation:	Clear	Live	Clear

Pier Scour

All piers have the same scour depth

Input Data		
	Pier Shape:	Round nose
	Pier Width (m):	0.31
	Grain Size D50 (mm):	1.75000
	Depth Upstream (m):	4.19
	Velocity Upstream (m/s):	1.04
	K1 Nose Shape:	1.00
	Pier Angle:	0.00
	Pier Length (m):	8.53
	K2 Angle Coef:	1.00
	K3 Bed Cond Coef:	1.10
	Grain Size D90 (mm):	2.00000
	K4 Armouring Coef:	1.00
Results		
	Scour Depth Ys (m):	0.77
	Froude #:	0.16
	Equation:	CSU equation

Q50 flood year event:

Pier Scour

All piers have the same scour depth

Input Data

Pier Shape:	Round nose
Pier Width (m):	0.31
Grain Size D50 (mm):	1.75000
Depth Upstream (m):	4.79
Velocity Upstream (m/s):	1.18
K1 Nose Shape:	1.00
Pier Angle:	0.00
Pier Length (m):	8.53
K2 Angle Coef:	1.00
K3 Bed Cond Coef:	1.10
Grain Size D90 (mm):	2.00000
K4 Armouring Coef:	1.00

Results

Scour Depth Ys (m):	0.83
Froude #:	0.17
Equation:	CSU equation

Q100 flood year event:

Contraction Scour

		Left	Channel	Right
Input Data				
	Average Depth (m):	0.95	4.00	1.01
	Approach Velocity (m/s):	0.08	2.70	0.08
	Br Average Depth (m):	1.20	2.30	2.00
	BR Opening Flow (m3/s):	2.73	432.68	3.25
	BR Top WD (m):	8.60	85.00	7.70
	Grain Size D50 (mm):	1.75	1.75	1.75
	Approach Flow (m3/s):	12.43	417.66	8.57
	Approach Top WD (m):	171.23	55.57	106.21
	K1 Coefficient:	0.590	0.640	0.590
Results				
	Scour Depth Ys (m):	0.00	0.84	0.00
	Critical Velocity (m/s):	0.74	0.94	0.75
	Equation:	Clear	Live	Clear

Pier Scour

All piers have the same scour depth

Input Data		
	Pier Shape:	Round nose
	Pier Width (m):	0.31
	Grain Size D50 (mm):	1.75000
	Depth Upstream (m):	5.43
	Velocity Upstream (m/s):	1.32
	K1 Nose Shape:	1.00
	Pier Angle:	
	Pier Length (m):	8.53
	K2 Angle Coef:	1.00
	K3 Bed Cond Coef:	1.10
	Grain Size D90 (mm):	2.50000
	K4 Armouring Coef:	1.00
	Set K1 value to 1.0 because angle > 5 degrees	
Results		
	Scour Depth Ys (m):	0.89
	Froude #:	0.18
	Equation:	CSU equation

Abutment Scour

		Left	Right
Input Data			
	Station at Toe (m):	170.80	244.16
	Toe Sta at appr (m):	165.02	233.86
	Abutment Length (m):	171.23	106.21
	Depth at Toe (m):	2.54	2.74
	K1 Shape Coef:	1.00 - Vertical abutment	
	Degree of Skew (degrees):	0.00	0.00
	K2 Skew Coef:	0.00	0.00
	Projected Length L' (m):	171.23	106.21
	Avg Depth Obstructed Ya (m):	0.95	1.01
	Flow Obstructed Qe (m3/s):	12.43	8.57

	Area Obstructed Ae (m2):	162.78	107.10
Results			
	Scour Depth Ys (m):	0.00	0.00
	Froude #:	0.01	0.01
	Equation:	HIRE	HIRE

Combined Scour Depths

Pier Scour + Contraction Scour (m):		
	Channel:	1.73
Left abutment scour + contraction scour (m):	0.00	
Right abutment scour + contraction scour (m):	0.00	

Q500 flood year event:

Contraction Scour

		Left	Channel	Right
Input Data				
	Average Depth (m):	2.56	7.04	2.52
	Approach Velocity (m/s):	0.14	1.58	0.14
	Br Average Depth (m):	1.38	5.77	1.43
	BR Opening Flow (m3/s):	61.24	615.76	45.11
	BR Top WD (m):	177.00	80.10	126.20
	Grain Size D50 (mm):	1.75	1.75	1.75
	Approach Flow (m3/s):	61.89	619.16	41.05
	Approach Top WD (m):	171.23	55.57	116.63
	K1 Coefficient:	0.590	0.640	0.590
Results				
	Scour Depth Ys (m):	0.00	0.00	0.00
	Critical Velocity (m/s):	0.87	1.03	0.87
	Equation:	Clear	Live	Clear

Pier Scour

All piers have the same scour depth

Input Data		
	Pier Shape:	Round nose
	Pier Width (m):	0.31
	Grain Size D50 (mm):	1.75000
	Depth Upstream (m):	6.10
	Velocity Upstream (m/s):	1.53
	K1 Nose Shape:	1.00
	Pier Angle:	0.00
	Pier Length (m):	8.53
	K2 Angle Coef:	1.00
	K3 Bed Cond Coef:	1.10
	Grain Size D90 (mm):	5.00000
	K4 Armouring Coef:	1.00
Results		
	Scour Depth Ys (m):	0.96
	Froude #:	0.20
	Equation:	CSU equation

Peak discharge event 1:

Contraction Scour

		Left	Channel	Right
Input Data				
	Average Depth (m):		1.06	
	Approach Velocity (m/s):		0.22	
	Br Average Depth (m):		1.03	
	BR Opening Flow (m3/s):		4.33	
	BR Top WD (m):		21.01	
	Grain Size D50 (mm):	1.75	1.75	1.75
	Approach Flow (m3/s):		4.33	
	Approach Top WD (m):		18.44	
	K1 Coefficient:		0.590	
Results				
	Scour Depth Ys (m):		0.00	
	Critical Velocity (m/s):		0.75	
	Equation:		Clear	

Pier Scour

All piers have the same scour depth

Input Data		
	Pier Shape:	Round nose
	Pier Width (m):	0.31
	Grain Size D50 (mm):	1.75000
	Depth Upstream (m):	1.03
	Velocity Upstream (m/s):	0.20
	K1 Nose Shape:	1.00
	Pier Angle:	0.00
	Pier Length (m):	8.53
	K2 Angle Coef:	1.00
	K3 Bed Cond Coef:	1.10
	Grain Size D90 (mm):	2.00000
	K4 Armouring Coef:	1.00
Results		
	Scour Depth Ys (m):	0.31
	Froude #:	0.06
	Equation:	CSU equation

Peak discharge event 2:

Contraction Scour

		Left	Channel	Right
Input Data				
	Average Depth (m):	0.19	1.93	0.27
	Approach Velocity (m/s):	0.02	0.62	0.03
	Br Average Depth (m):	0.12	1.92	0.18
	BR Opening Flow (m3/s):	0.01	65.96	0.01
	BR Top WD (m):	2.76	59.49	3.02
	Grain Size D50 (mm):	1.75	1.75	1.75
	Approach Flow (m3/s):	0.01	65.94	0.03
	Approach Top WD (m):	2.52	55.57	3.25
	K1 Coefficient:	0.590	0.590	0.590
Results				
	Scour Depth Ys (m):	0.00	0.00	0.00
	Critical Velocity (m/s):	0.56	0.83	0.60
	Equation:	Clear	Clear	Clear

Pier Scour

All piers have the same scour depth

Input Data		
	Pier Shape:	Round nose
	Pier Width (m):	0.31
	Grain Size D50 (mm):	1.75000
	Depth Upstream (m):	1.92
	Velocity Upstream (m/s):	0.57
	K1 Nose Shape:	1.00
	Pier Angle:	0.00
	Pier Length (m):	8.53
	K2 Angle Coef:	1.00
	K3 Bed Cond Coef:	1.10
	Grain Size D90 (mm):	2.00000
	K4 Armouring Coef:	1.00
Results		
	Scour Depth Ys (m):	0.54
	Froude #:	0.13
	Equation:	CSU equation

Peak discharge event 3:

Contraction Scour

		Left	Channel	Right
Input Data				
	Average Depth (m):		2.02	
	Approach Velocity (m/s):		0.59	
	Br Average Depth (m):		1.96	
	BR Opening Flow (m3/s):		39.36	
	BR Top WD (m):		35.43	
	Grain Size D50 (mm):	1.75	1.75	1.75
	Approach Flow (m3/s):		39.36	
	Approach Top WD (m):		32.91	
	K1 Coefficient:		0.590	
Results				
	Scour Depth Ys (m):		0.00	
	Critical Velocity (m/s):		0.84	
	Equation:		Clear	

Pier Scour

All piers have the same scour depth

Input Data		
	Pier Shape:	Round nose
	Pier Width (m):	0.31
	Grain Size D50 (mm):	1.75000
	Depth Upstream (m):	1.97
	Velocity Upstream (m/s):	0.56
	K1 Nose Shape:	1.00
	Pier Angle:	0.00
	Pier Length (m):	8.53
	K2 Angle Coef:	1.00
	K3 Bed Cond Coef:	1.10
	Grain Size D90 (mm):	2.00000
	K4 Armouring Coef:	1.00
Results		
	Scour Depth Ys (m):	0.54
	Froude #:	0.13
	Equation:	CSU equation

Peak discharge event 4:

Contraction Scour

		Left	Channel	Right
Input Data				
	Average Depth (m):		1.13	
	Approach Velocity (m/s):		0.25	
	Br Average Depth (m):		1.13	
	BR Opening Flow (m3/s):		5.41	
	BR Top WD (m):		21.24	
	Grain Size D50 (mm):	1.75	1.75	1.75
	Approach Flow (m3/s):		5.41	
	Approach Top WD (m):		19.13	
	K1 Coefficient:		0.590	
Results				
	Scour Depth Ys (m):		0.00	
	Critical Velocity (m/s):		0.76	
	Equation:		Clear	

Pier Scour

All piers have the same scour depth

Input Data		
	Pier Shape:	Round nose
	Pier Width (m):	0.31
	Grain Size D50 (mm):	1.75000
	Depth Upstream (m):	1.12
	Velocity Upstream (m/s):	0.22
	K1 Nose Shape:	1.00
	Pier Angle:	0.00
	Pier Length (m):	8.53
	K2 Angle Coef:	1.00
	K3 Bed Cond Coef:	1.10
	Grain Size D90 (mm):	2.00000
	K4 Armouring Coef:	1.00
Results		
	Scour Depth Ys (m):	0.34
	Froude #:	0.07
	Equation:	CSU equation

BEATRICE:

Q2 flood year event:

Contraction Scour

		Left	Channel	Right
Input Data				
	Average Depth (m):		3.21	
	Approach Velocity (m/s):		0.94	
	Br Average Depth (m):		3.31	
	BR Opening Flow (m3/s):		255.70	
	BR Top WD (m):		83.75	
	Grain Size D50 (mm):	2.21	2.21	2.21
	Approach Flow (m3/s):		255.70	
	Approach Top WD (m):		84.41	
	K1 Coefficient:		0.590	
Results				
	Scour Depth Ys (m):		0.00	
	Critical Velocity (m/s):		0.98	
	Equation:		Clear	

Pier Scour

Pier: #1 (CL = 111.3)

Input Data		
	Pier Shape:	Round nose
	Pier Width (m):	0.99
	Grain Size D50 (mm):	2.21000
	Depth Upstream (m):	3.31
	Velocity Upstream (m/s):	0.89
	K1 Nose Shape:	1.00
	Pier Angle:	
	Pier Length (m):	3.20
	K2 Angle Coef:	1.00
	K3 Bed Cond Coef:	1.10
	Grain Size D90 (mm):	2.50000
	K4 Armouring Coef:	1.00
	Set K1 value to 1.0 because angle > 5 degrees	
Results		
	Scour Depth Ys (m):	1.50
	Froude #:	0.16
	Equation:	CSU equation

Pier: #2 (CL = 140.25)

Input Data

Pier Shape:	Round nose
Pier Width (m):	1.05
Grain Size D50 (mm):	2.21000
Depth Upstream (m):	3.31
Velocity Upstream (m/s):	0.89
K1 Nose Shape:	1.00
Pier Angle:	
Pier Length (m):	3.20
K2 Angle Coef:	1.00
K3 Bed Cond Coef:	1.10
Grain Size D90 (mm):	2.50000
K4 Armouring Coef:	1.00

Set K1 value to 1.0 because angle > 5 degrees

Results

Scour Depth Ys (m):	1.56
Froude #:	0.16

Equation:	CSU equation

Pier: #3 (CL = 170.75)

Input Data

Pier Shape:	Round nose
Pier Width (m):	1.05
Grain Size D50 (mm):	2.21000
Depth Upstream (m):	3.31
Velocity Upstream (m/s):	0.89
K1 Nose Shape:	1.00
Pier Angle:	
Pier Length (m):	3.20
K2 Angle Coef:	1.00
K3 Bed Cond Coef:	1.10
Grain Size D90 (mm):	2.50000
K4 Armouring Coef:	1.00

Set K1 value to 1.0 because angle > 5 degrees

Results

Scour Depth Ys (m):	1.55
Froude #:	0.16
Equation:	CSU equation

Pier: #4 (CL = 199.7)

Input Data

Pier Shape:	Round nose
Pier Width (m):	0.91
Grain Size D50 (mm):	2.21000
Depth Upstream (m):	3.31
Velocity Upstream (m/s):	0.89
K1 Nose Shape:	1.00
Pier Angle:	
Pier Length (m):	3.20
K2 Angle Coef:	1.00
K3 Bed Cond Coef:	1.10
Grain Size D90 (mm):	2.50000
K4 Armouring Coef:	1.00

Set K1 value to 1.0 because angle > 5 degrees

Results

Scour Depth Ys (m):	1.42
Froude #:	0.16
Equation:	CSU equation

Q10 flood year event:

Pier Scour

Pier: #1 (CL = 111.3)

Input Data

Pier Shape:	Round nose
Pier Width (m):	0.99
Grain Size D50 (mm):	2.21000
Depth Upstream (m):	5.83
Velocity Upstream (m/s):	1.33
K1 Nose Shape:	1.00
Pier Angle:	
Pier Length (m):	3.20
K2 Angle Coef:	1.00
K3 Bed Cond Coef:	1.10
Grain Size D90 (mm):	2.50000
K4 Armouring Coef:	1.00

Set K1 value to 1.0 because angle > 5 degrees

Results

Scour Depth Ys (m):	1.92
Froude #:	0.18
Equation:	CSU equation

Pier: #2 (CL = 140.25)

Input Data

Pier Shape:	Round nose
Pier Width (m):	1.05
Grain Size D50 (mm):	2.21000
Depth Upstream (m):	5.83
Velocity Upstream (m/s):	1.33
K1 Nose Shape:	1.00
Pier Angle:	
Pier Length (m):	3.20
K2 Angle Coef:	1.00
K3 Bed Cond Coef:	1.10
Grain Size D90 (mm):	2.50000
K4 Armouring Coef:	1.00

Set K1 value to 1.0 because angle > 5 degrees

Results

Scour Depth Ys (m):	2.00
Froude #:	0.18
Equation:	CSU equation

Pier: #3 (CL = 170.75)

Input Data

Pier Shape:	Round nose
Pier Width (m):	1.05
Grain Size D50 (mm):	2.21000
Depth Upstream (m):	5.83
Velocity Upstream (m/s):	1.33
K1 Nose Shape:	1.00
Pier Angle:	
Pier Length (m):	3.20
K2 Angle Coef:	1.00
K3 Bed Cond Coef:	1.10
Grain Size D90 (mm):	2.50000

K4 Armouring Coef:	1.00

Set K1 value to 1.0 because angle > 5 degrees

Results

Scour Depth Ys (m):	1.99	
Froude #:	0.18	
Equation:	CSU equation	

Pier: #4 (CL = 199.7)

Input Data

Pier Shape:	Round nose	
Pier Width (m):	0.91	
Grain Size D50 (mm):	2.21000	
Depth Upstream (m):	5.83	
Velocity Upstream (m/s):	1.33	
K1 Nose Shape:	1.00	
Pier Angle:		
Pier Length (m):	3.20	
K2 Angle Coef:	1.00	
K3 Bed Cond Coef:	1.10	
Grain Size D90 (mm):	2.50000	
K4 Armouring Coef:	1.00	
Set K1 value to 1.0 because angle > 5 degrees		

Results

Scour Depth Ys (m):	1.82	
Froude #:	0.18	
Equation:	CSU equation	

Abutment Scour

	Left	Right
Input Data		
Station at Toe (m):	89.20	221.80
Toe Sta at appr (m):	85.34	214.54
Abutment Length (m):	1.23	27.75
Depth at Toe (m):	-0.94	0.46
K1 Shape Coef:	1.00 - Vertical abutment	
Degree of Skew (degrees):	90.00	90.00
K2 Skew Coef:	1.00	1.00
Projected Length L' (m):	1.23	27.75
Avg Depth Obstructed Ya (m):	0.11	1.97
Flow Obstructed Qe (m3/s):	0.01	14.79
Area Obstructed Ae (m2):	0.14	54.66
Results		
Scour Depth Ys (m):		1.65
Froude #:		0.12
Equation:	Default	HIRE

Q25 flood year event:

Contraction Scour

		Left	Channel	Right
Input Data				
	Average Depth (m):	0.49	7.03	1.50
	Approach Velocity (m/s):	0.11	1.66	0.28
	Br Average Depth (m):	0.33	8.60	2.30
	BR Opening Flow (m3/s):	1.10	1183.27	30.71
	BR Top WD (m):	24.41	135.50	33.76
	Grain Size D50 (mm):	2.21	2.21	2.21
	Approach Flow (m3/s):	3.63	1180.20	31.25
	Approach Top WD (m):	64.39	101.00	75.75
	K1 Coefficient:	0.590	0.640	0.590
Results				
	Scour Depth Ys (m):	0.00	0.00	0.00
	Critical Velocity (m/s):	0.71	1.11	0.86
	Equation:	Clear	Live	Clear

Pier Scour

Pier: #1 (CL = 111.3)

Input Data

Pier Shape:	Round nose
Pier Width (m):	0.99
Grain Size D50 (mm):	2.21000
Depth Upstream (m):	7.09
Velocity Upstream (m/s):	1.60
K1 Nose Shape:	1.00
Pier Angle:	
Pier Length (m):	3.20
K2 Angle Coef:	1.00
K3 Bed Cond Coef:	1.10
Grain Size D90 (mm):	2.50000
K4 Armouring Coef:	1.00
Set K1 value to 1.0 because angle > 5 degrees	

Results

Scour Depth Ys (m):	2.14
Froude #:	0.19
Equation:	CSU equation

Pier: #2 (CL = 140.25)

Input Data

Pier Shape:	Round nose
Pier Width (m):	1.05
Grain Size D50 (mm):	2.21000
Depth Upstream (m):	7.09
Velocity Upstream (m/s):	1.60
K1 Nose Shape:	1.00
Pier Angle:	
Pier Length (m):	3.20
K2 Angle Coef:	1.00
K3 Bed Cond Coef:	1.10
Grain Size D90 (mm):	2.50000
K4 Armouring Coef:	1.00
Set K1 value to 1.0 because angle > 5 degrees	

Results

Scour Depth Ys (m):	2.22
Froude #:	0.19

Equation:	CSU equation

Pier: #3 (CL = 170.75)

Input Data

Pier Shape:	Round nose
Pier Width (m):	1.05
Grain Size D50 (mm):	2.21000
Depth Upstream (m):	7.09
Velocity Upstream (m/s):	1.60
K1 Nose Shape:	1.00
Pier Angle:	
Pier Length (m):	3.20
K2 Angle Coef:	1.00
K3 Bed Cond Coef:	1.10
Grain Size D90 (mm):	2.50000
K4 Armouring Coef:	1.00

Set K1 value to 1.0 because angle > 5 degrees

Results

Scour Depth Ys (m):	2.22
Froude #:	0.19
Equation:	CSU equation

Pier: #4 (CL = 199.7)

Input Data

Pier Shape:	Round nose
Pier Width (m):	0.91
Grain Size D50 (mm):	2.21000
Depth Upstream (m):	7.09
Velocity Upstream (m/s):	1.60
K1 Nose Shape:	1.00
Pier Angle:	
Pier Length (m):	3.20
K2 Angle Coef:	1.00
K3 Bed Cond Coef:	1.10
Grain Size D90 (mm):	2.50000
K4 Armouring Coef:	1.00

Set K1 value to 1.0 because angle > 5 degrees

Results

Scour Depth Ys (m):	2.03
Froude #:	0.19
Equation:	CSU equation

Q50 flood year event:

Contraction Scour

		Left	Channel	Right
Input Data				
	Average Depth (m):	1.19	7.91	2.20
	Approach Velocity (m/s):	0.21	1.83	0.31
	Br Average Depth (m):	0.73	11.75	3.42
	BR Opening Flow (m3/s):	9.27	1498.91	38.06
	BR Top WD (m):	60.27	68.07	31.78
	Grain Size D50 (mm):	2.21	2.21	2.21
	Approach Flow (m3/s):	22.15	1465.89	58.20
	Approach Top WD (m):	89.64	101.00	85.04
	K1 Coefficient:	0.590	0.640	0.590
Results				
	Scour Depth Ys (m):	0.00	0.00	0.00
	Critical Velocity (m/s):	0.83	1.14	0.92
	Equation:	Clear	Live	Clear

Pier Scour

Pier: #1 (CL = 111.3)

Input Data

Pier Shape:	Round nose
Pier Width (m):	0.99
Grain Size D50 (mm):	2.21000
Depth Upstream (m):	7.96
Velocity Upstream (m/s):	1.78
K1 Nose Shape:	1.00
Pier Angle:	
Pier Length (m):	3.20
K2 Angle Coef:	1.00
K3 Bed Cond Coef:	1.10
Grain Size D90 (mm):	2.50000
K4 Armouring Coef:	1.00
Set K1 value to 1.0 because angle > 5 degrees	

Results

Scour Depth Ys (m):	2.27
Froude #:	0.20
Equation:	CSU equation

Pier: #2 (CL = 140.25)

Input Data

Pier Shape:	Round nose
Pier Width (m):	1.05
Grain Size D50 (mm):	2.21000
Depth Upstream (m):	7.96
Velocity Upstream (m/s):	1.78
K1 Nose Shape:	1.00
Pier Angle:	
Pier Length (m):	3.20
K2 Angle Coef:	1.00
K3 Bed Cond Coef:	1.10
Grain Size D90 (mm):	2.50000
K4 Armouring Coef:	1.00
Set K1 value to 1.0 because angle > 5 degrees	

Scour Depth Ys (m):	2.36
Froude #:	0.20

Results

Equation:	CSU equation

Pier: #3 (CL = 170.75)

Input Data

Pier Shape:	Round nose
Pier Width (m):	1.05
Grain Size D50 (mm):	2.21000
Depth Upstream (m):	7.96
Velocity Upstream (m/s):	1.78
K1 Nose Shape:	1.00
Pier Angle:	
Pier Length (m):	3.20
K2 Angle Coef:	1.00
K3 Bed Cond Coef:	1.10
Grain Size D90 (mm):	2.50000
K4 Armouring Coef:	1.00

Set K1 value to 1.0 because angle > 5 degrees

Results

Scour Depth Ys (m):	2.36
Froude #:	0.20
Equation:	CSU equation

Pier: #4 (CL = 199.7)

Input Data

Pier Shape:	Round nose
Pier Width (m):	0.91
Grain Size D50 (mm):	2.21000
Depth Upstream (m):	7.96
Velocity Upstream (m/s):	1.78
K1 Nose Shape:	1.00
Pier Angle:	
Pier Length (m):	3.20
K2 Angle Coef:	1.00
K3 Bed Cond Coef:	1.10
Grain Size D90 (mm):	2.50000
K4 Armouring Coef:	1.00

Set K1 value to 1.0 because angle > 5 degrees

Results

Scour Depth Ys (m):	2.16
Froude #:	0.20
Equation:	CSU equation

Q100 flood year event:

Contraction Scour

		Left	Channel	Right
Input Data				
	Average Depth (m):	2.06	8.78	3.07
	Approach Velocity (m/s):	0.30	2.40	0.39
	Br Average Depth (m):	1.18	8.70	2.27
	BR Opening Flow (m3/s):	48.78	1508.80	74.31
	BR Top WD (m):	93.50	85.80	65.29
	Grain Size D50 (mm):	2.21	2.21	2.21
	Approach Flow (m3/s):	55.18	1750.83	101.13
	Approach Top WD (m):	89.64	101.00	85.04
	K1 Coefficient:	0.590	0.640	0.590
Results				
	Scour Depth Ys (m):	0.00	0.00	0.00
	Critical Velocity (m/s):	0.91	1.16	0.97
	Equation:	Clear	Live	Clear

Pier Scour

Pier: #1 (CL = 111.3)

Input Data

	Pier Shape:	Round nose
	Pier Width (m):	0.99
	Grain Size D50 (mm):	2.21000
	Depth Upstream (m):	8.83
	Velocity Upstream (m/s):	1.92
	K1 Nose Shape:	1.00
	Pier Angle:	
	Pier Length (m):	3.20
	K2 Angle Coef:	1.00
	K3 Bed Cond Coef:	1.10
	Grain Size D90 (mm):	5.00000
	K4 Armouring Coef:	1.00
	Set K1 value to 1.0 because angle > 5 degrees	

Results

	Scour Depth Ys (m):	2.38
	Froude #:	0.21
	Equation:	CSU equation

Pier: #2 (CL = 140.25)

Input Data

Pier Shape:	Round nose
Pier Width (m):	1.05
Grain Size D50 (mm):	2.21000
Depth Upstream (m):	8.83
Velocity Upstream (m/s):	1.92
K1 Nose Shape:	1.00
Pier Angle:	
Pier Length (m):	3.20
K2 Angle Coef:	1.00
K3 Bed Cond Coef:	1.10
Grain Size D90 (mm):	5.00000
K4 Armouring Coef:	1.00

Set K1 value to 1.0 because angle > 5 degrees

Results

Scour Depth Ys (m):	2.47
Froude #:	0.21

Equation:	CSU equation

Pier: #3 (CL = 170.75)

Input Data

Pier Shape:	Round nose
Pier Width (m):	1.05
Grain Size D50 (mm):	2.21000
Depth Upstream (m):	8.83
Velocity Upstream (m/s):	1.92
K1 Nose Shape:	1.00
Pier Angle:	
Pier Length (m):	3.20
K2 Angle Coef:	1.00
K3 Bed Cond Coef:	1.10
Grain Size D90 (mm):	5.00000
K4 Armouring Coef:	1.00

Set K1 value to 1.0 because angle > 5 degrees

Results

Scour Depth Ys (m):	2.47
Froude #:	0.21
Equation:	CSU equation

Pier: #4 (CL = 199.7)

Input Data

Pier Shape:	Round nose
Pier Width (m):	0.91
Grain Size D50 (mm):	2.21000
Depth Upstream (m):	8.83
Velocity Upstream (m/s):	1.92
K1 Nose Shape:	1.00
Pier Angle:	
Pier Length (m):	3.20
K2 Angle Coef:	1.00
K3 Bed Cond Coef:	1.10
Grain Size D90 (mm):	5.00000
K4 Armouring Coef:	1.00

Set K1 value to 1.0 because angle > 5 degrees

Results

Scour Depth Ys (m):	2.26
Froude #:	0.21
Equation:	CSU equation

Q500 flood year event:

Contraction Scour

		Left	Channel	Right
Input Data				
	Average Depth (m):	3.99	10.71	5.00
	Approach Velocity (m/s):	0.46	2.28	0.53
	Br Average Depth (m):	3.15	9.32	3.82
	BR Opening Flow (m3/s):	293.85	2307.65	257.06
	BR Top WD (m):	93.50	104.40	79.20
	Grain Size D50 (mm):	2.21	2.21	2.21
	Approach Flow (m3/s):	165.57	2465.83	227.15
	Approach Top WD (m):	89.64	101.00	85.04
	K1 Coefficient:	0.640	0.640	0.640
Results				
	Scour Depth Ys (m):	0.00	0.59	0.00
	Critical Velocity (m/s):	1.01	1.20	1.05
	Equation:	Clear	Live	Clear

Pier Scour

Pier: #1 (CL = 111.3)

Input Data		
	Pier Shape:	Round nose
	Pier Width (m):	0.99
	Grain Size D50 (mm):	2.21000
	Depth Upstream (m):	10.76
	Velocity Upstream (m/s):	2.23
	K1 Nose Shape:	1.00
	Pier Angle:	
	Pier Length (m):	3.20
	K2 Angle Coef:	1.00
	K3 Bed Cond Coef:	1.10
	Grain Size D90 (mm):	2.50000
	K4 Armouring Coef:	1.00
	Set K1 value to 1.0 because angle > 5 degrees	
Results		
	Scour Depth Ys (m):	2.61
	Froude #:	0.22
	Equation:	CSU equation

Pier: #2 (CL = 140.25)

Input Data

Pier Shape:	Round nose
Pier Width (m):	1.05
Grain Size D50 (mm):	2.21000
Depth Upstream (m):	10.76
Velocity Upstream (m/s):	2.23
K1 Nose Shape:	1.00
Pier Angle:	
Pier Length (m):	3.20
K2 Angle Coef:	1.00
K3 Bed Cond Coef:	1.10
Grain Size D90 (mm):	2.50000
K4 Armouring Coef:	1.00

Set K1 value to 1.0 because angle > 5 degrees

Results

Scour Depth Ys (m):	2.71
Froude #:	0.22

Equation:	CSU equation

Pier: #3 (CL = 170.75)

Input Data

Pier Shape:	Round nose
Pier Width (m):	1.05
Grain Size D50 (mm):	2.21000
Depth Upstream (m):	10.76
Velocity Upstream (m/s):	2.23
K1 Nose Shape:	1.00
Pier Angle:	
Pier Length (m):	3.20
K2 Angle Coef:	1.00
K3 Bed Cond Coef:	1.10
Grain Size D90 (mm):	2.50000
K4 Armouring Coef:	1.00

Set K1 value to 1.0 because angle > 5 degrees

Results

Scour Depth Ys (m):	2.70
Froude #:	0.22
Equation:	CSU equation

Pier: #4 (CL = 199.7)

Input Data

Pier Shape:	Round nose
Pier Width (m):	0.91
Grain Size D50 (mm):	2.21000
Depth Upstream (m):	10.76
Velocity Upstream (m/s):	2.23
K1 Nose Shape:	1.00
Pier Angle:	
Pier Length (m):	3.20
K2 Angle Coef:	1.00
K3 Bed Cond Coef:	1.10
Grain Size D90 (mm):	2.50000
K4 Armouring Coef:	1.00

Set K1 value to 1.0 because angle > 5 degrees

Results

Scour Depth Ys (m):	2.47
Froude #:	0.22
Equation:	CSU equation

Combined Scour Depths

Pier : #1 (CL = 111.3) (Contr + Pier) (m):	3.19
Pier : #2 (CL = 140.25) (Contr + Pier) (m):	3.29
Pier : #3 (CL = 170.75) (Contr + Pier) (m):	3.29
Pier : #4 (CL = 199.7) (Contr + Pier) (m):	2.47

Peak discharge event 1:

Contraction Scour

		Left	Channel	Right
Input Data				
	Average Depth (m):		3.38	
	Approach Velocity (m/s):		0.98	
	Br Average Depth (m):		3.50	
	BR Opening Flow (m3/s):		288.83	
	BR Top WD (m):		85.53	
	Grain Size D50 (mm):	2.21	2.21	2.21
	Approach Flow (m3/s):		288.83	
	Approach Top WD (m):		86.75	
	K1 Coefficient:		0.590	
Results				
	Scour Depth Ys (m):		0.00	
	Critical Velocity (m/s):		0.99	
	Equation:		Clear	

Pier Scour

Pier: #1 (CL = 111.3)

Input Data		
	Pier Shape:	Round nose
	Pier Width (m):	0.99
	Grain Size D50 (mm):	2.21000
	Depth Upstream (m):	3.51
	Velocity Upstream (m/s):	0.93
	K1 Nose Shape:	1.00
	Pier Angle:	
	Pier Length (m):	3.20
	K2 Angle Coef:	1.00
	K3 Bed Cond Coef:	1.10
	Grain Size D90 (mm):	2.50000
	K4 Armouring Coef:	1.00
	Set K1 value to 1.0 because angle > 5 degrees	
Results		
	Scour Depth Ys (m):	1.54
	Froude #:	0.16
	Equation:	CSU equation

Pier: #2 (CL = 140.25)

Input Data

Pier Shape:	Round nose
Pier Width (m):	1.05
Grain Size D50 (mm):	2.21000
Depth Upstream (m):	3.51
Velocity Upstream (m/s):	0.93
K1 Nose Shape:	1.00
Pier Angle:	
Pier Length (m):	3.20
K2 Angle Coef:	1.00
K3 Bed Cond Coef:	1.10
Grain Size D90 (mm):	2.50000
K4 Armouring Coef:	1.00

Set K1 value to 1.0 because angle > 5 degrees

Results

Scour Depth Ys (m):	1.60
Froude #:	0.16

Equation:	CSU equation

Pier: #3 (CL = 170.75)

Input Data

Pier Shape:	Round nose
Pier Width (m):	1.05
Grain Size D50 (mm):	2.21000
Depth Upstream (m):	3.51
Velocity Upstream (m/s):	0.93
K1 Nose Shape:	1.00
Pier Angle:	
Pier Length (m):	3.20
K2 Angle Coef:	1.00
K3 Bed Cond Coef:	1.10
Grain Size D90 (mm):	2.50000
K4 Armouring Coef:	1.00

Set K1 value to 1.0 because angle > 5 degrees

Results

Scour Depth Ys (m):	1.60
Froude #:	0.16
Equation:	CSU equation

Pier: #4 (CL = 199.7)

Input Data

Pier Shape:	Round nose
Pier Width (m):	0.91
Grain Size D50 (mm):	2.21000
Depth Upstream (m):	3.51
Velocity Upstream (m/s):	0.93
K1 Nose Shape:	1.00
Pier Angle:	
Pier Length (m):	3.20
K2 Angle Coef:	1.00
K3 Bed Cond Coef:	1.10
Grain Size D90 (mm):	2.50000
K4 Armouring Coef:	1.00

Set K1 value to 1.0 because angle > 5 degrees

Results

Scour Depth Ys (m):	1.46
Froude #:	0.16
Equation:	CSU equation

Peak discharge event 3:

Pier Scour

Pier: #1 (CL = 111.3)

Input Data

Pier Shape:	Round nose
Pier Width (m):	0.99
Grain Size D50 (mm):	2.21000
Depth Upstream (m):	2.59
Velocity Upstream (m/s):	0.75
K1 Nose Shape:	1.00
Pier Angle:	
Pier Length (m):	3.20
K2 Angle Coef:	1.00
K3 Bed Cond Coef:	1.10
Grain Size D90 (mm):	2.50000
K4 Armouring Coef:	1.00

Set K1 value to 1.0 because angle > 5 degrees

Results

Scour Depth Ys (m):	1.35
Froude #:	0.15
Equation:	CSU equation

Pier: #2 (CL = 140.25)

Input Data

Pier Shape:	Round nose
Pier Width (m):	1.05
Grain Size D50 (mm):	2.21000
Depth Upstream (m):	2.59
Velocity Upstream (m/s):	0.75
K1 Nose Shape:	1.00
Pier Angle:	
Pier Length (m):	3.20
K2 Angle Coef:	1.00
K3 Bed Cond Coef:	1.10
Grain Size D90 (mm):	2.50000
K4 Armouring Coef:	1.00

Set K1 value to 1.0 because angle > 5 degrees

Results

Scour Depth Ys (m):	1.40
Froude #:	0.15
Equation:	CSU equation

Pier: #3 (CL = 170.75)

Input Data

Pier Shape:	Round nose
Pier Width (m):	1.05
Grain Size D50 (mm):	2.21000
Depth Upstream (m):	2.59
Velocity Upstream (m/s):	0.75
K1 Nose Shape:	1.00
Pier Angle:	
Pier Length (m):	3.20
K2 Angle Coef:	1.00
K3 Bed Cond Coef:	1.10
Grain Size D90 (mm):	2.50000
K4 Armouring Coef:	1.00

Set K1 value to 1.0 because angle > 5 degrees

Scour Depth Ys (m):	1.40
Froude #:	0.15
Equation:	CSU equation

Pier: #4 (CL = 199.7)

Input Data

Pier Shape:	Round nose
Pier Width (m):	0.91
Grain Size D50 (mm):	2.21000
Depth Upstream (m):	2.59
Velocity Upstream (m/s):	0.75
K1 Nose Shape:	1.00
Pier Angle:	
Pier Length (m):	3.20
K2 Angle Coef:	1.00
K3 Bed Cond Coef:	1.10
Grain Size D90 (mm):	2.50000
K4 Armouring Coef:	1.00

Set K1 value to 1.0 because angle > 5 degrees

Results

Scour Depth Ys (m):	1.28
Froude #:	0.15
Equation:	CSU equation

Peak discharge event 3:

Contraction Scour

		Left	Channel	Right
Input Data				
	Average Depth (m):		0.95	
	Approach Velocity (m/s):		0.46	
	Br Average Depth (m):		1.04	
	BR Opening Flow (m3/s):		30.87	
	BR Top WD (m):		71.40	
	Grain Size D50 (mm):	2.21	2.21	2.21
	Approach Flow (m3/s):		30.87	
	Approach Top WD (m):		70.44	
	K1 Coefficient:		0.590	
Results				
	Scour Depth Ys (m):		0.00	
	Critical Velocity (m/s):		0.80	
	Equation:		Clear	

Pier Scour

Pier: #1 (CL = 111.3)

Input Data		
	Pier Shape:	Round nose
	Pier Width (m):	0.99
	Grain Size D50 (mm):	2.21000
	Depth Upstream (m):	1.04
	Velocity Upstream (m/s):	0.40
	K1 Nose Shape:	1.00
	Pier Angle:	
	Pier Length (m):	3.20
	K2 Angle Coef:	1.00
	K3 Bed Cond Coef:	1.10
	Grain Size D90 (mm):	2.50000
	K4 Armouring Coef:	1.00
	Set K1 value to 1.0 because angle > 5 degrees	
Results		
	Scour Depth Ys (m):	0.91
	Froude #:	0.13
	Equation:	CSU equation

Pier: #2 (CL = 140.25)

Input Data		
	Pier Shape:	Round nose
	Pier Width (m):	1.05
	Grain Size D50 (mm):	2.21000
	Depth Upstream (m):	1.04
	Velocity Upstream (m/s):	0.40
	K1 Nose Shape:	1.00
	Pier Angle:	
	Pier Length (m):	3.20
	K2 Angle Coef:	1.00
	K3 Bed Cond Coef:	1.10
	Grain Size D90 (mm):	2.50000
	K4 Armouring Coef:	1.00
	Set K1 value to 1.0 because angle > 5 degrees	
Results		
	Scour Depth Ys (m):	0.95
	Froude #:	0.13

Equation:	CSU equation

Pier: #3 (CL = 170.75)

Input Data

Pier Shape:	Round nose
Pier Width (m):	1.05
Grain Size D50 (mm):	2.21000
Depth Upstream (m):	1.04
Velocity Upstream (m/s):	0.40
K1 Nose Shape:	1.00
Pier Angle:	
Pier Length (m):	3.20
K2 Angle Coef:	1.00
K3 Bed Cond Coef:	1.10
Grain Size D90 (mm):	2.50000
K4 Armouring Coef:	1.00

Set K1 value to 1.0 because angle > 5 degrees

Results

Scour Depth Ys (m):	0.95
Froude #:	0.13
Equation:	CSU equation

Pier: #4 (CL = 199.7)

Input Data

Pier Shape:	Round nose
Pier Width (m):	0.91
Grain Size D50 (mm):	2.21000
Depth Upstream (m):	1.04
Velocity Upstream (m/s):	0.40
K1 Nose Shape:	1.00
Pier Angle:	
Pier Length (m):	3.20
K2 Angle Coef:	1.00
K3 Bed Cond Coef:	1.10
Grain Size D90 (mm):	2.50000
K4 Armouring Coef:	1.00

Set K1 value to 1.0 because angle > 5 degrees

Results

Scour Depth Ys (m):	0.87
Froude #:	0.13
Equation:	CSU equation

Appendix D

NDOT Provided D50 values

List of Tables

Table D.1: Previous NDOT D50 values for Lincoln's site.

Lincoln		
NDOT	Sample 2	Sample 3
N/A	0.18	0.085
	Average	
	0.1325	

Table D.2: Previous NDOT D50 values for Wilber's site.

Wilber				
NDOT	Sample 1	Sample 2	Sample 3	Sample 4
0.1	0.035	0.425	0.82	1.3
	Average			
	0.645			

Table D.3: Previous NDOT D50 values for Hooper's site.

Hooper				
NDOT	Sample 1	Sample 2	Sample 3	Sample 4
0.01	0.056	0.07	0.053	0.068
	Average			
	0.06175			

Table D.4: Previous NDOT D50 values for Beatrice's site.

Beatrice					
NDOT	Sample 1	Sample 2	Sample 3	Sample 4	Sample 5
0.1	0.56	0.04	1.2	0.07	0.037
	Average				
	0.3814				

Appendix E

NDOT's HEC-RAS Models

List of Figure

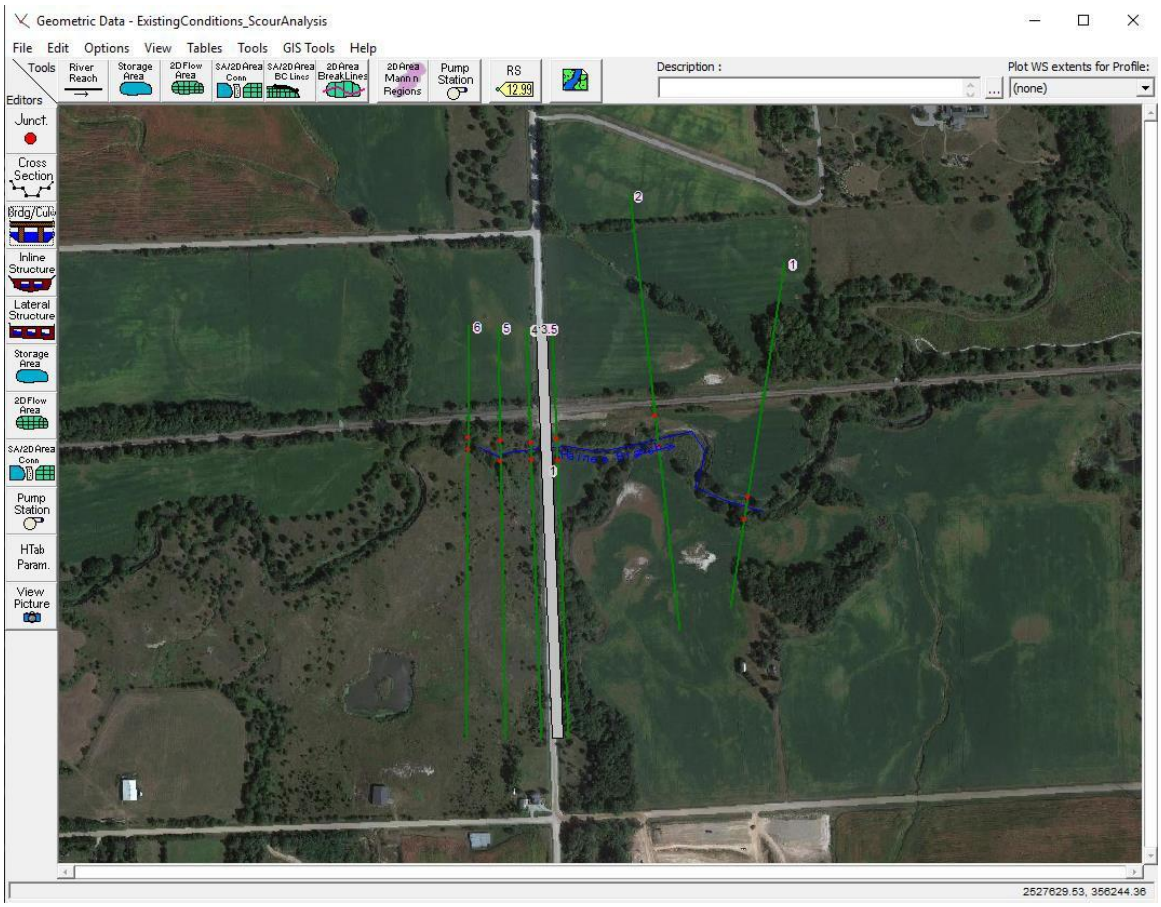

Figure E.1: NDOT's HEC-RAS geometric data (Lincoln).

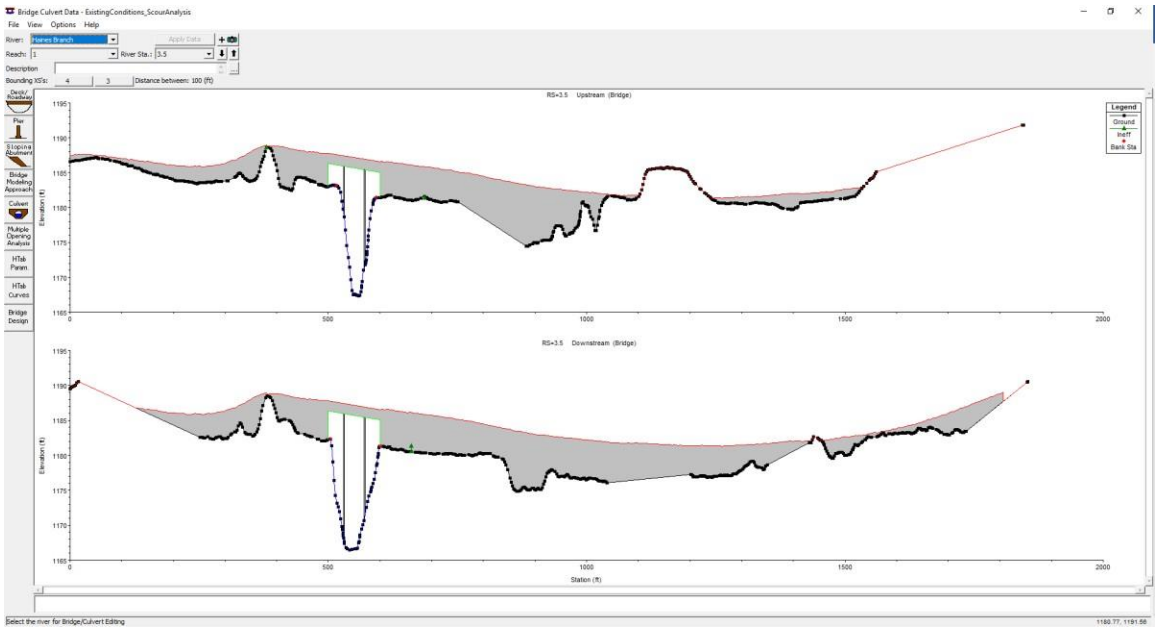

Figure E.2: NDOT's HEC-RAS Bridge geometry data (Lincoln).

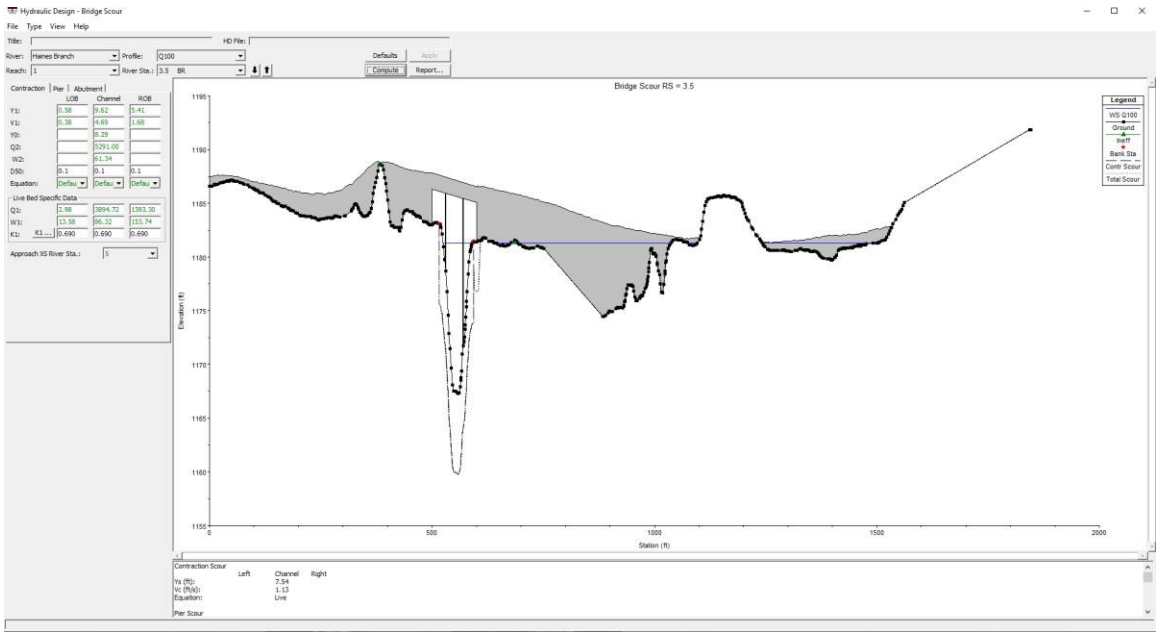

Figure E.3: NDOT's HEC-RAS Hydraulic design computation (Lincoln).

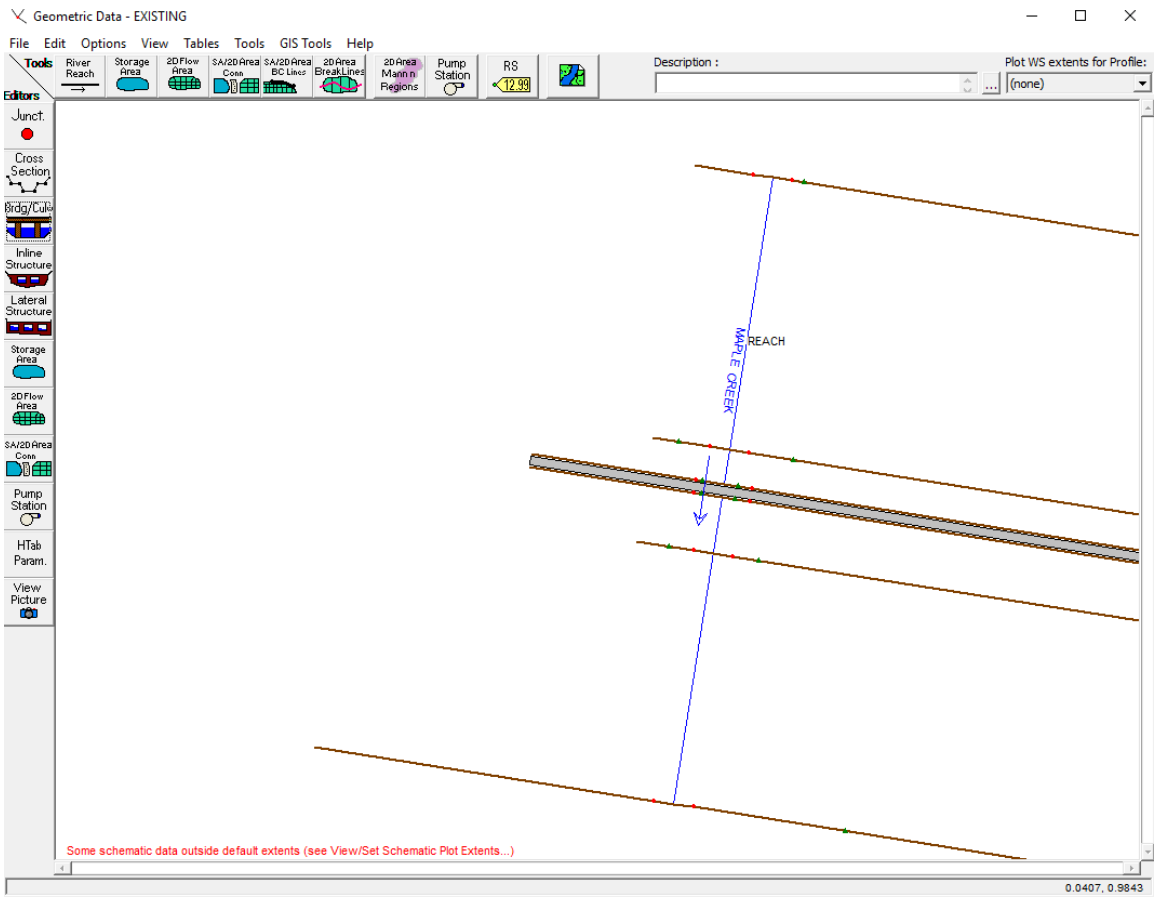

Figure E.4: NDOT's HEC-RAS geometric data (Hooper).

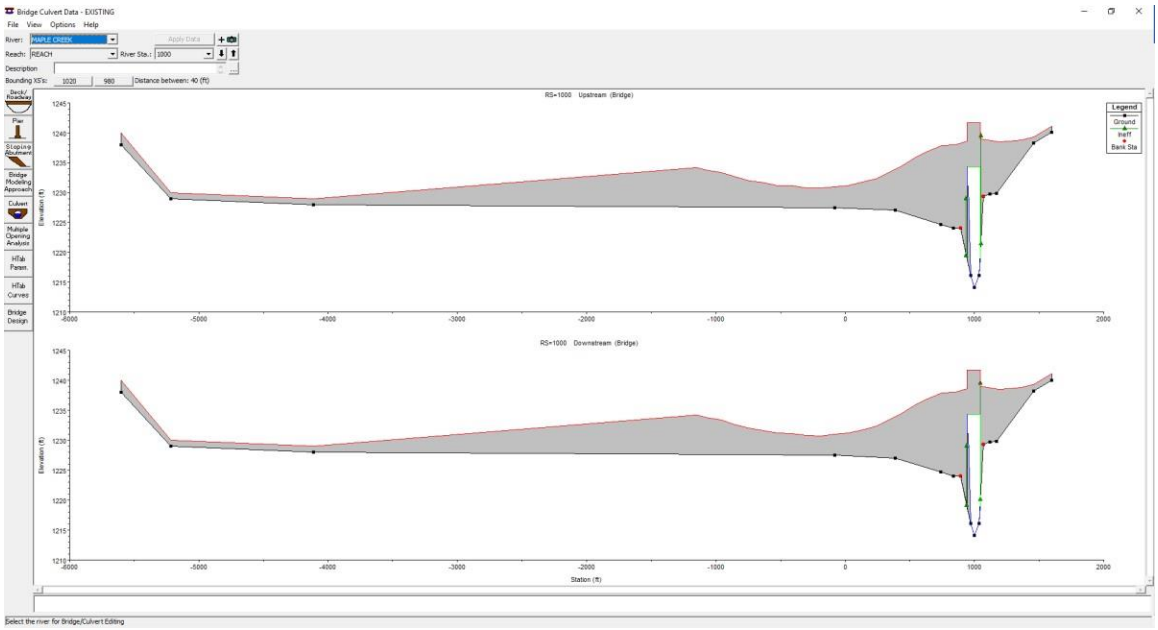

Figure E.5: NDOT's HEC-RAS bridge geometry data (Hooper).

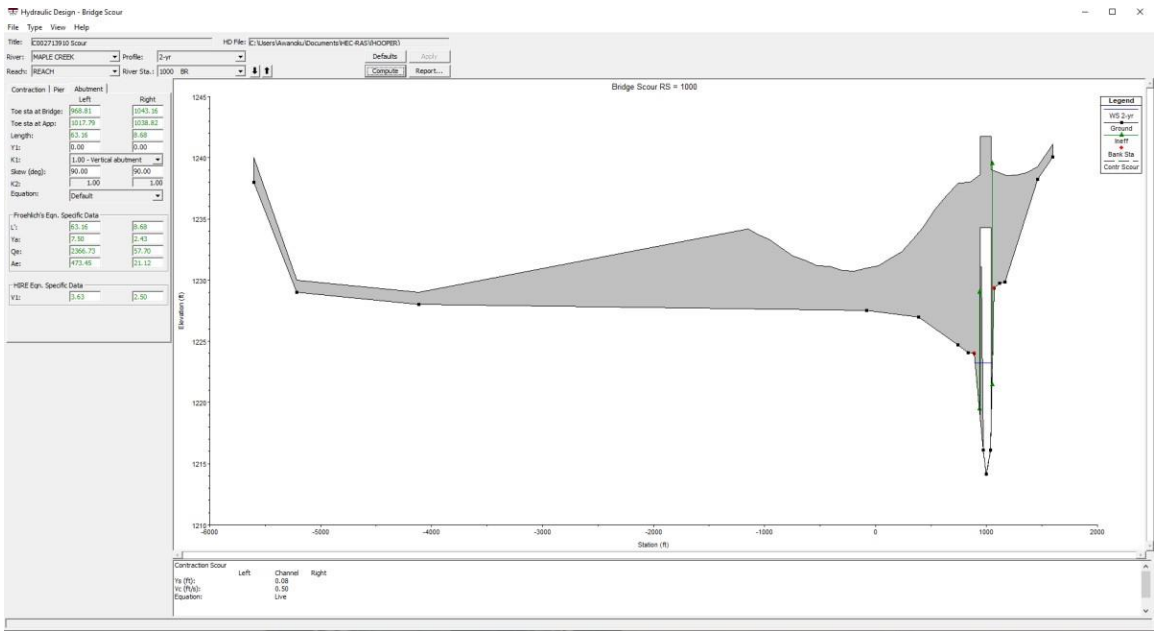

Figure E.6: NDOT's HEC-RAS hydraulic design computation (Hooper).

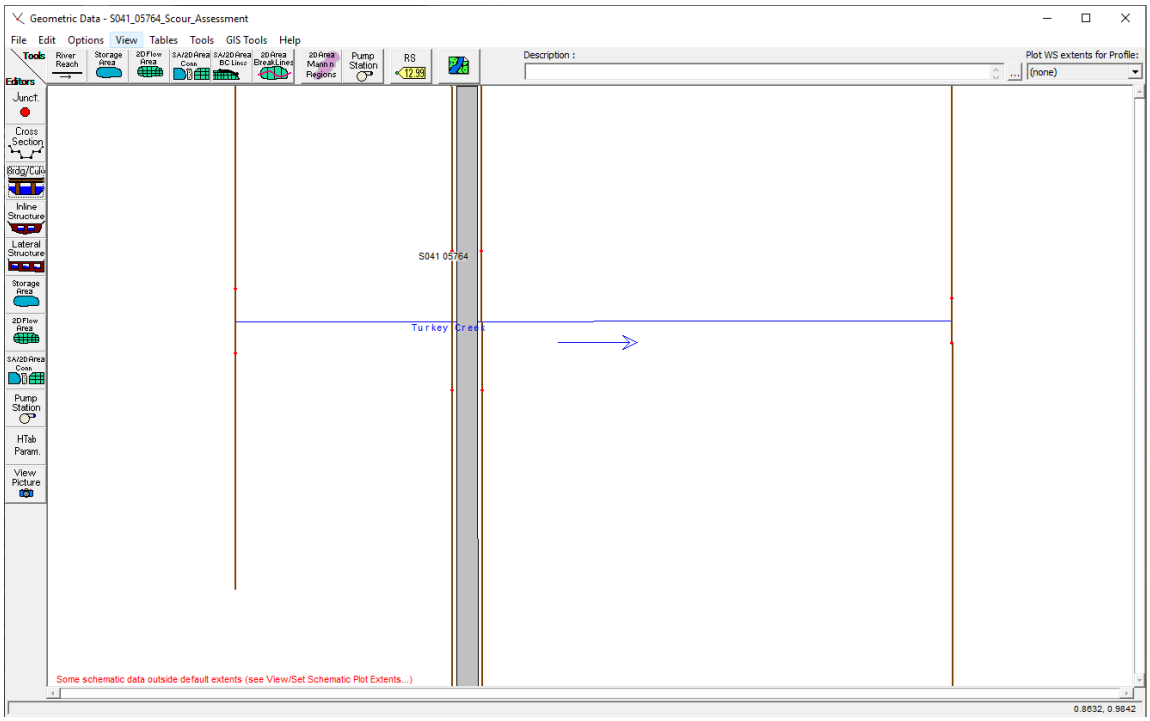

Figure E.7: NDOT's HEC-RAS geometric data (Wilber).

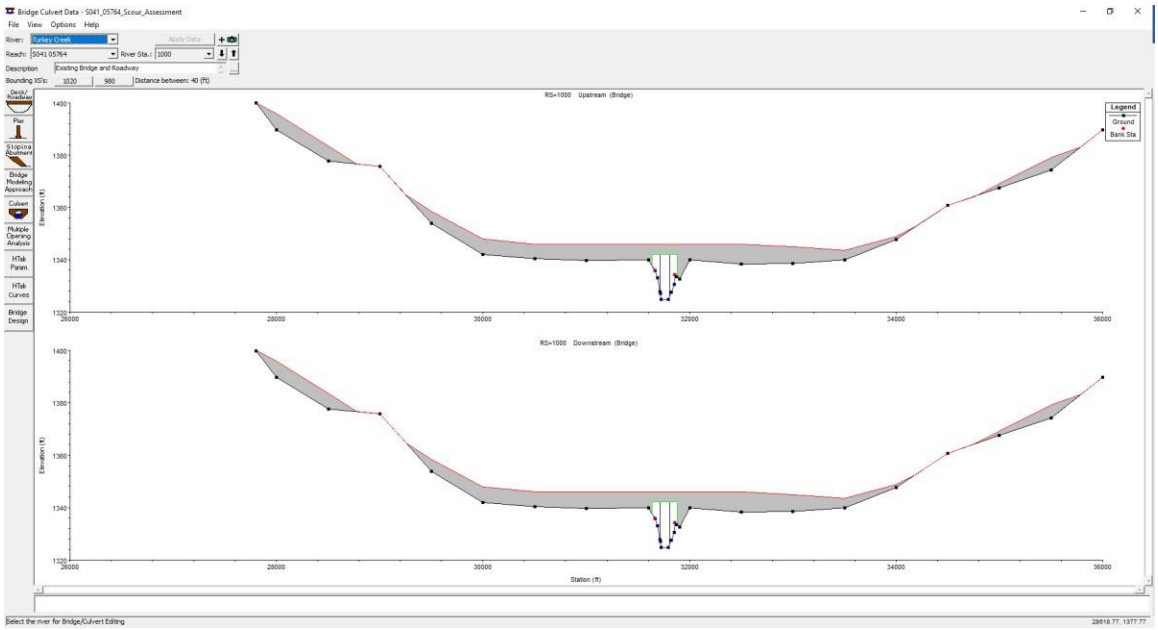

Figure E.8: NDOT's HEC-RAS bridge geometry data (Wilber).

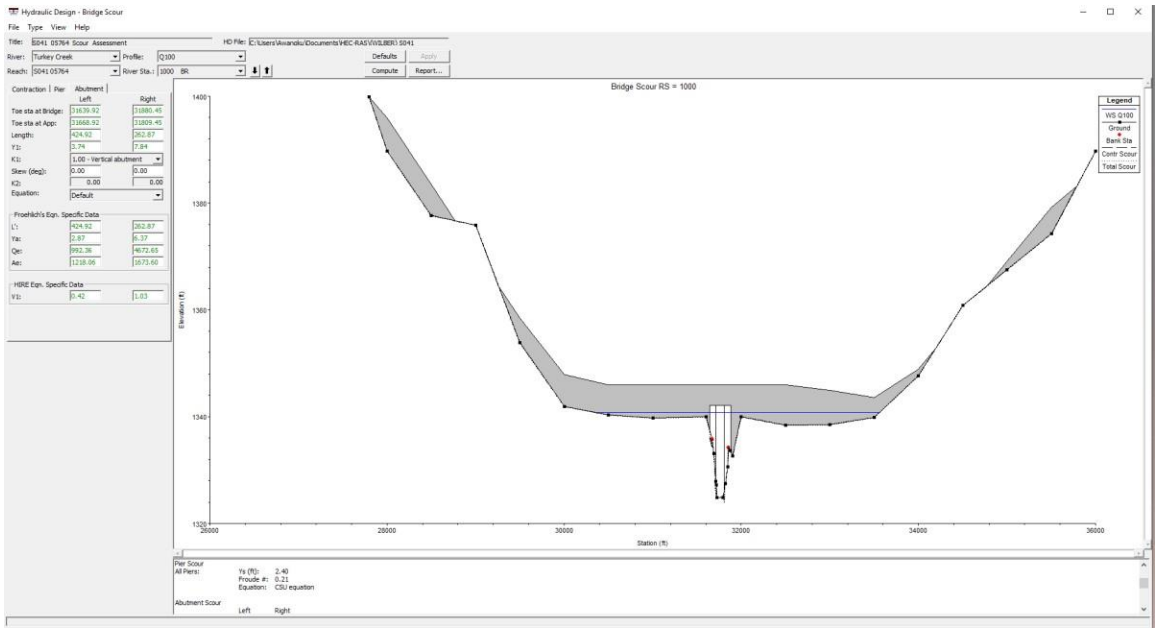

Figure E.9: NDOT's HEC-RAS hydraulic design computation (Wilber).

Appendix F

NDOT Provided HEC-RAS Output Reports

NDOT HOOPER MODEL:

Q100 flood year event:

Contraction Scour

		Left	Channel	Right
Input Data				
	Average Depth (ft):	2.46	12.23	1.16
	Approach Velocity (ft/s):	1.07	3.46	0.65
	Br Average Depth (ft):	0.00	13.67	0.00
	BR Opening Flow (cfs):	0.00	8981.80	0.00
	BR Top WD (ft):	0.00	88.83	0.00
	Grain Size D50 (mm):	0.01	0.01	0.01
	Approach Flow (cfs):	16383.40	5340.56	76.03
	Approach Top WD (ft):	6213.63	126.37	100.91
	K1 Coefficient:	0.690	0.690	0.690
Results				
	Scour Depth Ys (ft):		10.68	
	Critical Velocity (ft/s):		0.55	
	Equation:		Live	

Combined Scour Depths

Peak discharge event 1:

Contraction Scour

		Left	Channel	Right
Input Data				
	Average Depth (ft):		1.98	
	Approach Velocity (ft/s):		2.23	
	Br Average Depth (ft):		2.10	
	BR Opening Flow (cfs):		325.00	
	BR Top WD (ft):		71.41	
	Grain Size D50 (mm):	0.01	0.01	0.01
	Approach Flow (cfs):		325.00	
	Approach Top WD (ft):		73.66	
	K1 Coefficient:		0.690	
Results				
	Scour Depth Ys (ft):		0.00	
	Critical Velocity (ft/s):		0.40	
	Equation:		Live	

Peak discharge event 2:

Contraction Scour

		Left	Channel	Right
Input Data				
	Average Depth (ft):		4.14	
	Approach Velocity (ft/s):		3.52	
	Br Average Depth (ft):		4.27	
	BR Opening Flow (cfs):		1180.00	
	BR Top WD (ft):		78.07	
	Grain Size D50 (mm):		0.01	
	Approach Flow (cfs):		1180.00	
	Approach Top WD (ft):		80.87	
	K1 Coefficient:		0.690	
Results				
	Scour Depth Ys (ft):		0.00	
	Critical Velocity (ft/s):		0.45	
	Equation:		Live	

Peak discharge event 3:

Contraction Scour

		Left	Channel	Right
Input Data				
	Average Depth (ft):		3.97	
	Approach Velocity (ft/s):		3.42	
	Br Average Depth (ft):		4.07	
	BR Opening Flow (cfs):		1090.00	
	BR Top WD (ft):		77.85	
	Grain Size D50 (mm):		0.10	
	Approach Flow (cfs):		1090.00	
	Approach Top WD (ft):		80.25	
	K1 Coefficient:		0.690	
Results				
	Scour Depth Ys (ft):		0.00	
	Critical Velocity (ft/s):		0.97	
	Equation:		Live	

Peak discharge event 4:

Contraction Scour

		Left	Channel	Right
Input Data				
	Average Depth (ft):		3.13	
	Approach Velocity (ft/s):		2.96	
	Br Average Depth (ft):		3.20	
	BR Opening Flow (cfs):		716.00	
	BR Top WD (ft):		76.02	
	Grain Size D50 (mm):		0.10	
	Approach Flow (cfs):		716.00	
	Approach Top WD (ft):		77.42	
	K1 Coefficient:		0.690	
Results				
	Scour Depth Ys (ft):		0.00	
	Critical Velocity (ft/s):		0.93	
	Equation:		Live	

NDOT LINCOLN MODEL:

Q100 flood year event:

Contraction Scour

		Left	Channel	Right
Input Data				
	Average Depth (ft):	0.58	9.62	5.41
	Approach Velocity (ft/s):	0.38	4.69	1.68
	Br Average Depth (ft):		8.29	
	BR Opening Flow (cfs):		5291.00	
	BR Top WD (ft):		61.34	
	Grain Size D50 (mm):	0.13	0.13	0.13
	Approach Flow (cfs):	2.98	3894.72	1393.30
	Approach Top WD (ft):	13.58	86.32	153.74
	K1 Coefficient:	0.640	0.690	0.690
Results				
	Scour Depth Ys (ft):		7.54	
	Critical Velocity (ft/s):		1.23	
	Equation:		Live	

Pier Scour

All piers have the same scour depth

Input Data		
	Pier Shape:	Round nose
	Pier Width (ft):	2.00
	Grain Size D50 (mm):	0.13000
	Depth Upstream (ft):	8.63
	Velocity Upstream (ft/s):	6.99
	K1 Nose Shape:	1.00
	Pier Angle:	0.00
	Pier Length (ft):	40.00
	K2 Angle Coef:	1.00
	K3 Bed Cond Coef:	1.10
	Grain Size D90 (mm):	1.00000
	K4 Armouring Coef:	1.00
Results		
	Scour Depth Ys (ft):	4.80
	Froude #:	0.42
	Equation:	CSU equation
	Pier Scour Limited to Maximum of Ys = 2.4 * a	

Abutment Scour

		Left	Right
Input Data			
	Station at Toe (ft):	500.00	600.00
	Toe Sta at appr (ft):	501.63	616.60
	Abutment Length (ft):	13.58	153.74
	Depth at Toe (ft):	-0.44	1.16
	K1 Shape Coef:	1.00 - Vertical abutment	
	Degree of Skew (degrees):	90.00	90.00
	K2 Skew Coef:	1.00	1.00
	Projected Length L' (ft):	13.58	153.74
	Avg Depth Obstructed Ya (ft):	0.58	5.41
	Flow Obstructed Qe (cfs):	2.98	1393.30

	Area Obstructed Ae (sq ft):	7.89	831.13
Results			
	Scour Depth Ys (ft):		4.63

Froude #:		0.16
Equation:	Default	HIRE

Combined Scour Depths

Pier Scour + Contraction Scour (ft):		
	Channel:	12.34
Right abutment scour + contraction scour (ft):	4.63	

Peak discharge event 1:

Contraction Scour

		Left	Channel	Right
Input Data				
	Average Depth (ft):		1.13	
	Approach Velocity (ft/s):		0.93	
	Br Average Depth (ft):		0.51	
	BR Opening Flow (cfs):		27.60	
	BR Top WD (ft):		17.59	
	Grain Size D50 (mm):	0.13	0.13	0.13
	Approach Flow (cfs):		27.60	
	Approach Top WD (ft):		26.27	
	K1 Coefficient:		0.640	
Results				
	Scour Depth Ys (ft):		0.95	
	Critical Velocity (ft/s):		0.86	
	Equation:		Live	

Pier Scour

All piers have the same scour depth

Input Data		
	Pier Shape:	Round nose
	Pier Width (ft):	2.00
	Grain Size D50 (mm):	0.13000
	Depth Upstream (ft):	0.74
	Velocity Upstream (ft/s):	2.02
	K1 Nose Shape:	1.00
	Pier Angle:	0.00
	Pier Length (ft):	40.00
	K2 Angle Coef:	1.00
	K3 Bed Cond Coef:	1.10
	Grain Size D90 (mm):	1.00000
	K4 Armouring Coef:	1.00
Results		
	Scour Depth Ys (ft):	2.12
	Froude #:	0.41
	Equation:	CSU equation

Combined Scour Depths

Pier Scour + Contraction Scour (ft):

	Channel:	3.07

Peak discharge event 2:

Contraction Scour

		Left	Channel	Right
Input Data				
	Average Depth (ft):		4.97	
	Approach Velocity (ft/s):		2.94	
	Br Average Depth (ft):		4.51	
	BR Opening Flow (cfs):		630.00	
	BR Top WD (ft):		35.90	
	Grain Size D50 (mm):	0.13	0.13	0.13
	Approach Flow (cfs):		630.00	
	Approach Top WD (ft):		43.22	
	K1 Coefficient:		0.690	
Results				
	Scour Depth Ys (ft):		1.14	
	Critical Velocity (ft/s):		1.10	
	Equation:		Live	

Pier Scour

All piers have the same scour depth

Input Data		
	Pier Shape:	Round nose
	Pier Width (ft):	2.00
	Grain Size D50 (mm):	0.13000
	Depth Upstream (ft):	4.43
	Velocity Upstream (ft/s):	3.74
	K1 Nose Shape:	1.00
	Pier Angle:	0.00
	Pier Length (ft):	40.00
	K2 Angle Coef:	1.00
	K3 Bed Cond Coef:	1.10
	Grain Size D90 (mm):	1.00000
	K4 Armouring Coef:	1.00
Results		
	Scour Depth Ys (ft):	3.53
	Froude #:	0.31
	Equation:	CSU equation

Combined Scour Depths

Pier Scour + Contraction Scour (ft):

	Channel:	4.66

Peak discharge event 3:

Contraction Scour

		Left	Channel	Right
Input Data				
	Average Depth (ft):		4.04	
	Approach Velocity (ft/s):		2.36	
	Br Average Depth (ft):		3.43	
	BR Opening Flow (cfs):		336.00	
	BR Top WD (ft):		29.30	
	Grain Size D50 (mm):	0.13	0.13	0.13
	Approach Flow (cfs):		336.00	
	Approach Top WD (ft):		35.21	
	K1 Coefficient:		0.690	
Results				
	Scour Depth Ys (ft):		1.16	
	Critical Velocity (ft/s):		1.06	
	Equation:		Live	

Pier Scour

All piers have the same scour depth

Input Data		
	Pier Shape:	Round nose
	Pier Width (ft):	2.00
	Grain Size D50 (mm):	0.13000
	Depth Upstream (ft):	3.26
	Velocity Upstream (ft/s):	3.27
	K1 Nose Shape:	1.00
	Pier Angle:	0.00
	Pier Length (ft):	40.00
	K2 Angle Coef:	1.00
	K3 Bed Cond Coef:	1.10
	Grain Size D90 (mm):	1.00000
	K4 Armouring Coef:	1.00
Results		
	Scour Depth Ys (ft):	3.20
	Froude #:	0.32
	Equation:	CSU equation

Combined Scour Depths

	Pier Scour + Contraction Scour (ft):		
		Channel:	4.35

Peak discharge event 4:

Contraction Scour

		Left	Channel	Right
Input Data				
	Average Depth (ft):		1.41	
	Approach Velocity (ft/s):		1.18	
	Br Average Depth (ft):		0.89	
	BR Opening Flow (cfs):		45.30	
	BR Top WD (ft):		19.11	
	Grain Size D50 (mm):	0.13	0.13	0.13
	Approach Flow (cfs):		45.30	
	Approach Top WD (ft):		27.35	
	K1 Coefficient:		0.690	
Results				
	Scour Depth Ys (ft):		0.92	
	Critical Velocity (ft/s):		0.89	
	Equation:		Live	

Pier Scour

All piers have the same scour depth

Input Data		
	Pier Shape:	Round nose
	Pier Width (ft):	2.00
	Grain Size D50 (mm):	0.13000
	Depth Upstream (ft):	1.01
	Velocity Upstream (ft/s):	2.30
	K1 Nose Shape:	1.00
	Pier Angle:	0.00
	Pier Length (ft):	40.00
	K2 Angle Coef:	1.00
	K3 Bed Cond Coef:	1.10
	Grain Size D90 (mm):	1.00000
	K4 Armouring Coef:	1.00
Results		
	Scour Depth Ys (ft):	2.35
	Froude #:	0.40
	Equation:	CSU equation

Combined Scour Depths

	Pier Scour + Contraction Scour (ft):		
		Channel:	3.26

NDOT WILBER MODEL:
Q100 flood year event:

Contraction Scour

		Left	Channel	Right
Input Data				
	Average Depth (ft):	3.05	12.29	6.49
	Approach Velocity (ft/s):	0.85	8.93	2.82
	Br Average Depth (ft):	4.08	12.88	6.96
	BR Opening Flow (cfs):	174.71	15090.44	734.85
	BR Top WD (ft):	28.02	185.00	25.07
	Grain Size D50 (mm):	0.10	0.10	0.10
	Approach Flow (cfs):	1177.02	9547.16	5275.82
	Approach Top WD (ft):	453.00	87.00	288.33
	K1 Coefficient:	0.690	0.690	0.690
Results				
	Scour Depth Ys (ft):	1.47	0.00	0.00
	Critical Velocity (ft/s):	0.93	1.17	1.06
	Equation:	Clear	Live	Live

Pier Scour

All piers have the same scour depth

Input Data		
	Pier Shape:	Round nose
	Pier Width (ft):	1.00
	Grain Size D50 (mm):	0.10000
	Depth Upstream (ft):	16.48
	Velocity Upstream (ft/s):	4.75
	K1 Nose Shape:	1.00
	Pier Angle:	0.00
	Pier Length (ft):	28.00
	K2 Angle Coef:	1.00
	K3 Bed Cond Coef:	1.10
	Grain Size D90 (mm):	0.20000
	K4 Armouring Coef:	1.00
Results		
	Scour Depth Ys (ft):	2.40
	Froude #:	0.21
	Equation:	CSU equation
	Pier Scour Limited to Maximum of Ys = 2.4 * a	

Abutment Scour

		Left	Right
Input Data			
	Station at Toe (ft):	31639.92	31880.45
	Toe Sta at appr (ft):	31668.92	31809.45
	Abutment Length (ft):	424.92	262.88
	Depth at Toe (ft):	3.74	7.84
	K1 Shape Coef:	1.00 - Vertical abutment	
	Degree of Skew (degrees):	0.00	0.00
	K2 Skew Coef:	0.00	0.00
	Projected Length L' (ft):	424.92	262.88
	Avg Depth Obstructed Ya (ft):	2.87	6.37
	Flow Obstructed Qe (cfs):	993.31	4673.21

	Area Obstructed Ae (sq ft):	1219.15	1674.27
Results			
	Scour Depth Ys (ft):	0.00	0.00
	Froude #:	0.04	0.06
	Equation:	HIRE	HIRE

Combined Scour Depths

Pier Scour + Contraction Scour (ft):		
	Channel:	2.40
Left abutment scour + contraction scour (ft):	1.47	
Right abutment scour + contraction scour (ft):	0.00	

Peak discharge event 1:

Contraction Scour

		Left	Channel	Right
Input Data				
	Average Depth (ft):		1.82	
	Approach Velocity (ft/s):		1.98	
	Br Average Depth (ft):		1.90	
	BR Opening Flow (cfs):		153.00	
	BR Top WD (ft):		95.88	
	Grain Size D50 (mm):	0.10	0.10	0.10
	Approach Flow (cfs):		153.00	
	Approach Top WD (ft):		42.40	
	K1 Coefficient:		0.690	
Results				
	Scour Depth Ys (ft):		0.00	
	Critical Velocity (ft/s):		0.85	
	Equation:		Live	

Pier Scour

All piers have the same scour depth

Input Data		
	Pier Shape:	Round nose
	Pier Width (ft):	1.00
	Grain Size D50 (mm):	0.10000
	Depth Upstream (ft):	2.23
	Velocity Upstream (ft/s):	0.89
	K1 Nose Shape:	1.00
	Pier Angle:	0.00
	Pier Length (ft):	28.00
	K2 Angle Coef:	1.00
	K3 Bed Cond Coef:	1.10
	Grain Size D90 (mm):	0.20000
	K4 Armouring Coef:	1.00
Results		
	Scour Depth Ys (ft):	1.10
	Froude #:	0.10
	Equation:	CSU equation

Peak discharge event 2:

Contraction Scour

		Left	Channel	Right
Input Data				
	Average Depth (ft):	0.02	6.47	1.45
	Approach Velocity (ft/s):	0.02	3.82	0.70
	Br Average Depth (ft):		7.56	1.36
	BR Opening Flow (cfs):		2309.89	20.11
	BR Top WD (ft):		179.58	25.36
	Grain Size D50 (mm):	0.10	0.10	0.10
	Approach Flow (cfs):	0.00	2122.37	207.63
	Approach Top WD (ft):	9.30	85.90	205.42
	K1 Coefficient:	0.640	0.690	0.690
Results				
	Scour Depth Ys (ft):		0.00	0.00
	Critical Velocity (ft/s):		1.06	0.82
	Equation:		Live	Clear

Pier Scour

All piers have the same scour depth

Input Data		
	Pier Shape:	Round nose
	Pier Width (ft):	1.00
	Grain Size D50 (mm):	0.10000
	Depth Upstream (ft):	10.40
	Velocity Upstream (ft/s):	1.85
	K1 Nose Shape:	1.00
	Pier Angle:	0.00
	Pier Length (ft):	28.00
	K2 Angle Coef:	1.00
	K3 Bed Cond Coef:	1.10
	Grain Size D90 (mm):	0.20000
	K4 Armouring Coef:	1.00
Results		
	Scour Depth Ys (ft):	1.87
	Froude #:	0.10
	Equation:	CSU equation

Abutment Scour

		Left	Right	
Input Data				
	Station at Toe (ft):	31639.92	31880.45	
	Toe Sta at appr (ft):	31668.92	31809.45	
	Abutment Length (ft):	9.68	179.97	
	Depth at Toe (ft):	-2.34	1.76	
	K1 Shape Coef:	1.00 - Vertical abutment		
	Degree of Skew (degrees):			
	K2 Skew Coef:	0.00	0.00	
	Projected Length L' (ft):	9.68	179.97	
	Avg Depth Obstructed Ya (ft):	133522600000000000000000000000000000.00		1.40
	Flow Obstructed Qe (cfs):	129262700000000000000000000000000000.00		172.75

	Area Obstructed Ae (sq ft):	1292627000000000000000000000000000000.00	251.99

Results

Scour Depth Ys (ft):	0.00
Froude #:	0.08

Peak discharge event 3:

Contraction Scour

		Left	Channel	Right
Input Data				
	Average Depth (ft):		5.37	
	Approach Velocity (ft/s):		3.76	
	Br Average Depth (ft):		6.13	
	BR Opening Flow (cfs):		1390.00	
	BR Top WD (ft):		158.09	
	Grain Size D50 (mm):	0.10	0.10	0.10
	Approach Flow (cfs):		1390.00	
	Approach Top WD (ft):		68.90	
	K1 Coefficient:		0.690	
Results				
	Scour Depth Ys (ft):		0.00	
	Critical Velocity (ft/s):		1.02	
	Equation:		Live	

Pier Scour

All piers have the same scour depth

Input Data		
	Pier Shape:	Round nose
	Pier Width (ft):	1.00
	Grain Size D50 (mm):	0.10000
	Depth Upstream (ft):	8.09
	Velocity Upstream (ft/s):	1.59
	K1 Nose Shape:	1.00
	Pier Angle:	0.00
	Pier Length (ft):	28.00
	K2 Angle Coef:	1.00
	K3 Bed Cond Coef:	1.10
	Grain Size D90 (mm):	0.20000
	K4 Armouring Coef:	1.00
Results		
	Scour Depth Ys (ft):	1.69
	Froude #:	0.10
	Equation:	CSU equation

Peak discharge event 4:

Contraction Scour

		Left	Channel	Right
Input Data				
	Average Depth (ft):		2.09	
	Approach Velocity (ft/s):		2.11	
	Br Average Depth (ft):		2.11	
	BR Opening Flow (cfs):		191.00	
	BR Top WD (ft):		101.28	
	Grain Size D50 (mm):	0.10	0.10	0.10
	Approach Flow (cfs):		191.00	
	Approach Top WD (ft):		43.26	
	K1 Coefficient:		0.690	
Results				
	Scour Depth Ys (ft):		0.00	
	Critical Velocity (ft/s):		0.87	
	Equation:		Live	

Pier Scour

All piers have the same scour depth

Input Data		
	Pier Shape:	Round nose
	Pier Width (ft):	1.00
	Grain Size D50 (mm):	0.10000
	Depth Upstream (ft):	2.55
	Velocity Upstream (ft/s):	0.95
	K1 Nose Shape:	1.00
	Pier Angle:	0.00
	Pier Length (ft):	28.00
	K2 Angle Coef:	1.00
	K3 Bed Cond Coef:	1.10
	Grain Size D90 (mm):	0.20000
	K4 Armouring Coef:	1.00
Results		
	Scour Depth Ys (ft):	1.16
	Froude #:	0.11
	Equation:	CSU equation

NDOT BEATRICE MODEL:
Q100 flood year event:

Contraction Scour

		Left	Channel	Right
Input Data				
	Average Depth (ft):	4.91	28.60	5.97
	Approach Velocity (ft/s):	1.62	7.82	1.85
	Br Average Depth (ft):	3.25	28.46	4.82
	BR Opening Flow (cfs):	2699.01	53282.70	4018.29
	BR Top WD (ft):	639.47	278.09	576.72
	Grain Size D50 (mm):	0.10	0.10	0.10
	Approach Flow (cfs):	7071.97	44733.30	8194.73
	Approach Top WD (ft):	887.84	200.00	741.69
	K1 Coefficient:	0.690	0.690	0.690
Results				
	Scour Depth Ys (ft):	0.00	0.00	0.00
	Critical Velocity (ft/s):	1.01	1.35	1.04
	Equation:	Live	Live	Live

Pier Scour

Pier: #1 (CL = 637)

Input Data

	Pier Shape:	Round nose
	Pier Width (ft):	3.08
	Grain Size D50 (mm):	0.10000
	Depth Upstream (ft):	30.07
	Velocity Upstream (ft/s):	6.35
	K1 Nose Shape:	1.00
	Pier Angle:	0.00
	Pier Length (ft):	58.00
	K2 Angle Coef:	1.00
	K3 Bed Cond Coef:	1.10
	Grain Size D90 (mm):	0.20000
	K4 Armouring Coef:	1.00

Results

	Scour Depth Ys (ft):	7.40
	Froude #:	0.20
	Equation:	CSU equation
	Pier Scour Limited to Maximum of Ys = 2.4 * a	

Pier: #2 (CL = 732)

Input Data

	Pier Shape:	Round nose
	Pier Width (ft):	3.40
	Grain Size D50 (mm):	0.10000
	Depth Upstream (ft):	30.07
	Velocity Upstream (ft/s):	6.35
	K1 Nose Shape:	1.00
	Pier Angle:	0.00
	Pier Length (ft):	58.00
	K2 Angle Coef:	1.00
	K3 Bed Cond Coef:	1.10
	Grain Size D90 (mm):	0.20000
	K4 Armouring Coef:	1.00

Results

	Scour Depth Ys (ft):	8.09
	Froude #:	0.20

	Equation:	CSU equation

Pier: #3 (CL = 832)

Input Data

Pier Shape:	Round nose
Pier Width (ft):	3.45
Grain Size D50 (mm):	0.10000
Depth Upstream (ft):	30.07
Velocity Upstream (ft/s):	6.35
K1 Nose Shape:	1.00
Pier Angle:	0.00
Pier Length (ft):	58.00
K2 Angle Coef:	1.00
K3 Bed Cond Coef:	1.10
Grain Size D90 (mm):	0.20000
K4 Armouring Coef:	1.00

Results

Scour Depth Ys (ft):	8.17
Froude #:	0.20
Equation:	CSU equation

Pier: #4 (CL = 927)

Input Data

Pier Shape:	Round nose
Pier Width (ft):	3.07
Grain Size D50 (mm):	0.10000
Depth Upstream (ft):	30.07
Velocity Upstream (ft/s):	6.35
K1 Nose Shape:	1.00
Pier Angle:	0.00
Pier Length (ft):	58.00
K2 Angle Coef:	1.00
K3 Bed Cond Coef:	1.10
Grain Size D90 (mm):	0.20000
K4 Armouring Coef:	1.00

Results

Scour Depth Ys (ft):	7.36
Froude #:	0.20
Equation:	CSU equation
Pier Scour Limited to Maximum of Ys = 2.4 * a	

Abutment Scour

	Left	Right
Input Data		
Station at Toe (ft):	565.00	1000.00
Toe Sta at appr (ft):	660.00	1002.00
Abutment Length (ft):	817.84	669.69
Depth at Toe (ft):	7.82	7.42
K1 Shape Coef:	1.00 - Vertical abutment	
Degree of Skew (degrees):		
K2 Skew Coef:	0.00	0.00
Projected Length L' (ft):	817.84	669.69
Avg Depth Obstructed Ya (ft):	4.49	5.59
Flow Obstructed Qe (cfs):	5603.77	6605.41
Area Obstructed Ae (sq ft):	3671.71	3741.49

Results

Scour Depth Ys (ft):	0.00	0.00
Froude #:	0.09	0.11
Equation:	HIRE	HIRE

Peak discharge event 1:

Contraction Scour

		Left	Channel	Right
Input Data				
	Average Depth (ft):	1.86	11.65	1.71
	Approach Velocity (ft/s):	0.85	4.36	0.79
	Br Average Depth (ft):		11.25	
	BR Opening Flow (cfs):		10200.00	
	BR Top WD (ft):		280.84	
	Grain Size D50 (mm):	0.10	0.10	0.10
	Approach Flow (cfs):	23.44	10163.29	13.27
	Approach Top WD (ft):	14.89	200.00	9.86
	K1 Coefficient:	0.690	0.690	0.690
Results				
	Scour Depth Ys (ft):		0.00	
	Critical Velocity (ft/s):		1.16	
	Equation:		Live	

Pier Scour

Pier: #1 (CL = 637)

Input Data		
	Pier Shape:	Round nose
	Pier Width (ft):	3.08
	Grain Size D50 (mm):	0.10000
	Depth Upstream (ft):	13.05
	Velocity Upstream (ft/s):	3.48
	K1 Nose Shape:	1.00
	Pier Angle:	0.00
	Pier Length (ft):	58.00
	K2 Angle Coef:	1.00
	K3 Bed Cond Coef:	1.10
	Grain Size D90 (mm):	0.20000
	K4 Armouring Coef:	1.00
Results		
	Scour Depth Ys (ft):	5.24
	Froude #:	0.17
	Equation:	CSU equation

Pier: #2 (CL = 732)

Input Data		
	Pier Shape:	Round nose
	Pier Width (ft):	3.40
	Grain Size D50 (mm):	0.10000
	Depth Upstream (ft):	13.05
	Velocity Upstream (ft/s):	3.48
	K1 Nose Shape:	1.00
	Pier Angle:	0.00
	Pier Length (ft):	58.00
	K2 Angle Coef:	1.00
	K3 Bed Cond Coef:	1.10
	Grain Size D90 (mm):	0.20000
	K4 Armouring Coef:	1.00
Results		
	Scour Depth Ys (ft):	5.58
	Froude #:	0.17
	Equation:	CSU equation

Pier: #3 (CL = 832)

Input Data

Pier Shape:	Round nose
Pier Width (ft):	3.45
Grain Size D50 (mm):	0.10000
Depth Upstream (ft):	13.05
Velocity Upstream (ft/s):	3.48
K1 Nose Shape:	1.00
Pier Angle:	0.00
Pier Length (ft):	58.00
K2 Angle Coef:	1.00
K3 Bed Cond Coef:	1.10
Grain Size D90 (mm):	0.20000
K4 Armouring Coef:	1.00

Results

Scour Depth Ys (ft):	5.64
Froude #:	0.17
Equation:	CSU equation

Pier: #4 (CL = 927)

Input Data

Pier Shape:	Round nose
Pier Width (ft):	3.07
Grain Size D50 (mm):	0.10000
Depth Upstream (ft):	13.05
Velocity Upstream (ft/s):	3.48
K1 Nose Shape:	1.00
Pier Angle:	0.00
Pier Length (ft):	58.00
K2 Angle Coef:	1.00
K3 Bed Cond Coef:	1.10
Grain Size D90 (mm):	0.20000
K4 Armouring Coef:	1.00

Results

Scour Depth Ys (ft):	5.22
Froude #:	0.17
Equation:	CSU equation

Peak discharge event 2:

Contraction Scour

		Left	Channel	Right
Input Data				
	Average Depth (ft):	0.06	8.09	
	Approach Velocity (ft/s):	0.09	3.45	
	Br Average Depth (ft):		7.79	
	BR Opening Flow (cfs):		5560.00	
	BR Top WD (ft):		275.59	
	Grain Size D50 (mm):	0.10	0.10	0.10
	Approach Flow (cfs):	0.00	5560.00	
	Approach Top WD (ft):	0.51	199.27	
	K1 Coefficient:	0.640	0.690	
Results				
	Scour Depth Ys (ft):		0.00	
	Critical Velocity (ft/s):		1.10	
	Equation:		Live	

Pier Scour

Pier: #1 (CL = 637)

Input Data		
	Pier Shape:	Round nose
	Pier Width (ft):	3.08
	Grain Size D50 (mm):	0.10000
	Depth Upstream (ft):	9.42
	Velocity Upstream (ft/s):	2.84
	K1 Nose Shape:	1.00
	Pier Angle:	0.00
	Pier Length (ft):	58.00
	K2 Angle Coef:	1.00
	K3 Bed Cond Coef:	1.10
	Grain Size D90 (mm):	0.20000
	K4 Armouring Coef:	1.00
Results		
	Scour Depth Ys (ft):	4.60
	Froude #:	0.16
	Equation:	CSU equation

Pier: #2 (CL = 732)

Input Data		
	Pier Shape:	Round nose
	Pier Width (ft):	3.40
	Grain Size D50 (mm):	0.10000
	Depth Upstream (ft):	9.42
	Velocity Upstream (ft/s):	2.84
	K1 Nose Shape:	1.00
	Pier Angle:	0.00
	Pier Length (ft):	58.00
	K2 Angle Coef:	1.00
	K3 Bed Cond Coef:	1.10
	Grain Size D90 (mm):	0.20000
	K4 Armouring Coef:	1.00
Results		
	Scour Depth Ys (ft):	4.89
	Froude #:	0.16
	Equation:	CSU equation

Pier: #3 (CL = 832)

Input Data

Pier Shape:	Round nose
Pier Width (ft):	3.45
Grain Size D50 (mm):	0.10000
Depth Upstream (ft):	9.42
Velocity Upstream (ft/s):	2.84
K1 Nose Shape:	1.00
Pier Angle:	0.00
Pier Length (ft):	58.00
K2 Angle Coef:	1.00
K3 Bed Cond Coef:	1.10
Grain Size D90 (mm):	0.20000
K4 Armouring Coef:	1.00

Results

Scour Depth Ys (ft):	4.94
Froude #:	0.16
Equation:	CSU equation

Pier: #4 (CL = 927)

Input Data

Pier Shape:	Round nose
Pier Width (ft):	3.07
Grain Size D50 (mm):	0.10000
Depth Upstream (ft):	9.42
Velocity Upstream (ft/s):	2.84
K1 Nose Shape:	1.00
Pier Angle:	0.00
Pier Length (ft):	58.00
K2 Angle Coef:	1.00
K3 Bed Cond Coef:	1.10
Grain Size D90 (mm):	0.20000
K4 Armouring Coef:	1.00

Results

Scour Depth Ys (ft):	4.58
Froude #:	0.16
Equation:	CSU equation

Peak discharge event 3:

Contraction Scour

		Left	Channel	Right
Input Data				
	Average Depth (ft):		3.69	
	Approach Velocity (ft/s):		1.88	
	Br Average Depth (ft):		2.22	
	BR Opening Flow (cfs):		1090.00	
	BR Top WD (ft):		255.48	
	Grain Size D50 (mm):	0.10	0.10	0.10
	Approach Flow (cfs):		1090.00	
	Approach Top WD (ft):		157.40	
	K1 Coefficient:		0.690	
Results				
	Scour Depth Ys (ft):		0.42	
	Critical Velocity (ft/s):		0.96	
	Equation:		Live	

Pier Scour

Pier: #1 (CL = 637)

Input Data		
	Pier Shape:	Round nose
	Pier Width (ft):	3.08
	Grain Size D50 (mm):	0.10000
	Depth Upstream (ft):	3.51
	Velocity Upstream (ft/s):	2.37
	K1 Nose Shape:	1.00
	Pier Angle:	0.00
	Pier Length (ft):	58.00
	K2 Angle Coef:	1.00
	K3 Bed Cond Coef:	1.10
	Grain Size D90 (mm):	0.20000
	K4 Armouring Coef:	1.00
Results		
	Scour Depth Ys (ft):	3.72
	Froude #:	0.22
	Equation:	CSU equation

Pier: #2 (CL = 732)

Input Data		
	Pier Shape:	Round nose
	Pier Width (ft):	3.40
	Grain Size D50 (mm):	0.10000
	Depth Upstream (ft):	3.51
	Velocity Upstream (ft/s):	2.37
	K1 Nose Shape:	1.00
	Pier Angle:	0.00
	Pier Length (ft):	58.00
	K2 Angle Coef:	1.00
	K3 Bed Cond Coef:	1.10
	Grain Size D90 (mm):	0.20000
	K4 Armouring Coef:	1.00
Results		
	Scour Depth Ys (ft):	3.97
	Froude #:	0.22
	Equation:	CSU equation

Pier: #3 (CL = 832)

Input Data

Pier Shape:	Round nose
Pier Width (ft):	3.45
Grain Size D50 (mm):	0.10000
Depth Upstream (ft):	3.51
Velocity Upstream (ft/s):	2.37
K1 Nose Shape:	1.00
Pier Angle:	0.00
Pier Length (ft):	58.00
K2 Angle Coef:	1.00
K3 Bed Cond Coef:	1.10
Grain Size D90 (mm):	0.20000
K4 Armouring Coef:	1.00

Results

Scour Depth Ys (ft):	4.01
Froude #:	0.22
Equation:	CSU equation

Pier: #4 (CL = 927)

Input Data

Pier Shape:	Round nose
Pier Width (ft):	3.07
Grain Size D50 (mm):	0.10000
Depth Upstream (ft):	3.51
Velocity Upstream (ft/s):	2.37
K1 Nose Shape:	1.00
Pier Angle:	0.00
Pier Length (ft):	58.00
K2 Angle Coef:	1.00
K3 Bed Cond Coef:	1.10
Grain Size D90 (mm):	0.20000
K4 Armouring Coef:	1.00

Results

Scour Depth Ys (ft):	3.71
Froude #:	0.22
Equation:	CSU equation

Combined Scour Depths

Pier : #1 (CL = 637) (Contr + Pier) (ft):	4.15
Pier : #2 (CL = 732) (Contr + Pier) (ft):	4.39
Pier : #3 (CL = 832) (Contr + Pier) (ft):	4.43
Pier : #4 (CL = 927) (Contr + Pier) (ft):	4.13